

**Assessing rare earth element concentrations in geothermal and oil and gas
produced waters: A potential domestic source of strategic mineral
commodities**

Final Report to U.S. Department of Energy, Geothermal Technologies Office

Reporting Period Start Date: July 1, 2016
Reporting Period End Date: June 30, 2018

Authors: Scott Quillinan, Charles Nye, Mark Engle, Timothy Bartos, Ghanashyam
Neupane, Jonathan Brant, Davin Bagdonas, Travis McLing, J. Fred McLaughlin

Contributors: Erin Phillips, Laura Hallberg, Mahdi Shahabadi, Matthew Johnson

Date Report was issued: July 2018

DOE Award Number: DE-EE0007603

Carbon Management Institute
University of Wyoming
1020 E. Lewis Street
Laramie, WY 82072

Idaho National Laboratory
1955 N. Fremont Ave.
Idaho Falls, ID 83415

USGS Eastern Energy Resources Science Center
12201 Sunrise Valley Drive
956 National Center
Reston, VA 20192

USGS Wyoming-Montana Water Science Center
521 Progress Circle
Suite 6
Cheyenne, WY 82007

ACKNOWLEDGEMENT

This material is based upon work supported by the U.S. Department of Energy's Office of Energy Efficiency and Renewable Energy (EERE) under the Geothermal Technologies Office Award Number DE-EE0007603.

DISCLAIMER

This report was prepared as an account of work sponsored by an agency of the United States Government. Neither the United States Government nor any agency thereof, nor any of their employees, makes any warranty, express or implied, or assumes any legal liability or responsibility for the accuracy, completeness, or usefulness of any information, apparatus, product, or process disclosed, or represents that its use would not infringe privately owned rights. Reference herein to any specific commercial product, process, or service by trade name, trademark, manufacturer, or otherwise does not necessarily constitute or imply its endorsement, recommendation, or favoring by the United States Government or any agency thereof. The views and opinions of authors expressed herein do not necessarily state or reflect those of the United States Government or any agency thereof.

EXECUTIVE SUMMARY

The project team collected and analyzed 224 water samples and 101 matching rock samples. INL's improved method of measuring aqueous REEs allows study of samples previously thought too volume limited to measure.

The study found that aqueous REEs occur at trace levels in all analyzed samples, and sometimes exceed ocean REE concentrations by a factor of 1,000. No significant predictive relationship to lithology, reservoir temperature, nor salinity was discovered, but aqueous REE concentration appears spatially controlled.

Future work is needed to find the spatially-dependent variable that controls aqueous REE concentration.

ABSTRACT

This study, funded by U.S. Department of Energy Geothermal Technology Laboratory award DE-EE0007603, sought to discover the concentration of aqueous Rare Earth Elements (REEs) in geothermal produced waters. The project team collected 224 samples of geothermal produced water from wells and libraries, as well as 101 rock samples from outcrop and core libraries. These samples were studied with a variety of rock/fluid analyses, a neural network, and human expertise. This project resulted in a characterization of aqueous REEs in United States geothermal resources which will allow future work to: (1) measure aqueous REEs in volumes of water as small as 30mL, (2) extrapolate characteristics and constituents which indicate a prospective REE resource, (3) intelligently predict the most promising areas of the United States for further study and development, and (4) evaluate technologies for extracting extra value from water produced for geothermal energy to off-set costs.

To obtain a characterization of dissolved REEs in geothermal produced waters, it was necessary to determine REE concentrations in small volume samples, which form the majority of sample libraries in the United States. To that end, researchers at Idaho National Laboratory improved the methods of McLing 2014 to allow a 33-fold reduction in sample size. This improvement resulted in the addition of samples from the USGS water sample library which expanded the project to national scope.

The samples collected showed that a given basin had fairly consistent REE behavior. The basin a sample came from was a better predictor of REE concentration than salinity, temperature, or host rock lithology. The mechanism or variable by which this basin-by-basin control operates is unknown, and is among our top suggestions for future work.

The results of the nation-wide REE database were input to an Emergent Self Organizing Map (ESOM). The ESOM output a network of compositional "closeness" of each sample to the others, seen in Chapter 6. By using this network the researchers were able to estimate unmeasured parameters, such as the REE content of the samples in the USGS National Produced Waters Geochemical Database v2.3. The results of this method support the above finding that REE content follows the basin-by-basin trend seen in the measured samples.

The set of water samples was compared with a matching sample set of rocks that represented the reservoir the waters were hosted in. The researchers expected a rock type to match high REE waters, however, rock-type associations were less significant than the basin-to-basin trend.

The researchers also investigated possible technologies to concentrate and extract REEs. Their conclusion was that methods which can process large volumes are most favorable, even if the increase in concentration is incremental. The concept of treatment-trains allows such incremental increases in concentration to be summed and an ultimately favorable output to be achieved with near-optimal economic efficiency.

The ESOM's predicted REE concentrations are the first attempt to map-out REE concentrations in geothermal produced waters. By doing so researchers can better inform future studies seeking to understand REE concentration in geothermal produced waters. If future work measures the REEs in one of the areas covered by the database, the ESOM could be refined with the new information, and produce improved estimates. The present predictions should not be used for business decisions, but future estimates might be suitable.

This project has assessed the REE resources in geothermal produced waters, suggested explanations for the observed behavior, and recommended future research to answer remaining questions.

Acknowledgements

The authors and project team would like to thank and acknowledge the following groups and individuals. Their assistance during this project made work progress smoothly, facilitated research, made data available, improved the project's design, and polished the project's delivered products. Many others, too numerous to list, contributed to this work in other ways and the project team is indebted to them for their support, and guidance.

The Geothermal Technologies Office

Holly Thomas

Josh Mengers

The Technical Monitoring Team

Thomas Moore

Madalyn Blondes

Tanya Gallegos

Elisabeth Rowan

Colin Doolan

Mathew Varonka

Debbie Lacroix

Savannah Bachman

Kipp Codington

Sitian Xiong

Mackensie Swift

TABLE OF CONTENTS

Executive Summary and Abstract	3
Table of Contents	6
Chapter 1: Project Objectives and Motivation	8
Past Work and Remaining Questions	
Milestones and Deliverables	
Conclusion	
Chapter 2: Sample Collection and Library Selection (Task 1)	16
Existing Samples in Team Member Libraries	
New Samples Collected for this Project	
Analogous Rock Sample Collection	
Conclusion	
Chapter 3: Rare earth element hydrogeology/groundwater-quality sections for individual lithostratigraphic/hydrogeologic units within specific Wyoming hydrocarbon production fields	24
Greater Green River Basin	
Powder River Basin	
Wind River Basin	
Conclusion	
Chapter 4: Aqueous Sample Analysis (Task 2)	47
Methods for Aqueous REE and Geochemical Analysis	
Results of REE and Geochemical Analysis	
New Options for Aqueous REE Normalization	
Conclusion	
Chapter 5: Rock Sample Analysis (Task 3)	66
Introduction	
Data Collection	
Rock Sample Results and Discussion	
Conclusion	
Chapter 6: Predicting Rare Earth Element Potential in Produced and Geothermal waters of the United States: Application of Emergent Self-Organizing Maps (Task 5)	75
Introduction	
Methods and Data	

Results	
Summary	
Chapter 7: Technology screening (Task 6)	106
Review of Processes for Recovering Rare Earth Elements (REEs) from Geothermal Brines	
Review of Separation Processes for REEs in Mixed Brines	
Conclusion	
Chapter 8: Conclusions and Future Work	114
Conclusions of this Study	
Opportunities for Future Work	
Conclusion	
Appendices:	119
A0: Uploads – ESOM, Membrane Recovery Cost Tool, Rock Data	
A1: Sample List	
A2: Aqueous Geochemistry	
A3: Aqueous Rare Earth Element Concentration	

Chapter 1: Project Objectives and Motivation

Charles Nye, Scott Quillinan, Jonathan Brant, Travis McLing

Scott Quillinan, Director of Research and Communications, University of Wyoming, 1000 E. University Ave., Laramie, WY 82072
scottyq@uwyo.edu

Keywords: Rare Earth Elements, REE, Project Management, Review, Critical Minerals

ABSTRACT

In the years after the discovery of Rare Earth Elements (REEs) they were considered insoluble except in acidic solutions. Some studies that were ahead of their time, like (Goldschmit, 1937), showed that REEs occurred in neutral aqueous systems like the ocean, but reports of REEs as inert tracers for physical processes gained more attention (Bhatia and Crook, 1986). REE solubility at neutral pH survived in the cannon of geologists studying ocean chemistry such as Goldberg et al 1963, HWJ Baar et al 1985, and Alibo and Nozaki 1999. The work of Wood, 2002, Mcling 2014, and Migdisov et al. 2016 marked the renewal of non-fluvial continental investigations of REE solubility, and inspired the present project.

The present project resulted in an aqueous analytical method with a smaller sample volume than past studies, an expanded dataset of aqueous REEs in natural produced waters, a continental produced waters normalization, a screening tool, and a prediction of REEs across the United States.

1. PAST WORK AND REMAINING QUESTIONS

The REEs have similar chemical behavior, which is part of the reason their isolation as elements took nearly 160 years (Gupta and Krishnamurthy 2005). The currently favored explanation for the REE's similar properties is their similar electron configuration resulting from similar energies in the *5d* and *4f* electron shells, which results in similar ionic radii in the 3+ state. REEs most often occur in the 3+ state, with the exceptions of cerium and europium which can sometimes occur in nature as Ce⁴⁺ or Eu²⁺ instead.

1.1 Historical Research in Rock REEs

REEs allowed past researchers to provide evidence for rock processes. REEs provided important support for foundational theories about the rock cycle and planetary differentiation (Frey, et al. 1968). REEs even allowed estimation of compositions that would have be otherwise prohibitive to measure, such as the entire upper continental crust of earth (Taylor and McLennan 1985). In almost every case where REEs provided support or comparisons that advanced scientific understanding of the world, those REEs were visualized with an REE plot. Such plots were conceived of by Coryell et al. (1963) and used in their modern style by Evensen et al. (1978).

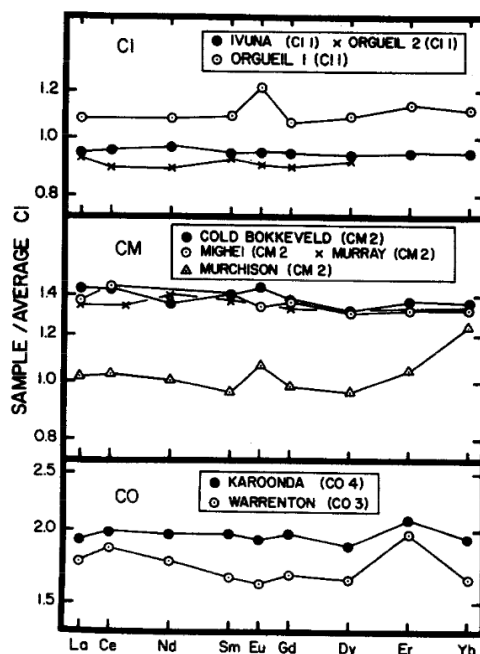


Fig. 1. REE abundances in carbonaceous chondrites from this study, normalized to average CI chondritic abundances.

Figure 1: A reproduction from Evensen 1978, showing how an REE plot allows visual comparison of multiple rare earth elements in multiple samples. This method emphasizes relative anomalies such as the europium anomaly in the top frame, and deemphasizes differences in absolute concentration. Note that even with missing data this method allows for meaningful conclusions. The data for Pr, Tb, Ho, and Tm is likely omitted because those elements occur at concentrations below the detection limits of Evensen’s 1978 instrumentation. At present, these elements are routinely measured in rocks thanks to modern advancements in instrumentation. The Pm data is omitted as this element does not naturally occur on earth.

These REE patterns allowed past researchers a means to test hypothetical mixing and partitioning of reservoirs. A famous use of this was the estimation of the bulk composition of the upper continental crust of earth by Taylor and McLennan (1985). Their estimation was made possible by comparing REE patterns of the Hadean earth to rocks that represented removal of material from the Earth’s core. An over-simplified version of this process would involve starting with the composition of meteorites thought to be similar to the composition of the Hadean proto-earth, and subtracting the composition of the modern mantle, to produce an estimation of the crust’s composition. Such process would hinge upon knowing the proportion of crust to mantle and the assumption that all material in the proto-earth partitioned into either the crust or the mantle.

More recent work, has applied the same principle to show that REE ratios in parent rock fragments that are preserved during weathering and transport into sedimentary basins (Heller, 1983). REEs allow identification of which rocks were weathered to produce the sediment, and the proportion of their contribution. This ability to trace parent rock material reliably has revolutionized sedimentology and allowed exciting assessments of basin evolution.

1.1.1 Importance to this project

The above past achievements in rock REEs contributed to the present project’s development in two important ways.

Firstly, as the study of rocks showed, REE measurements become more important and more meaningful when they are compared to each other or to other parts of their system. This is seen in rocks when a mountain range outcrop is compared to a basin sediment. The team was inspired to consider that aqueous REEs should be compared to their host reservoir, which is the most likely part of the water system to be a source/sink for REEs. This inspiration is reflected in the Statement Of Project Objectives (SOPO) tasks two and three.

Secondly, authors of early rock REE literature struggled to agree on the exact concentrations they would normalize to. Chondrite normalization alone has had at least fourteen distinct concentration values proposed over the last fifty years (Korotev, 2018). During the project the team considered a normalization for REEs in aqueous systems, which became the Wyoming Basin Produced Waters Normalization explained in chapter 4 (Nye et al. 2017).

1.2 Aqueous REE study

Conventional wisdom for much of the 20th century was that REEs do not dissolve in water or form aqueous complexes except in acidic conditions (Pearson, 1963). The discovery of naturally-occurring REEs in neutral waters at the end of the 20th century showed that these

species do dissolve, but at very small concentrations that often require analysis by ICP-MS to detect (Johannesson et al., 1995). As a result of this work various researchers have quantified the REE content of most oceans, rivers, and even some wines (Alibo, 1999, Goldstein and Jacobsen 1988, Piper and Bau 2013). Some of these authors have suggested a normalization based on their work.

However, all of these studies of aqueous REEs suffered from three limits on the ICP-MS method. First, the ICP-MS method is sensitive to the solution's salinity which can affect the background structure and obscure small signals from trace analytes like REEs. Second, the ICP-MS method has an inference between barium and some REEs, which limits precision in high-barium waters. Third, ICP-MS instruments are delicate, and can easily be fouled by oils, waxes, or particles. For these three reasons high salinity, high barium, and hydrocarbon-bearing waters are understudied. At the start of this project the USGS National Produced Waters Geochemical Database v2.3 contained less than five samples that reported an REE. Expanding the number of REE analyses was the primary motivator for the present work.

1.2.1 Importance to this project

The present work benefited from a unique methodology first performed by Strachan et al. (1989) with subsequent improvements by Stetzenbach et al. (1994), Wood (2002), and McLing (2014). Strachan et al. (1989) showed that the Chelex-100 resin could selectively hold most REEs as an ion-rich solution passed over it. With subsequent development this method was able to retain all REEs at such high efficiency that after removing them from the sample, the REEs could be released from the resin and measured on a common ICP-MS with analytical accuracy. The remaining weakness in this technique was that the minimum sample volume (>1L) much larger than normal for analytical chemistry.

The 1 Liter sample volume had not been a problem for the researchers who developed the resin pre-concentration method because when collecting sample from natural systems, they knew in advance that the analysis would require this large volume, and could modify their collection procedure to match the analytical method. However, sample libraries in the United States normally store only 10-100mL of sample. This limited library volume means that the only option for REE analysis is to modify the analytical method to match these smaller sample volumes. The development of such a method, to measure smaller sample sizes, was another goal of our work.

1.3 Interdisciplinary expansions

As described above the motivation for this work included: (1) comparison of REE fractionation between water and rock in the subsurface system, (2) development of a normalization that describes continental subsurface waters, (3) sample collection, and (4) method development. In addition the team saw that (5) identifying screening parameters and (6) identifying reservoirs with high REE potential were easy extensions that would contribute to the project's value.

1.3.1 Geochemistry

Extraction of value from otherwise unused water has been a topic of vigorous research, recently culminating with the work of Smith et al. (2017). The contribution of the University of Wyoming's Center for Excellence in Produced Waters Management (CEPWM) to this project developed the understanding of past researchers like Smith to see if REEs in produced waters were economic. Smith et al (2017)'s conclusion was that REEs were not economic, but with a new technique or through combination of many different products, they might become so.

Researchers at the CEPWM have been studying and developing technologies for the purpose of extracting/recovering resources from mixed brines, like produced waters and brackish ground waters, in manners that are both economical and environmentally sustainable. Resources of specific interest to the CEPWM have historically been water, precious metals, and rare earth elements (REEs), as these resources are of great value and interest to Wyoming. The technological focus of these previous efforts has centered on understanding the transport and rejection mechanisms, and their subsequent manipulation, of dense membrane films for metals and REEs. Broadening the types of waters that may be included in these types of analyses was the central motivation for CEPWM researchers in the current effort.

The unique chemistries and compositions of geothermal brines, relative to those waters generally included in CEPWM's analyses, made the application and efficiencies of technologies aimed at REE separation possibly unique from other studies. Like other sources, the concentrations of REEs are relatively low, particularly when compared to other salts and minerals in geothermal brines. At such low concentrations, typically at the nanogram to microgram per liter level, the use of REE extraction technologies, like solvent based extraction, is economically and practically infeasible. This observation was not wholly surprising as many of these technologies were designed for extracting REEs from solid matrices and/or concentrated liquid flows.

This challenge provided motivation for identifying new and effective technologies for REE extraction from dilute mixtures. To this end, it was determined through a survey of the literature that significant knowledge and technology gaps exist in terms of how to selectively extract REEs at low concentrations from mixed brines, where competition for adsorption sites, co-precipitation, and simple economics can be overcome. The majority of recent studies in this area have centered on developing new adsorptive materials for REEs; however, these efforts focus on simple matrix solutions composed of a single REE and at concentrations that exceed those occurring in geothermal waters and produced brines. Preliminary advancements have been made for REE separation using nanofiltration membranes, though these studies too are limited by the same factors as the aforementioned adsorption studies. The CEPWM therefore concluded that while REE separation is technically feasible using any number of methods, there is a chasm that exists between these technologies and the practical recovery of REEs from geothermal waters and produced brines.

1.3.2 Emergent Self-Organizing Map (ESOM)

The advancement of computer science and machine-learning techniques offers a low-bias means to study large datasets. Although the data generated as part of this work is the largest source of REEs in geothermal and produced waters in the U.S., on a national scale the total sample count is still relatively low. Moreover, the likely existence of subpopulations within the data set (as designed) prevents estimation attempts using traditional regression methods. Thus, newer more innovative data analysis methods are needed. Our team selected a technique called an Emergent Self-Organizing Map (ESOM) to extrapolate our measured discoveries in geothermal produced waters to the national scale. ESOM, a type of neural network, are particularly useful in organizing data based on their similarities and can be used in prediction even when some of the parameters are missing. This ESOM would help identify areas of particular promise for REE value-added or cost-offset development.

2. MILESTONES AND DELIVERABLES

The project was divided into two budget periods spread over two years. These tasks were generally in chronological order but had significant overlap so project duration could be used effectively. The Budget Periods were separated by a Go/No-go decision point, which the project team passed with a “Go” recommendation. There were some modifications to the SOPO as the project advanced, most significantly the re-listing of task 2.4 in both budget periods to clarify its intended duration and rewriting Task 5 to avoid overlap with a different DOE project. The only other project management change was the retirement from the Geothermal Technology Office of the Project Officer, Holly Thomas, who had proven very helpful to the team.

The project team was spread over three organizations – University of Wyoming, USGS, and Idaho National Laboratories. The team’s cooperation was directed by the PI, Scott Quillinan, and guided by the Milestones and Deliverables in Table 2.1.

Project Milestones By Task	Milestone Description	Planned month of completion	Quarter	Verification Method
Task 1	Collect matching/analogous rock and water samples			
1-1	Identify which existing samples will be submitted for REE analysis from USGS catalog	3	Q1	Data to DOE-GDR and quarterly reports DOE
1-2	Process, split, and transfer of existing samples to INL	6	Q2	Data to DOE-GDR and quarterly reports DOE
1-3	Identify available corresponding rock samples for analysis	9	Q3	Data to DOE-GDR and quarterly reports DOE
1-4	Complete report and data upload to the DOE-GDR in the appropriate templates for water and rock samples and well fluid production content.	12	Q4	Data to DOE-GDR and quarterly reports DOE
Task 1 Deliverable	Completed sample inventory of all selected OGTW samples for REE analysis containing sample ID, site description, geologic formation and basin, pH, temperature, salinity, and any field notes and parameters from sample collection provides as a report and data uploaded to the DOE-GDR in the appropriate templates.	12	Q4	Data to DOE-GDR and quarterly reports DOE
Task 2	Characterize geothermal water, and co-produced oil and gas waters			

Project Milestones By Task	Milestone Description	Planned month of completion	Quarter	Verification Method
2-1	Complete geochemical analysis of water samples and upload data to the NGDS in the appropriate templates.	12	Q4	Quick look report and Data to DOE-GDR and quarterly reports DOE
2-2	Format OGTW data into provided templates and upload to the DOE-GDR along with accompanying report	12	Q4	Data to DOE-GDR and quarterly reports DOE
2-3	Complete flow rate and temperature data collection	16	Q6	Data to DOE-GDR and quarterly reports DOE
2-4	Complete geochemical modeling to help inform geologic interpretations.	20	Q7	Data to DOE-GDR and quarterly reports DOE
Deliverable	Task 2 Deliverable: Report and data table uploaded to the DOE-GDR including: Sample inventory data, REE and trace element geochemistry, major and minor element geochemistry, and stable isotope geochemistry of analyzed OGTWS and methodologies used for sample collection and analysis			
Task 3	Characterize rock associated with water samples			
3-1	Rock samples obtained and analysis initiated.	3	Q1	Quarterly report
3-2	Complete analysis of major, minor elements, and REEs, in rock samples related to OGTW	12	Q4	Summary report and data uploaded to DOE-GDR
3-3	Format rock related OGTW-data into provided templates and upload to the DOE-GDR.	12	Q4	Data to DOE-GDR and quarterly reports DOE
Deliverable	Task 3: Deliverable: Report and data on the geochemical analysis of rock samples associated with OGTWs including: major oxides, trace elements, REEs, mineral assessment, porosity, mineral stability, and cation exchange capacity and methodologies used for sample collection and analysis. Data and reports uploaded to the DOE-GDR	12	Q4	Data and reports uploaded to the DOE-GDR.

Project Milestones By Task	Milestone Description	Planned month of completion	Quarter	Verification Method
Go/No-Go	Complete OGTW and GTW fluid and corresponding rock sample analysis and all results uploaded in the correct templates with accompanying explanatory reports and available for public access. Content as defined in the milestones for Tasks 1, 2, and 3 and the Data Management Plan.	10	Q4	Continuation report submitted 60 days before end of the period
BUDGET PERIOD 2				
Task 5	Geostatistics and REE distribution			
5-1	Generation of a trained emergent self-organizing map (ESOM) using REE data.	16	Q6	Data to DOE-GDR and quarterly reports DOE
5-2	Complete mapping of pre-existing data to trained ESOM.	20	Q7	Data to DOE-GDR and quarterly reports DOE
5-3	Collect and analyze a minimum of five samples produced water samples to validate the ESOM analysis	22	Q8	Data to DOE-GDR and quarterly reports DOE
5-4	Upload report including all supporting data, maps and graphs to the National Geothermal Repository on potential OGTW reservoir types and geologic regions with respect to REEs.	24	Q8	Data to DOE-GDR and quarterly reports DOE
Task 6	Technology screening			
6-1	Economic and sustainability models complete and upload report data to the DOE-GDR in accordance with the DMP.	18	Q7	Data to DOE-GDR, preliminary model demonstration and quarterly report DOE
6-2	Upload data and report to the National Geothermal Repository on evaluated technologies for REE separation. Recommend areas for future work.	24	Q8	Data to DOE-GDR and quarterly report DOE
Deliverable	Task 6: Excel-based screening tool and operating instructions to evaluate fluid, economic and engineering variables with respect to REE recovery and an example case study using up to 3 sites to illustrate variables of economic recovery process. Report and data uploaded to the DOE-GDR in accordance with the DMP.	24	Q8	Data to DOE-GDR, model demonstration, and Final Report.

Table 2.1: The table of milestones and deliverables as revised at the start of the project’s second year. All milestones and deliverables were fulfilled during the performance period.

2.1 Milestones

All milestones were met before project completion. Any milestones that required modification from the planned delivery date and method were coordinated with the Project Officer, and completed accordingly. As explained above these changes occurred between budget period 1 and budget period 2 with an end-date modification to task 2.4 and a rewrite of task 5. These changes were reflected in the milestones as well as the SOPO text.

2.2 Deliverables

Deliverables included a sample inventory of waters, a sample inventory of rocks, a chemistry report of waters, a chemistry report of rocks, maps of the ESOM prediction, and an excel-based screening tool. These were delivered as scheduled, again with the modifications that occurred between budget periods.

To fulfill the project’s data management plan all data appropriate for release to the public was uploaded to the Geothermal Data Repository (GDR). The GDR is the submission point for all data collected from research funded by the U.S. Department of Energy's Geothermal Technologies Office. These data are intended to contribute to the scientific communities’ resources, and to assist stakeholders with decision making.

Type	Description	Location on the GDR
Rock	Rare Earth Geochemistry of Rock Core from WY Reservoirs	https://gdr.openei.org/submissions/926
Rock	Technical Report-Rare Earth Element Data Associated with Oil and Gas Reservoir Rock	https://gdr.openei.org/submissions/953
Rock	Rare Earth Element and Trace Element Data Associated with Hydrothermal Spring Reservoir Rock, Idaho	https://gdr.openei.org/submissions/989
Water	Rare Earth Element Geochemistry for Produced Waters, WY	https://gdr.openei.org/submissions/925
Water	Aqueous Rare Earth Element Patterns and Concentration in Thermal Brines Associated with Oil and Gas Production	https://gdr.openei.org/submissions/930
Water	Soda Geyser Geochemistry	https://gdr.openei.org/submissions/937
Water	Aqueous Rare Earth Elements, Concentration, and Stable Isotopes in Deep Basin Brines, Wyoming	https://gdr.openei.org/submissions/933
Water	Rare Earth Element Concentration of Wyoming Thermal Waters Update	https://gdr.openei.org/submissions/931
Water	Rare Earth Element Geochemistry of Produced Waters in WY	https://gdr.openei.org/submissions/932
Water	Rare Earth Element Concentrations in Wyoming's Produced Waters	https://gdr.openei.org/submissions/960
Water	Technical Report-Rare Earth Element Concentrations in Wyoming's Produced Waters	https://gdr.openei.org/submissions/952

3. CONCLUSION

REEs have been an exciting area of research since their discovery. Few other elements have such similar behavior under such a wide range of environments, and surprising differences in the details. The historical applications of REEs in hard rocks have always been a few decades ahead of those same applications in aqueous systems. This work was inspired by Idaho National Lab’s improved method (McLing et al. 2014) to advance aqueous REEs in the same way rock REEs have been.

The project resulted in a further improved method that could use a smaller sample volume (~30mL), an expanded nation-wide dataset that multiplied the existing data on aqueous REEs in produced waters by more than ten times, a normalization expressing their typical behavior, a fluid evaluation screening tool, and a set of predicted potential maps suggested by the ESOM.

CONTRIBUTIONS AND ACKNOWLEDGMENTS

CN drafted this chapter manuscript and compiled edits. JB wrote section 1.3.1. SQ and TM conceived of the work presented in this chapter. All authors reviewed the chapter manuscript. Contributors include: Kipp Coddington who managed facilities and relationships used in the work. Funding for this work was provided by U.S. Department of Energy, Geothermal Technologies Office under Award DE-EE0007603. The authors would like to thank our DOE project managers Holly Thomas and Josh Mengers and also our Technical Monitoring Team for their support, advice, and insight.

REFERENCES

- Alibo D.S., Y. Nozaki. Rare earth elements in seawater: particle association, shale-normalization, and Ce oxidation. *Geochimica et Cosmochimica Acta*, **63** (3), (1999) pp. 363–372. [http://dx.doi.org/10.1016/S0016-7037\(98\)00279-8](http://dx.doi.org/10.1016/S0016-7037(98)00279-8).
- Bhatia, M.R. & Crook, K.A.W. “Trace element characteristics of graywackes and tectonic setting discrimination of sedimentary basins” in Contributions to Mineralogy and Petrology. (1986) 92: 181-193. Accessed from: <https://doi.org/10.1007/BF00375292>
- Coryell, Charles. D., John. W. Chase, and John. W. Winchester (1963), A procedure for geochemical interpretation of terrestrial rare-earth abundance patterns, Journal of Geophysical Research, 68(2), 559–566, <https://doi.org/10.1029/JZ068i002p00559>.
- De Baar, Hein J.W., Michael P. Bacon, Peter G. Brewer, Kenneth W. Bruland. *Rare earth elements in the Pacific and Atlantic Oceans*. *Geochimica et Cosmochimica Acta*, v49 i9 (1985), pp. 1943-1959 Accessed from <https://www.sciencedirect.com/science/article/pii/0016703785900894>
- Frey, Fred A., Mary A. Haskin, Jo Ann Poetz, and Larry A. Haskin. 1968 *Rare Earth Abundances in Some Basin Rocks* Journal of Geophysical Research. Vol 73 No 18. Accessed from <https://agupubs.onlinelibrary.wiley.com/doi/pdf/10.1029/JB073i018p06085>
- Goldberg, Edward D., M. Koide, R.A. Schmitt, R.H. Smith. *Rare-earth distributions in the marine environment* Journal of Geophysical Research, 68 (1963), pp. 4209-4217 Accessed from <https://agupubs.onlinelibrary.wiley.com/doi/pdf/10.1029/JZ068i014p04209>
- Goldschmidt, V M. *The principles of distribution of chemical elements in mineral and rocks*. Hugo Müller Lecture, Journal of the Chemical Society March 17th 1937. Pages 655-673. Accessed from <https://pubs.rsc.org/en/content/articlepdf/1937/jr/jr9370000655>
- Goldstein, S.J. and S.B. Jacobsen, 1988. *Rare earth elements in river waters*. Earth Planet. Sci. Lett., 89 (1988), pp. 35-47
- Heller, Paul Lewis. 1983. “Sedimentary Response to Eocene Tectonic Rotation in Western Oregon.” University of Arizona. Accessed from <https://doi.org/10.1501/187393>.
- Johannesson, Kevin H., W. Berry Lyons, Klaus J. Stetzenbach, and Robert H. Byrne. *The solubility control of rare earth elements in natural terrestrial waters and the significance of PO 4 3- and CO 3 2- in limiting dissolved rare earth concentrations: A review of recent information* (1995)
- Korotev, Randy L. “*Rare Earth Plots*” and the Concentrations of Rare Earth Elements (REE) in Chondritic Meteorites. Department of Earth and Planetary Sciences, Washington University in St. Louis. Accessed from: <http://meteorites.wustl.edu/goodstuff/ree-chon.htm> (September, 2018)
- McLing, W. Smith, R. Smith, *Utilizing rare earth elements as tracers in high TDS reservoir brines in CCS applications*, Energy Procedia 63 (2014) 3963-3974, <https://doi.org/10.1016/j.egypro.2014.11.426>.
- Migdisov A., A.E. Williams-Jones, J. Brugger, F.A. Caporuscio. Hydrothermal transport, deposition, and fractionation of the REE: experimental data and thermodynamic calculations. *Chemical Geology*, **439**, (2016) pages 13–42. <http://dx.doi.org/10.1016/j.chemgeo.2016.06.005>.
- Nye, Charles, Davin Bagdonas, Scott Quillinan: *A New Wyoming Basin Produced Waters REE Normalization and Its Application*, Proceedings, 43rd Workshop on Geothermal Reservoir Engineering, Stanford University, Stanford, CA (2018). SGP-TR-212.
- Pearson, Ralph G. 1963 *Hard and Soft Acids and Bases* in the Journal of the American Chemical Society 85 (22), 3533-3539. Accessed from: <https://pubs.acs.org/doi/pdf/10.1021/ja00905a001>
- Piper, David Z. and Michael Bau, *Normalized Rare Earth Elements in Water, Sediments, and Wine: Identifying Sources and Environmental Redox Conditions*, American Journal of Analytical Chemistry (2013) 69-83, https://file.scirp.org/pdf/AJAC_2013102515543528.pdf.
- Smith, Y.R., P. Kumar, and J.D. McLennan, *On the Extraction of Rare Earth Elements from Geothermal Brines*. Resources, 2017. 6(3). DOI:[10.3390/resources6030039](https://doi.org/10.3390/resources6030039).
- Taylor, S.R., and McLennan, S.M., 1985, *The Continental Crust: Its composition and Evolution*: Oxford, Blackwell, 312 pages.

Chapter 2: Sample Collection and Library Selection

Charles Nye, Hari Neupane, Scott Quillinan, Travis McLing, Davin Bagdonas, Fred McLaughlin

Scott Quillinan, Director of Research and Communications, University of Wyoming, 1000 E. University Ave., Laramie, WY 82072

scottyq@uwyo.edu

Keywords: Sample Collection, Sample Library, Collection, Methods, Research Areas

ABSTRACT

The USGS, and INL entered this project with existing samples from Geothermal resources. These Geothermal resources included the Eastern Snake River Plain (ESRP), Kevin-Sunburst Dome, the Appalachian Basin, the Permian Basin, and the Williston Basin.

In the last several years, INL has re-visited and evaluated the geothermal resource potential in the ESRP and surrounding areas using geological, geochemical, isotopic, and thermal tools (e.g., Neupane et al., 2014; Dobson et al., 2015; Mattson et al., 2016; McLing et al., 2016). These studies resulted in new samples from several geothermal features and concentration data for major cations and anions that were expected to allow estimation of deep reservoir temperatures (e.g., Cannon et al., 2014; Mattson et al., 2016).

UW expanded upon the USGS and INL libraries by sampling from four major Wyoming basins, each with a different stratigraphy and structural setting. This collection was facilitated by UW’s experience of working with oil and gas operators, and familiarity with their hope for an improved method of produced water use or disposal. UW also collected samples of rock matching each Wyoming sample and Idaho lithology.

1. EXISTING SAMPLES IN TEAM MEMBER LIBRARIES

INL and the USGS contributed samples to this project from their pre-existing libraries. The USGS contribution included larger-volume samples of over 100mL (n=18) which proved invaluable to incremental improvement of the INL methods, and more typical 30mL samples (n=31) which were analyzed as INL improved the extraction and analytical protocols. The USGS samples covered three basins, the Williston, the Appalachian, and the Permian. The INL contribution (n=142) focused on Idaho geothermal resources that resulted from migration of the Yellowstone hot spot over the ESRP. INL’s samples were collected with awareness of the sample volume limitation of Wood 2014’s method and are a much larger volume (>2L) than most samples (~500mL). Their large volume meant they could be analyzed before method development occurred. INL’s existing collection benefited from the work of Earl D. Mattson (INL) and Thomas Wood (University of Idaho).

Team Member Contributing	Area	Aqueous REE	Aqueous Geochemistry	Rock REE	Rock Geochemistry
University of Wyoming	Wind River Basin	X	X	X	X
University of Wyoming	Powder River Basin	X	X	X	X
University of Wyoming	Green River Basin	X	X	X	X
University of Wyoming	Washakie Basin	X	X	X	X
Idaho National Laboratory	Eastern Snake River Plain	X	Cannon et al. 2014 Mattson et al. 2015 Neupane et al. 2016a Neupane et al. 2016b Neupane et al. 2017	X	X
Idaho National Laboratory	Kevin-Sunburst Dome	X	previously unpublished		
USGS	Appalachian Basin	X	Rowan et al. 2015 Akob et al. 2015 Blondes (USGS)		
USGS	Permian Basin	X	Engle et al. 2016		
USGS	Williston Basin	X	Gallegos (USGS)		

Table 1: A Table of the sample groups studied under this project. “X” indicates a sample group analyzed for the first time during this work. Citations indicate a sample group whose data may be found elsewhere, but which was expanded in this work.

In addition to these libraries of physical samples, the USGS maintains a vast database of previous water quality analyses called the “National Produced Waters Geochemical Database v2.3” (NPWGD v2.3) roughly 115,000 of which were used for the ESOM (See Chapter 6) that featured in the second half of the project. Because this database contained less than 5 REE analyses at the start of this project, one of the project’s goals was to impute the REE concentrations to these ~115,000 samples to aid selection of future research sites. This goal was achieved, as described in Chapters 6 and 8.

2. NEW SAMPLES COLLECTED FOR THIS PROJECT

Samples were collected during the project by INL and by UW. The INL contribution focused on water samples from the Eastern Snake River Plain and Kevin-Sunburst Dome areas. UW’s contribution focused on water samples from four hydrocarbon-bearing basins in Wyoming. These samples sets were accompanied by rock sample collection. In Idaho, these rock samples came from outcrops and in Wyoming the samples came from drill core held at the Core Research Center (CRC) in Golden, Colorado (see Section 3). The rock samples were collected by UW. The Idaho water samples were collected according to the methods of McLing et al, 2014. This resulted in over a liter of sample volume.

To ensure successful partnerships with industry, the Wyoming water sample collection procedure had to accommodate rapid collection from an unfamiliar source. While very similar to McLing et al. (2014) some modifications were made. Three field blanks showed that these modifications were insignificant, but for caution, the strict methods of McLing et al. (2014) are recommended whenever feasible. The two main modifications were in bottle preparation, and transport prior to filtration.

All samples were collected in 500mL Low Density Polyethylene (LDPE) bottles that were pre-washed with hydrochloric acid, rinsed in the laboratory with ultra-pure water ($>18 \text{ M}\Omega\text{-cm}$), and then rinsed again in the field with the sample before final collection. In two cases, where limited water sample volumes precluded rinsing in the field that final step was omitted. There was no noticeable difference between field rinsed and un-rinsed samples.

Following collection, the sample bottles were transported on dry ice in a cooler. Upon return to the University of Wyoming (a trip of less than 8 hours) the samples were frozen overnight, and then thawed, filtered, split, and acidified the following morning. Freezing was important to arrest biologic activity that can change isotopes and reduction-oxidation sensitive chemical species. Filtering used 0.45 micron mixed-cellulose ether filter papers to remove particulate and microbes. The split allowed analysis for anions that require an unacidified sample, and also cations (including REEs) that can be better preserved in an acidified sample. The acid used for acidification was trace metal grade 69% Optima nitric acid. Only a few drops were needed to lower the pH of the samples to ~2 as measured with pH test strips.

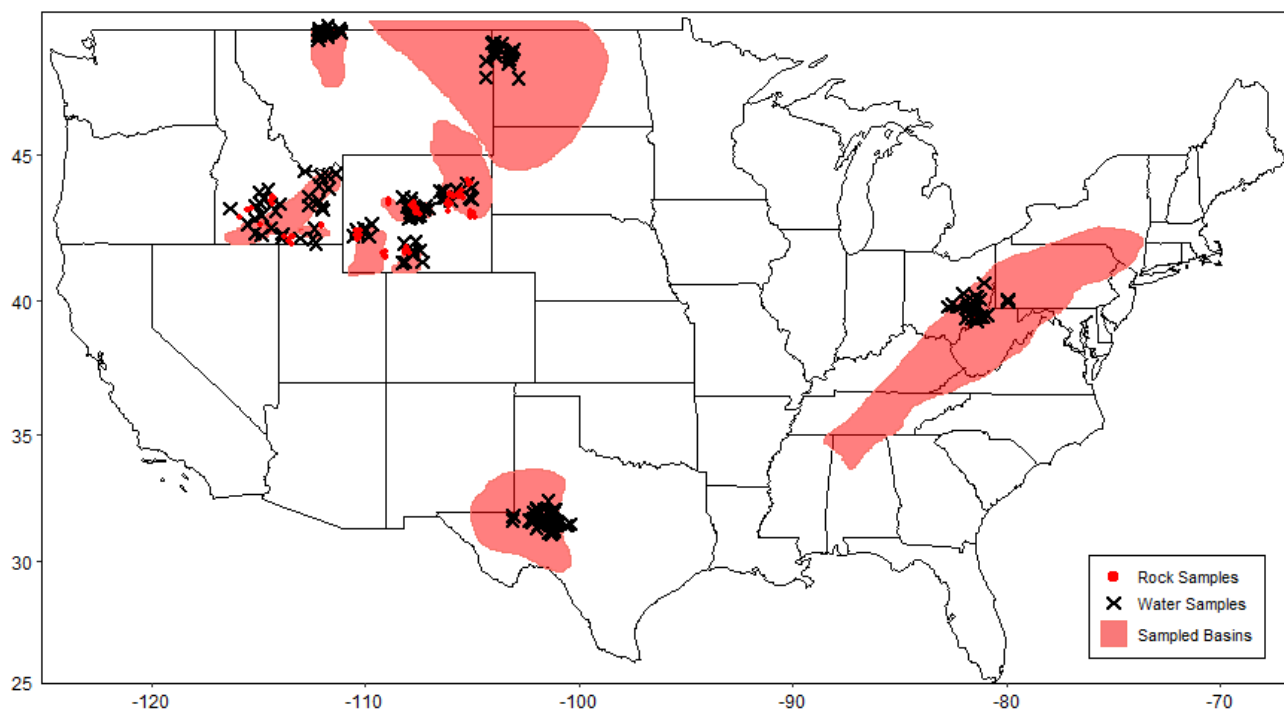


Figure 2: Basins in the United States that were analyzed for REEs in this project. The red points in Wyoming and Idaho are rock samples collected and analyzed for REEs and geochemistry during this project. The black “X”s indicate the location of water sample analyzed for REEs in this project. A jitter-function has been applied to all sample locations to show their density better.

The six areas of water sample collection were: the Eastern Snake River Plain (ESRP), Kevin-Sunburst dome, Wind River Basin, Powder River basin, Green River Basin and Washakie Basin. The following sections detail the context of these locations, and the general properties of their water samples.

2.1 Snake River Plain Geothermal Brines, Idaho

The Snake River Plain (SRP) is a topographic depression along the Snake River in south Idaho. The SRP is divided into two parts, the Western Snake River Plain (WSRP) and ESRP. The WSRP is a basalt and sediment filled tectonic feature defined by normal fault-bounded graben whereas the ESRP is formed by crustal down-warping, faulting, and successive caldera formation that is linked to the middle Miocene to recent volcanic activities associated with the migration of the Yellowstone-Snake River hotspot (Pierce and Morgan, 1992; Rodgers et al., 2002). The 100 km wide ESRP extends over 600 km (Hughes et al., 1999).

The ESRP consists of thick rhyolitic ash-flow tuffs, which are overlain by >1 km of basaltic flows. The rhyolitic volcanic rocks at depth are the product of super volcanic eruptions associated with the Yellowstone Hotspot activities. These rocks progressively become younger to the northeast towards the Yellowstone Plateau (Pierce and Morgan, 1992; Hughes et al., 1999). The younger basalt (predominantly, olivine tholeiite basalt) layers are the result of several low-volume, monogenetic shield-forming eruptions of short-duration that emanated from northwest trending volcanic rifts in the wake of the Yellowstone Hot Spot (Hughes et al., 1999). The thick sequences of coalescing basalt flows with interlayered fluvial and eolian sediments in the ESRP constitute the very productive Eastern Snake River Plain Aquifer (ESRPA) system above the rhyolitic ash-flow tuffs (Whitehead, 1992). This aquifer system rapidly transports cold recharge from the Yellowstone Plateau and surrounding mountain basins to springs along the Snake River Canyon west of Twin Falls, Idaho. The geothermal gradient below the ESRPA system was found to be increasing rapidly (Blackwell, 1989; McLing et al., 2002; Nielson et al., 2012).

The ESRP geothermal brine water samples were collected mostly from hot springs and hot wells distributed within and along the margins of the SRP and analyzed for their major, minor, trace, and REEs. These samples were initially collected for determining general chemistry needed for estimating reservoir temperatures (Mattson et al., 2016). These geothermal brines were also used for REE analysis for this project, because the sample collection procedure was as robust as the REE analysis collection procedure.

2.2 Brine Samples from the Kevin Dome Area, Montana

Kevin Dome (also called Kevin-Sunburst Dome) is a large underground, doubling plunging anticline in north central Montana, near the Canadian border (Stein, 2008). The dome feature extends for 700 square miles and is roughly circular (Collier, 1929). The water samples collected for this study came from surface features near the dome and domestic water wells. These 23 samples from Kevin Dome were collected during the Big Sky Carbon Sequestration Partnership. These samples were collected by affiliates of INL, according to INL collection procedures. INL analyzed these water samples for major, minor, trace elements, and REE.

2.3 Wind River Basin Geothermal Produced Waters, Wyoming

The Wind River Basin (WRB) is a structural basin in central Wyoming. Like most Wyoming basins, it formed in the Laramide. The basin is bounded by the Wind River Range on the west, the Granite Mountains on the south, the Casper Arch on the east, and the Owl Creek Mountains on the north. The basin's deepest contact with granitic basement (24,000ft below sea level) occurs just south of the Owl Creek Mountains (Keefer, 1970). Samples for this project came from this area in the deepest part of the basin. There are some anomalous geothermal resources in the WRB that deviate from the expected geothermal gradient. The cause of this activity is unknown but could be related to stresses caused by the failed extreme northern branch of the Rio-Grand Rift, tertiary volcanic plugs, thermal insulation by coal seams, or blind faults that connect the deep basin to shallower units. The last option is the preferred explanation at present.

The WRB samples came from three well fields. These fields spanned shallow, hot units like the Fort Union, deeper, cooler units like the Cody, and deep very hot units like the Madison. With the exception of two holding-tank samples all samples were taken from the phase-separator.

2.4 Powder River Basin Geothermal Produced Waters, Wyoming

The Powder River Basin (PRB) is an asymmetric syncline in Northeast Wyoming possessing both stratigraphic and structural features. The basin is bounded by the Big Horn Mountains on the west, the Laramie Range on the south, and on the northeast partially by the Black Hills. The basin axis trends north-south, with a significant dip on the west limb, and a much gentler dip on the eastern limb. Samples from the PRB came from two fields, one on the basin axis, and the other on the eastern limb. Almost all modern production in the PRB is from horizontal wells enhanced with near-well rock fracturing.

2.5 Green River Basin Geothermal Produced Waters, Wyoming

The Green River Basin (GRB) is distinguished from the Greater Green River Basin (GGRB) in this work. The Greater Green River Basin refers to the combined areas of the Green River Basin, Great Divide Basin, and also the Washakie Basin (see subsection 2.6). The Green River Basin is a structural basin in far western Wyoming. The GRB is bounded by the Wyoming Fold-and-Thrust Belt on the west, the Uinta Mountains on the south, partially by the Rock Springs Uplift on the east, and the Wind River Range on the north. Water samples for this project came from two fields in the northeast of the GRB. This area is sometimes designated the Hoback Sub-Basin of the GGRB. The fields bordered the fold and thrust belt and were designed to harness the structural traps of that area rather than the less dramatic traps commonly found in the center of the GRB.

2.6 Washakie Basin Geothermal Produced Waters, Wyoming

The Washakie Basin of south central Wyoming is centered around a small syncline. The basin is partially bounded by the Rock Springs Uplift on the west, Cherokee Ridge on the south, the Sierra Madre on the east, and the Wamsutter Arch on the north (Roehler, 1973). The basin's vague borders contribute to its frequent grouping in the better delineated GGRB. The Washakie basin produces a great deal of gas and gas condensate, which sometimes made water recovery challenging. Water samples in this basin came from phase separators with the exception of one sample that came from a water-holding tank.

3. ANALOGOUS ROCK SAMPLE COLLECTION

Researchers at the University of Wyoming identified the rock formations most likely to be in contact with the water samples in Idaho and Wyoming. In Wyoming, this formation was the producing interval listed with the WOGCC. In Idaho, this formation was identified from expert knowledge of field relationships, and checked with a literature search. The samples were collected from the Core Research Center’s (CRC) repository in Golden Colorado, and in cooperation with landowners in Idaho. The exact location or locations within the targeted formation were selected to be representative of the full reservoir interval or, if additional information was known, the relevant substrata. An example of such additional information would be the perforated depth within a producing formation.

The result of these collections was 65 core plug samples from the CRC for Wyoming, and 18 traditional outcrop samples from Idaho. Rock sample collection was the same for all rock samples, exempting that outcrop samples were trimmed to ensure fresh rock was analyzed. Subsequent preparation and analysis was then the same for all Idaho and Wyoming samples. The total 83 samples are listed with analysis in appendix A4. The CRC formations for Wyoming are given on Figure 3 and the outcrop rock type is given for Idaho on Figure 4.

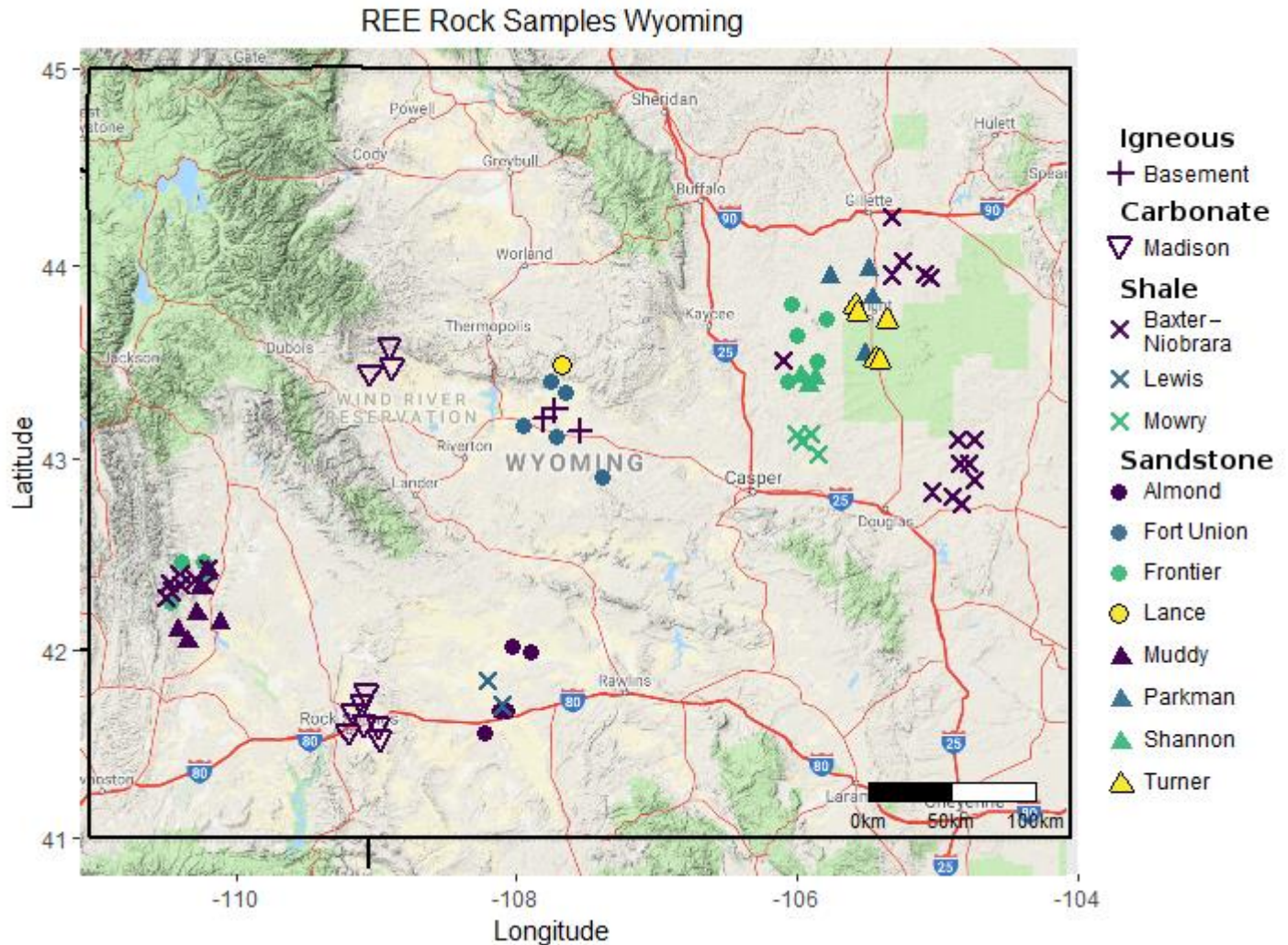


Figure 3: Location and formation of core collected at the USGS Core Research Center. Core is representative of the four basins where produced water samples were collected, and correlates to sampled intervals.

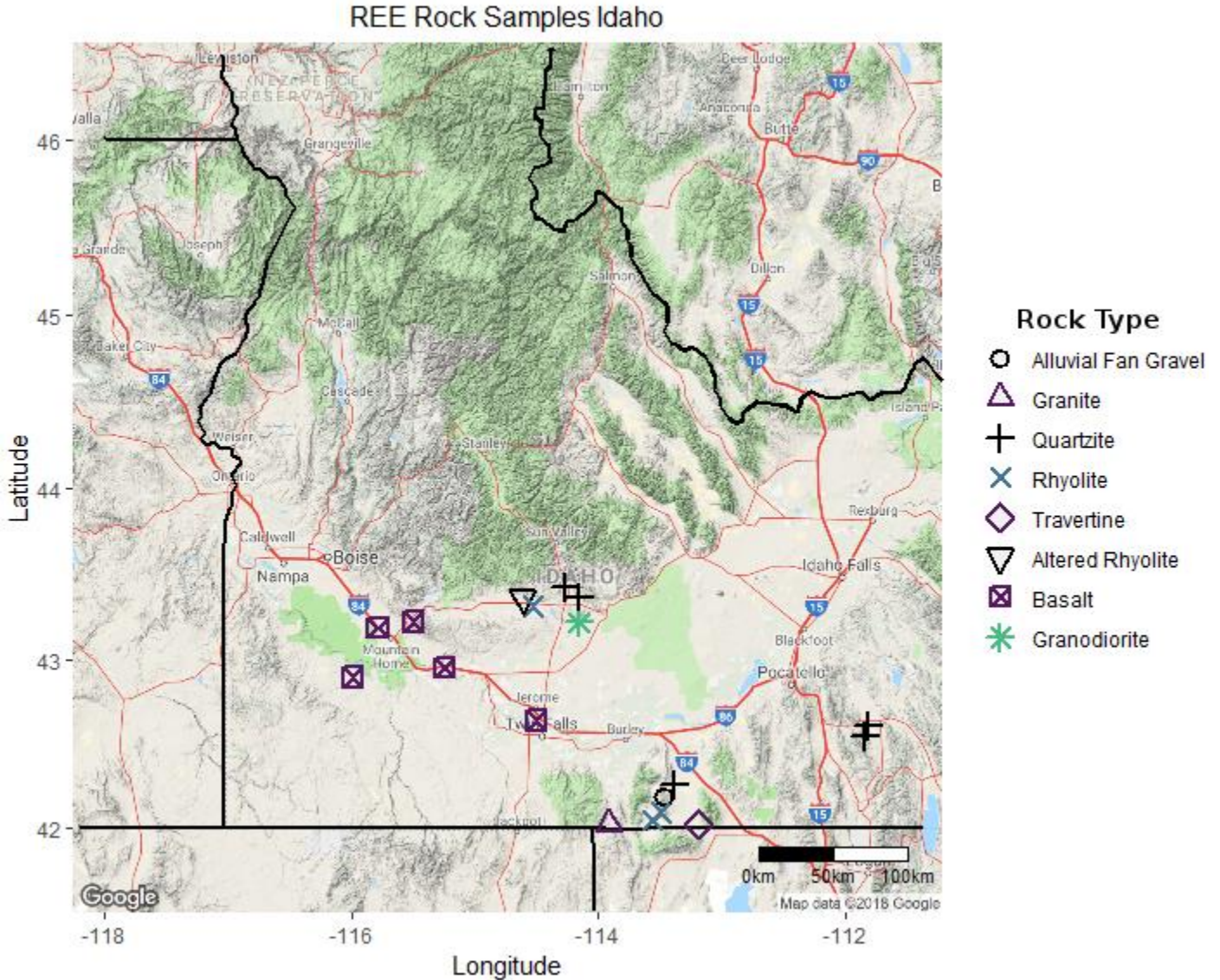


Figure 4: Sample locations and lithology of samples collected to represent geothermal water samples in Idaho. All collections in Idaho were from outcrop, and performed with consenting land owners.

4. CONCLUSION

This work contains the largest collection of aqueous REE data to date in the United States. The dataset shown in the appendices is distinctive for its consistent methodology. Similarly, the pairing of aqueous REE with their likely host rock formations provided a unique opportunity to study the nature of REE distributions in geothermal systems. Our extensive REE database was coupled with the general chemistry of geothermal waters through an ESOM, and resulted in a statistical inference of the likely REE contents in thousands of brines from several other basins.

The consistent methodology of McLing et al. (2014), and the rapid-sampling modifications of Nye et al. (2017), were performed by a common set of people who ensured sampling methodology was consistent. The use of the same instrumentation for each analysis further reduces the probability for systemic error to be introduced to the dataset. Other areas where this uniformity benefited include the HDPE (McLing et al., 2014) and LDPE (Nye et al., 2017) sample bottles, which were bought from the same vendor for the duration of the project. This uniformity has the added benefit of allowing each blank to raise the confidence in a greater number of samples.

By linking water REE data to the rock REE data, researchers in this project were able to study the exchange of aqueous REEs with reservoir rock. This project design was inspired by a previous cooperation between INL and UW at the Rock Springs Uplift RSU#1 well (Bentley and Surdam 2013), where core plugs and well water were studied together, resulting in conclusions neither half could have produced on its own.

The samples collected in this project were diverse and represent many significant lithologies for geothermal resources and produced waters. If future work collected water samples from hard, hot rock, such as basement systems, a full picture of geothermal resources and REE resources could be produced.

CONTRIBUTIONS AND ACKNOWLEDGMENTS

CN and GN drafted this chapter manuscript. CN compiled edits. SQ and TM conceived of the work presented in this chapter. Water samples presented in this chapter were collected by SQ, TM, CN, GN, Thomas Wood, Cody Canon, Wade Worthing, and USGS personnel including Mark Engle, Madalyn Blondes, Tanya Gallegos, Elisabeth Rowan, Colin Doolan, and Mathew Varonka. Rock samples presented in this chapter were collected by DB and FM. All authors reviewed the chapter manuscript. Contributors include: Tom Moore who prepared figures 2-4. Funding for this work was provided by U.S. Department of Energy, Geothermal Technologies Office under Award DE-EE0007603. The authors would like to thank our industry partners who allowed water sample collection, the landowners who allowed rock collection, our DOE project managers Holly Thomas and Josh Mengers and also our Technical Monitoring Team for their support, advice, and insight.

REFERENCES

Engle, M. A., Reyes, F. R., Varonka, M. S., Orem, W. H., Ma, L., Ianno, A. J., et al. (2016). Geochemistry of formation waters from the Wolfcamp and “Cline” shales: Insights into brine origin, reservoir connectivity, and fluid flow in the Permian Basin, USA. *Chemical Geology*, 425, 76–92. <http://doi.org/10.1016/j.chemgeo.2016.01.025>

Rowan, E. L., Engle, M. A., Kraemer, T. F., Schroeder, K. T., Hammack, R. W., & Doughten, M. W. (2015). Geochemical and isotopic evolution of water produced from Middle Devonian Marcellus shale gas wells, Appalachian basin, Pennsylvania. *AAPG Bulletin*, 99(02), 181–206. <http://doi.org/10.1306/07071413146>

Akob, D. M., Cozzarelli, I. M., Dunlap, D. S., Rowan, E. L., & Lorah, M. M. (2015). Organic and inorganic composition and microbiology of produced waters from Pennsylvania shale gas wells. *Applied Geochemistry*, 60, 116–125. <http://doi.org/10.1016/j.apgeochem.2015.04.011>

M. Blondes (USGS), unpublished data. (In submission 2019).

T. Gallegos (USGS), unpublished data. (In submission 2019).

Bentley, Ramsey D., Ronald C. Surdam (2013) *The Story of the Wyoming Carbon Underground Storage Project (WY-CUSP), and the Regional Inventory and Prioritization of Potential CO2 Storage Reservoirs in Wyoming* in *Geological CO2 Storage Characterization* ed: Surdam, Ronald C. Accessed from <https://link.springer.com/book/10.1007%2F978-1-4614-5788-6>

Earl D Mattson, Robert W Smith, Ghanashayam Neupane, Carl D Palmer, Yoshiko Fujita, Travis L McLing, David W Reed, DC Cooper, VS Thompson, 2015. Improved geothermometry through multivariate reaction-path modeling and evaluation of geomicrobiological influences on geochemical temperature indicators: Final Report, INL/EXT-14-33959, DOI: 10.2172/1177234, p. 227. [<https://inldigitallibrary.inl.gov/sites/sti/sti/6360447.pdf>]

Ghanashayam Neupane, Earl D Mattson, Nicolas Spycher, Patrick F Dobson, Mark E Conrad, Dennis L Newell, 2017. Geochemical Evaluation of the Geothermal Resources of Camas Prairie, Idaho. 42nd Workshop on Geothermal Reservoir Engineering Stanford University, Stanford, California, February 13-15, 2017.

Ghanashayam Neupane, Earl D. Mattson, Cody J. Cannon, Trevor A. Atkinson, Travis L. McLing, Thomas R. Wood, Wade C. Worthing, Patrick F. Dobson, Mark E. Conrad, 2016. Potential Hydrothermal Resource Areas and Their Reservoir Temperatures in the Eastern Snake River Plain, Idaho. PROCEEDINGS, 41st Workshop on Geothermal Reservoir Engineering Stanford University, Stanford, California, February 22-24, 2016 SGP-TR-209.

Ghanashayam Neupane, Earl D. Mattson, Cody J. Cannon, Trevor A. Atkinson, Travis L. McLing, Thomas R. Wood, Wade C. Worthing, Mark E. Conrad, 2016. Mixing Effects on Geothermometric Calculations of the Newdale Geothermal Area in the Eastern Snake River Plain, Idaho. PROCEEDINGS, 41st Workshop on Geothermal Reservoir Engineering Stanford University, Stanford, California, February 22-24, 2016 SGP-TR-209

Cody Cannon, Thomas Wood, Ghanashayam Neupane, Travis McLing, Earl Mattson, Patrick Dobson, Mark Conrad, 2014. Geochemistry Sampling for Traditional and Multicomponent Equilibrium Geothermometry in Southeast Idaho. *GRC Transactions* 38, 524-431.

Nye, C., Quillinan S., Neupane G., and McLing T. L. (2017) “Aqueous Rare Earth Element Patterns and Concentration in Thermal Brines Associated With Oil and Gas Production” PROCEEDINGS, 42nd Workshop on Geothermal Reservoir Engineering. Stanford University, Stanford, California, February 13-15, 2017. SGP-TR-212.

Roehler, Henry W. (1973) “Stratigraphy of the Washakie Formation in the Washakie Basin, Wyoming.” *USGS Bulletin* 1369. Accessed from: <https://doi.org/10.3133/b1369>

Keefer, William R. (1970) "Geology of the Wind River Basin, Central Wyoming" USGS Professional Paper 495-D. Accessed from: <https://doi.org/10.3133/pp495D>.

Stein, Jason (2008) "Analysis of Porosity Trends in the Kevin-Sunburst Dome Using 3D Seismic Reflection Data, Toole County, Montana" Masters Thesis. University of Arizona. Accessed from: <https://www.geo.arizona.edu/Antevs/Theses/SteinJason08.pdf>

Collier, Arthur J. (1929). "The Kevin-Sunburst Oil Field and Other Possibilities of Oil and Gas in the Sweetgrass Arch, Montana" In Contributions to economic geology, 1929, Part II, Mineral fuels. USGS Bulletin 812-B. Accessed from: <https://doi.org/10.3133/b812B>.

Chapter 3: Geologic and hydrogeologic characteristics of selected hydrocarbon-producing lithostratigraphic units within three Wyoming Laramide structural basins

Timothy T. Bartos and Laura L. Hallberg

U.S. Geological Survey Wyoming-Montana Water Science Center, 521 Progress Cir., Suite 6, Cheyenne, WY 82007

ttbartos@usgs.gov, lhallber@usgs.gov

Keywords: Geology, hydrogeology, reservoir, porosity, permeability, groundwater, aquifer, confining unit, groundwater quality

ABSTRACT

Hydrocarbons (gas and oil) are produced from deeply buried siliciclastic and carbonate reservoirs in numerous lithostratigraphic units found in the various Laramide structural basins of Wyoming. Lithostratigraphic units and associated reservoirs described herein are in select production fields located within the Greater Green River, Powder River, and Wind River structural basins. Production is from both conventional-style stratigraphic and (or) structural traps, as well as unconventional continuous accumulations. Many of these reservoirs are low-permeability “tight” sandstones. Pressures measured in the reservoirs can be normal (hydrostatic) or anomalous (under or overpressured). Reservoir fluids typically are multi-phase accumulations, consisting of oil, gas, and (or) groundwater in varying proportions. Many reservoirs are found within areas of basinwide cross-formational overpressure. Above the overpressured zone, pressures typically are normal or near-normal, and fluids largely consist of a single phase (groundwater). Groundwater in this shallower normally pressured zone is in hydrologic/hydraulic connection with local and regional groundwater-flow systems associated with meteoric groundwater circulation and may be hydraulically disconnected from the underlying overpressured areas/reservoirs by different types of low permeability/impermeable barriers. Aquifers used to provide water for most uses are located within the shallower normally pressured zone; waters from these aquifers are much fresher than waters from the underlying reservoirs/aquifers present at depths sufficient for petroleum generation and accumulation. Groundwater coproduced with the hydrocarbons varies widely in both quantity and quality with salinity ranging from brackish to saline, and sodium and chloride are almost always the predominant ions regardless of salinity.

1. INTRODUCTION

Hydrocarbons (gas and oil) are produced from deeply buried reservoirs in the various Laramide structural basins of Wyoming. This chapter briefly describes the geologic and hydrogeologic characteristics of some of these reservoirs and the lithostratigraphic units containing them. Reservoirs described herein were selected because they were sampled for rare-earth elements as part of this study. Results of this sampling are described in other parts of this project report. Lithostratigraphic units and associated reservoirs described herein are in various production fields located within the Greater Green River, Powder River, and Wind River structural basins. Groundwater-quality data presented herein were obtained from the U.S. Geological Survey Produced Waters Database (Blondes and others, 2017).

2. GREATER GREEN RIVER BASIN

2.1 Lewis Shale (Wamsutter field in the Greater Wamsutter arch development area)

The Upper Cretaceous Lewis Shale consists of marine shale with many interbedded lenticular sandstone beds deposited in nearshore marine environments (deltaic, shelf, ramp-slope, and deep marine basin) during the last major transgressive/regressive sequence of the Western Interior Seaway (Weimer, 1961; Gill and others, 1970; Winn and others, 1985, 1987; Van Horn and Shannon, 1989; Witton, 1999; Pyles, 2000, and references therein; Pyles and Slatt, 2000, 2002). Thickness of the formation ranges from 2,100- to 2,300-feet (ft) thick along the eastern Greater Green River Basin (GGRB; eastern GGRB defined herein consists of Great Divide and Washakie Basins and intervening Wamsutter arch) and decreases to the north and west (Hettinger and Roberts, 2005). The formation is overlain by and interfingers with the Fox Hills Sandstone and is underlain by the Almond Formation of the Mesaverde Group. Where divided, the formation consists of an upper unnamed part and a lower part known as the Dad Sandstone Member; both parts consist of varying amounts of fine-grained rocks (mudrocks/shale and siltstone) and beds of very fine- to medium-grained sandstone (Gill and others, 1970).

Lewis Shale hydrocarbons (oil and gas) are found in lenticular sandstone beds/reservoirs self-sourced from intraformation organic-rich mudrock (Law, 1996; Hettinger and Roberts, 2005). Hydrocarbon production consists primarily of gas from conventional-style stratigraphic and (or) structural traps in the shallower parts of the eastern GGRB, and where deeply buried, an unconventional, basin-centered gas system that also includes the underlying Almond Formation (Law, 1996; Law and others, 1989; Hettinger and Roberts, 2005). Most production is from Dad Sandstone Member reservoirs consisting of turbidite sandstones surrounded by and sealed by clay-rich mudrocks. These reservoir sandstones were described by Thyne and others (2003, p. 93) as consisting of “fine-to medium-grained, poorly to moderately sorted, angular to subangular grains of subarkose to arkosic arenite composition.” Dad Sandstone Member thickness is as much as 1,400 ft in the eastern Washakie Basin. Thickness of individual lenticular sandstone beds is as much as 100 ft, and sandstone beds may be stacked into units as much as 350-ft thick (Hettinger and Roberts, 2005). Cumulative sandstone thickness near Wamsutter field and the Greater Wamsutter arch development area (GWADA) is about 200 to 400 ft (Hettinger and Roberts, 2005, fig. 10).

For producing sandstones in the eastern GGRB, porosity ranges from 8 to 25 percent and permeability ranges from 0.01 to 50 millidarcies (mD) (Hettinger and Roberts, 2005). Thyne and others (2003) reported that Lewis Shale sandstone porosity and permeability varied over a wide range for individual wells and fields. The investigators concluded that these characteristics were not directly related to depth of burial, and that the principal factors that control reservoir quality include mechanical compaction, alteration of detrital components to clay, and the formation of secondary porosity.

Because the formation consists of thousands of feet of fine-grained marine shale, the Lewis Shale is defined as a confining unit (Lewis confining unit) throughout the eastern GGRB (Collentine and others, 1981; Freethey and Cordy, 1991), including Wamsutter field and the GWADA. Sandstone beds in the formation at depths much shallower than depths associated with hydrocarbon production have been considered to have some limited/local aquifer development potential (Collentine and others, 1981; Bartos and others, 2010). The Lewis confining unit separates the underlying Mesaverde aquifer from the overlying Lance-Fox Hills aquifer composed of the water-saturated and permeable parts of the Lance Formation and Fox Hill Sandstone; collectively, all three of these hydrogeologic units compose the Mesaverde aquifer system (Freethey and Cordy, 1991). The Lewis Shale also serves as a hydrocarbon seal preventing upward vertical migration of gas from the underlying Almond Formation (Johnson and others, 2005). Where the Lewis Shale/confining unit is absent, the Mesaverde aquifer may be in direct hydraulic connection with the Lance-Fox Hills aquifer.

Total dissolved solids (TDS) concentrations in Lewis Shale produced-water samples from the Wamsutter field ranged from 1,633 to 20,377 milligrams per liter (mg/L), with a median of 12,650 mg/L [(number of samples (N)=10)] (Blondes and others, 2017). Waters were brackish (TDS=1,000 to 10,000 mg/L; definition of brackish water TDS range from National Groundwater Association, 2018) and saline (TDS>10,000 mg/L). Almost all waters were sodium-chloride type. Sample-collection depths ranged from about 7,400 to 9,800 ft below land surface (bls). Bartos and others (2010) characterized Lewis Shale groundwater quality for the entire eastern GGRB using 56 produced-water samples. TDS concentrations ranged from 720 to 54,600 mg/L, indicating a larger/more variable TDS range than in the Wamsutter field samples, and the median TDS concentration (9,200 mg/L) was lower.

2.2 Almond Formation of the Mesaverde Group (Wamsutter field in Greater Wamsutter arch development area)

The Upper Cretaceous Almond Formation is the uppermost formation of the Mesaverde Group in the eastern GGRB, including the Wamsutter field in the GWADA (Gill and others, 1970; Roehler, 1990). The 250- to 500-ft thick formation was deposited in fluvial, shallow/marginal marine, and coastal plain environments during early Maastrichtian transgression of the Western Interior Seaway (Roehler, 1990; Finn and others, 2005). Two informal intervals are recognized in the Almond Formation in the eastern GGRB by many investigators—(1) an upper interval (“upper Almond”) composed of laterally extensive marginal marine very fine- to fine-grained sandstone interbedded with tongues of the marine Lewis Shale, and (2) a lower or main interval (“main Almond”) composed of lenticular, very fine- to fine-grained sandstone, nonmarine shale and mudstone, and coal (Weimer, 1965; Gill and others, 1970; Martinsen and others, 1995; Sturm and others, 2001; Tobin and others, 2010).

Parts of the Mesaverde Group, including the Almond Formation, contain hydrocarbons (oil and gas) in sandstone and coal reservoirs self-sourced from various intraformation coals and carbonaceous shales (Garcia-Gonzales and others, 1993; Finn and others, 2005; Tobin and others, 2010). Mesaverde Group hydrocarbon production is from conventional-style stratigraphic and (or) structural traps, and a basin-centered gas system (Finn and others, 2005). Within the Almond Formation, most produced hydrocarbons have been gas and gas liquids from reservoirs consisting of laterally continuous marginal marine bar sandstones in the upper Almond. Because of low sandstone reservoir porosity and permeability and the presence of clay minerals in pore space, the deeply buried Almond Formation from which gas is produced in the eastern GGRB, including the Wamsutter field in the GWADA, commonly is described broadly as a “tight-gas sandstone;” however, this description presently cannot be applied universally to Almond Formation sandstones in the GWADA because upper Almond sandstone permeability and porosity are not uniformly low (Nelson and others, 2010). These deeply buried Almond Formation tight-gas sandstones from which gas is produced are immature, very fine- to fine-grained, moderately well to well-sorted sublitharenites and litharenites that have experienced substantial diagenetic alteration (Tobin and others, 2010). Almond Formation sandstone permeability in the GWADA and parts of the Great Divide Basin decreases with increasing present-day burial depth (Keighin and others, 1989). Both porosity and permeability generally are greater in the upper than in the main Almond Formation. Porosity of the Almond Formation in the Washakie Basin area was reported by Martinsen (1998) to range from 10 to 20 percent and most permeabilities to range from 0.1 to 20 mD in the upper Almond Formation; main body Almond Formation porosity ranged from 1 to 15 percent, and permeabilities generally were less than 1 mD. Tobin and others (2010) noted that measured Almond Formation sandstone porosities in the GWADA generally are less than 12 percent, and measured permeabilities generally are less than 0.1 mD.

Deeply buried parts of the Mesaverde Group from which gas is produced, including the Almond Formation, are part of an abnormally pressured (overpressured) basin-centered gas system present throughout much of the eastern GGRB, including the Wamsutter field in the GWADA (McPeck, 1981; Law, 1984, 2002; Law and Dickinson, 1985; Surdam and others, 2005; Martinsen and Christensen, 1992; Finn and others, 2005). This basin-centered gas system crosses lithostratigraphic units, and parts of many different deeply buried Upper Cretaceous and Neogene units within the system (for example, Law, 2002, fig. 6). Depth of the overpressured part of the GWADA [Township (T.) 18 North (N.) to T. 23 N. and Range (R.) 88 West (W.) to R. 112 W.] occurs below a depth of about 7,800 ft bls (Forster and Horne, 2005). Water production was minimal/low from drill-stem tests conducted below this depth (Forster and Horne, 2005).

In addition to gas, some oil or condensate is produced from all wells and no dry gas is produced (Nelson and others, 2010). Most GWADA Almond Formation wells produce from 1 to 10 barrels of water per day, and water production does not vary much among the different fields within the GWADA (Nelson and others, 2010). Water-gas ratios in the GWADA are lowest in areas with the highest rates of gas production and are greatest in areas with the lowest rates of gas production (Nelson and others, 2010). Mapping of expected water-gas ratios for different depths by Nelson and others (2010) indicated that the water-gas ratio from the upper Almond and combined upper and

main Almond typically is less than 3 barrels of water per million cubic feet of gas (bbl/mmcf) in many wells within the GWADA; this led the investigators to conclude that a fraction (up to one-half) of the produced water is water of condensation. Conversely, the investigators noted that water-gas ratios from the main Almond generally were greater than 3 bbl/mmcf and concluded that water of condensation could only be a small fraction of total produced water with most of it being free, mobile water. Water production rates decrease with time in most wells, but production rates increase with time in about one-fourth of wells in the central part of the GWADA (Nelson and others, 2010). Changes (increases or decreases) in water production over a five-year period were independent of the rate of gas production (Nelson and others, 2010). The water-saturated and permeable parts of the entire Mesaverde Group, including the Almond Formation, compose an aquifer (Mesaverde aquifer) throughout the GGRB, including the GWADA (Collentine and others, 1981; Freethey and Cordy, 1991). The Mesaverde aquifer is the lowermost of three hydrogeologic units composing a thick, regionally extensive aquifer system identified as the Mesaverde aquifer system (Freethey and Cordy, 1991). Overlying the Mesaverde aquifer are the two other units of the aquifer system—the Lewis confining unit, consisting of the Lewis Shale, and the Lance-Fox Hills aquifer consisting of the water-saturated and permeable parts of the Lance Formation and Fox Hills Sandstone. On a regional scale, the Mesaverde aquifer and aquifer system is confined from above by the Lewis confining unit and below by the Baxter-Mowry confining unit composed of several underlying Upper and Lower Cretaceous lithostratigraphic units (Cody/Steele Shales to Thermopolis Shale). The Lewis Shale also serves as a seal preventing upward vertical migration of gas from the underlying Almond Formation (Finn and others, 2005). Where the Lewis Shale/confining unit is absent, the Mesaverde aquifer may be in direct hydraulic connection with the Lance-Fox Hills aquifer.

Individual water-saturated and permeable sandstone and coal beds in the various formations (including Almond Formation) collectively form the Mesaverde aquifer (and Mesaverde aquifer system) in the eastern GGRB (Welder and McGreevy, 1966; Fisk, 1967; Collentine and others, 1981; Freethey and Cordy, 1991). The sandstone beds also contain oil and gas in many parts of the GGRB where buried at depths sufficient for hydrocarbon generation and accumulation (Finn and others, 2005). Fine-grained rocks (typically shale) throughout these formations laterally and vertically confine and seal these water- and hydrocarbon-bearing aquifers/reservoirs to varying degrees, resulting in differing amounts of hydraulic connection/compartimentalization (Fisk, 1967; Collentine and others, 1981; Freethey and Cordy, 1991; Heasler and Surdam, 1992). Upper Almond Formation marine bar sandstones have been compartmentalized by faulting in parts of the Washakie Basin (Martinsen, 1998). Because of deep burial below younger rocks (generally 2,000 to more than 12,000 ft bls) in most areas (Freethey and Cordy, 1991), the Mesaverde aquifer/aquifer system is rarely utilized as a source of water in most parts of the GGRB, including the eastern GGRB/GWADA (Fisk, 1967; Collentine and others, 1981; Bartos and others, 2010). Few wells are completed in the Mesaverde aquifer and aquifer system in the eastern GGRB, and development generally is limited to areas where the Mesaverde aquifer is exposed along uplifts such as the Rock Springs Uplift and adjacent areas where buried at shallow economical drilling depths thousands of feet above hydrocarbon-bearing zones, and where waters are sufficiently fresh for intended uses (Fisk, 1967; Collentine and others, 1981; Freethey and others, 1988; Bartos and others, 2010; Bartos and Hallberg, 2010). These aquifer outcrop areas along uplifted areas such as the Rock Springs uplift also are interpreted as the source of much of the recharge to the Mesaverde aquifer (Collentine and others, 1981; Freethey and Cordy, 1991), although the small outcrop extent likely provides limited opportunities for substantial volumes of recharge (Freethey and Cordy, 1991). Where buried, recharge from adjacent underlying and overlying lithostratigraphic/hydrogeologic units (cross-stratigraphic flow) is likely limited because of numerous intervening fine-grained confining layers/units.

Fluids in the deeply buried, regionally overpressured sandstone aquifers/reservoirs of the Mesaverde Group (various lithostratigraphic units, including the Almond Formation) in the eastern GGRB (including Wamsutter field and other fields in the GWADA) from which hydrocarbons (primarily gas) are produced are not likely in hydrologic connection with the overlying shallower hydro pressured (primarily normally pressured) parts of these and other units. Normally pressured areas in the upper shallow parts of sedimentary basins typically are in hydrologic connection with regional groundwater-flow systems associated with meteoric groundwater circulation [and predominantly, single-phase (groundwater) flow], and these areas can be hydrologically disconnected from regionally overpressured areas/reservoirs to varying degrees by some low-permeability/impermeable barriers such as lithologic/facies changes (commonly pinch-outs), diagenetically altered areas, faults, water-block (capillary) trap/seal (seal developed by up-dip expulsion of water from low-permeability overpressured system) or some combination of these and other potential contributing factors (Masters, 1979; Law, 1984, 2002, and references therein; Kreidler, 1989; Hunt, 1990; Heasler and Surdam, 1992; Scott and Kaiser, 1994; Surdam, 1997; Surdam and others, 2005). Overpressure can be caused by a variety of mechanisms (for example, Law and Dickinson, 1985; Hunt, 1990; Law, 2002, and references therein). Most investigators attribute overpressure associated with the basin-centered gas accumulations in the eastern GGRB within Upper Cretaceous and Neogene units to thermal gas generation at a rate that exceeds the rate at which gas can escape from low-permeability tight-gas reservoirs, resulting in a gas-saturated/gas-charged overpressured area (Surdam and others, 1995; Law, 2002, and references therein; Surdam and others, 2005). This prevents groundwater from reentering the overpressured zone because the resulting pore pressure is greater than the regional hydrostatic pressure (Law and Dickinson, 1985; Law and others, 1989). However, this interpretation, including the presence of a regional gas saturation outside conventional traps in the eastern GGRB, has been challenged recently by other investigators (for example, Shanley, 2004; Bartberger and Pasternack, 2015).

Several studies have described the presence and characteristics of these two “pressure regimes” in the eastern GGRB. The top of the eastern GGRB hydrocarbon overpressure zone was interpreted by Scott and Kaiser (1994) to be a “no-flow” boundary between the hydro pressured and overpressured zones in the Washakie and Sand Wash Basins. The investigators (Scott and Kaiser, 1994, p. 74) concluded that groundwater in Cretaceous and younger Neogene strata enters aquifers (including Mesaverde aquifer) from recharge areas along bordering uplifts, flows basinward to some depth in response to hydraulic/topographic gradients and structural depth, and then turns upward “upon convergence from the basin margins, aquifer pinch-out, encountering the top of overpressure, or combination of these” mechanisms. Scott and Kaiser (1994) indicated that the transition between hydro pressure and overpressure in the Sand Wash Basin was often abrupt, and that the hydro pressured zone was variable, consisting of underpressure, normal pressure, and overpressure zones/compartments, conclusions similar to that described for Mesaverde Group reservoirs in the Washakie Basin by Heasler and Surdam

(1992). Scott and Kaiser (1994) also noted that no pressure regimes in the hydro pressured zone were regionally dominant, although they noted vertical pressure gradients indicated slight underpressure to normal pressure. Heasler and Surdam (1992) concluded the Mesaverde Group reservoirs in the Washakie Basin characterized by anomalously high or low pressures were areas of pressure compartmentalization similar to those conceptually described by Hunt (1990). Subsequently, similar conclusions were reached by Surdam and others (2005) in their examination of the Almond Formation in part of the Washakie Basin. The investigators (Surdam and others, 2005, p. 65) noted the entire deeply buried Almond Formation in the area examined was within a “gas-charged domain where the rock/fluid system contains a ubiquitous gas phase dominated by capillarity” coinciding with a “regional anomalously pressured depletion-drive, multi-phase fluid-flow system” that was overlain by a “water-rich, predominantly single-phase fluid-flow system under water-drive.”

Bartos and others (2010) characterized the quality of groundwater sampled from springs issuing from or wells completed in the Mesaverde aquifer (all lithostratigraphic units) in the eastern GGRB where utilized as a source of water supply for various uses not associated with hydrocarbon exploration and development (defined hereinafter as “environmental water samples”). TDS concentrations ranged from 477 to 2,300 mg/L, with a median of 985 mg/L (N= 18). Slightly more than one-half (56 percent) of the environmental water samples were fresh (TDS<1,000 mg/L) whereas the remaining samples were brackish (TDS=1,000 to 10,000 mg/L). The investigators also characterized the quality of groundwater collected exclusively from wells completed at shallow depths in the Almond Formation in the eastern GGRB. Environmental water samples indicated TDS concentrations ranged from 337 to 1,090 mg/L, with a median of 483 mg/L (N=7). Most environmental waters were fresh (TDS<1,000 mg/L), and the remaining waters were slightly brackish (TDS=1,000 to 10,000 mg/L). Trilinear diagrams constructed using environmental water samples from both the Mesaverde aquifer and the Almond Formation indicated ionic composition varied with salinity (Bartos and others, 2010).

Groundwater quality in the deeply buried overpressured parts of the Almond Formation in the Wamsutter field associated with hydrocarbon production is substantially different than the overlying shallower and fresher parts associated with the Mesaverde aquifer/aquifer system described above using environmental water samples. TDS concentrations in the Wamsutter field produced-water samples ranged from 1,447 to 66,462 mg/L, with a median of 12,188 mg/L (N= 67). Waters were brackish (TDS=1,000 to 10,000 mg/L) and saline TDS>10,000 mg/L). Almost all waters were sodium-chloride type. Sample-collection depths ranged from about 8,800 to 11,000 ft bls, Bartos and others (2010) characterized Almond Formation groundwater quality for the entire eastern GGRB using 269 produced-water samples. TDS concentrations ranged from 115 to 95,300 mg/L, indicating a larger/more variable TDS range than in the Wamsutter field samples, and the median TDS (9,600 mg/L) was lower.

2.3 Baxter/Hilliard Shale (Hogsback field in northern Moxa arch/La Barge platform area)

The Baxter and Hilliard Shales are names applied to a thick sequence of nearshore to offshore marine sediments (primarily marine shale) deposited during the Late Cretaceous (Finn and Johnson, 2005a, b, and references therein). The two lithostratigraphic units are considered equivalent and use of “Hilliard” or “Baxter” depends upon the location examined and (or) study, as use of the names for specific parts of the GGRB is not consistent among the geologic literature (consequently, “Baxter/Hilliard Shale” will be used hereinafter). In the northern Moxa arch/La Barge platform area, the formation is overlain by the Adaville Formation and underlain by the Frontier Formation (Love and others, 1993).

Although consisting largely of shale, interbedded lenticular discontinuous sandstone beds deposited in marine nearshore, shelf, slope, and deep basin-floor environments are present throughout the Baxter/Hilliard Shale (Roehler, 1990); however, total (net) sandstone thickness (hundreds of feet) is small compared to the total thickness of the remainder of the formation composed primarily of shale (thousands of feet) (Finn and Johnson, 2005a, b, and references therein). Hydrocarbons, primarily gas, are produced from these sandstone beds/reservoirs from conventional-style stratigraphic and (or) structural traps in the shallower less thermally mature parts of the western GGRB, and from an unconventional, gas-saturated basin-centered continuous gas system where deeply buried and more thermally mature (Law, 1996; Law and others, 1989; Finn and Johnson, 2005a, b, and references therein). Size of the sandstone reservoirs ranges from “single sandstone bodies covering many square miles, with thicknesses ranging to 100 ft or more, to thin interbeds of sandstone and siltstone in thick mudstone and shale intervals” (Finn and Johnson, 2005a, b). Seals for the sandstone reservoirs typically are clay-rich mudrocks, and less commonly faults, whereas the continuous gas accumulations likely are sealed by a capillary seal/water block (Finn and Johnson, 2005a, b, and references therein). For depths ranging from 3,500 to 6,000 ft, the porosity of Baxter Shale reservoir sandstones in the GGRB likely averages 15 percent, and permeability ranges from 0.01 to 70 mD with a most likely permeability of 1 mD. (Buursink and others, 2014).

The Baxter/Hilliard Shale and equivalents are part of a large regional confining unit composed of numerous lithostratigraphic units throughout the GGRB. Identified by Freethey and Cordy (1991) as the Mancos confining unit and renamed by Bartos and Hallberg (2010) as the Baxter-Mowry confining unit to reflect Wyoming stratigraphic nomenclature, the unit hydraulically separates the overlying Mesaverde aquifer from the underlying Dakota/Cloverly aquifer. In the northwestern GGRB, including the Moxa arch/La Barge area, the Baxter-Mowry confining unit consists of, in descending (youngest to oldest) order, (1) the Baxter Shale and equivalent Hilliard Shale; (2) Frontier Formation; (3) Mowry Shale and equivalent/correlative Aspen Shale; (4) the Muddy Sandstone; and (5) Thermopolis Shale and stratigraphic equivalents (Bear River Formation and Dakota Sandstone) (Freethey and Cordy, 1991). The Baxter-Mowry confining unit consists largely of thousands of feet of predominantly fine-grained rocks such as marine shale, but interbedded sandstones in the Baxter/Hilliard Shale and other lithostratigraphic units within the larger confining unit can contain discontinuous (local) aquifers (Ahern and others, 1981; Collentine and others, 1981; Freethey and Cordy, 1991) in addition to hydrocarbon reservoirs (Kirschbaum and Roberts, 2005a, b). The discontinuous (local) aquifers in the Baxter/Hilliard Shale, consisting of water-saturated and permeable sandstone beds, are rarely utilized in the western GGRB because of deep burial and poor groundwater quality in most areas (Ahern and others, 1981; Bartos and Hallberg, 2010; Bartos and others, 2010).

The TDS concentration in one Baxter/Hilliard Shale produced-water sample from Hogsback field in the Moxa arch/La Barge platform area was 23,296 mg/L, indicating the water was saline (TDS>10,000 mg/L) (Blondes and others, 2017). The water was sodium-chloride type. Bartos and others (2010) characterized Baxter Shale groundwater quality for the entire western GGRB using produced-water samples. TDS concentrations ranged from 660 to 23,300 mg/L, with a median of 16,300 mg/L, and most waters were brackish and saline (N=6).

2.4 Frontier Formation (Tip Top, Hogsback, and LaBarge fields in northern Moxa arch/La Barge platform area)

The Upper Cretaceous Frontier Formation along the Moxa arch consists of marine (offshore and nearshore) and nonmarine fine-grained rocks (shale and siltstone) and sandstone (Winn and Smithwick, 1980; Merewether, 1983; Merewether and others, 1984; Stonecipher and others, 1984; Winn and others, 1984; Stonecipher and Diedrich, 1993). Four informal intervals, known as the first through fourth Frontier, are recognized in the Frontier Formation in the western GGRB (DeChadenedes, 1975; McDonald, 1976; Merewether and others, 1984; Stands, 1999; Kirschbaum and Roberts, 2005a, b). The first Frontier is a tongue encased from above and below by fine-grained offshore marine deposits within the lower Hilliard Shale (Merewether and others, 1984; Ryer and others, 1987; Stands, 1999; Kirschbaum and Roberts, 2005a, fig. 2). The second Frontier is overlain by the Hilliard Shale and underlain by the third and fourth Frontier or Mowry Shale; the third and fourth Frontier are underlain by the Mowry Shale (Merewether and others, 1984; Ryer and others, 1987; Stands, 1999; Kirschbaum and Roberts, 2005a, fig. 2). The second Frontier (considered equivalent to the Dry Hollow Member of the Frontier Formation in parts of the western GGRB and Overthrust Belt area) is subdivided into five “benches” (in descending order, benches 1–5), all included in the northern Moxa arch/LaBarge area (Kirschbaum and Roberts, 2005a, fig. 2). In the northern Moxa arch/LaBarge area, sandstone beds in the second Frontier (including all 5 benches) contain the primary reservoirs from which hydrocarbons (primarily gas from tight sandstones) are produced (“Moxa arch column” shown in fig. 2 of Kirschbaum and Roberts, 2005a).

Sandstone beds comprising hydrocarbon reservoirs of the Frontier Formation were deposited in fluvial, estuarine, and shoreface/deltaic environments (DeChadenedes, 1975; McDonald, 1976; Merewether and others, 1984; Stands, 1999; Kirschbaum and Roberts, 2005a, b). Most reservoir sandstones are sublitharenites and litharenites, with minor amounts of feldspathic litharenites and lithic arkoses present (Dutton and others, 1992). Buursink and others (2014) indicated the “most likely” porosities for GGRB Frontier Formation sandstones at depths between 3,000 to 13,000 ft bls range from 12 to 18 percent, with a most likely porosity of 15 percent. Porosity of Frontier Formation sandstones (fluvial, shoreface, and tidal) in the Moxa arch area range from an average of about 7 to 11 percent (Winn and others, 1984; Stonecipher and Diedrich, 1993). Maximum permeability of Frontier Formation sandstones (fluvial, shoreface, and tidal in the second Frontier) in the Moxa arch area ranges from less than 0.1 to about 39 mD, and average permeability ranges from 0.1 to about 6 mD; tidal sandstones are more permeable than fluvial sandstones (Stonecipher and Diedrich, 1993).

The Frontier Formation is part of a large regional confining unit composed of numerous lithostratigraphic units throughout the GGRB. Identified by Freethey and Cordy (1991) as the Mancos confining unit and renamed by Bartos and Hallberg (2010) as the Baxter-Mowry confining unit to reflect Wyoming stratigraphic nomenclature, the unit separates the overlying Mesaverde aquifer from the underlying Cloverly aquifer. In the northwestern GGRB, including the Moxa arch/La Barge area, the Baxter-Mowry confining unit consists of, in descending (youngest to oldest) order, the Baxter Shale and equivalent Hilliard Shale, Frontier Formation, Mowry Shale and equivalent/correlative Aspen Shale, and the Muddy Sandstone and Thermopolis Shale and equivalents (Bear River Formation and Dakota Sandstone) (Freethey and Cordy, 1991). The Baxter-Mowry confining unit consists largely of thousands of feet of predominantly fine-grained rocks such as marine shale, but interbedded sandstones in the Frontier Formation and other lithostratigraphic units within the larger confining unit can contain aquifers (Ahern and others, 1981; Collentine and others, 1981; Freethey and Cordy, 1991) and (or) hydrocarbon reservoirs (Kirschbaum and Roberts, 2005a, b). The interbedded Frontier Formation sandstone beds, where water-saturated and permeable, collectively compose a rarely utilized aquifer in the western GGRB and adjacent Overthrust Belt (Frontier aquifer; Ahern and others, 1981). Permeability of the sandstones composing the Frontier aquifer is intergranular except where fractured, and permeability corresponds largely to the degree of sandstone cementation (Ahern and others, 1981).

Excluding wells used to produce hydrocarbons in the deeply buried part of the formation, most wells are located along the eastern and western flanks of the eastern GGRB where the Frontier Formation crops out or is buried at shallow depths (Collentine and others, 1981; Bartos and Hallberg, 2010). Recharge to the aquifer has been speculated to occur in the various uplifts surrounding the eastern GGRB where the formation crops out, with regional groundwater flow from these recharge areas toward the centers of the Great Divide and Washakie Basins (Collentine and others, 1981).

TDS concentrations in Frontier Formation produced-water samples from Tip Top field in the Moxa arch/La Barge platform area ranged from 2,879 to 34,788 mg/L, with a median of 17,255 mg/L (N= 7) (Blondes and others, 2017). Waters were brackish (TDS=1,000 to 10,000 mg/L) and saline (TDS>10,000 mg/L). All waters were sodium-chloride type. Sample-collection depths ranged from about 6,000 to 7,700 ft bls.

TDS concentrations in Frontier Formation produced-water samples from Hogsback field in the Moxa arch/La Barge platform area ranged from 1,138 to 65,920 mg/L, with a median of 7,534 mg/L (N=12) (Blondes and others, 2017). Waters were brackish (TDS=1,000 to 10,000 mg/L) and saline (TDS>10,000 mg/L). All waters were sodium-chloride type. Sample-collection depths ranged from about 5,300 to 8,400 ft bls.

TDS concentrations in produced-water samples from La Barge field in the Moxa arch/La Barge platform area ranged from 1,061 to 66,500 mg/L, with a median of 12,324 mg/L (N=26) (Blondes and others, 2017). Waters were brackish (TDS=1,000 to 10,000 mg/L) and saline (TDS>10,000 mg/L). Almost all waters were sodium-chloride type. Sample-collection depths ranged from about 4,700 to 7,500 ft bls.

2.5 “Muddy Sandstone” (Hogsback field in northern Moxa arch/La Barge platform area)

Hydrocarbons produced from Lower Cretaceous reservoirs in the western GGRB that includes the northern Moxa arch/LaBarge platform area are in continental and shoreface/deltaic strata located below offshore marine strata (primarily shale) assigned to one or more lithostratigraphic units, depending on location (Mowry Shale or equivalent Aspen Shale, or Shell Creek Shale, where present) (Kirschbaum and Roberts, 2005a, b). Lithostratigraphic nomenclature assigned to continental and shoreface strata containing these hydrocarbon reservoirs is inconsistent among studies. Inconsistencies are due primarily to differences between lithostratigraphic units named from outcrop studies and subsurface equivalent names (generally informal) typically associated with hydrocarbon exploration and development. Further complicating matters are difficulties in correlation of Lower Cretaceous strata deposited during complicated transgressive-regressive sequences over large distances using primarily subsurface data; substantial facies changes occur in Lower Cretaceous strata over these large distances (Ryer and others, 1987; Kirschbaum and Roberts, 2005a, b). For example, the “Muddy Sandstone” is not a formally recognized lithostratigraphic unit in the northern and western GGRB, including the entire length of the Moxa arch (Love and others, 1993; Wyoming Geological Association, 2014). Hydrocarbon-producing sandstone reservoirs assigned to the “Muddy Sandstone” and the underlying offshore marine shale commonly assigned to the Thermopolis Shale are likely part of/wholly or partially correlative to part of the Bear River Formation (Ryer and others, 1987; Kirschbaum and Roberts, 2005a, b). The Bear River Formation is the formally recognized lithostratigraphic unit in the northern and western GGRB and immediately adjacent Overthrust Belt that contains strata equivalent in age to the “Muddy Sandstone” and the Thermopolis Shale (Love and others, 1993, column O; Wyoming Geological Association, 2014). Along the Moxa arch, strata equivalent to the Bear River Formation (as well as the “Muddy Sandstone” and Thermopolis Shale) have been given an informal subsurface equivalent name (Dakota Sandstone) that is widely utilized for hydrocarbon exploration and development in the area (Ryer and others, 1987; Kirschbaum and Roberts, 2005a, b; Lehrer, 2006). However, usage of the subsurface “Muddy Sandstone” and “Thermopolis Shale” is retained in addition to use of the “Dakota Sandstone” along parts of the Moxa arch (Kirschbaum and Roberts, 2005a, b). Because of these complexities, characteristics of these Lower Cretaceous hydrocarbon-bearing sandstone reservoirs below the Mowry Shale assigned to the various formally and informally recognized units commonly are grouped together for descriptive purposes (for example, “Dakota and Muddy Sandstone and equivalents” utilized by Kirschbaum and Roberts, 2005a, b). Hydrocarbons are produced from the Lower Cretaceous Muddy/Dakota/Bear River (hereinafter identified as “Muddy Sandstone and equivalents”) reservoirs along the Moxa arch. The formations containing these reservoirs consist of marine (offshore and nearshore) and continental (nonmarine) fine-grained rocks (shale and siltstone) and sandstone (Ryer and others, 1987). The Aspen and Mowry Shales form the top seal(s) for hydrocarbon accumulations in these units (Kirschbaum and Roberts, 2005a, b). Gas from conventional and/or unconventional accumulations is the primary hydrocarbon produced from these sandstone reservoirs in the northern Moxa arch/LaBarge platform area (Kirschbaum and Roberts, 2005a). Most sandstones composing these reservoirs are classified as sublitharenites, with fewer classified as quartz. arenites, subarkoses, and litharenites (Muller and Coalson, 1989). Porosity of these reservoir sandstones ranges from 8–23 percent, and permeability ranges from 0.06–750 mD (Cardinal and Stewart, 1979; Miller and others, 1992).

The Muddy Sandstone and equivalents are part of a large regional confining unit composed of numerous lithostratigraphic units throughout the GGRB. Identified by Freethey and Cordy (1991) as the Mancos confining unit and renamed by Bartos and Hallberg (2010) as the Baxter-Mowry confining unit to reflect Wyoming stratigraphic nomenclature, the unit hydraulically separates the overlying Mesaverde aquifer from the underlying Dakota/Cloverly aquifer. In the northwestern GGRB, including the Moxa arch/La Barge area, the Baxter-Mowry confining unit consists of, in descending (youngest to oldest) order, the Baxter Shale and equivalent Hilliard Shale, Frontier Formation, Mowry Shale and equivalent/correlative Aspen Shale, and the Muddy Sandstone and Thermopolis Shale and stratigraphic equivalents (Bear River Formation and Dakota Sandstone) (Freethey and Cordy, 1991). The Baxter-Mowry confining unit consists largely of thousands of feet of predominantly fine-grained rocks such as marine shale, but interbedded sandstones in the Muddy Sandstone and other lithostratigraphic units within the larger confining unit can contain discontinuous aquifers (Ahern and others, 1981; Collentine and others, 1981; Freethey and Cordy, 1991) and (or) hydrocarbon reservoirs (Kirschbaum and Roberts, 2005a, b). Sandstone beds in the Muddy Sandstone and equivalents (parts of the Bear River Formation and Dakota Sandstone), where water-saturated and permeable, collectively compose rarely utilized aquifers in the western GGRB and adjacent Overthrust Belt named after their respective lithostratigraphic units (for example, Muddy aquifer for the Muddy Sandstone; Ahern and others, 1981; Bartos and Hallberg, 2010). These aquifers are rarely utilized in the western GGRB because of deep burial and poor groundwater quality in most areas except near outcrop areas where waters likely are fresher, and wells can be completed at economical drilling depths (Ahern and others, 1981; Bartos and Hallberg, 2010; Bartos and others, 2010).

TDS concentrations in Muddy Sandstone produced-water samples from Hogsback field in the Moxa arch/La Barge platform area ranged from 3,994 to 64,366 mg/L, with a median of 8,169 mg/L (N=7) (Blondes and others, 2017). Waters were brackish (TDS=1,000 to 10,000 mg/L) and saline (TDS>10,000 mg/L). Almost all waters were sodium-chloride type. Sample-collection depths ranged from about 7,800 to 9,000 ft bls.

TDS concentrations in Muddy Sandstone produced-water samples from La Barge field in the Moxa arch/La Barge platform area ranged from 8,343 to 21,105 mg/L, with a median of 15,829 mg/L (N=6) (Blondes and others, 2017). Waters were brackish (TDS=1,000 to 10,000 mg/L) and saline (TDS>10,000 mg/L). All waters were sodium-chloride type. Sample-collection depths ranged from about 7,600 to 8,000 ft bls.

2.6 Madison Limestone (Tip Top field in northern Moxa arch/La Barge platform area)

The Mississippian Madison Limestone in the western GGRB, including the northern Moxa arch/La Barge platform area, consists of varying proportions of dolomite and limestone (Geldon, 2003a, b; Sonnenfeld, 1996; Thyne and others, 2010; Kaszuba and others, 2011). The lithostratigraphic unit has been affected by fracturing, brecciation, stylolitization, karstification, and dolomitization in the area (Sonnenfeld, 1996; Thyne and others, 2010; Becker and Lynds, 2012). Substantial quantities of various gases, including methane, carbon

dioxide, hydrogen sulfide, and helium are present in the Madison Limestone in the northern Moxa arch/La Barge platform area, and the formation is considered the most productive gas reservoir in the western GGRB (Huang and others, 2007; Smith and others, 2010; Becker, and Lynds, 2012).

Subsurface Madison Limestone porosity and permeability in the northern Moxa arch/La Barge platform area was studied extensively by Thyne and others (2010). Both characteristics varied substantially, both laterally and vertically. Porosity was found to be related to depositional facies and secondary dolomitization and dedolomitization. Core-determined porosities ranged from 0 to 31 percent, but very few values were larger than 24 percent; most values were less than 8 percent, with only 20 percent of the values greater than 15 percent. Porosities were highest in the lower part of the formation in the packstone- to grainstone-dominated facies and were lowest in micritic- to wackestone-facies as well as thinly bedded packstones and grainstones. Fractures were interpreted to provide “permeable migration pathways between and through intervals of matrix permeability” (Thyne and others, 2010, p. 148). Core-determined permeabilities ranged from less than 0.1 to more than 1,000 mD.

Water-saturated and permeable parts of the Madison Limestone, in combination with the overlying Darwin Sandstone Member of the Amsden Formation where present, compose an aquifer (Madison aquifer) throughout the GGRB (Collentine and others, 1981; Geldon, 2003a, b). The Madison aquifer is confined from above by the parts of the Amsden Formation above the Darwin Sandstone Member of the Amsden Formation and from below by the Darby confining unit composed of the Devonian Darby Formation (Collentine and others, 1981; Geldon, 2003a, b; Campbell-Stone and others, 2011). The aquifer is rarely utilized in the western GGRB because of deep burial throughout most of the basin. Permeability in the aquifer is primarily secondary, and is well-developed in places; examples include fractures, as well as various karstic features such as solution cavities and channels and caverns (Collentine and others, 1981; Geldon, 2003a, b). Groundwater in the Madison aquifer generally flows away from outcrop areas surrounding the western GGRB (and source of recharge) and towards the basin center (Geldon, 2003a, b).

The TDS concentration in one Madison Limestone produced-water sample from Tip Top field in the Moxa arch/La Barge platform area was 25,253 mg/L, indicating the water was saline (TDS>10,000 mg/L). (Blondes and others, 2017). The water was a sodium-sulfate type, but remaining anions (bicarbonate and chloride) still represented substantial percentages of the total anions (21 and 27 percent, respectively). Bartos and others (2010) described two produced groundwater-quality samples from the Madison Limestone in the western GGRB. TDS concentrations were 20,800 and 76,800 mg/L, indicating both waters were saline.

3. POWDER RIVER STRUCTURAL BASIN

3.1 Parkman Sandstone Member of the Mesaverde Formation (House Creek field)

Sediments composing the Mesaverde Formation were deposited in marine and nonmarine environments (Gill and Burkholder, 1979; Merewether, 1996, and references therein). Thickness of the Mesaverde Formation in the Powder River structural basin (PRSB) increases from the north to south, and for the part of the southwestern PRSB that includes the House Creek field area, thickness ranges from about 800 to 900 ft (Fox and Higley, 1987a; Merewether, 1996, fig. 22). Sandstone beds are found primarily in the uppermost member of the formation, known as the Teapot Sandstone Member, and the lowermost member, known as the Parkman Sandstone Member; the members are separated by an unnamed intervening unit known by various informal names, including the “unnamed member” or “unnamed marine shale member” (Wegemann, 1918; Gill and Cobban, 1966a, b, 1973; Merewether and others, 1977a, b, c, d; Gill and Burkholder, 1979; Merewether, 1996). Some studies elevate the Teapot and Parkman Sandstone Members to formation rank, and thus elevate the Mesaverde Formation to group rank (for example, Dogan, 1984).

Composed of marine and nonmarine, very fine- to medium-grained sandstone with locally occurring silty and sandy shale, coal, and shale pebbles, the Teapot Sandstone Member disconformably overlies either the unnamed marine shale member or the Parkman Sandstone Member and is conformably overlain by the marine Lewis Shale (Gill and Cobban, 1966a, b; Gill and Burkholder, 1979; Dogan, 1984). Thickness of the Teapot Sandstone Member measured at outcrops in the western PRSB ranged from about 60 to 165 ft (Rich, 1962; Gill and Burkholder, 1979). In the subsurface, thickness of the Teapot Sandstone Member increases southward from less than 60 ft in northeastern Campbell County to more than 200 ft in a north-northwest-trending area in Converse, Campbell, Johnson, and Sheridan Counties (Fox and Higley, 1987b).

The marine shale member separating the two sandstone members is not present in all parts of the PRSB; the unit conformably overlies the Parkman Sandstone Member and is disconformably overlain by the Teapot Sandstone Member in parts of Converse, Natrona, and Johnson Counties, but it is replaced laterally by the Parkman Sandstone Member in southern and western Natrona County, northern Johnson County, and Sheridan County (Gill and Cobban, 1966a, b). The unnamed marine shale member is composed primarily of silty or sandy shale, clayey or sandy siltstone, and lesser amounts of very fine- to medium-grained sandstone (Gill and Burkholder, 1979). Composed largely of fine-grained rocks, sandstone beds in the unnamed marine shale member can be as much as 155-ft thick (Gill and Burkholder, 1979).

The Parkman Sandstone Member is composed mainly of marine and nonmarine, thin-bedded, very fine- to fine-grained sandstone with partly carbonaceous and coaly, sandy shale (Merewether and others, 1977a, b, c, d; Dogan, 1984). In the western PRSB in Wyoming, the Parkman Sandstone Member conformably overlies and grades into the Cody Shale and is either conformably overlain by the unnamed marine shale member or is disconformably overlain by the Teapot Sandstone Member (Merewether and others, 1977a, b, c, d). Measurements at outcrops near the western PRSB indicate thickness of the Parkman Sandstone Member increases southward from about 356 ft in northwestern Sheridan County to about 553 ft in south-central Natrona County (Rich, 1962; Gill and Cobban, 1966a). In the

subsurface, thickness of the Parkman Sandstone Member increases generally to the south from less than 75 ft in north-central Campbell County to about 700 ft in southwestern Converse County [Fox and Higley, 1987c (actual subsurface thickness likely smaller in some areas because mapped thickness in the report included Red Bird Silty Member of the Pierre Shale where present)].

On the basis of large sandstone content in the Teapot and Parkman Sandstone Members that compose much of the total formation thickness, the Mesaverde Formation is identified as an aquifer (Mesaverde aquifer) in previous studies (Warner, 1947; Babcock and Morris, 1954; Kohout, 1957; Whitcomb, 1960, 1965; Lowry and Cummings, 1966; Whitcomb and others, 1966; Crist and Lowry, 1972; Hodson and others, 1973; Feathers and others, 1981; Western Water Consultants, Inc., 1982, 1983; WWC Engineering and others, 2007, fig. 4-9). Individual water-saturated and permeable sandstone beds such as those that compose parts of the Teapot and Parkman Sandstone Members collectively form the Mesaverde aquifer. Because sandstone is interbedded with substantial amounts of shale throughout the formation, Western Water Consultants, Inc. (1983, fig. 2) described the Mesaverde Formation in the southwestern PRSB near the town of Kaycee as a “secondary aquifer with leaky confining layers.” Despite being classified as an aquifer, the Mesaverde Formation is considered part of a regionally extensive confining unit (Upper Cretaceous confining unit) because net thickness of water-saturated and permeable sandstone composing the aquifer (likely hundreds of feet) is still very small in comparison with the thousands of feet of fine-grained low-permeability strata (primarily shale) in the various overlying and underlying lithostratigraphic units composing the confining unit (Downey, 1986; Downey and Dinwiddie, 1988; Whitehead, 1996).

Development of the Mesaverde aquifer as a water supply in the PRSB is limited to the basin margin area where water-saturated and sufficiently permeable sandstone beds can be penetrated at economical drilling depths, and where groundwater is likely to be fresher and less mineralized (Crist and Lowry, 1972; Hodson and others, 1973; Feathers and others, 1981). Wells completed in the Mesaverde aquifer in these areas are used primarily to provide water for livestock. Crist and Lowry (1972) suggested that both the Teapot and Parkman Sandstone Members should be fully penetrated to provide maximum yield from wells completed in the Mesaverde aquifer.

Bartos and others (2018) characterized the quality of groundwater sampled from seven wells completed in the Mesaverde aquifer throughout the PRSB where utilized as a source of water supply for various uses not associated with oil and gas exploration and development (environmental water samples). TDS concentrations in environmental water samples ranged from 370 to 4,430 mg/L, with a median of 1,490 mg/L. A majority (about 71 percent, 5 of 7 samples) of the waters were brackish (TDS=1,000 to 10,000 mg/L), whereas the remaining waters were fresh (about 29 percent, 2 of 7 samples; TDS<1,000 mg/L). Trilinear diagrams constructed using environmental water samples collected from the Mesaverde aquifer indicated ionic composition varied with salinity (Bartos and others, 2018).

The quality of groundwater from deeply buried parts of the Parkman Sandstone Member of the Mesaverde Formation in House Creek field associated with hydrocarbon production is different than the overlying shallower and fresher parts associated with the Mesaverde aquifer in the PRSB described above using environmental water samples. TDS concentrations in 38 produced-water samples from House Creek Field ranged from 3,390 to 19,009 mg/L, with a median of 11,100 mg/L, indicating waters were brackish (TDS=1,000 to 10,000 mg/L) and saline (TDS>10,000 mg/L). Sample-collection depths ranged from about 800 to 12,200 ft bls. All waters were sodium-chloride type. Bartos and others (2018) described the chemical composition of produced waters from the Mesaverde Formation (including Parkman Sandstone Member) throughout the PRSB using 466 produced-water samples. TDS concentrations varied substantially, ranging from 399 to 48,670 mg/L, with a median of 14,170 mg/L. The majority of samples (about 76 percent, or 354 of 463 samples) were saline, whereas the remaining were brackish (about 23 percent, or 107 of 463 samples with complete chemical analysis) or fresh (less than 1 percent, or 2 of 463 samples). Sodium was the predominant cation in almost all samples, but the predominant anion varied in relation to TDS concentrations. In saline waters, chloride was the dominant anion as is the case with the 38 House Creek field produced-water samples.

3.2 Turner Sandy Member/Sandstone of Carlile Shale (House Creek field)

The Turner Sandy Member/Sandstone of the Carlile Shale in the PRSB consists of shale, siltstone, and minor sandstone (Merewether, 1996). Most sandstone is silty, very fine grained, and calcareous, and most sandstone beds are less than 16 ft thick (Merewether, 1996).

Hydrocarbons (oil and gas, but primarily oil) are produced from sandstone beds in the Turner Sandy Member/Sandstone. Craddock and others (2012) indicated the “most likely” porosities for PRSB sandstones at depths between 3,000 to 13,000 ft bls range from 10 to 16 percent, with a most likely porosity of 12 percent. Anna (2010) briefly described permeabilities determined from sandstone core plugs collected at two producing fields in the PRSB (Finn-Shurley and Porcupine fields). Measured permeability was greater than 2 darcies for medium-grained, clean, well-sorted sandstones at the Finn-Shurley field. For the Porcupine field, measured permeability was greater than 10 mD for slightly argillaceous, fine-grained sandstone, but less than 10 mD for argillaceous, fine-grained, and slightly bioturbated sandstone.

The deeply buried Cretaceous shale section in the PRSB, including the Carlile Shale, is overpressured on a basinwide scale below present-day burial depths of about $8,000 \pm 2,000$ ft (Surdam and others, 1994, 1997, 2005; Jiao and Surdam, 1997). Collectively, the shale section contained within parts of numerous lithostratigraphic units forms a basinwide dynamic pressure compartment/regime that extends across the PRSB. The bottom of the overpressured shale section occurs at the deepest organic-rich Cretaceous shales. Overpressure in this large basinwide pressure compartment has been attributed to generation and storage of liquid hydrocarbons, and subsequent reaction to gas in the organic-rich shales (Surdam and others, 1994). This converted the fluid-flow system “from a water-dominated single-phase regime to a hydrocarbon-dominated multi-phase regime where capillarity dominates the relative permeability, creating elevated displacement pressures within the shales” (Surdam and others, 1994, p. 213 and 223). In contrast, the pressure regime of Upper Cretaceous sandstones interbedded within the overpressured shale section is different. These sandstones, including the Turner Sandy Member/Sandstone, are not part of the basinwide overpressured pressure compartment; the pressure systems and fluid flow systems of individual sandstones are vertically and horizontally separated, and can be subdivided into small, isolated compartments (Heasler and others, 1994; Martinsen,

1994). Pressures within the sandstones/sandstone compartments can be normal or anomalous (above or below normal hydrostatic gradient), even though shales at the same depths are overpressured. Within the PRSB below 8,000 to 9,000 ft, most of the sandstones within the various Upper and Lower Cretaceous lithostratigraphic units are overpressured (Surdam and others, 1994, fig. 23). Fluids in these deeply buried overpressured sandstone aquifers/reservoirs (various lithostratigraphic units, including the Turner Sandy Member/Sandstone) from which hydrocarbons are produced likely are not in hydrologic connection with the overlying shallower hydropressured (primarily normally pressured) parts of these and other units. The overlying normally pressured areas are in hydrologic connection with groundwater-flow systems associated with meteoric groundwater circulation (and predominantly, single-phase groundwater flow, and these areas likely are hydrologically disconnected from overpressured areas/reservoirs to varying degrees (Surdam and others, 1994). However, normally pressured sandstones within the overpressured shale section may represent “fluid conduits” out of the overpressured shale section (Surdam and others, 1994).

Numerous Upper Cretaceous lithostratigraphic units, including the Carlile Shale containing the Turner Sandy Member/Sandstone, collectively compose a thick, geographically extensive regional confining unit present throughout much of the PRSB (Feathers and others, 1981, fig. II-4; Downey, 1986; Downey and Dinwiddie, 1988; Busby and others, 1995; Whitehead, 1996). Named the Upper Cretaceous confining unit by Bartos and others (2018), the regional confining unit separates and hydraulically isolates an overlying Upper Cretaceous aquifer system and all overlying Cenozoic aquifers/aquifer systems from all stratigraphically older aquifers/aquifer systems. Within the PRSB, the lithostratigraphic units composing the confining unit differ by geographic area. Individual lithostratigraphic units and (or) parts of the units composing the Upper Cretaceous confining unit laterally grade and intertongue in outcrops and in the subsurface, chronicling the multiple westward transgressions and eastward regressions of the north-trending epeiric sea in the Western Interior Seaway (Merewether, 1996, and references therein). The confining unit consists largely of thousands of feet of predominantly fine-grained rocks such as marine shale, but interbedded sandstones such as the Turner Sandstone Member/Sandstone of the Carlile Shale and other lithostratigraphic units within the larger confining unit can contain or have been speculated to possibly contain discontinuous (local) aquifers (Ahern and others, 1981; Collentine and others, 1981) in addition to hydrocarbon reservoirs (Kirschbaum and Roberts, 2005a, b). However, Bartos and others (2018) conducted a detailed overview of the hydrogeology of the PRSB and the investigators did not document any use of waters from the Carlile Shale, including the Turner Sandstone Member/Sandstone. Even where hydrocarbons are absent, the unit is unlikely be developed as a source of water supply because of deep burial and poor groundwater quality in most areas (Bartos and others, 2018).

TDS concentrations available for two produced-water samples from the Turner Sandy Member/Sandstone in House Creek field were 61,747 and 62,810 mg/L, indicating both waters were saline (TDS>10,000 mg/L). Both waters were sodium-chloride type. Bartos and others (2018) described the chemical composition of groundwater from the Turner Sandstone Member/Sandstone (identified as the Carlile confining unit) throughout the PRSB using 70 produced-water samples. TDS concentrations ranged from 1,430 to 84,100 mg/L, with a median of 40,400 mg/L, indicating most waters were saline. Almost all waters were sodium-chloride type.

3.3 Frontier Formation (Pine Tree field)

Marine and nonmarine siliciclastic sediments composing the Upper Cretaceous Frontier Formation in what is now the western and southwestern PRSB were deposited in numerous depositional environments (Hares, 1916; Towse, 1952; Merewether and others, 1979, and references therein; Merewether, 1983, 1996, and references therein). Two or three different members of the Frontier Formation are recognized, including, from stratigraphically youngest to oldest, the Wall Creek Sandstone (also known as the Wall Creek Member; Merewether, 1996), Emigrant Gap Member (formerly known as the “unnamed member”; Merewether and others, 1979), and the Belle Fourche Shale (Wegemann, 1911; Hares, 1916; Hose, 1955; Mapel, 1959; Merewether and others, 1979; Merewether, 1996) (also known as the Belle Fourche Member; Merewether, 1996). All three members are not present at all locations in the PRSB, and some members grade laterally into other lithostratigraphic units (Merewether and others, 1979; Merewether, 1996). The Wall Creek Sandstone consists of very fine- to fine-grained sandstone, silty sandstone, siltstone, sandy siltstone, silty shale, and shale; the sandstone beds generally grade into underlying siltstone and are abruptly overlain by shale or siltstone (Merewether and others, 1979; Merewether, 1996). Sandstone content and thickness of the Wall Creek Sandstone is greatest in the southwestern PRSB; thickness in this area ranges from 10 to 280 ft (Merewether, 1996). In the southwestern PRSB, the Wall Creek Sandstone disconformably overlies either the Emigrant Gap Member or the Belle Fourche Member and is conformably overlain by the Cody Shale (Merewether and others, 1979; Merewether, 1996). Composition of the Emigrant Gap and Belle Fourche Shale is similar to the Wall Creek Sandstone, consisting primarily of varying proportions of interstratified very fine- to medium-grained sandstone, siltstone, and mudstone; the sandstone is locally conglomeratic, calcareous, and concretionary (Merewether and others, 1979; Merewether, 1996). Anna (2010) estimated that fine-grained rocks typically compose about one-half of total formation thickness.

Hydrocarbons (oil and gas, but primarily oil) are produced from sandstone beds in the various members of the Frontier Formation. Porosity of Belle Fourche Member sandstones ranges from 5 to 15 percent, and permeability ranges from 1 to less than 100 mD (Anna, 2010). Wall Creek Sandstone Member sandstones have porosities ranging from near 0 to 20 percent; hydrocarbon-producing reservoir sandstones in the member have porosities ranging from 10 to 20 percent (Anna, 2010). Permeability of Wall Creek Sandstone Member sandstones averages much less than 100 mD, but some can be as much as 100 mD (Anna, 2010). Craddock and others (2012) indicated the “most likely” porosities for PRSB Frontier Formation sandstones at depths between 3,000 to 13,000 ft bls range from 10 to 16 percent, with a most likely porosity of 12 percent.

The deeply buried Cretaceous shale section in the PRSB, including the Frontier Formation, is overpressured on a basinwide scale below present-day burial depths of about 8,000 ± 2,000 ft (Surdam and others, 1994, 1997, 2005; Jiao and Surdam, 1997). Collectively, the shale section contained within parts of numerous lithostratigraphic units forms a basinwide dynamic pressure compartment/regime that extends across the PRSB. The bottom of the overpressured shale section occurs at the deepest organic-rich Cretaceous shales. Overpressure in this

large basinwide pressure compartment has been attributed to generation and storage of liquid hydrocarbons, and subsequent reaction to gas in the organic-rich shales (Surdam and others, 1994). This converted the fluid-flow system “from a water-dominated single-phase regime to a hydrocarbon-dominated multi-phase regime where capillarity dominates the relative permeability, creating elevated displacement pressures within the shales” (Surdam and others, 1994, p. 213 and 223). In contrast, the pressure regime of Upper Cretaceous sandstones interbedded within the overpressured shale section is different. These sandstones, including the sandstone within the Frontier Formation, are not part of the basinwide overpressured pressure compartment; the pressure systems and fluid flow systems of individual sandstones are vertically and horizontally separated, and can be subdivided into small, isolated compartments (Heasler and others, 1994; Martinsen, 1994). Pressures within the sandstones/sandstone compartments can be normal or anomalous (above or below normal hydrostatic gradient), even though shales at the same depths are overpressured. Within the PRSB below 8,000 to 9,000 ft, most of the sandstones within the various Upper and Lower Cretaceous lithostratigraphic units are overpressured (Surdam and others, 1994, fig. 23). Fluids in these deeply buried overpressured sandstone aquifers/reservoirs (various lithostratigraphic units, including the Frontier Formation) from which hydrocarbons are produced likely are sealed from/not likely in hydrologic connection with the overlying shallower hydropressured (primarily normally pressured) parts of these and other units. The overlying normally pressured areas are in hydrologic connection with groundwater-flow systems associated with meteoric groundwater circulation (and predominantly, single-phase groundwater flow), and these areas likely are hydrologically disconnected from overpressured areas/reservoirs to varying degrees (Surdam and others, 1994). However, normally pressured sandstones within the overpressured shale section may represent “fluid conduits” out of the overpressured shale section (Surdam and others, 1994).

Because of substantial sandstone content, the Frontier Formation was speculated to be or was defined as an aquifer or minor aquifer by previous investigators (Warner, 1947; Babcock and Morris, 1954; Kohout, 1957; Whitcomb, 1960, 1965; Lowry and Cummings, 1966; Whitcomb and others, 1966; Crist and Lowry, 1972; Hodson and others, 1973; Feathers and others, 1981; Western Water Consultants, Inc., 1982, 1983; WWC Engineering and others, 2007). Water-saturated and permeable sandstone beds are interbedded with substantial thicknesses of fine-grained rocks throughout the formation, so Western Water Consultants, Inc. (1983, fig. 2) described the Frontier Formation in the southwestern PRSB near the town of Kaycee as a series of “alternating leaky confining layers and secondary aquifers.” Although classified as an aquifer, the Frontier Formation is still considered part of the regionally extensive confining unit (Upper Cretaceous confining unit) because net thickness of water-saturated and permeable sandstone composing the aquifer (likely hundreds of feet) is still very small in comparison with the thousands of feet of fine-grained low-permeability strata (primarily shale) in the various overlying lithostratigraphic units and the additional hundreds of feet in underlying units composing the confining unit (Downey, 1986; Downey and Dinwiddie, 1988; Whitehead, 1996).

The Frontier aquifer is rarely utilized in the PRSB because of deep burial throughout most of the basin. Development of the Frontier aquifer as a water supply is limited to areas in or near outcrops along the PRSB margin and adjacent Casper arch area in Natrona County where sufficiently water-saturated and permeable sandstone beds can be penetrated at economical drilling depths and where groundwater is likely to be fresher and less mineralized (Crist and Lowry, 1972; Hodson and others, 1973; Feathers and others, 1981; Western Water Consultants, Inc., 1983, fig. 2; Banner Associates, Inc., 2002). Many groundwater wells have been completed in the Frontier aquifer in these areas, and many of those wells have artesian pressure sufficient to cause wells completed in the aquifer to flow (Crist and Lowry, 1972; Banner Associates, Inc., 2002). Much of the water withdrawn from the Frontier aquifer is used to provide water for stock supply. Several investigators have noted the potential for development of secondary porosity and permeability from fractures in the sandstones composing the Frontier aquifer (Western Water Consultants, Inc., 1983, fig. 2; Banner Associates, Inc., 2002). Except near outcrop areas, groundwater in the Frontier aquifer generally is under confined conditions at most locations (Feathers and others, 1981). Warner (1947) speculated that recharge to the Wall Creek Sandstone of the Frontier Formation in the southwestern PRSB near Kaycee was by infiltration of precipitation on outcrops and streamflow losses (seepage) from the Middle Fork of the Powder River.

Bartos and others (2018) characterized the quality of groundwater sampled from wells completed in the Frontier aquifer throughout the PRSB where utilized as a source of water supply for various uses not associated with oil and gas exploration and development (environmental water samples). TDS concentrations in environmental water samples ranged from 348 to 2,270 mg/L, with a median of 1,120 mg/L (N= 12). A majority (about 67 percent, 8 of 12 samples) of the waters were brackish (TDS=1,000 to 10,000 mg/L), whereas the remaining waters were fresh (TDS<1,000 mg/L). Trilinear diagrams constructed for environmental waters from the Frontier aquifer indicated ionic composition varied with salinity (Bartos and others, 2018).

Groundwater quality in the deeply buried overpressured parts of the Frontier Formation in the Pine Tree field associated with hydrocarbon production is substantially different than the overlying shallower and fresher parts associated with the Frontier aquifer in the PRSB described above using environmental water samples. TDS concentrations in three produced-water samples were 2,250, 40,367, and 50,709 mg/L, indicating one sample was brackish (TDS=1,000 to 10,000 mg/L) and two samples were saline (TDS>10,000 mg/L). All three waters were sodium-chloride type. Bartos and others (2018) described the chemical composition of the Frontier aquifer throughout the PRSB using 320 produced-water samples. TDS concentrations varied substantially, ranging from 227 to 156,600 mg/L, with a median of 7,019 mg/L. Sodium was the predominant cation in almost all samples, but the predominant anion varied in relation to TDS concentrations. In saline waters, chloride was the dominant anion as is the case with the three Pine Tree field produced-water samples.

3.4 Mowry Shale (Pine Tree field)

Deposited by an inland sea during the Early to Late Cretaceous transition, the marine Mowry Shale in the PRSB consists of largely of organic-rich siliceous shale, with minor non-siliceous silty or sandy shale and sandstone (Byers and Larson, 1979; Merewether, 1996) and possibly siltstone (Anna, 2010). The Mowry Shale is overlain by the Upper Cretaceous Frontier Formation and underlain by the Lower Cretaceous Muddy Sandstone (Merewether, 1996). The Mowry Shale is a hydrocarbon source rock for Lower Cretaceous reservoirs as

well as for an intraformational continuous (unconventional) accumulation/reservoir. Mowry Shale hydrocarbon production may be enhanced by fracture permeability and storage (Anna, 2010).

The deeply buried Cretaceous shale section in the PRSB, including the Mowry Shale, is overpressured on a basinwide scale below present-day burial depths of about $8,000 \pm 2,000$ ft (Surdam and others, 1994, 1997, 2005; Jiao and Surdam, 1997). Collectively, the shale section contained within parts of numerous lithostratigraphic units forms a basinwide dynamic pressure compartment/regime that extends across the PRSB. The bottom of the overpressured shale section occurs at the deepest organic-rich Cretaceous shales. Overpressure in this large basinwide pressure compartment has been attributed to generation and storage of liquid hydrocarbons, and subsequent reaction to gas in the organic-rich shales (Surdam and others, 1994). This converted the fluid-flow system “from a water-dominated single-phase regime to a hydrocarbon-dominated multi-phase regime where capillarity dominates the relative permeability, creating elevated displacement pressures within the shales” (Surdam and others, 1994, p. 213 and 223).

Numerous Upper Cretaceous lithostratigraphic units, including the Mowry Shale, collectively compose a thick, geographically extensive regional confining unit present throughout much of the PRSB (Feathers and others, 1981, fig. II-4; Downey, 1986; Downey and Dinwiddie, 1988; Busby and others, 1995; Whitehead, 1996). Named the Upper Cretaceous confining unit by Bartos and others (2018), the regional confining unit separates and hydraulically isolates an overlying Upper Cretaceous aquifer system and all overlying Cenozoic aquifers/aquifer systems from all stratigraphically older aquifers/aquifer systems. Within the PRSB, the lithostratigraphic units composing the confining unit differ by geographic area. Individual lithostratigraphic units and (or) parts of the units composing the Upper Cretaceous confining unit laterally grade and intertongue in outcrops and in the subsurface, chronicling the multiple westward transgressions and eastward regressions of the north-trending epeiric sea in the Western Interior Seaway (Merewether, 1996, and references therein). The confining unit consists largely of thousands of feet of predominantly fine-grained rocks such as marine shale in the Mowry Shale, but interbedded sandstones within the larger confining unit can contain or have been speculated to possibly contain discontinuous (local) aquifers (Ahern and others, 1981; Collentine and others, 1981; Freethey and Cordy, 1991) in addition to hydrocarbon reservoirs (Kirschbaum and Roberts, 2005a, b). Bartos and others (2018) noted use of the Mowry Shale as a source of water in parts of the PRSB was restricted to areas where the formation is buried at shallow depths or is exposed at land surface, and that deep burial, small well yields, and poor groundwater quality limits development of the formation in most areas.

The TDS concentration in one Mowry Shale produced-water sample from Pine Tree field was 51,778 mg/L, indicating the water was saline (TDS > 10,000 mg/L) (Blondes and others, 2017). The water was sodium-chloride type. Bartos and others (2018) described the chemical composition of the Mowry Shale in the PRSB using nine produced-water samples. TDS concentrations from produced-water samples were variable, ranging from 1,608 to 38,600 mg/L, with a median of 27,500 mg/L. Most waters were saline (about 89 percent, or 8 of 9 samples; TDS > 10,000 mg/L), and remaining waters were brackish (about 11 percent, or 1 of 9 samples; TDS > 1,000 to < 10,000 mg/L).

4. WIND RIVER STRUCTURAL BASIN

4.1 Fort Union Formation (Madden and Moneta Hills fields)

The nonmarine Paleocene Fort Union Formation in the Wind River structural basin (WRSB) is divided into an upper fluvial and marginal lacustrine interval that were deposited within and adjacent to a major lake known as Lake Waltman, and a lower fluvial and paludal interval (Keefer, 1965). The upper interval is further subdivided into two members, the Shotgun Member, consisting of fine- to coarse-grained, partly conglomeratic, fluvial and marginal lacustrine rocks, and the underlying Waltman Shale Member, consisting mainly of lacustrine shale. The lower interval, consisting of sandstone, shale/carbonaceous shale, and coal, is known as the “lower unnamed member” or “lower Fort Union.” Overlying the formation are Eocene strata assigned to the Wind River or Indian Meadows Formations. Reported thickness of the lower unnamed member is more than 3,000 ft along the basin trough south of the Bighorn Mountains that includes the Madden and Moneta Hills fields (Johnson and others, 2007, fig. 16).

Gas from conventional and/or unconventional (basin-centered gas) accumulations is the primary hydrocarbon produced from Fort Union Formation sandstone reservoirs in the WRSB (Johnson and others, 2007). Gas production from the formation in the Madden and Moneta fields area is limited to the lower Fort Union below the Waltman Shale. Where present in the WRSB, the Waltman Shale Member may act as a barrier to vertical hydrocarbon and meteoric water movement (Nelson and Kibler, 2007; Nelson and others, 2009). In the Madden field area, the shaley interval of the Waltman Shale Member is more than 2,000-ft thick and serves as a pressure seal to an underlying, overpressured gas compartment in the lower Fort Union and several other underlying units (described below; Nelson and Kibler, 2007).

All or parts of the deeply buried Fort Union Formation in the Madden field are overpressured (Surdam and others, 2003, 2005; Johnson and others, 2007; Nelson and others, 2009). Nelson and Kibler (2007) and Nelson and others (2009) considered the Fort Union Formation to be within the uppermost of two stacked overpressured compartments in the Madden field area. The upper pressure compartment extends from the top of the Mesaverde Formation upward to the base of the Waltman Shale Member (upper pressure seal), including the lower unnamed member of the Fort Union Formation. Overpressure in the upper pressure compartment has been attributed primarily to gas generation in the Upper Cretaceous Mowry and Cody Shales and Mesaverde Formation (Nelson and others, 2009). The produced water-to-gas ratios for the Fort Union Formation in this Madden field upper pressure compartment were estimated to be about 24 bbl/mmcft (Nelson and Kibler, 2007, table 2). Nelson and Kibler (2007) noted that fluids recovered by drillstem tests in the Fort Union and Lance Formations in the Madden field area below the Waltman Shale had a range of hydrocarbon-to-water ratios, and that no drillstem tests within the pressure compartment yielded only hydrocarbons. Nelson and others (2009) concluded that gas and water production from tight-gas accumulations in the lower Fort Union Formation and two other formations (Cody Shale and Mesaverde Formation) within the

Madden field area showed little or no correlation between gas and water production. The investigators also noted that lower Fort Union Formation produced water-to-gas ratios and produced-water rates were not related to depth in the Madden field area.

Surdam and others (2003, 2005) examined the pressure regimes and fluid-flow systems throughout the WRSB with an emphasis on selected Tertiary and Cretaceous lithostratigraphic units. The investigators proposed that the WRSB on a basinwide scale to some depth can be broadly divided into at least two regional pressure/fluid-flow compartments separated by a regional velocity inversion surface (typically 6,000-8,000 ft below present-day burial depth). The upper component is primarily normally pressured, water-dominated/under water-drive, and consists largely of single-phase fluid-flow systems, whereas the lower compartment is normally or anomalously pressured (in relation to hydrostatic gradient), regionally gas-charged, and consists of multi-phase fluid-flow systems dominated by capillarity. The lower boundary of the lower compartment was speculated to be located in the lowermost organic-rich Mesozoic shale. The upper compartment largely is in hydrologic connection with groundwater-flow systems associated with meteoric groundwater circulation, and likely is hydrologically disconnected from underlying lower compartment rock/fluid-flow systems to varying degrees (Surdam and others, 2005). Below the regional velocity inversion surface and above a present-day burial depth of about 12,000 ft, the lower compartment rock/fluid flow systems in the lower Fort Union Formation and Lance or Mesaverde Formations throughout much of the WRSB were interpreted to be typically (1) normally pressured or underpressured; (2) compartmentalized (subcompartments); (3) isolated from overlying meteoric water circulation (not under strong water-drive); (4) gas-charged; and (5) multi-phase fluid-flow systems dominated by capillarity. At depths approaching or greater than about 12,000 ft, rock/fluid-flow systems in these units have the same characteristics except the systems commonly are substantially overpressured. Fluid-flow subcompartments present in these and other units have shapes and boundaries controlled by faults and other geologic structures, low-permeability rocks, depositional setting, and diagenetic history. Despite being largely isolated from meteoric water recharge, “trapped water” or even substantial water-dominated “domains” within the lower regional gas-charged compartment may be present in parts of the lower Fort Union Formation and Lance or Mesaverde Formations away from the WRSB basin margins and presumed source of meteoric groundwater recharge (Surdam and others, 2003, 2005).

Water-saturated and permeable sandstones and conglomerates in the Fort Union Formation collectively comprise an aquifer (Fort Union aquifer) in the WRSB (Whitcomb and Lowry, 1968; Richter, 1981; Flores et al., 1993). The Fort Union aquifer in the WRSB was grouped by Richter (1981) with the underlying Lance aquifer (named after Lance Formation) into a broader hydrogeologic unit identified as the Fort Union-Lance aquifer. Few data are available describing the hydrogeologic characteristics of the Fort Union Formation/aquifer (Bartos and others, 2012).

The Waltman Shale Member may act as a confining unit (and seal for hydrocarbon accumulations) within the Fort Union Formation/aquifer throughout much of the WRSB where present, including the Madden field area (Nelson and Kibler, 2007; Nelson and others, 2009). Nelson and Kibler (2007) believe the Waltman Shale Member prevents downward movement of meteoric water to depths greater than the top of the unit, although the investigators noted that lateral migration of meteoric waters within units deeper than the Waltman Shale Member may be possible. In addition, the investigators noted the Waltman Shale Member may not “form a continuous barrier to fluid flow” everywhere present because shale may represent only a small percentage of total unit thickness in some areas.

Individual sandstone and conglomerate aquifers composing the Fort Union aquifer likely are confined at most locations in the WRSB because of deep burial, but unconfined conditions are likely in outcrop areas or where buried at shallow depths (Richter, 1981). Permeability likely is both primary and secondary, and permeability may be fracture-enhanced in structurally deformed areas (Richter, 1981). Apart from oil and gas wells, very few wells have been installed in the Fort Union Formation/aquifer in the WRSB because of limited outcrop/shallow subcrop and deep burial at most locations, or poor hydrogeologic characteristics for intended uses (Richter, 1981; Bartos and others, 2012). Most wells completed in the aquifer are for livestock use (Richter, 1981; Bartos and others, 2012).

TDS concentrations in Fort Union Formation produced-water samples from Madden field ranged from 949 to 51,237 mg/L, with a median of 9,149 mg/L (N=182) (Blondes and others, 2017). Almost all waters were brackish (TDS=1,000 to 10,000 mg/L) and saline (TDS>10,000 mg/L). Most waters were sodium-chloride. Sample-collection depths ranged from about 3,000 to 13,400 ft bls.

TDS concentrations in Fort Union Formation produced-water samples from Moneta Hills field ranged from 2,517 to 11,523 mg/L, with a median of 6,297 mg/L (N=20) (Blondes and others, 2017). Waters were brackish (TDS=1,000 to 10,000 mg/L) and saline (TDS>10,000 mg/L). Waters were sodium-chloride, sodium-bicarbonate, or sodium-bicarbonate-chloride/sodium-chloride-bicarbonate type. Sample-collection depths ranged from about 7,500 to 10,800 ft bls.

4.2 Lance Formation (Madden and Moneta Hills fields)

The Upper Cretaceous Lance Formation in the WRSB consists of nonmarine (continental) sandstone interbedded with shale, claystone, siltstone, and thin coal (Keefer, 1965). Reported thickness of the Lance Formation is more than 5,000 ft along the basin trough south of the Bighorn Mountains that includes the Madden and Moneta Hills fields (Johnson and others, 2007, fig. 15). The formation is overlain by the Paleocene Fort Union Formation and underlain by the Upper Cretaceous Meetetse Formation. Gas from conventional and/or unconventional (basin-centered gas) accumulations is the primary hydrocarbon produced from Lance Formation sandstone reservoirs in the WRSB, including the Madden and Moneta Hills fields area (Johnson and others, 2007).

Lance Formation cores collected from Madden field indicate sandstones typically are fine-grained and moderately well-sorted, with a fining upward grain size (Dunleavy and Gilbertson, 1986). Reid (1978) reported an average core-determined porosity of 5.5 percent, and an average core-determined permeability of 0.58 mD for Lance Formation reservoir sandstones from one Madden field well. Fractures may enhance Madden field sandstone productivity in parts of the formation (Reid, 1978; Dunleavy and Gilbertson, 1986). Additional insight into Lance Formation reservoir sandstone properties is available from a study of the unit at Cave Gulch field located about 20

miles southeast of Madden field (Montgomery and others, 2001), although it is unknown how comparable reservoir sandstone properties are between the locations. Sandstones composing these reservoirs were described as very fine- to fine-grained, moderately well-sorted, and sublithic. Core-determined porosities of Lance Formation reservoir sandstones ranged from 9–19 percent, and permeabilities ranged from 0.1–50 mD. Porosity was both primary (original intergranular pores) and secondary (dissolution pores), and both properties decreased with depth. Fractures were noted, especially in the middle Lance Formation, and these fractures may facilitate increased gas production in some areas.

All or parts of the deeply buried Lance Formation in Madden field are overpressured (Reid, 1978; Dunleavy and Gilbertson, 1986; Surdam and others, 2003, 2005; Johnson and others, 2007; Nelson and Kibler, 2007; Nelson and others, 2009). Two studies (Nelson and Kibler, 2007; Nelson and others, 2009) considered the Lance Formation to be within the uppermost of two stacked overpressured compartments in the Madden field area. The upper pressure compartment extends from the top of the Mesaverde Formation upward to the base of the Waltman Shale Member (pressure seal), including the Lance Formation. Overpressure in the upper pressure compartment has been attributed primarily to gas generation in the Upper Cretaceous Mowry and Cody Shales and Mesaverde Formation (Nelson and others, 2009). The produced water-to-gas ratios for the Lance Formation in this Madden field upper pressure compartment were estimated to be about 102 bbl/mmcf (Nelson and Kibler, 2007, table 2). Fluids recovered by Fort Union and Lance Formation drillstem tests in the Madden field area below the Waltman Shale show a range of hydrocarbon-to-water ratios, and no drillstem tests within the pressure compartment yield only hydrocarbons (Nelson and Kibler, 2007).

Surdam and others (2003, 2005) examined the pressure regimes and fluid-flow systems throughout the WRSB with an emphasis on selected Tertiary and Cretaceous lithostratigraphic units. The investigators proposed that the WRSB on a basinwide scale to some depth can be broadly divided into at least two regional pressure/fluid-flow compartments separated by a regional velocity inversion surface (typically 6,000–8,000 ft below present-day burial depth). The upper component is primarily normally pressured, water-dominated/under water-drive, and consists largely of single-phase fluid-flow systems, whereas the lower compartment is normally or anomalously pressured (in relation to hydrostatic gradient), regionally gas-charged, and consists of multi-phase fluid-flow systems dominated by capillarity. The lower boundary of the lower compartment was speculated to be located in the lowermost organic-rich Mesozoic shale. The upper compartment largely is in hydrologic connection with groundwater-flow systems associated with meteoric groundwater circulation, and likely is hydrologically disconnected from underlying lower compartment rock/fluid-flow systems to varying degrees (Surdam and others, 2005). Below the regional velocity inversion surface and above a present-day burial depth of about 12,000 ft, the lower compartment rock/fluid flow systems in the lower Fort Union Formation and Lance or Mesaverde Formations throughout much of the WRSB were interpreted to be typically (1) normally pressured or underpressured; (2) compartmentalized (subcompartments); (3) isolated from overlying meteoric water circulation (not under strong water-drive); (4) gas-charged; and (5) multi-phase fluid-flow systems dominated by capillarity. At depths approaching or greater than about 12,000 ft, rock/fluid-flow systems in these units have the same characteristics except the systems commonly are substantially overpressured. Fluid-flow subcompartments present in these and other units have shapes and boundaries controlled by faults and other geologic structures, low-permeability rocks, depositional setting, and diagenetic history. Despite being largely isolated from meteoric water recharge, “trapped water” or even substantial water-dominated “domains” within the lower regional gas-charged compartment may be present in parts of the lower Fort Union Formation and Lance or Mesaverde Formations away from the WRSB basin margins and presumed sourced of meteoric groundwater recharge.

Water-saturated and permeable parts of the Upper Cretaceous Lance Formation (primarily sandstone beds) collectively compose an aquifer (Lance aquifer) in the WRSB (Richter, 1981). The Lance aquifer in the WRSB was grouped by Richter (1981) with the overlying Fort Union aquifer into a broader hydrogeologic unit identified as the Fort Union-Lance aquifer. The aquifer is overlain by the Fort Union aquifer and underlain by the Meeteetse-Lewis confining unit consisting of the Meeteetse Formation and Lewis Shale, respectively (Richter, 1981). Individual sandstone aquifers composing the Lance aquifer likely are confined at most locations in the WRSB because of deep burial, but unconfined conditions are likely in outcrop areas or where buried at shallow depths. Richter (1981, table IV-1, p. 48) speculated the aquifer had “large development potential” in the WRSB. Apart from oil and gas wells, very few wells have been installed in the Lance aquifer in the WRSB because of limited outcrop/shallow subcrop and deep burial at most locations, or poor hydrogeologic characteristics for intended uses (Richter, 1981; Bartos and others, 2012).

TDS concentrations in Lance Formation produced-water samples from Madden field ranged from 3,322 to 15,025 mg/L, with a median of 7,271 mg/L (N=19) (Blondes and others, 2017). Waters were brackish (TDS=1,000 to 10,000 mg/L) and saline (TDS>10,000 mg/L). Almost all waters were sodium-chloride type. Sample-collection depths ranged from about 7,200 to 15,400 ft bls.

TDS concentrations in Lance Formation produced-water samples from Moneta Hills field ranged from 4,090 to 20,916 mg/L, with a median of 7,664 mg/L (N=4) (Blondes and others, 2017). Waters were brackish (TDS=1,000 to 10,000 mg/L) and saline (TDS>10,000 mg/L). Waters were sodium-chloride-type (two samples), calcium-sodium-chloride type (one sample), and sodium-bicarbonate-sulfate type (one sample). Sample-collection depths ranged from about 9,700 to 11,300 ft bls.

4.3 Mesaverde Formation (Madden field)

The Upper Cretaceous Mesaverde Formation consists of a variable sequence of massive to lenticular, fine- to coarse-grained sandstone, carbonaceous shale, and lesser amounts of coal (Keefer, 1972; Johnson and others, 2007, and references therein). Sediments composing the formation were deposited in coastal plain and fluvial settings as the Western Interior Seaway shoreline retreated. Thickness of the Mesaverde Formation (including all members) in the Madden field area is between 1,000 and 1,200 ft (Johnson and others, 2007, fig. 9). As many as four members of the Mesaverde Formation are recognized in the eastern and southeastern WRSB—the uppermost Teapot Sandstone Member, an unnamed middle member, the Parkman Sandstone Member, and the lowermost Fales Sandstone Member (Keefer, 1972). Where present, the Wallace Creek Tongue of the Cody Shale intertongues with the Mesaverde Formation and separates the Parkman

and Fales Sandstone Members. Most of these members cannot be identified in the remainder of the WRSB, and the formation is divided into an upper interval (Teapot Sandstone Member) and lower interval typically identified as the “lower part” (for example, Johnson and others, 2007, fig. 2).

Gas from conventional and/or unconventional (primarily basin-centered gas) accumulations is the primary hydrocarbon produced from Mesaverde Formation reservoirs in the WRSB, including Madden field (Johnson and others, 2007). Most WRSB Mesaverde reservoirs are fluvial channel and marginal marine sandstones, with the latter sandstone type being confined to the lower part of the formation (Johnson and others, 2007). Mesaverde Formation reservoir sandstones can be highly productive in Madden field (Johnson and others, 2007). Productive reservoirs at Madden field are located in the lower part of the formation and consist of marginal marine sandstones with a shape described as “blanket-like” (Johnson and others, 2007; Dunleavy and Gilbertson, 1986). Dunleavy and Gilbertson (1986) attributed high productivity to a combination of the “blanket-like” shape and fractures associated with the Madden anticline.

The deeply buried Mesaverde Formation in the Madden field is overpressured (Johnson and others, 2007; Nelson and others, 2009). Two studies (Nelson and Kibler, 2007; Nelson and others, 2009) considered the Mesaverde Formation to be within the lowermost of two stacked overpressured “pressure compartments” in the Madden field area. The lower overpressured compartment extends from the top of the Mesaverde Formation downward to a base described as being located “somewhat below the base of the Cretaceous” (Nelson and Kibler, 2007, p. 23) or alternatively at the top of the Jurassic Morrison Formation (Nelson and others, 2009). Nelson and Kibler (2007, p. 23) noted that Mesaverde Formation water production from the Madden field lower overpressure compartment was high (186 bbl/mmc) despite “the high pressure and preponderance of gas shows.” Gas and water production from tight-gas accumulations in the Mesaverde Formation and two other formations (Cody Shale and lower Fort Union Formation) within the Madden field area showed little or no correlation between gas and water production (Nelson and others, 2009). Overpressure in the lower pressure compartment may be attributable to earlier uplift of a sealed, water-dominated, normally pressured system rather than to overpressuring from gas generation (Nelson and Kibler, 2007).

The Mesaverde aquifer is overlain by the Fort Union aquifer and underlain by the Meeteetse-Lewis confining unit consisting of the Meeteetse Formation and Lewis Shale, respectively (Richter, 1981). Individual sandstone aquifers composing the Mesaverde aquifer likely are confined at most locations in the WRSB because of deep burial, but unconfined conditions are likely in outcrop areas or where buried at shallow depths. Richter (1981, table IV-1, p. 48) speculated the aquifer had “large development potential” in the WRSB. With the exception of oil and gas wells, very few wells have been installed in the Mesaverde aquifer in the WRSB because of limited outcrop/shallow subcrop and deep burial at most locations, or poor hydrogeologic characteristics for intended uses (Richter, 1981; Bartos and others, 2012).

Water-saturated and permeable parts of the Upper Cretaceous Mesaverde Formation (primarily sandstone beds) collectively compose an aquifer (Mesaverde aquifer) in the WRSB (Richter, 1981). Parts of the formation consisting largely of sandstone, including formally recognized members of the formation consisting substantially of sandstone (Teapot Sandstone, Parkman Sandstone, and Fales Sandstone Members), are considered aquifers or subaquifers within the broadly defined Mesaverde aquifer (Richter, 1981). The unnamed middle member is composed of siltstone, shale, carbonaceous shale, and thin-bedded, discontinuous sandstone; this member and the intertonguing Wallace Creek Tongue of the Cody Shale (where present) are defined as confining units dividing the larger Mesaverde aquifer (Richter, 1981). Division of the larger Mesaverde aquifer by these confining units, along with the overlying regionally extensive Meeteetse-Lewis and underlying Cody confining units, creates a series of confined sandstone subaquifers (Teapot Sandstone, Parkman Sandstone, and the Fales Sandstone Members) within the Mesaverde aquifer. In parts of the WRSB, subaquifers may be hydraulically connected by faults and fractures in underlying and overlying confining units (Richter, 1981).

Individual sandstone aquifers composing the Mesaverde aquifer likely are confined at most locations in the WRSB because of deep burial, but unconfined conditions are likely in outcrop areas or where buried at shallow depths. Aquifer permeability may be enhanced in areas where the Mesaverde aquifer is faulted and fractured (Richter, 1981). Excluding wells associated with petroleum exploration and development, few groundwater wells are installed in the Mesaverde aquifer in the WRSB because of deep burial, availability of shallower sources of groundwater, and/or poor groundwater quality, including the part of the basin that includes Madden field.

TDS concentrations in Mesaverde Formation produced-water samples from Madden field ranged from 1,835 to 15,291 mg/L, with a median of 11,593 mg/L (N=8) (Blondes and others, 2017). Waters were brackish (TDS=1,000 to 10,000 mg/L) and saline (TDS>10,000 mg/L). Almost all waters were sodium-chloride. Sample-collection depths ranged from about 15,400 to 16,000 ft bls.

4.4 “Shannon sandstone” of Cody Shale (Madden field)

The Upper Cretaceous Cody Shale in the WRSB consists of a thick sequence of marine shale, sandstone, and siltstone (Keefer, 1972; Finn, 2007, and references therein). The formation conformably intertongues with the overlying Mesaverde Formation and underlying Frontier Formation (Keefer, 1972). As many as four members of the Cody Shale are recognized in the WRSB (Keefer, 1972; Finn, 2007, and references therein). Most gas produced from the unit in the WRSB is from the “upper sandy member,” including Madden field. Marine sandstone, interbedded with shale and bentonite beds, serve as the reservoirs in the upper sandy member. Intraformational shales within the unit serve as local seals to the hydrocarbon accumulations in the reservoir sandstones (Johnson and others, 2007). Sandstones in the upper sandy member are identified informally as the “Shannon and Sussex sandstones” (Dunleavy and Gilbertson, 1986). Thickness of the upper sandy member in the Madden field area is about 3,000 ft (Johnson and others, 2007, fig. 8).

At Madden field, the Shannon and Sussex sandstones are very fine- to fine-grained, moderately sorted, subrounded to subangular, and shaley (Dunleavy and Gilbertson, 1986, and references therein). Porosity and permeability (as well as productivity) of these reservoir sandstones at Madden field largely are controlled by fractures along the crest of the Madden anticline (Dunleavy and Gilbertson, 1986).

The deeply buried Cody Shale in the Madden field is overpressured (Johnson and others, 2007; Nelson and others, 2009). Two studies (Nelson and Kibler, 2007; Nelson and others, 2009) considered the Cody Shale to be within the lowermost of two stacked overpressured pressure compartments in the Madden field area. The lower pressure compartment containing the Cody Shale extends from the top of the Mesaverde Formation downward to a base described as being located “somewhat below the base of the Cretaceous” (Nelson and Kibler, 2007, p. 23) or alternatively at the top of the Jurassic Morrison Formation (Nelson and others, 2009). Gas and water production from tight-gas accumulations in the Cody Shale and two other formations (Mesaverde Formation and lower Fort Union Formation) within the Madden field area showed little or no correlation between gas and water production (Nelson and others, 2009).

Because the formation is composed substantially of marine shale, the Cody Shale in the WRSB is classified as a basinwide confining unit or leaky confining unit (Richter, 1981). Sandstones and fractured zones of the formation may potentially yield small quantities of water to groundwater wells, although deep burial and poor water quality likely limits most potential uses (Richter, 1981; Bartos and others, 2012).

TDS concentrations in Shannon sandstone produced-water samples from Madden field ranged from 1,640 to 22,098 mg/L, with a median of 9,678 mg/L (N=4) (Blondes and others, 2017). Waters were brackish (TDS=1,000 to 10,000 mg/L) and saline (TDS>10,000 mg/L). All waters were sodium-chloride type. Sample-collection depths ranged from about 17,000 to 17,900 ft bls.

4.5 Madison Limestone (Madden field)

The Mississippian Madison Limestone (or Madison Formation) in the WRSB consists of marine carbonate strata of varying lithology (Keefer and Van Lieu, 1966; Westphal and others, 2004). The formation is unconformably overlain by the Mississippian and Pennsylvanian Amsden Formation and unconformably underlain by the Devonian Darby Formation. Thickness of the Madison Limestone in the Madden field area ranges from 300 to more than 400 ft (Keefer and Van Lieu, 1966, fig. 14).

Substantial quantities of gas are produced from Madden field wells completed in deeply buried Madison reservoirs (between 23,600 to 24,400 ft bls; Nelson and others, 2009). The highest gas-production rates in Madden field are from the Madison Limestone (Nelson and others, 2009, pl. 7).

Gas produced from the Madison Limestone at Madden field is dry (no condensate produced) (Nelson others, 2009). Nelson and others (2009) attributed water-gas ratios of about 10 bbl/mmcf to water in solution in reservoir gas, and the investigators noted the “dissolved water volume is high because of a reservoir temperature of 420 degrees Fahrenheit (°F) (Brown and Shannon, 1989).”

Westphal and others (2004) concluded Madison Limestone reservoir quality variations in the WRSB are the result of a combination of cyclic stacking of reservoir facies, diagenetic overprinting by dolomitization, and late-stage hydrothermal brecciation and calcite cementation. Extensively brecciated limestone at the top of the formation in the WRSB and at Madden field creates a seal for the lower parts/underlying carbonate sequences of the unit (Westphal and others, 2004; Kirschbaum and others, 2007). Low-permeability beds bounding internal carbonate sequences serve as vertical seals and flow boundaries (Westphal and others, 2004). Within individual carbonate sequences, late-stage calcite cement surrounding the clasts of hydrothermal breccias can create horizontal flow barriers.

Water-saturated and permeable parts of the Madison Limestone compose the Madison aquifer in the WRB (Richter, 1981). The Madison aquifer is overlain by the Amsden aquifer and underlain by the Darby aquifer, composed of the Amsden and Darby Formations, respectively (Richter, 1981). No regional confining units separate the Madison aquifer from these two aquifers. The Madison aquifer is used as a source of water for domestic, commercial, stock, public supply, industrial, and (rarely) irrigation purposes, primarily along the WRSB margin where the aquifer crops out or is buried at relatively shallow depths (Bartos and others, 2012). Water typically is confined, and most wells flow at land surface due to artesian pressure.

Permeability in the Madison aquifer is primarily secondary and is attributed to solution-enhanced fractures, joints, and caverns (Whitcomb and Lowry, 1968; McGreevy and others, 1969; Richter, 1981). Primary permeability is very low to nonexistent because of the dense and finely crystalline structure of the carbonates composing the aquifer (Richter, 1981). Without development of secondary permeability, well yields in the Madison Limestone are likely to be relatively small. The most productive (permeable) parts of the Madison Limestone are in areas with substantial fractures and cavernous zones (Whitcomb and Lowry, 1968; McGreevy and others, 1969; Richter, 1981; Jorgensen Engineering and Land Surveying, 1995).

A produced groundwater-quality sample collected from the Madison Limestone at a depth of 23,758 ft bls at Madden field had a TDS concentration (370 mg/L) indicating freshwater (fresh=TDS<1,000 mg/L). The water was a sodium-chloride type. It is unclear if this groundwater-quality sample represents the true chemical composition of Madison Limestone waters at Madden field because this sample is much fresher than expected for a sample collected from this depth and from a reservoir known for high temperatures (420°F; Brown and Shannon, 1989). Kharaka and Hanor (2003) indicate that chemical analyses from gas wells completed in high-temperature reservoirs may not represent the true chemical composition of formation waters because of dilution by condensed water vapor produced with natural gas. The investigators note that “water vapor condenses because of the drop in temperature and pressure as the gases expand on entering the well” and that “this problem is not generally recognized and is probably responsible for many of the reports of fresh or brackish water in petroleum reservoirs” (Kharaka and Hanor, 2003, p. 5).

5. CONCLUSION

Hydrocarbons (gas and oil) are produced from deeply buried siliciclastic and carbonate reservoirs in numerous lithostratigraphic units found in the various Laramide structural basins of Wyoming. In many cases, reservoir extent represents only a small percentage of the total thickness and (or) areal extent of the lithostratigraphic unit hosting the reservoir.

Production is from both conventional-style stratigraphic and (or) structural traps as well as unconventional continuous accumulations. Some lithostratigraphic units contain both types of accumulation. Many reservoirs are low-permeability “tight” sandstones.

Pressures measured in the reservoirs can be normal (hydrostatic) or anomalous (under or overpressured), but these within-reservoir pressures may not be the same as the adjacent lithofacies or host lithostratigraphic unit surrounding the reservoir. Reservoir fluids typically are multi-phase accumulations, consisting of oil, gas, and (or) groundwater in varying proportions. In the structural basins examined, many of these multi-phase hydrocarbon-bearing reservoirs are found within areas of basinwide cross-formational overpressure. Above the overpressured zone, pressures typically are normal or near-normal, and fluids largely consist of a single phase (groundwater). Groundwater in this shallower normally pressured zone is in hydrologic/hydraulic connection with local and regional groundwater-flow systems associated with meteoric groundwater circulation. Furthermore, waters circulating in the shallow system likely are hydrologically disconnected from the underlying overpressured areas/reservoirs to varying degrees by different types of low permeability/impermeable barriers. Aquifers used to provide water for most uses are located within the shallow normally pressured zone; waters from these aquifers are much fresher than waters from the underlying reservoirs/aquifers present at depths sufficient for petroleum generation and accumulation.

Groundwater coproduced with the hydrocarbons varies widely in both quantity and quality. Coproduced water salinity ranges from brackish (TDS=1,000-10,000 mg/L) to saline (TDS >10,000 mg/L), and sodium and chloride are almost always the predominant ions regardless of salinity.

CONTRIBUTIONS AND ACKNOWLEDGMENTS

Timothy Bartos and Laura Hallberg wrote and revised this chapter manuscript. Both authors reviewed the chapter manuscript. Scott Quillinan (former project manager) and Timothy Bartos conceived of the work presented in this chapter. Funding for this work was provided by U.S. Department of Energy, Geothermal Technologies Office under Award DE-EE0007603. The authors would like to thank our DOE project managers Holly Thomas and Josh Mengers and also our Technical Monitoring Team for their support, advice, and insight. Peter Wright and Greg Boughton (both USGS) provided helpful reviews of this chapter.

REFERENCES

- Ahern, J., Collentine, M., and Cook, S.: Occurrence and characteristics of groundwater in the Green River Basin and Overthrust Belt, Wyoming. report prepared for U.S. Environmental Protection Agency, Water Resources Research Institute, University of Wyoming, Laramie, Wyoming, **V-A**, (1981), 123 p.
- Anna, L.O.: Geologic assessment of undiscovered oil and gas in the Powder River Basin Province Wyoming and Montana. In Total Petroleum Systems and Geologic Assessment of Oil and Gas Resources in the Powder River Basin Province, Wyoming and Montana. U.S. Geological Survey Series DDS-69-U, chap. 1, (2010 [revised April 2010]), 97 p.
- Babcock, H.M., and Morris, D.A.: Ground water in the vicinity of Edgerton, Wyoming. U.S. Geological Survey Open-File Report 54-13, (1954), 9 p. [Number assigned after report was published].
- Banner Associates, Inc.: Powder River water supply level I study. report prepared for the Wyoming Water Development Commission, (2002), 53 p.
- Bartberger, C.E., and Pasternack, Ira: Spontaneous potential—Key to understanding continuous and conventional gas in Upper Cretaceous sandstones, deep eastern Greater Green River Basin, southwest Wyoming. American Association of Petroleum Geologists *Bulletin*, **99**(5), (2015), p. 889–925.
- Bartos, T.T., and Hallberg, L.L.: Groundwater and hydrogeologic units. In Clarey, K.E., Bartos, T.T., Copeland, David, Hallberg, L.L., Clark, M.L., and Thompson, M.L., Available groundwater determination technical memorandum—WWDC Green River Basin Water Plan II—Groundwater study, level I (2007–2009). Wyoming State Geological Survey, Laramie, Wyo., chapter 5, (2010), p. 5-1–5-93.
- Bartos, T.T., Hallberg, L.L., and Clark, M.L.: Groundwater quality. In Clarey, K.E., Bartos, T.T., Copeland, David, Hallberg, L.L., Clark, M.L., and Thompson, M.L., Available groundwater determination technical memorandum—WWDC Green River Basin Water Plan II—Groundwater study, level I (2007–2009). Wyoming State Geological Survey, Laramie, Wyo., chap. 6, (2010), p. 6-1–6-94.
- Bartos, T.T., Hallberg, L.L., and Clark, M.L.: WBRB [Wind/Bighorn River Basin] hydrogeologic units—physical and chemical characteristics. Chapter 7 of Taucher, Paul, Bartos, T.T., Clarey, K.E., Quillinan, S.A., Hallberg, L.L., Clark, M.L., Thompson, Melissa, Gribb, Nikolaus, Worman, Brett, and Gracias, Tomas, 2012, Available groundwater determination technical memorandum, WWDC [Wyoming Water Development Commission] Wind/Bighorn River Basin water plan update, Groundwater study level I (2008–2011), report prepared by the Wyoming State Geological Survey for the Wyoming Water Development Commission, Laramie, Wyo., (2012), p. 7-101–7-179.
- Bartos, T.T., Hallberg, L.L., and Clark, M.L.: Northeastern River Basins hydrogeologic units—physical and chemical characteristics, Chapter 7 of Available groundwater determination technical memorandum, WWDC [Wyoming Water Development Commission]

- Northeastern River Basins water plan update. Groundwater study level 1, report prepared by the Wyoming State Geological Survey for the Wyoming Water Development Commission, Laramie, Wyo., (2018 [in press]).
- Becker, T.P., and Lynds, R.: A geologic deconstruction of one of the world's largest natural accumulations of CO₂, Moxa arch, southwestern Wyoming. *American Association of Petroleum Geologists Bulletin*, **96**(9), (2012), p. 1643–1664.
- Blondes, M.S., Gans, K.D., Engle, M.A., Kharaka, Y.K., Reidy, M.E., Saraswathula, V., Thordsen, J., Rowan, E.L., Morrissey, E.A.: U.S. Geological Survey National Produced Waters Geochemical Database, version 2.3. U.S. Geological Survey, (2017). Retrieved from <https://energy.usgs.gov/EnvironmentalAspects/EnvironmentalAspectsofEnergyProductionandUse/ProducedWaters.aspx#3822349-data>
- Brown, R.G., and Shannon, L.T.: The #2–3 Bighorn—An ultra-deep confirmation well on the Madden anticline. In *Gas resources of Wyoming. 40th Annual Field Conference Guidebook*, Wyoming Geological Association, (1989), p. 181–187.
- Busby, J.F., Kimball, B.A., Downey, J.S., and Peter, K.D.: Geochemistry of water in aquifers and confining units of the Northern Great Plains in parts of Montana, North Dakota, South Dakota, and Wyoming. U.S. Geological Survey Professional Paper 1402–F, U.S. Geological Survey, (1995), 146 p.
- Buursink, M.L., Slucher, E.R., Brennan, S.T., Doolan, C.A., Drake, R.M., II, Merrill, M.D., Warwick, P.D., Blondes, M.S., Freeman, P.A., Cahan, S.M., DeVera, C.A., and Lohr, C.D.: Geologic framework for the national assessment of carbon dioxide storage resources—Greater Green River Basin, Wyoming, Colorado, and Utah, and Wyoming-Idaho-Utah Thrust Belt. Chap. E of Warwick, P.D., and Corum, M.D. (Eds.), *Geologic framework for the national assessment of carbon dioxide storage resources*. U.S. Geological Survey Open-File Report 2012–1024–E, U.S. Geological Survey, (2014), 50 p., <http://dx.doi.org/10.3133/ofr20121024E>.
- Byers, C.W., and Larson, D.W.: Paleoenvironments of Mowry Shale (Lower Cretaceous), western and central Wyoming. *American Association of Petroleum Geologists Bulletin*, **63**(3), (1979), p. 354–375.
- Campbell-Stone, E., Lynds, R., Frost, C., Becker, T.P., Diem, B.: The Wyoming carbon underground storage project—geologic characterization of the Moxa arch and Rock Springs uplift. *Energy Procedia* **4**, (2011), p. 4656–4663.
- Cardinal, D.F., and Stewart, W.W.: Wyoming Oil and Gas Fields Symposium, Greater Green River Basin. Wyoming Geological Association, (1979), 428 p.
- Collentine, M., Libra, R., Feathers, K.R., and Hamden, L.: Occurrence and characteristics of groundwater in the Great Divide and Washakie Basins, Wyoming. Report for U.S. Environmental Protection Agency, Water Resources Research Institute, University of Wyoming, Laramie, Wyoming, **VI-A**, (1981), 112 p.
- Craddock, W.H., Drake, R.M., II, Mars, J.C., Merrill, M.D., Warwick, P.D., Blondes, M.S., Gosai, M.A., Freeman, P.A., Cahan, S.M., DeVera, C.A., and Lohr, C.D.: Geologic framework for the national assessment of carbon dioxide storage resources—Powder River Basin, Wyoming, Montana, South Dakota, and Nebraska. Chap. B of Warwick, P.D., and Corum, M.D. (Eds.), *Geologic framework for the national assessment of carbon dioxide storage resources*. U.S. Geological Survey Open-File Report 2012–1024–B, U.S. Geological Survey, (2012), 30 p.
- Crist, M.A., and Lowry, M.E.: Ground-water resources of Natrona County, Wyoming. U.S. Geological Survey Water-Supply Paper 1897, U.S. Geological Survey, (1972), 92 p., 3 pls.
- DeChadenedes, J.F.: Frontier deltas of the western Green River Basin, Wyoming. In *Deep drilling frontiers of the central Rocky Mountains*. Rocky Mountain Association of Geologists Symposium, 1975, Denver, Colo., (1975), p. 149–157.
- Dogan, U.D.: Stratigraphy, petrology, depositional and post-depositional histories and their effects upon reservoir properties of the Parkman Formation of the Mesaverde Group, Powder River Basin, Wyoming. Ph.D. thesis, University of Iowa, Iowa City, Iowa, (1984), 265 p.
- Downey, J.S.: Geohydrology of bedrock aquifers in the Northern Great Plains in parts of Montana, North Dakota, South Dakota, and Wyoming. U.S. Geological Survey Professional Paper 1402–E, U.S. Geological Survey, (1986), 87 p.
- Downey, J.S., and Dinwiddie, G.A.: The regional aquifer system underlying the northern Great Plains in parts of Montana, North Dakota, South Dakota, and Wyoming—Summary. U.S. Geological Survey Professional Paper 1402–A, U.S. Geological Survey, (1988), 64 p.
- Dunleavy, J.M., and Gilbertson, R.L.: Madden anticline—growing giant. *Rocky Mountain Oil and Gas Fields Symposium*, Wyoming Geological Association, (1986), p. 107–157.
- Dutton, S.P., Hamlin, H.S., and Laubach, S.E.: Geologic controls on reservoir properties of low-permeability sandstone, Frontier Formation, Moxa arch, southwest Wyoming. *Gas Research Institute publication GRI–92/012*, (1992), 199 p.
- Feathers, K.R., Libra, Robert, and Stephenson, T.R.: Occurrence and characteristics of ground water in the Powder River Basin, Wyoming. Water Resources Research Institute, University of Wyoming, Laramie, Wyoming, **I(A, B)**, (1981), 171 p., 4 append., 8 pls..
- Finn, T.M.: Subsurface stratigraphic cross sections of Cretaceous and lower tertiary rocks in the Wind River Basin, central Wyoming. In *USGS Wind River Basin Province Assessment Team, Petroleum systems and geologic assessment of oil and gas in the Wind River Basin Province, Wyoming*. U.S. Geological Survey Digital Data Series DDS–69–J, ch. 9, (2007), 28 p.

- Finn, T.M., and Johnson, R.C.: The Hilliard-Baxter-Mancos Total Petroleum System, Southwestern Wyoming Province. Chap. 7 of USGS Southwestern Wyoming Province Assessment Team (Eds.), Petroleum systems and geologic assessment of oil and gas in the Southwestern Wyoming Province, Wyoming, Colorado, and Utah. U.S. Geological Survey Digital Data Series DDS-69-D, version 1.0, (2005a), 43 p.
- Finn, T.M., and Johnson, R.C.: Subsurface stratigraphic cross sections of Cretaceous and lower Tertiary rocks in the Southwestern Wyoming Province, Wyoming, Colorado, and Utah. Chap. 14 in USGS Southwestern Wyoming Province Assessment Team (Eds.), Petroleum systems and geologic assessment of oil and gas in the Southwestern Wyoming Province, Wyoming, Colorado, and Utah. U.S. Geological Survey Digital Data Series DDS-69-D, version 1.0, (2005b), 43 p.
- Finn, T.M., Johnson, R.C., and Roberts, S.B.: The Mesaverde-Lance-Fort Union composite total petroleum system, southwestern Wyoming province, Wyoming, Colorado, and Utah. Chapter 10 of Petroleum systems and geologic assessment of oil and gas in the southwestern Wyoming province, Wyoming, Colorado, and Utah. U.S. Geological Survey Digital Data Series DDS-69-D, (2005), 33 p., https://pubs.usgs.gov/dds/dds-069/dds-069-d/REPORTS/69_D_CH_10.pdf.
- Fisk, E.P.: Groundwater geology and hydrology of the Great Divide and Washakie Basins, south-central Wyoming. M.S. thesis, University of Southern California, Los Angeles, Calif., (1967), 132 p.
- Flores, R.M., Clark, A.C., Keighin, W.C.: Architecture of Fort Union paleovalley conglomerates related to aquifer potential in the western Wind River Basin, Wyoming. In Keefer, W.R., Metzger, W.J., and Godwin, L.H. (Eds.), Oil and gas and other resources of the Wind River Basin, Wyoming. Special Symposium Guidebook, 1993, Wyoming Geological Association, (1993), p. 143-162.
- Forster, J.F., and Horne, J.C.: The interpretation of fluids and pressures in determining conventional and unconventional gas resources in the Rocky Mountain region. Chapter 7 of Bishop, M.G., Cumella, S.P., Robinson, J.W., and Silverman, M.R. (Eds.), Gas in low permeability reservoirs of the Rocky Mountain region. Rocky Mountain Association of Geologists 2005 Guidebook, Denver, Colo., (2005), p. 187-210.
- Fox, J.E., and Higley, D. K.: Thickness of Upper Cretaceous Mesaverde Formation, Powder River Basin, Wyoming and Montana. U.S. Geological Survey Open-File Report 87-340-D, U.S. Geological Survey, (1987a), 1 sheet, scale 1:500,000.
- Fox, J.E., and Higley, D. K.: Thickness of the Teapot Sandstone Member of the Upper Cretaceous Mesaverde Formation, Powder River Basin, Wyoming and Montana. U.S. Geological Survey Open-File Report 87-340-I, U.S. Geological Survey, (1987b), 1 sheet, scale 1:500,000.
- Fox, J.E., and Higley, D. K.: Thickness of Parkman Sandstone Member of the Upper Cretaceous Mesaverde Formation and the Redbird Silty Member of the Upper Cretaceous Pierre Shale, Powder River Basin, Wyoming and Montana. U.S. Geological Survey Open-File Report 87-340-E, U.S. Geological Survey, (1987c), 1 sheet, scale 1:500,000.
- Freethy, G.W., and Cordy, G.E.: Geohydrology of Mesozoic rocks in the Upper Colorado River Basin in Arizona, Colorado, New Mexico, Utah, and Wyoming, excluding the San Juan Basin. U.S. Geological Survey Professional Paper 1411-C, U.S. Geological Survey, (1991), 118 p.
- Freethy, G.W., Kimball, B.A., Wilberg, D.E., and Hood, J.W.: General hydrogeology of the aquifers of Mesozoic age, Upper Colorado River Basin, excluding the San Juan Basin, Colorado, Utah, Wyoming, and Arizona. U.S. Geological Survey Hydrologic Investigations Atlas HA-698, U.S. Geological Survey, (1988), 2 sheets, scale 1:2,500,000.
- Garcia-Gonzalez, Mario, MacGowan, D.B., and Surdam, R.C.: Mechanisms of petroleum generation from coal, as evidenced from petrographic and geochemical studies—Examples from Almond Formation coals in the Greater Green River Basin. In Stroock, Betty, and Andrew, Sam (Eds.), Jubilee Anniversary Field Conference Guidebook. Wyoming Geological Association, (1993), p. 311-321.
- Geldon, A.L.: Geology of Paleozoic rocks in the Upper Colorado River Basin in Arizona, Colorado, New Mexico, Utah, and Wyoming, excluding the San Juan Basin. U.S. Geological Survey Professional Paper 1411-A, U.S. Geological Survey, (2003a), 85 p., 17 pls. and 1 oversize table in pocket.
- Geldon, A.L.: Hydrologic properties and ground-water flow systems of the Paleozoic rocks in the Upper Colorado River Basin in Arizona, Colorado, New Mexico, Utah, and Wyoming, excluding the San Juan Basin. U.S. Geological Survey Professional Paper 1411-B, U.S. Geological Survey, (2003b), 153 p., 13 pls. In separate volume.
- Gill, J.R., and Burkholder, R.R.: Measured sections of the Montana Group and equivalent rocks from Montana and Wyoming. U.S. Geological Survey Open-File Report 79-1143, U.S. Geological Survey, (1979), 202 p.
- Gill, J.R., and Cobban, W.A.: The Red Bird section of the Upper Cretaceous Pierre Shale in Wyoming, with a section on A new echinoid from the Cretaceous Pierre Shale of eastern Wyoming, by P.M. Kier. U.S. Geological Survey Professional Paper 393-A, U.S. Geological Survey, (1966a), p. A1-A73.
- Gill, J.R., and Cobban, W.A.: Regional unconformity in Late Cretaceous, Wyoming. U.S. Geological Survey Professional Paper 550-B, U.S. Geological Survey, (1966b), p. B20-B27.
- Gill, J.R., and Cobban, W.A.: Stratigraphy and geologic history of the Montana Group and equivalent rocks, Montana, Wyoming, and North and South Dakota. U.S. Geological Survey Professional Paper 776, U.S. Geological Survey, (1973), 37 p.
- Gill, J.R., Merewether, F.A., and Cobban, W.A.: Stratigraphy and nomenclature of some Upper Cretaceous and lower Tertiary rocks in south-central Wyoming. U.S. Geological Survey Professional Paper 667, U.S. Geological Survey, (1970), 53 p.

- Hares, C.J.: Anticlines in central Wyoming. U.S. Geological Survey Bulletin 641-I, U.S. Geological Survey, (1916), p. 233–279.
- Heasler, H.P., and Surdam, R.C.: Pressure compartments in the Mesaverde Formation of the Green River and Washakie Basins, as determined from drill-stem test data. In Mullen, C.E. (Ed.), *Rediscover the Rockies. Forty-Third Field Conference Guidebook*, Wyoming Geological Association, (1992), p. 207–220.
- Heasler, H.P., Surdam, R.C., and George, J.H.: Pressure compartments in the Powder River Basin, Wyoming and Montana, as determined from drill-stem test data. In Ortoleva, P.J. (Ed.), *Basin compartments in seals: American Association of Petroleum Geologists Memoir 61*, (1994), p. 235–262.
- Hettinger, R.D., and Roberts, L.N.R.: Lewis total petroleum system of the southwestern Wyoming province, Wyoming, Colorado, and Utah. Chapter 9 of *Petroleum systems and geologic assessment of oil and gas in the southwestern Wyoming province, Wyoming, Colorado, and Utah*, U.S. Geological Survey Digital Data Series DDS-69-D, (2005), 39 p., https://pubs.usgs.gov/dds/dds-069/dds-069-d/REPORTS/69_D_CH_9.pdf.
- Hodson, W.G., Pearl, R.H., and Druse, S.A.: Water resources of the Powder River Basin and adjacent areas, northeastern Wyoming. U.S. Geological Survey Hydrologic Investigations Atlas HA-465, U.S. Geological Survey, (1973 [1974]), 4 sheets.
- Hose, R.K.: Geology of the Crazy Woman Creek area, Johnson County, Wyoming. U.S. Geological Survey Bulletin 1027-B, U.S. Geological Survey, (1955), p. 33–118.
- Huang, N.S., Aho, G.E., Baker, B.H., Matthews, T.R., and Pottorf, R.J.: Integrated reservoir modeling to maximize the value of a large sour-gas field with high concentrations of inerts. *International Petroleum Technology Conference 11202*, (2007), 16 p.
- Hunt, L.M.: Generation and migration of petroleum from abnormally pressured fluid compartments. *American Association of Petroleum Geologists Bulletin*, **74**(1), (1990), p. 1–12.
- Jiao, Z.S., and Surdam, R.C.: Characteristics of anomalously pressured Cretaceous shales in the Laramide basins of Wyoming. In Surdam, R.C. (Ed.), *Seals, traps, and the petroleum system*. American Association of Petroleum Geologists Memoir 67, (1997), p. 243–254.
- Johnson, R.C., Finn, T.M. and Roberts, L.N.R.: The Mesaverde total petroleum system, southwestern Wyoming province. Chapter 8 of *Petroleum systems and geologic assessment of oil and gas in the southwestern Wyoming province, Wyoming, Colorado, and Utah*. U.S. Geological Survey Digital Data Series DDS-69-D, (2005), 38 p.
- Johnson, R.C., Finn, T.M., Kirschbaum, M.A., Roberts, S.B., Roberts, Laura N.R., Cook, Troy, and Taylor, D.J.: The Cretaceous-lower Tertiary composite total petroleum system, Wind River Basin, Wyoming. In U.S. Geological Survey Wind River Basin province assessment team, *Petroleum systems and geologic assessment of oil and gas in the Wind River Basin Province, Wyoming*. U.S. Geological Survey Digital Data Series DDS-69-J, ch. 4, (2007), 96 p.
- Jorgensen Engineering and Land Surveying, in association with Hinckley Consulting, and Hydrokinetics, Inc.: Final level II (Phase III) study report, Upper Little Warm Springs water supply project. Prepared for the Wyoming Water Development Commission, (1995), variously paged.
- Kaszuba, J.P., Navarre-Sitchler, A., Thyne, G., Chopping, C., Meuzelaar, T.: Supercritical carbon dioxide and sulfur in the Madison Limestone: A natural analog in southwest Wyoming for geologic carbon-sulfur co-sequestration. *Earth and Planetary Science Letters*, **309**, (2011), p. 131–140.
- Keefer, W.R.: Stratigraphy and geologic history of the uppermost Cretaceous, Paleocene, and lower Eocene rocks in the Wind River Basin, Wyoming. U.S. Geological Survey Professional Paper 495-A, U.S. Geological Survey, (1965), 77 p.
- Keefer, W.R.: Frontier, Cody, and Mesaverde Formations in the Wind River Basin and southern Bighorn Basins, Wyoming. U.S. Geological Survey Professional Paper 495-E, U.S. Geological Survey, (1972), 23 p.
- Keefer, W.R., and Van Lieu, J.A.: Paleozoic formations in the wind River basin, Wyoming. U.S. Geological Survey Professional Paper 495-D, U.S. Geological Survey, (1966), 60 p., 6 pl.
- Keighin, C.W., Law, B.E., and Pollastro, R.M.: Petrology and reservoir characteristics of the Almond Formation, Greater Green River Basin, Wyoming. In Coalson, E.B., and others (Eds.), *Petrogenesis and petrophysics of selected sandstone reservoirs of the Rocky Mountain region*. Rocky Mountain Association of Geologists, Denver, Colo., (1989), p. 281–298.
- Kharaka, Y.K., and Hanor, J.S.: Deep fluids in the continents [5.16]—I. Sedimentary basins. In Drever, J.I. (Ed.), *Treatise on geochemistry*, **5**, Elsevier, (2003), p. 1–48.
- Kirschbaum, M.A., and Roberts, L.N.R.: Geologic assessment of undiscovered oil and gas resources in the Mowry composite total petroleum system, southwestern Wyoming province, Wyoming, Colorado, and Utah. Chapter 5 of *Petroleum systems and geologic assessment of oil and gas in the southwestern Wyoming province, Wyoming, Colorado, and Utah*. U.S. Geological Survey Digital Data Series DDS-69-D, (2005a), 23 p., https://pubs.usgs.gov/dds/dds-069/dds-069-d/REPORTS/69_D_CH_5.pdf.
- Kirschbaum, M.A., and Roberts, L.N.R.: Stratigraphic framework of the Cretaceous Mowry Shale, Frontier Formation and adjacent units, southwestern Wyoming province, Wyoming, Colorado, and Utah. Chapter 15 of *Petroleum systems and geologic assessment of oil and gas in the southwestern Wyoming province, Wyoming, Colorado, and Utah*. U.S. Geological Survey Digital Data Series DDS-69-D, (2005b), 23 p., https://pubs.usgs.gov/dds/dds-069/dds-069-d/REPORTS/69_D_CH_15.pdf.

- Kirschbaum, M.A., Lillis, P.G., and Roberts, L.N.R.: Geologic assessment of undiscovered oil and gas resources in the Phosphoria Total Petroleum System of the Wind River Basin Province, Wyoming. In USGS Wind River Basin Province assessment team, Petroleum systems and geologic assessment of oil and gas in the Wind River Basin Province, WYOMING. U.S. Geological Survey Digital Data Series DDS-69-J, ch. 3, (2007), 27 p., https://pubs.usgs.gov/dds/dds-069/dds-069-j/REPORTS/69_J_CH_3.pdf.
- Kohout, F.A.: Geology and ground-water resources of the Kaycee irrigation project, Johnson County, Wyoming, with a section on Chemical quality of the ground water, by F.H. Rainwater. U.S. Geological Survey Water-Supply Paper 1360-E, U.S. Geological Survey, (1957), p. 321–374.
- Kreitler, C.W.: Hydrogeology of sedimentary basins. *Journal of Hydrology*, **106**(1-2), (1989), p. 29–53.
- Law, B.E.: Relationships of source-rock, thermal maturity, and overpressuring to gas generation and occurrence in low-permeability Upper Cretaceous and lower Tertiary rocks, Greater Green River Basin, Wyoming, Colorado and Utah. In Woodward, J., Meissner, F.F., and Clayton, J.L. (Eds.), Hydrocarbon source rocks of the greater Rocky Mountain Region. Rocky Mountain Association of Geologists Guidebook, (1984), p. 469–490.
- Law, B.E.: Southwestern Wyoming Province (037). In Gauthier, D.L., Dolton, G.L., Takahashi, K.I., and Varnes, K.L. (Eds.), 1995 National assessment of United States oil and gas resources—Results, methodology, and supporting data. U.S. Geological Survey Digital Data Series DDS-30, (1996), release 2.
- Law, B.E.: Basin-centered gas systems. American Association of Petroleum Geologists *Bulletin*, **86**(11), 2002, p. 1891–1919.
- Law, B.E., and Dickinson, W.W.: A conceptual model for the origin of abnormally pressured gas accumulations in low-permeability reservoirs. American Association of Petroleum Geologists *Bulletin*, **69**, (1985), p. 1295–1304.
- Law, B.E., Spencer, C.W., Charpentier, R.R., Crovelli, R.A., Mast, R.F., Dolton, G.L., and Wandrey, C.J.: Estimates of gas resources in overpressured low-permeability Cretaceous and Tertiary sandstone reservoirs, Greater Green River Basin, Wyoming, Colorado, and Utah. In Eisert, J.L. (Ed.), Gas resources of Wyoming. Fortieth Field Conference Guidebook, Wyoming Geological Association, (1989), p. 39–61.
- Lehrer, M.G.: Revitalizing the Moxa Arch—exploiting resource play. *The Mountain Geologist*, **43**, (2006), p. 201–205.
- Love, J.D., Christiansen, A.C., and Ver Ploeg, A.J., compilers: Stratigraphic chart showing Phanerozoic nomenclature for the State of Wyoming: Geological Survey of Wyoming Map Series MS-41, Geological Survey of Wyoming, Laramie, (1993), 1 sheet.
- Lowry, M.E., and Cummings, T.R.: Ground-water resources of Sheridan County, Wyoming. U.S. Geological Survey Water-Supply Paper 1807, U.S. Geological Survey, (1966), 77 p., 1 pl.
- Mapel, W.J.: Geology and coal resources of the Buffalo-Lake De Smet area, Johnson and Sheridan Counties, Wyoming. U.S. Geological Survey Bulletin 1078, U.S. Geological Survey, (1959), 148 p.
- Martinsen, R.S.: Stratigraphic compartmentation of reservoir sandstones—examples from the Muddy Sandstone, Powder River Basin, Wyoming. In Ortoleva, P.J. (Ed.), Basin compartments and seals. American Association of Petroleum Geologists Memoir 61, (1994), p. 273–296.
- Martinsen, R.S.: Compartmentalization of sandstone reservoirs due to syndepositional faulting, Almond Formation, Washakie Basin, Wyoming. In Slatt, R.M. (Ed.), Compartmentalized reservoirs in Rocky Mountain Basins. Rocky Mountain Association of Geologists Symposium, (1998), p. 71–98.
- Martinsen, R.S., and Christensen, G.: A stratigraphic and environmental study of the Almond Formation, Mesaverde Group, Greater Green River Basin, Wyoming. In Mullen, C.E. (Ed.), Rediscover the Rockies. Forty-Third Field Conference Guidebook, Rocky Mountain Association of Geologists, (1992), p. 171–190.
- Martinsen, R.S., Christiansen, G.E., Olson, M.A., and Surdam, R.C.: Stratigraphy and lithofacies of the Almond Formation, Washakie and Great Divide Basins, Wyoming. In Jones, R.W. (Ed.), Resources of southwestern Wyoming. Forty-Sixth Field Conference Guidebook, Wyoming Geological Association, (1995), p. 297–310.
- Masters, J.A.: Deep basin gas trap western Canada. American Association of Petroleum Geologists *Bulletin*, **63**(2), (1979), p. 151–181.
- McDonald, R.E.: Big Piney-La Barge producing complex, Sublette and Lincoln Counties, Wyoming. In North American oil and gas fields, American Association of Petroleum Geologists Memoir 24, (1976), p. 91–120.
- McGreevy, L.J., Hodson, W.G., and Rucker, S.J. IV: Ground-water resources of the Wind River Indian Reservation, Wyoming. U.S. Geological Survey Water-Supply Paper 1576-I, U.S. Geological Survey, (1969), 45 p., 3 pl.
- McPeck, L.A.: Eastern Green River Basin—A developing giant gas supply from deep, overpressured Upper Cretaceous sandstones. American Association of Petroleum Geologists *Bulletin*, **65**, (1981), p. 1078–1098.
- Merewether, E.A.: The Frontier Formation and mid-Cretaceous orogeny in the foreland of southwestern Wyoming. *The Mountain Geologist*, **20**, (1983), p. 121–138.
- Merewether, E.A.: Stratigraphy and tectonic implications of Upper Cretaceous rocks in the Powder River Basin, northeastern Wyoming and southeastern Montana. U.S. Geological Survey Bulletin 1917-T, U.S. Geological Survey, (1996), 92 p.

- Merewether, E.A., Cobban, W.A., and Cavanaugh, E.T.: Frontier Formation and equivalent rocks in eastern Wyoming. *The Mountain Geologist*, 6(3), (1979), p. 67–102.
- Merewether, E.A., Blackmon, P.D., and Webb, J.C.: The Mid-Cretaceous Frontier Formation near the Moxa arch, southwestern Wyoming. U.S. Geological Survey Professional Paper 1290, U.S. Geological Survey, (1984), 29 p.
- Merewether, E.A., Cobban, W.A., Matson, R.M., and Magathan, W.J.: Stratigraphic diagrams with electric logs of Upper Cretaceous rocks, Powder River Basin, Johnson, Campbell, and Crook Counties, Wyoming, Section A–A'. U.S. Geological Survey, Oil and Gas Investigations Chart OC–73, (1977a).
- Merewether, E.A., Cobban, W.A., Matson, R.M., and Magathan, W.J.: Stratigraphic diagrams with electric logs of Upper Cretaceous rocks, Powder River Basin, Natrona, Campbell, and Weston Counties, Wyoming, Section B–B'. U.S. Geological Survey Oil and Gas Investigations Chart OC–74, (1977b).
- Merewether, E.A., Cobban, W.A., Matson, R.M., and Magathan, W.J.: Stratigraphic diagrams with electric logs of Upper Cretaceous rocks, Powder River Basin, Natrona, Converse, and Niobrara Counties, Wyoming, Section C–C'. U.S. Geological Survey Oil and Gas Investigations Chart OC–75, (1977c).
- Merewether, E.A., Cobban, W.A., Matson, R.M., and Magathan, W.J.: Stratigraphic diagrams with electric logs of Upper Cretaceous rocks, Powder River Basin, Sheridan, Johnson, Campbell, and Converse Counties, Wyoming, Section D–D'. U.S. Geological Survey Oil and Gas Investigations Chart OC–76, (1977d).
- Miller, T.S., Crockett, F.J., and Hollis, S.H.: Wyoming oil and gas fields symposium, Greater Green River Basin and Overthrust Belt. Wyoming Geological Association Symposium, (1992), 372 p.
- Montgomery, S.L., Barrett, Fred, Vickery, Kim, Natali, Steve, Roux, Roy, and Dea, Peter: Cave Gulch field—large gas discovery in the Rocky Mountain foreland, Wind River Basin. American Association of Petroleum Geologists *Bulletin*, 85(9), (2001), p. 1543–1564.
- Muller, M.M., and Coalson, E.B.: Diagenetic and petro-physical variations of the Dakota Sandstone, Henry Field, Green River Basin, Wyoming. In Coalson, E.B., Kaplan, S.S., Keighin, C.W., Oglesby, C.A., and Robinson, J.W. (Eds.), Petrogenesis and petrophysics of selected sandstone reservoirs of the Rocky Mountain Region. Rocky Mountain Association of Geologists, (1989), p. 149–158.
- National Groundwater Association: Brackish groundwater. Information Brief, September 25, 2017, National Groundwater Association (NGWA), (2018), https://www.ngwa.org/docs/default-source/default-document-library/publications/brackish-groundwater.pdf?sfvrsn=5c89617d_2 (accessed August 28, 2018).
- Nelson, P.H., and Kibler, J.E.: Distribution of fluids and pressures in the Wind River Basin, Wyoming. In USGS Wind River Basin Province Assessment Team, Petroleum and geologic assessment of oil and gas in the Wind River Basin Province, Wyoming. U.S. Geological Survey Digital Data Series DDS–69–J, ch. 7, (2007), 35 p.
- Nelson, P.H., Trainor, P.K., and Finn, T.M.: Gas, oil, and water production in the Wind River Basin, Wyoming. U.S. Geological Survey Scientific Investigations Report 2008–5225, U.S. Geological Survey, (2009), 23 p, 8 pls.
- Nelson, P.H., Ewald, S.M., Santus, S.L., and Trainor, P.K.: Gas, oil, and water production from Jonah, Pinedale, Greater Wamsutter, and Stagecoach Draw fields in the Greater Green River Basin, Wyoming. U.S. Geological Survey Open-File Report 2009–1290, U.S. Geological Survey, (2010), 19 p., 5 pls., <https://pubs.usgs.gov/of/2009/1290/>.
- Pyles, D.R.: A high-frequency sequence stratigraphic framework for the Lewis Shale and Fox Hills Sandstone, Great Divide and Washakie Basins, Wyoming. M.S. thesis, Colorado School of Mines, Golden, Colo., (2000), 261 p.
- Pyles, D.R., and Slatt, R.M.: A high-frequency sequence stratigraphic framework for shallow through deep-water deposits of the Lewis Shale and Fox Hills Sandstone, Great Divide and Washakie Basins, Wyoming. In Weimer, P., and others (Eds.), Deep-water reservoirs of the world [electronic resource]. 20th annual Bob F. Perkins Research Conference, December 3–6, 2000, Gulf Coast Section Society of Economic Paleontologists and Mineralogists Foundation, Houston, Texas, (2000), p. 836–861.
- Pyles, D.R., and Slatt, R.M.: Stratigraphic response to tectonic forcing in the Cretaceous Western Interior Seaway, Lewis Shale, south-central Wyoming. American Association of Petroleum Geologists, Rocky Mountain Section, Official Program with Abstracts, (2002), p. 36.
- Reid, S.G.: Madden Deep unit—Fremont, and Natrona Counties, Wyoming. *Earth Science Bulletin*, September 1978, Wyoming Geological Association, (1978), p. 34–42.
- Rich, E.I.: Reconnaissance geology of Hiland-Clarkson Hill area, Natrona County, Wyoming. U.S. Geological Survey Bulletin 1107–G, U.S. Geological Survey, (1962), p. 447–540.
- Richter, H.R., Jr.: Occurrence and characteristics of groundwater in the Wind River Basin, Wyoming. Water Resources Research Institute, University of Wyoming, Laramie, Wyoming, IV(A, B), (1981), variously paged, 11 pls.
- Roehler, H.W.: Stratigraphy of the Mesaverde Group in the central and eastern Greater Green River Basin, Wyoming, Colorado, and Utah. U.S. Geological Survey Professional Paper 1508, U.S. Geological Survey, (1990), 52 p.
- Ryer, T.A., McClurg, J.J., and Muller, M.M.: Dakota–Bear River paleoenvironments, depositional history and shoreline trends—implications for foreland basin paleotectonics, southwestern Green River Basin and southern Wyoming overthrust belt. In Miller,

- W.R. (Ed.), The Thrust Belt revisited. Wyoming Geological Association Annual Field Conference Guidebook, v. 38, (1987), p. 179–206.
- Scott, A.R., and Kaiser, W.R.: Hydrologic setting of the upper Mesaverde Group, Sand Wash Basin. In Kaiser, W.R., Scott, A.R., Hamilton, D.S., Tyler, R., McMurry, R.G., Zhou, N., and Tremain, C.M., Geologic and hydrologic controls on coalbed methane, Sand Wash Basin, Colorado and Wyoming. Report sponsored by and prepared for the Gas Research Institute [GRI topical report no. 92/0420], The University of Texas at Austin Bureau of Economic Geology and Colorado Geological Survey, (1994), p. 63–76.
- Shanley, K.W.: Fluvial reservoir description for a giant, low-permeability gas field: Jonah Field, Green River Basin, Wyoming, U.S.A. Chapter 10 in Robinson, J.W., and Shanley, K.W. (Eds.), Jonah Field: case study of a tight-gas fluvial reservoir. American Association of Petroleum Geologists Studies in Geology 52, Rocky Mountain Association of Geologists 2004 Guidebook, (2004), p. 37–59.
- Smith, M.S., Sharma, S., Wyckoff, T.B., and Frost, C.D.: Baseline geochemical characterization of potential receiving reservoirs for carbon dioxide in the Greater Green River Basin, Wyoming. *Rocky Mountain Geology*, **45** (2), (2010), p. 93–111.
- Sonnenfeld, M.D.: Sequence evolution and hierarchy within the lower Mississippian Madison Limestone of Wyoming. In Longman, M.W., and Sonnenfeld, M.D. (Eds.), Paleozoic systems of the Rocky Mountain region. SEPM Rocky Mountain Section, (1996), p. 165–192.
- Stands, R.E.: Depositional sequence analysis of the Upper Cretaceous Frontier Formation, Darby thrust—Moxa arch area, southwestern Wyoming. Ph.D. dissertation, Colorado School of Mines, Golden, Colorado, (1999), 619 p.
- Stonecipher, S.A., and Diedrich, R.P.: Petrographic differentiation of fluvial and tidally influenced estuarine channels in second Frontier sandstones, Moxa arch area, Wyoming. In Strock, Betty, and Andrew, Sam (Eds.), Wyoming geology—Past, present and future. Jubilee Anniversary Field Conference Guidebook, Wyoming Geological Association, (1993), p. 181–200.
- Stonecipher, S.A., Winn, R.D., Jr., and Bishop, M.G.: Diagenesis of the Frontier Formation, Moxa arch—A function of sandstone geometry, texture and composition, and fluid flux. In McDonald, D.A., and Surdam, R.C. (Eds.), Clastic diagenesis. American Association of Petroleum Geologists Memoir 37, (1984), p. 289–316.
- Sturm, S.D., Evans, L.W., Keusch, B.F., and Clark, W.J.: Almond Formation reservoir characterization and sweet spot analysis in Siberia Ridge Field, Wyoming. In Anderson, D.S., Robinson, J.W., Estes-Jackson, J.E., and Coalson, E.B. (Eds.), Gas in the Rockies. Rocky Mountain Association of Geologists Guidebook, (2001), p. 145–169.
- Surdam, R.C.: A new paradigm for gas exploration in anomalously pressured “tight-gas sands” in the Rocky Mountain Laramide basins. In Surdam, R.C. (Ed.), Seals, traps, and the petroleum system. American Association of Petroleum Geologists Memoir no. 67, (1997), p. 283–298.
- Surdam, R.C., Jiao, Z.S., and Martinsen, R.S.: The regional pressure regime in Cretaceous sandstones and shales in the Powder River Basin. In Ortoleva, P.J. (Ed.), Basin compartments and seals. American Association of Petroleum Geologists Memoir 61, (1994), p. 213–233.
- Surdam, R.C., Jiao, Z.S., and Liu, J.: Pressure regime in the Upper Cretaceous shales and sandstones in the Washakie Basin, Wyoming. In Jones, R.W. (Ed.), Resources of southwestern Wyoming. Forty-Sixth Field Conference Guidebook, Wyoming Geological Association, (1995), p. 205–223.
- Surdam, R.C., Jiao, Z.S., and Ganshin, Yuri: Reducing risk and low-permeability gas formations—understanding the rock/fluid characteristics of Rocky Mountain Laramide basins. Department of Energy Final Technical Progress Report, award no. DE-FC26-01NT41325, (2003), 49 p.
- Surdam, R.C., Jiao, Z.S., and Ganshin, Yuri: A new approach to exploring for anomalously pressured gas accumulations—the key to unlocking huge, conventional gas resources. Wyoming State Geological Survey Exploration Memoir no. 1, (2005), 96 p.
- Thyne, G.D., Pasternack, Ira, and Anderson, D.S.: Preliminary assessment of reservoir quality controls in Lewis Shale sandstones, south-central Wyoming. Fifty-Third Field Conference Guidebook, Wyoming Geological Association, (2003), p. 89–99.
- Thyne, G.D., Tomasso, Mark, Bywater-Reyes, S.V., Budd, D.A., Reyes, B.M.: Characterization of porosity and permeability for CO₂ sequestration models in the Mississippian Madison Group, Moxa Arch-LaBarge platform, southwestern Wyoming. *Rocky Mountain Geology*, **45** (2), (2010), p. 133–150.
- Tobin, R.C., McClain, T., Lieber, R.B., Ozkan, A., Banfield, L.A., Marchand, A.M.E. and McRae, L.E.: Reservoir quality modeling of tight-gas sands in Wamsutter field— Integration of diagenesis, petroleum systems, and production data. Association of Petroleum Geologists *Bulletin*, **94** (8), (2010), p. 1229–1266.
- Towse, Donald: Frontier Formation, southwest Powder River Basin, Wyoming. American Association of Petroleum Geologists *Bulletin*, **36** (10), (1952), p. 1962–2010.
- Van Horn, M.D., and Shannon, L.T.: Hay Reservoir field—a submarine fan gas reservoir within the Lewis Shale, Sweetwater County, Wyoming. Fortieth Field Conference Guidebook, Wyoming Geological Association Guidebook, (1989), p. 155–180.
- Warner, D.A.: Geology and ground-water resources of the Kaycee area, Wyoming. U.S. Geological Survey Open-File Report, (1947), 9 p. [unnumbered report].

- Wegemann, C.H.: The Salt Creek oil field, Wyoming. U.S. Geological Survey Bulletin 452, U.S. Geological Survey, (1911), p. 37–38.
- Wegemann, C.H.: The Salt Creek oil field, Wyoming. U.S. Geological Survey Bulletin 670, U.S. Geological Survey, (1918), 52 p.
- Weimer, R.J.: Uppermost Cretaceous rocks in central and southern Wyoming and northwest Colorado. In Wiloth, G.J. (Ed.), Symposium of late Cretaceous rocks of Wyoming and adjacent areas. Sixteenth Field Conference Guidebook, Wyoming Geological Association, (1961), p. 17–28.
- Weimer, R.J.: Stratigraphy and petroleum occurrences, Almond and Lewis Formations (Upper Cretaceous), Wamsutter arch, Wyoming. Nineteenth Field Conference Guidebook, Wyoming Geological Association, (1965), p. 65–80.
- Welder, G.E., and McGreevy, L.J.: Groundwater reconnaissance of the Great Divide and Washakie Basins and some adjacent areas, Southwestern Wyoming. U.S. Geological Survey Hydrologic Investigations Atlas HA–219, (1966), 10 p., 3 sheets, scale 1:250,000.
- Western Water Consultants, Inc.: Potential for ground water development, city of Sheridan, Wyoming, feasibility report. Report prepared for the city of Sheridan and Wyoming Water Development Commission (1982), [variously paged].
- Western Water Consultants, Inc.: Ground water feasibility study for Kaycee. Report prepared for the Wyoming Water Development Commission, (1983), 62 p., 6 pls.
- Westphal, Hildegard, Eberli, G.P., Smith, L.B., Grammer, G.M., and Kislak, J.: Reservoir characterization of the Mississippian Madison Formation, Wind River Basin, Wyoming. American Association of Petroleum Geologists *Bulletin*, **88** (4), (2004), p. 405–432.
- Whitcomb, H.A.: Investigation of declining artesian pressures in the vicinity of Osage, Weston County, Wyoming. U.S. Geological Survey Open-File Report 60–153, (1960), 11 p.
- Whitcomb, H.A.: Ground-water resources and geology of Niobrara County, Wyoming, with a section on The chemical quality of the ground water by T.R. Cummings. U.S. Geological Survey Water-Supply Paper 1788, (1965), 101 p., 3 pls.
- Whitcomb, H.A., and Lowry, M.E.: Ground-water resources and geology of the Wind River Basin area, central Wyoming. U.S. Geological Survey Hydrologic Investigations Atlas HA–270, (1968), 3 sheets; accompanying text, 13 p.
- Whitcomb, H.A., Cummings, T.R., and McCullough, R.A.: Ground-water resources and geology of northern and central Johnson County, Wyoming. U.S. Geological Survey Water-Supply Paper 1806, (1966), 99 p., 2 pls.
- Whitehead, R.L.: Ground water atlas of the United States—Segment 8, Montana, North Dakota, South Dakota, Wyoming. U.S. Geological Survey Hydrologic Atlas 730–I, (1996), 24 p.
- Winn, R.D., Jr., and Smithwick, M.E.: Lower Frontier Formation, southwestern Wyoming—Depositional controls on sandstone compositions and on diagenesis. In Stratigraphy of Wyoming, Thirty-First Field Conference Guidebook, Wyoming Geological Association, (1980), p. 137–153.
- Winn, R.D., Jr., Stonecipher, S.A., and Bishop, M.G.: Sorting and wave abrasion—Controls on composition and diagenesis in lower Frontier sandstones, southwestern Wyoming. American Association of Petroleum Geologists *Bulletin*, **68**, (1984), p. 268–284.
- Winn, R.D., Jr., Bishop, M.G., and Gardner, P.S.: Lewis Shale reservoirs, southern Wyoming: Turbidite sandstones deposited in delta-tow settings. American Association of Petroleum Geologists *Bulletin*, **69** (2), (1985), p. 317.
- Winn, R.D. Jr., Bishop, M.G., and Gardner, P.S.: Shallow water and sub-storm-base deposition of Lewis Shale in Cretaceous Western Interior Seaway, south-central Wyoming. American Association of Petroleum Geologists *Bulletin*, **71** (7), (1987), p. 859–881.
- Witton, E.M.: Outcrop and subsurface characterization of the Lewis Shale, Carbon County, Wyoming. M.S. Thesis, Colorado School of Mines, Golden, Colo., (1999), 214 p.
- WWC Engineering, Hinckley Consulting, Collins Planning Associates, Greenwood Mapping, Inc., and States West Water Resources Corporation: Wyoming Framework Water Plan, v. 1. Report prepared for Wyoming Water Development Commission (2007), [variously paged].
- Wyoming Geological Association: Wyoming Stratigraphic Nomenclature Chart 2014. Stratigraphic Nomenclature Committee of the Wyoming Geological Association, (2014), numerous files on CD-ROM.

Chapter 4: Aqueous Sample Analysis

Charles Nye, Ghanashyam Neupane, Scott Quillinan, Travis McLing

Scott Quillinan, Director of Research, School of Energy Resources, University of Wyoming, 1000 E. University Ave., Laramie, WY 82072

scottyq@uwyo.edu

Keywords: Aqueous REE, Ion-exchange, Resin, Analytical Methods, WBPW, Normalization

ABSTRACT

All aqueous samples data, seen in the appendix, was processed with a variety of methods. These include multiple normalizations, parameter-specific statistical descriptions of the data groups, and enrichment-depletion indices. These processed data were then considered in their geologic context. The result is a concise set of observations, and models to explain them.

The samples exhibit two modes of samarium-gadolinium enrichment. They also show reduction-oxidation features in their cerium anomalies and europium anomalies. These observations may, with more work, link water chemistry to its flow history. This analysis also suggests support for other REE researchers and for structural geologists who have studied flow-path phenomena in these basins.

1. METHODS FOR AQUEOUS REE AND GEOCHEMICAL ANALYSIS

Natural spring samples were collected as close to the spring as safe. Produced water samples were collected post phase-separator from sampling valves. In the limited cases where this was not possible, the samples were taken from holding tanks on the well-pad. Those eight samples represent a longer-duration average of the water produced from the wells, but are subject to more significant cooling than those samples taken directly from the separator's valves. In some cases the separator valve released a sample containing significant hydrocarbon fractions. In these cases, the sample was allowed to gravity-separate, the light-fraction removed, and the bottle refilled to gain more heavy-fraction water. In all cases, blanks were poured in the field to ensure sample accuracy.

Waters were analyzed with field measurements of pH, temperature, conductivity, and Oxidation-Reduction Potential (ORP). Ion Chromatography anion analysis of the unacidified fraction was used to identify monoatomic and polyatomic anions. The acidified fraction was used for elemental analysis by ICP-OES to determine cation concentration. Other analyses that indirectly resulted from this work included stable carbon/oxygen/hydrogen isotopes and metagenomics sequencing. A separate acidified fraction was sent to INL for aqueous REE analysis with resin cleaning and pre-concentration under the methods of (McLing et al., 2014).

The concentrations of REE in natural waters of near-neutral pH tend to be extremely low (in parts-per-trillion, ppt), and measurement of such a low level of REE in the presence of high concentration background (and interfering) cations has been a major challenge. To overcome these difficulties, several selective preconcentration approaches were developed in the past by various researchers (e.g., Strachan et al., 1989; Stetzenbach et al., 1994; Wood, 2002). These preconcentration approaches range from selectively extracting REEs from natural samples by cation-exchange resin(s) or metal oxides (e.g., ferric hydroxides) and retrieving them by acid elution or acid digestion. In this study, we employed two preconcentration methods based on Strachan et al. (1989) and Stetzenbach et al. (1994) for low TDS (<4.5 g/sample size) and high TDS (>4.5 g/sample size) water samples, respectively. Both of these methods (Figure 1) were reported to be equally effective in concentrating REEs and removing interfering ions (McLing et al., 2014).

1.1 REEs extraction from low TDS brines

This REEs extraction procedure began with gravity-driven passing of brine (0.5 -1 L) through a column filled with 200-400 mesh AG-50-X8 hydrogen form resin. The volume of resin was determined by proportion to the volume of sample, TDS level, and type of dominant cations (Monovalent sodium or divalent calcium). After the sample was introduced to the resin, the monovalent and divalent metal ions were eluted with ultrapure (optima grade) 2.5 M nitric acid (8 times the resin volume) followed by a rinse of 25-50 mL of nano-pure water (>18 M Ω -cm). Finally, the REEs retained in resin were eluted with 8 M nitric acid (4 times the resin volume) and collected in a clean Teflon watch glass. The resin was also eluted with ca. 25-50 mL nano-pure water. The REEs extract was evaporated to dryness without boiling on a hot plate. The residue remained in the Teflon evaporating dish was dissolved in 5 mL 1% nitric acid solution resulting in about 100 to 200 times selective enrichment of REEs. Both chromatography and evaporation of REEs extract were conducted in dust-free environment to minimize contamination from aerosols. The final extracts were collected in clean 15 mL centrifuge tubes and stored at 4 °C until analysis by an ICP-MS in reaction/collision cell mode.

1.2 REEs extraction from high TDS brines

This extraction of REEs from high TDS brines was conducted using a different resin, 200-400 mesh Chelex-100 in ammoniated form. The pre-chromatography preparation for this procedure consisted of converting the resin into ammoniated form and treating the brines with ammonium acetate and pH adjustment. The resin was initially converted to hydrogen form by passing 50 mL 2.5 M ultra-pure nitric acid through a clean drip column containing about 8.15 to 16.25 g of Chelex 100 Na. Excess nitric acid was removed by passing 50 mL of nano-pure water followed by two drip-cycles of ultra-pure (optima grade) 50-100 mL of 2.0 M ammonium hydroxide solution.

The ammonium hydroxide treatment converts the resin from hydrogen form to ammonium form. The final column preparation was to rinse the resin with nano-pure water to reach a neutral pH.

The brine preparation involved buffer-treatment (about 1 g per 100 mL of brine) of brine with ultra-pure (optima grade) ammonium acetate and raising pH to the optimum pH of 5.3-5.4 (the brine samples had been acidified right after their collection) for sample chromatography with ammonium solution. When the resin column and sample brine were prepared to their optimum conditions, sample chromatography was conducted by adding about 50 mL of brine into the drip column initially and subsequently adding remaining brines. The sample chromatography was followed by washing the resin 5 times with about 250 mL of nano-pure water. Then monovalent and divalent metals were eluted with 3 to 5 elutions (125 to 250 mL depending upon the amount of resin) of 1 M ammonium hydroxide solutions. Excess ammonium solution in the column was removed with two nano-pure water circulations. Finally, the REEs retained by the resin were eluted with three cycles (one 25-50 mL followed by two 5 mL additions) of 2.5 M ultra-pure nitric acid solution. As with the low-TDS samples, the REEs extracts were evaporated to dryness on a hot plate (100 °C) and the residue was dissolved in 5 mL 1% ultra-pure nitric acid solution for ICP-MS analysis.

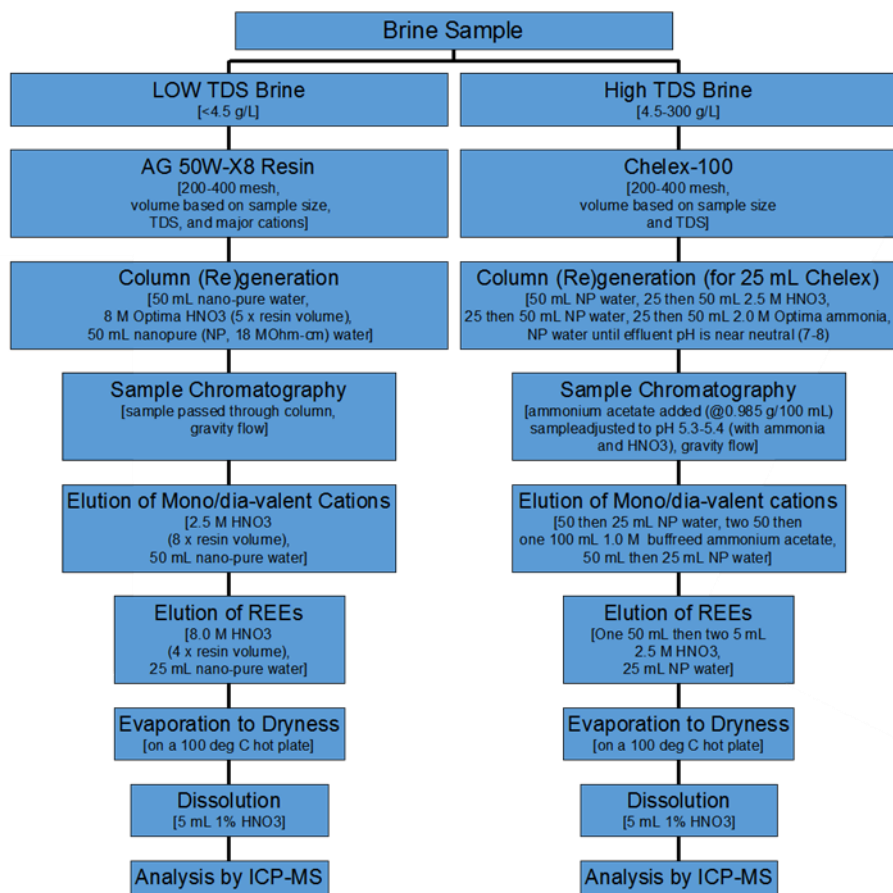


Figure 4.1: Schematic of the steps used for REE preconcentration in this study. There are two similar protocols depending on the brine’s characteristics, low-TDS and high-TDS.

1.3 Standard Analysis of Geochemistry

Three standard analyses were performed on the Wyoming samples to determine cation concentration, anion concentration, and stable isotope ratios. These analyses are in addition to basic field data such as sample temperature at the time of collection, initial pH, and conductivity as a proxy for Total Dissolved Solids (TDS).

Cations were measured as elements by Inductively Coupled Plasma Optical Emission Spectroscopy (ICP-OES). The ICP-OES analysis also measured the concentration of selected trace elements. Anions were measured by Ion Chromatograph (IC) exempting carbonate/bicarbonate which was calculated by charge balance, and supported by analysis from an external lab. Isotopes of Carbon ($\delta^{13}\text{C}$), Oxygen ($\delta^{18}\text{O}$), and Hydrogen ($\delta^2\text{H}$) were measured by Isotope Ratio Mass Spectrometer (IRMS).

2. RESULTS OF REE AND GEOCHEMICAL ANALYSIS

The following sections describe the brine samples context, present major ion chemistry, and present REE chemistry. Figure 4.2 gives the detection limits of the ICP-MS used to measure REE in this work, however, since each sample was pre-concentrated up to 200 times, the reported values can sometimes be much less than these.

REE	La	Ce	Pr	Nd	Sm	Eu	Gd	Tb	Dy	Ho	Er	Tm	Yb	Lu
ng/L	0.13	0.15	0.03	1.47	0.04	0.37	0.41	0.51	0.02	0.01	0.05	0.01	0.18	0.04

Figure 4.2: The Detection Limits of the ICP-MS used in this study. If the samples had not been pre-concentrated as described in section 1 these values would be the lowest detectable concentrations. Due to pre-concentration the actual limit was sometimes up to 200 times less than these. Lower values indicate greater ability to detect small amounts of the element. Often, but not always, a low detection limit also indicates a proportionally better sensitivity.

The charts in this section are typical REE diagrams, also called “Spider diagrams”. These diagrams show the REEs in the water samples normalized to a standard. In this case the standard chosen was the North American Shale Composite (NASC) as reported by Grommet et al. (1984). Spider diagrams were originally designed to allow visual comparison of the similarity or difference of two or more REE patterns which would indicate the similarity or difference of their formation and history. Two common observations on REE diagrams are LREE/HREE ratio (indicated by the overall slope from La to Lu), and anomalies (which are a disproportionate elevation of one REE above the level suggested by a geometric average of its two nearest neighbors).

Two modifications have been made to the diagrams. First, all water sample concentrations have been multiplied by 1,000,000 which is the approximate difference in concentration commonly found between rock REEs and water REEs. This modification makes water and rock (NASC) comparable. Second, they have been set on a linear rather than log scale to show absolute concentrations better. This second change assists economic resource assessment at the expense of scientific process description. This tradeoff emphasizes samples of significantly higher-REEs but suppresses negative anomalies and the details of REE behavior at low concentrations.

REE	La	Ce	Pr	Nd	Sm	Eu	Gd	Tb	Dy	Ho	Er	Tm	Yb	Lu
mg/L	31.1	66.7	7.7	27.4	5.59	1.18	4.9	0.85	4.17	1.02	2.84	0.48	3.06	0.46

Figure 4.3: The concentrations reported by Grommet et. al. (1984) for the North American Shale Composite (NASC). These values were chosen for normalization in this section because they allow comparison to the rock samples of chapter 5. Note that rock REEs are reported in parts-per-million (ppm) using the SI units of mg/L or mg/kg, whereas water REEs are reported in parts-per-trillion (ppt) using the SI units ng/L.

The REE-diagrams at the end of the appendix have been set to the same axis to allow easy comparison between basins. The REE-diagrams in this chapter use scales proportional to their largest value. The legend shows the brines’ source reservoir, with the exception of the ESRP’s 119 samples that overpopulate the legend. Each Idaho and Wyoming basin is listed below. The USGS library samples are listed after those.

2.1 Eastern Snake River Plain Geothermal Brines

Our REE database for ESRP waters includes both thermal ($T \geq 20$ °C) and cooler waters. Samples from the Raft River Geothermal (RRG) area have the highest recorded temperatures (up to 150 °C). Some hot springs and wells in the Twin Falls (Idaho) area have temperatures as high as 65 °C. Cooler water samples have temperatures as low as 10.6 °C. These cooler water samples represent the domestic or irrigation wells.

The ESRP thermal waters show a large range in total dissolved solids (TDS) from about 106 mg/L (Sturm Well) to more than 7,000 mg/L (Heise Hot Spring). Based on the dominant ions in water, the majority of the ESRP waters are of either sodium-bicarbonate or calcium-bicarbonate. Some samples are of sodium chloride types. In the ESRP, sodium-bicarbonate water is generally considered as deeper water whereas calcium-magnesium-bicarbonate water represents shallower water (McLing et al., 2002; Mattson Et al., 2016).

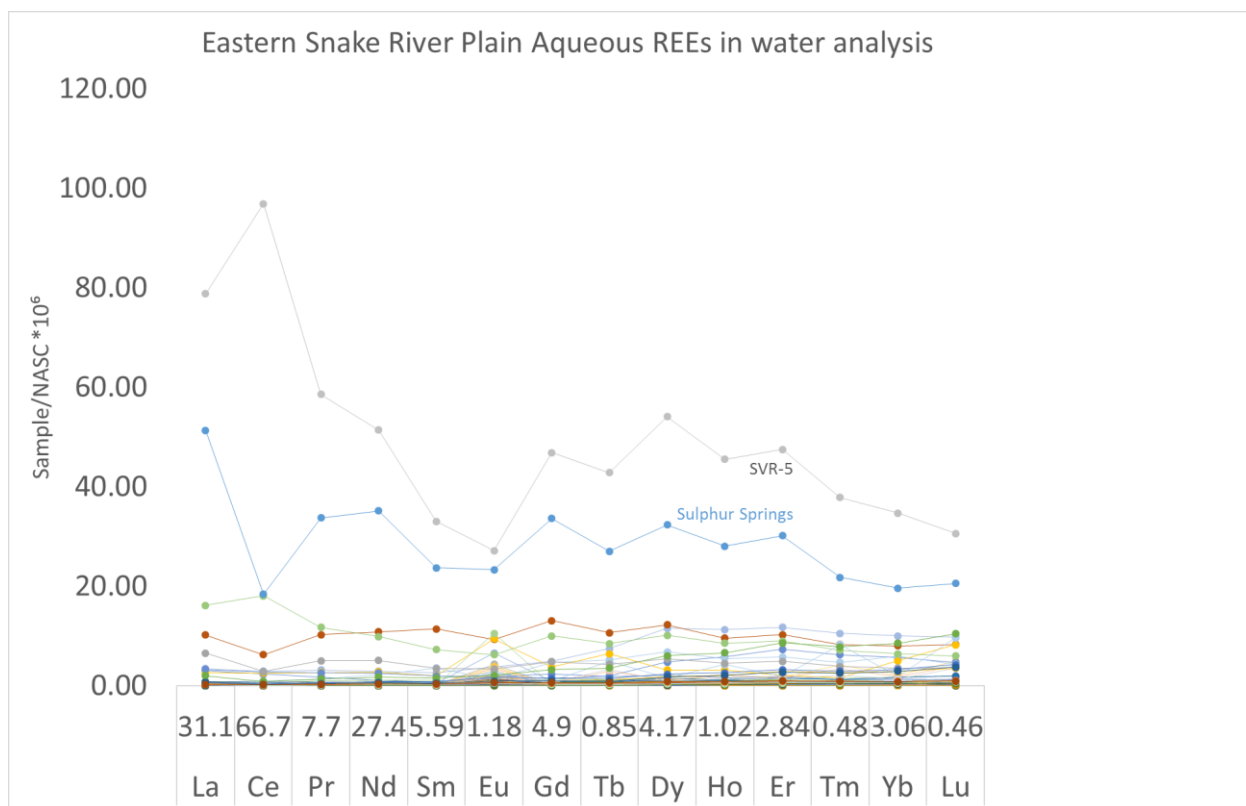


Figure 4.4: A REE diagram of 119 samples from the ESRP that were used in this study. As noted above, samples rarely occur at more than 10/1,000,000ths of NASC. Samples in this dataset include both positive and negative europium anomalies.

The sampled ESRP geothermal brines are generally unassociated with Oil and Gas production. The significant europium anomaly that is often seen in other waters (Figures 4.9-4.15) is almost non-existent here (Figure 4.4). Two samples present significantly higher REE concentrations than commonly found: SVR-5 and Sulphur Spring (Figure 4.4). These two have generally similar REE patterns, with the exception of the Ce anomaly being positive in SVR-5 and negative in Sulphur Spring.

The concentrations of REEs in near-neutral water samples are very low, almost exclusively in parts-per-trillions (or in ng/L) level. These concentration levels are consistent with the previously reported REE concentrations in near-neutral geothermal, groundwater, and oil-and-gas produced waters from several basins the United States (Wood, 2001; Nelson, 2005; Nelson et al., 2004; Nye et al., 2017). Element by element REE concentrations for all samples are given in the Appendix. In general, a total REE content of less than 10 ng/L is common in the near-neutral ESRP water samples (Figure 4.4).

2.2 Brines of the Kevin Dome Area, Montana

Figure 4.5 shows the North American Shale Composite (NASC) normalized values of REEs in water samples from the Kohls and Kohls, Nagy, Alme, and Pace wells. In general, the water samples from these wells show very low REEs values compared to NASC values. All water samples show Eu enrichment. Similarly, all samples, show general enrichment of heavier REEs (HREEs) compared to lighter REEs (LREEs). All three Paul George wells (Mule, Kitty, and House wells; Figure 4.6) show similar REEs trends (e.g., enrichment of Eu and HREEs). The water samples collected from Paul George reservoir show very strong HREEs enrichment. However, this sample does not show Eu enrichment. Furthermore, the later sample (October 2014) collected from this reservoir shows higher levels of REEs compared to the earlier sample (October 2013), however, the same enrichment towards HREEs is maintained between the two samples. Similarly, REE values for later samples from the Kern reservoir and Wallewein reservoir south end show higher concentrations in earlier samples (Figure 4.7). All these samples (except early Kern reservoir sample) show higher enrichment of HREEs. Wallewein evaporation pond samples collected in October 2013 show very strong Eu enrichment.

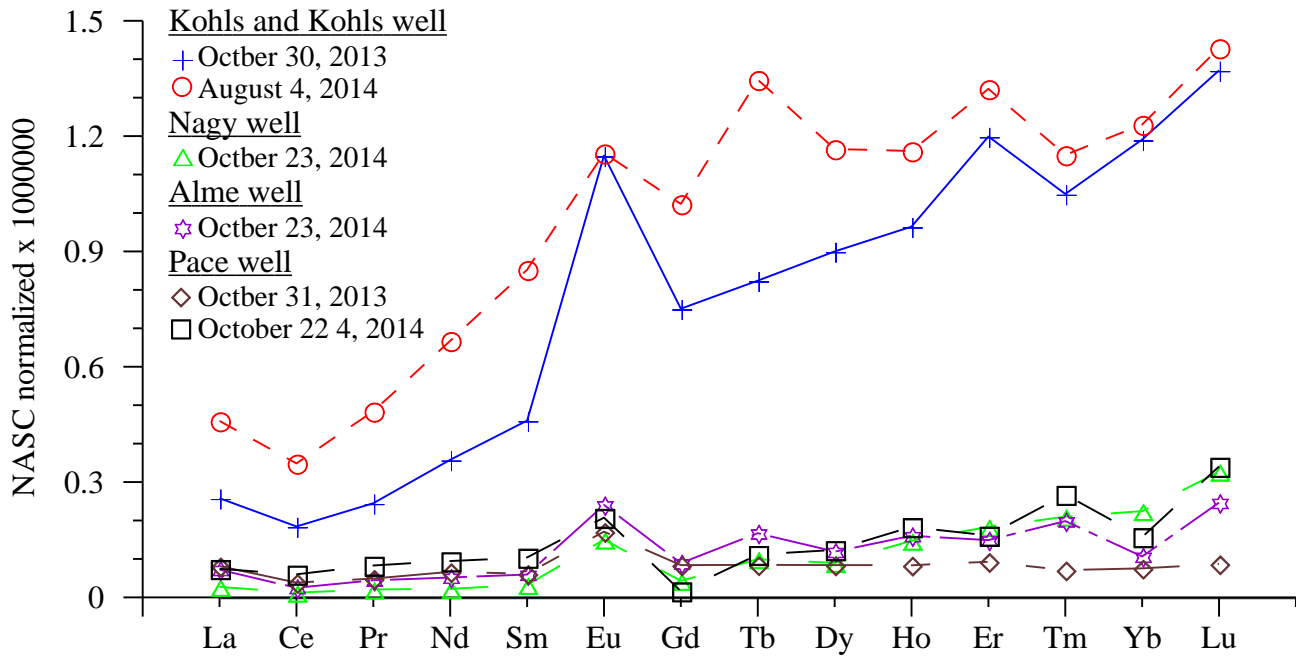


Figure 4.5: NASC normalized rare earth elements in water samples from Kohls and Kohls, Nagy, Alme, and Pace wells in Kevin Dome, Montana. Note that the scale is 0-1.5 rather than 0-100.

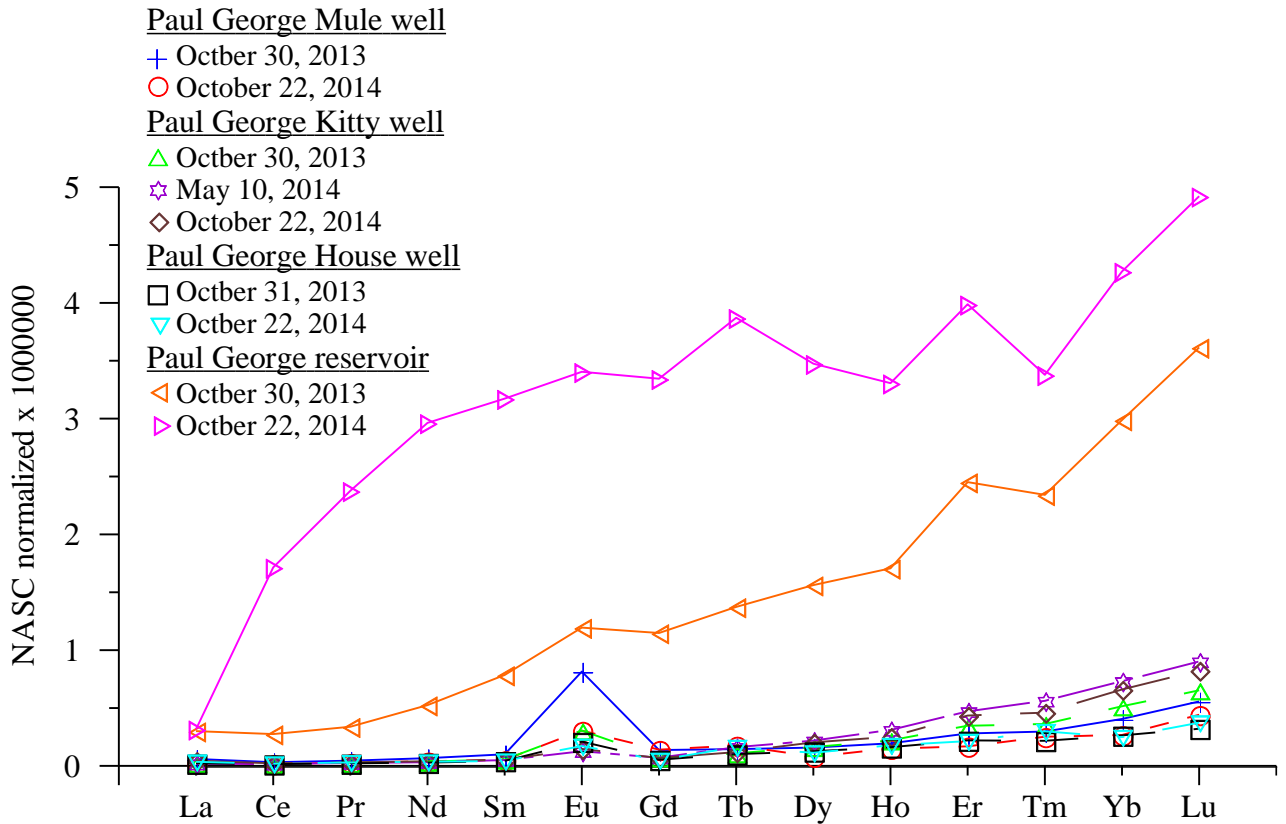


Figure 4.6: NASC normalized rare earth elements in water samples from Paul George wells and Paul George reservoir in Kevin Dome, Montana. Note that the scale is 0-5 rather than 0-100.

Water samples from Kern well (Figure 4.7) show REEs concentration trends similar to other shallow wells in the area (such as Pace, Nagy, Alme, Paul George wells; Figures 4.5 and 4.6) with Eu enrichment and slightly higher values for HREEs. Both samples collected from Kleinert Farm fishing pond show low and almost featureless NASC normalized REEs pattern (Figure 4.7).

In general, water samples from shallow wells in Kevin Dome area show distinct Eu enrichment. These samples also show enrichment trend towards HREEs. The surface water samples show slightly different REEs trends and temporal variabilities. In general, surface water samples reflect the HREEs enrichment in shallow subsurface waters; however, the strong Eu enrichment is not always appear in their distributions (with the exception of Wallewein evaporation pond). In some cases, surface water samples show featureless REEs distributions.

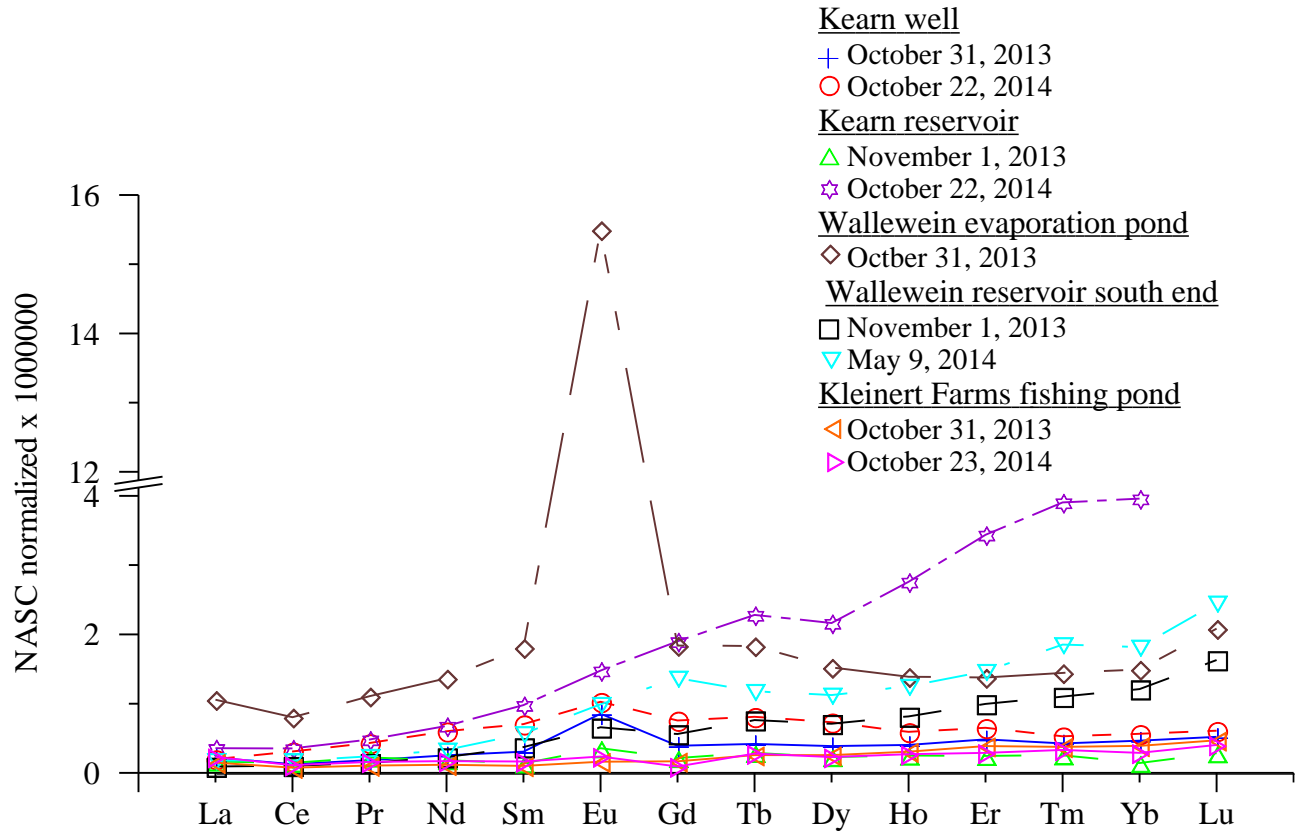


Figure 4.7: NASC normalized rare earth elements in water samples from Kern well and reservoir, Wallewein evaporation pond and reservoir, and Kleinert Farms fishing pond in Kevin Dome, Montana. Note that the scale is interrupted and run from 0-16 times NASC.

As stated above, these samples from the Kevin Dome area contain very low concentrations of REEs. This set of samples is among the most interesting because of the very low REE concentration of all samples. While samples such as Wallewein Reservoir have comparatively large anomalies as shown in 4.7, there are no anomalies that are significant at the scale of other sample sets in this research (Figure 4.8). Even the higher concentrations of HREEs over LREEs seen in the Kern's and Paul George Reservoirs are almost insignificant when compared to the other sample sets in this research.

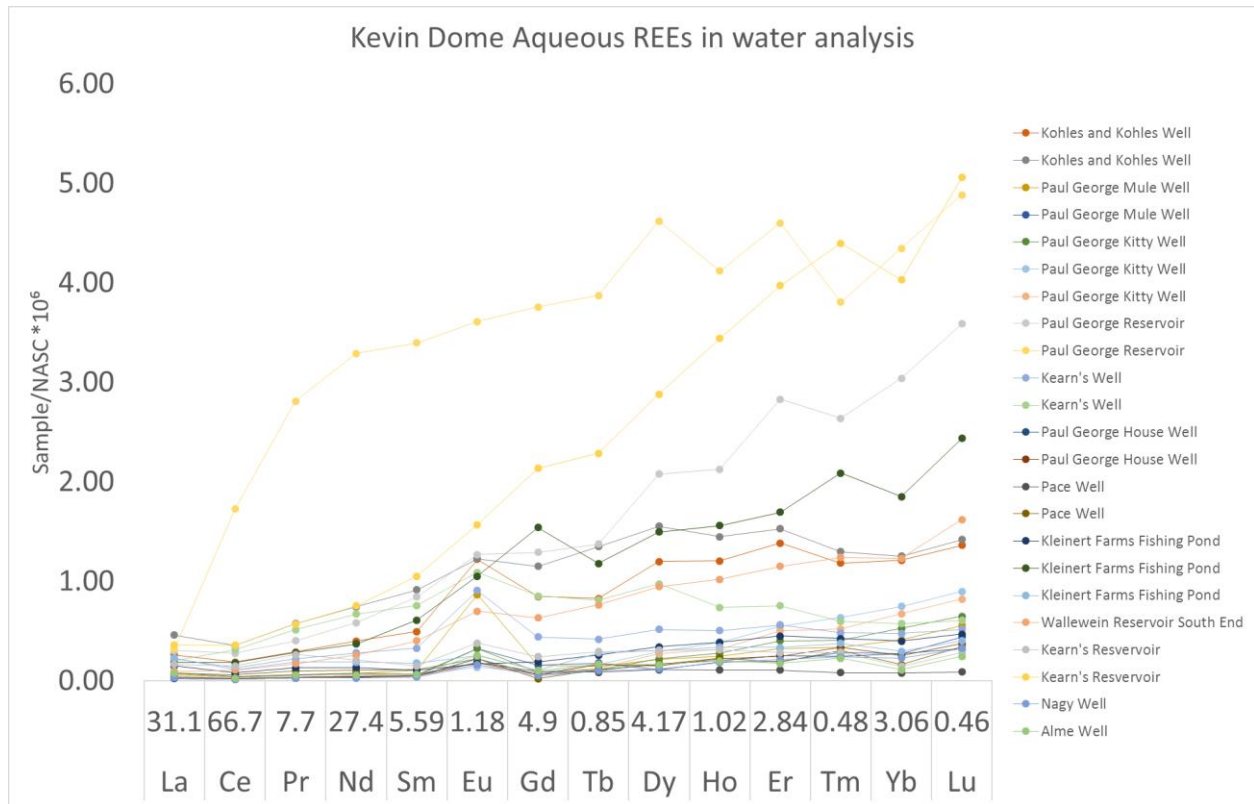


Figure 4.8: A composite REE diagram of 23 samples from the Kevin Dome area in Montana combining samples shown in Figures 4.5, 4.6, 4.7.

2.3 Produced Waters of the Wind River Basin, Wyoming

Produced Water samples in Wyoming typically have a Europium anomaly with balanced Samarium and Gadolinium rider-peaks (Figure 4.9). The WRB has this style of europium enrichment. The sample set from the Lance and Fort Union Formation of the Wind River Basin (also indicated by an MD prefix) shows this anomaly in all samples. There are also samples from clastic units deeper in the Wind River Basin (MS prefix), and from the deepest reservoir, the Madison limestone.

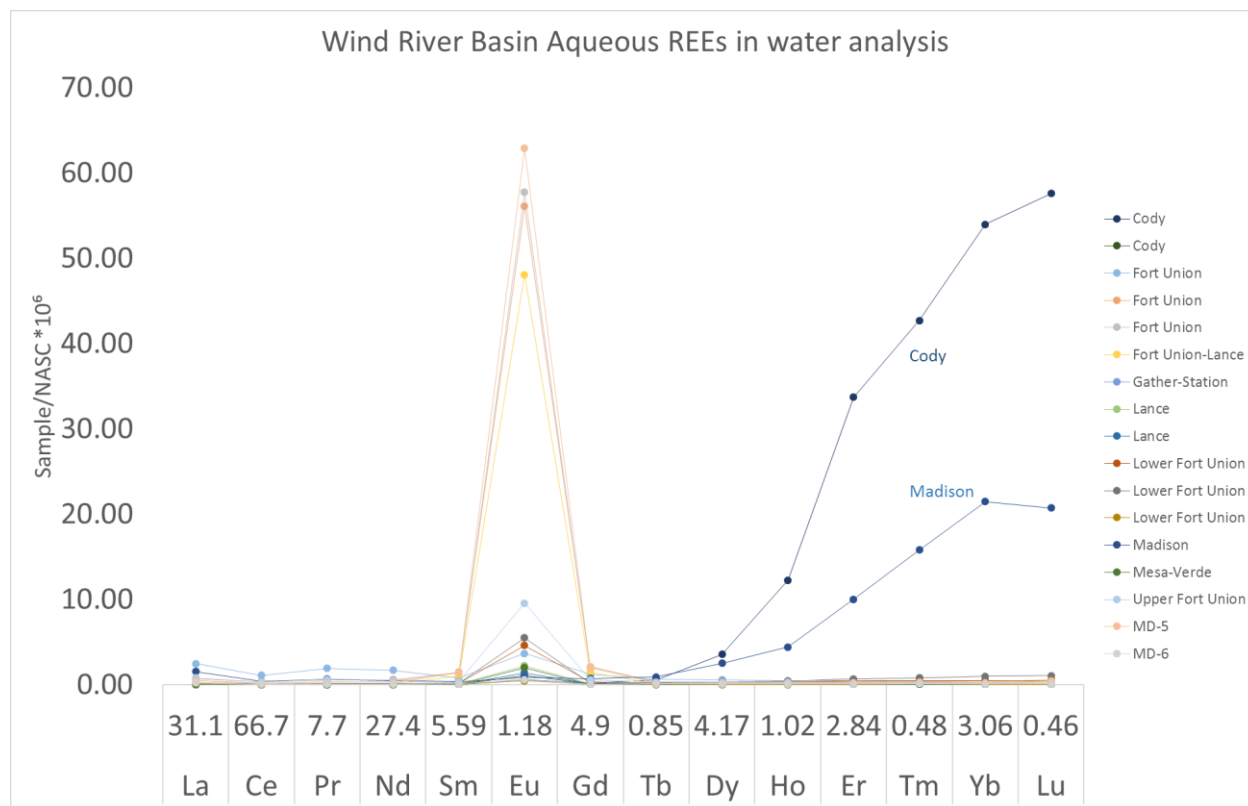


Figure 4.9: A NASC-normalized REE diagram for the WRB. Exempting one Cody sample and one Madison sample, there is a general but slight enrichment in LREE over HREE. Note that the scale runs from 0 to 70 times the shifted NASC.

The WRB water type in the collected samples is dominantly sodium-bicarbonate but transitions from bicarbonate to chloride with greater depths. Major cations other than sodium are virtually non-existent, as is sulfate (Geochemistry Appendix). The TDS of the WRB samples ranges from 3,800 to 19,100 mg/L with an outlier of 68,000 mg/L. The pH is slightly basic, averaging 7.6 units. These data are consistent with an oil and gas field in a carbonate-bearing rock system.

Europium behavior in the WRB falls into three categories: significant positive anomalies (greater than 11.8ng/L), typical positive anomalies (between 11.8ng/L and 1.18ng/L), and a significant negative anomaly (less than 1.18ng/L). The samples with a significant positive europium anomaly occur in samples from the Fort Union Formation (Figure 4.9) which is a mature, Paleocene, continental sandstone containing significant Oil and Gas fields. The sample with a significant negative Eu anomaly came from the Madison Limestone.

2.4 Produced Waters of the Powder River Basin, Wyoming

Samples from the PRB are most similar to the Kevin Dome samples, with the exception that they have a weak europium anomaly and gadolinium anomaly (Figure 4.10). Two samples, from the Frontier and Mowry have minor HREE enrichment.

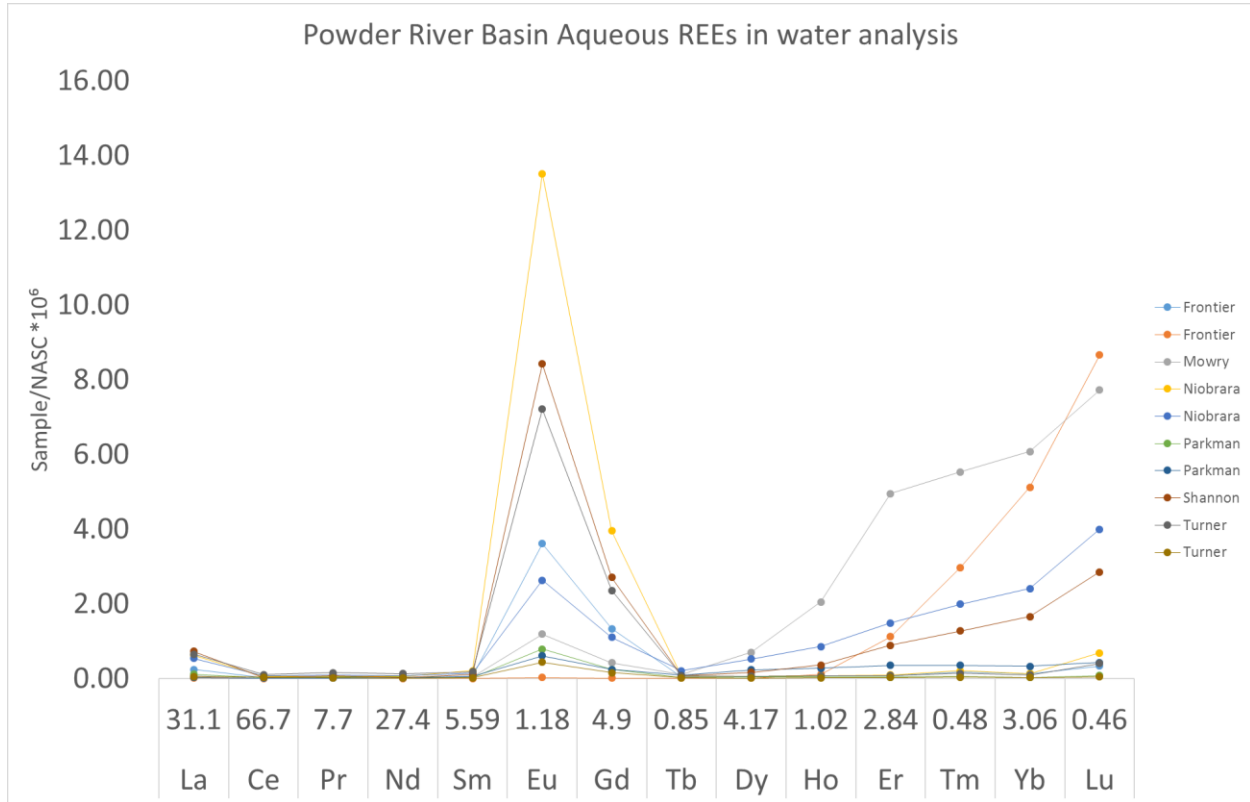


Figure 4.10: A NASC-normalized REE diagram for the PRB. The PRB has a small Eu anomaly. The Gd anomaly is unusual and unique to the PRB out of all samples in this project. The Mowry, one or two Frontier samples, and maybe the Shannon sample show HREE enrichment. Those four samples were collected from nearer the basin axis than the other samples. The visible europium anomaly is mostly in the typical range for produced waters. Note that the scale runs from 0 to 16 times the shifted NASC, the lowest of all Wyoming Basins.

The water type in all PRB samples is sodium chloride. The other major ions have very small contributions. Sulfate was not detected in any PRB sample. Despite being limited to an almost entirely sodium chloride chemistry, the TDS of these samples (~50,000 mg/L) is almost ten times higher than the average of other Wyoming samples. This high TDS but low REE content seen in the PRB dataset supports the conclusion of Chapter 6 that TDS and REE concentration are not significantly linked. The pH of these samples is neutral.

In produced water samples with high europium content there are often small “rider” peaks on either side for samarium and gadolinium. However, in the PRB the europium is below the level these riders are normally seen (compare with the high europium WRB samples). Further, the gadolinium rider is much larger than the samarium rider.

The four samples with elevated HREE were from wells on the basin axis, whereas the other samples were from the eastern limb of the basin. These four wells may have contributions from waters further south in the PRB (that traveled along the axis), or from the western limb (whose strata dip more steeply). A more southerly flow path would mean that the water reaching these middle-basin wells has had a greater exposure to the cretaceous host rocks and explain how the waters picked up more HREEs than the other PRB samples.

2.5 Produced Waters of the Green River Basin, Wyoming

All GRB samples except the Maddison were collected from holding tanks and exhibit very poor conformance to the reservoir rocks. This is most likely due to differential oxidation causing some REEs, especially europium, to fall out of solution. Another possible cause is the iron in the tanks. This iron could be removing REEs from solution analogous to the process of Shannon and Wood (2005) who used a ferric iron co-precipitation method to extract REE from aqueous samples for analysis.

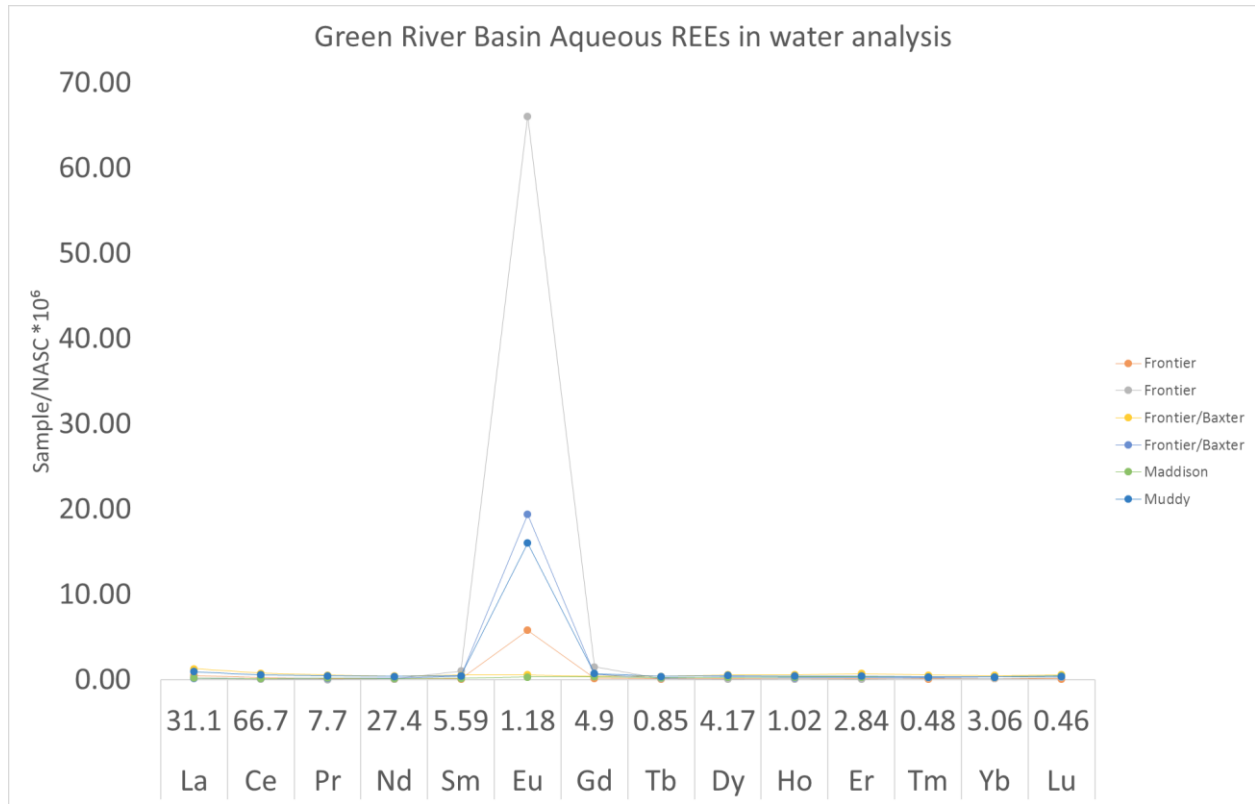


Figure 4.11: NASC-normalized REE diagram for the GRB. The GRB has few features at this scale. The Eu anomaly is most often small. The Frontier, Baxter, and Muddy samples which show more europium than typical for produced waters are similar to the WRB samples. Like the WRB, and unlike the PRB, these samples have balanced Sm-Gd rider peaks. Note that the scale runs from 0 to 70 times the shifted NASC.

The GRB water type ranges from sodium-chloride to sodium-bicarbonate. The TDS of the GRB samples ranges from 1,000 to 20,000 mg/L, and the pH is acidic, averaging 5.6 units. These data describe a relatively clean water. However the acidic pH emphasizes that this water could scavenge elements after it leaves the reservoir formation.

The Maddison sample from this area has the same europium negative anomaly seen in the WRB Maddison sample (not shown on figure 4.11). However, it lacks the HREE enrichment seen in that WRB sample (4.9). The most likely explanation for this is that the GRB has less hydrothermal fluid activity to transport HREEs out of the basement rock, but that the Maddison limestone is just as deficient in REEs as in the WRB.

2.6 Produced Waters of the Washakie Basin, Wyoming

Washakie Basin samples exhibit the same style of europium enrichment as the WRB samples. They are also similar to the GRB but without the poor-correlation to rocks which is hypothesized to come from iron interaction in the tanks. This is significant because one sample (4.12) came from a holding tank but did not exhibit the poor rock correlation seen in the GRB. That sample's good conformance could be caused by its near-neutral pH of 6.6 or by a company-specific maintenance procedure.

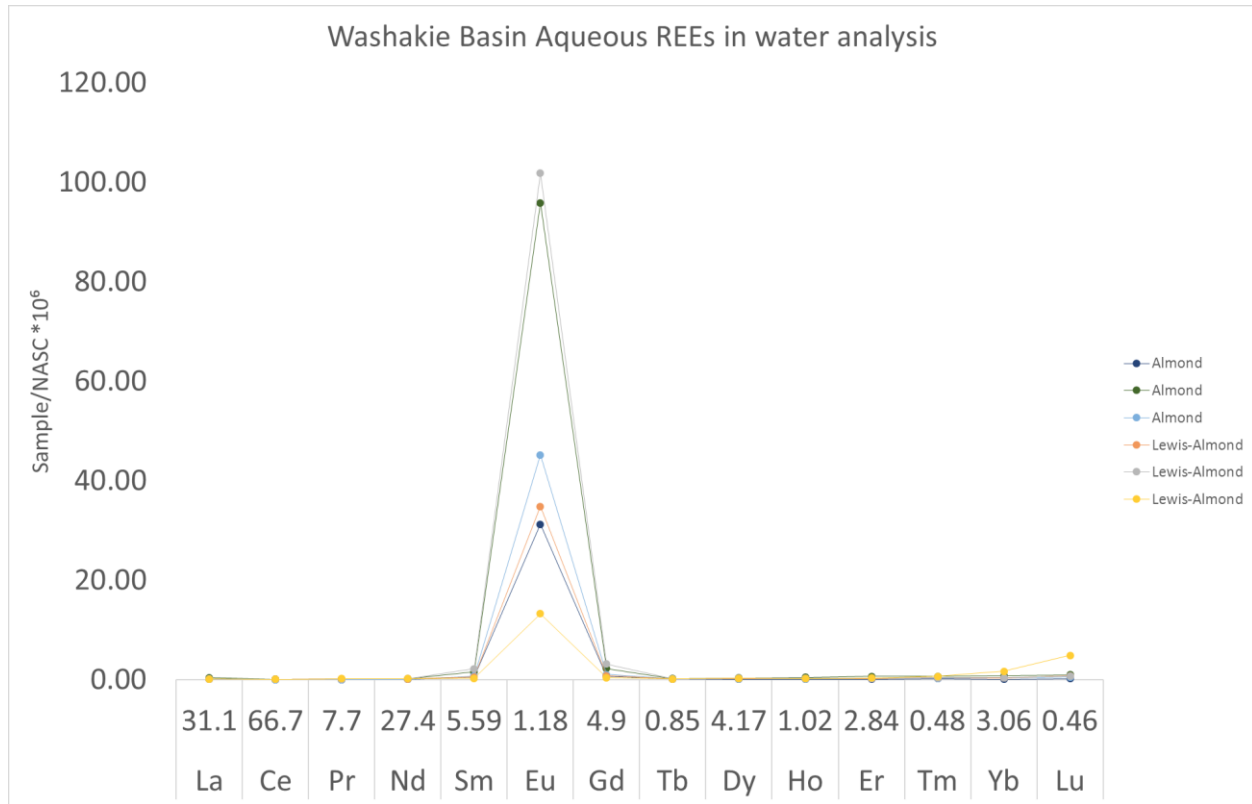


Figure 4.12: NASC-normalized REE diagram for the Washakie Basin. The Washakie Basin shows a pronounced Eu enrichment with balanced Sm-Gd riders. This style of enrichment is also seen in the WRB and GRB. As in those locations, this anomaly suggests a reduced water-rock environment. The low-europium sample from the Lewis-Almond, shown in yellow, was the only tank-collected sample in the Washakie. This tank sample shows HREE enrichment and better conformance to rock REEs than the tank-collected GRB samples. Note that the scale runs from 0 to 120 times the shifted NASC, the largest of the Wyoming basins.

The Washakie Basin's water type in the collected samples is sodium-chloride to sodium-bicarbonate but is unique among the Wyoming samples for its high sulfate, averaging 260 mg/L. The TDS of the Washakie Basin samples ranges from 5,300 to 10,700 mg/L, and the pH is near-neutral, averaging 7.1 units. The general water chemistry of the Washakie is like the Wind River and Green River basins with the exception of the sulfate concentration.

A possible challenge to the conventional interpretation of the europium peak comes from comparison of these Washakie waters to their reservoir rocks (Chapter 5). The strong Europium enrichment is normally interpreted to indicate inheritance from calcic minerals (Calcifeldspars and calcite), but the rock samples that hosted these fluids are low in calcium. Nye et al. (2018) cites the oxidation-reduction-potential (ORP or Eh) of the Washakie waters and the vanadium enrichment of the associated rock as evidence that the samples from the Washakie basin were so strongly reducing that they removed europium from untraditional non-calcic minerals.

The HREE enrichment in the Washakie basin tank-sample is limited to ytterbium and lutetium. This limitation to two elements suggests that the enrichment is from a source not found in other basins, whose HREE enrichment is evident in more elements from Tb to Lu. Company specific maintenance procedures remains a possibility, or it is possible that the Lewis and Almond contain a local Yb-Lu mineral not found in other basins.

2.7 Produced Waters of the Appalachian Basin, Eastern US.

The Appalachian Basin samples mostly came from Ohio, but also represent oil and gas fields in West Virginia and Pennsylvania. Like the Wyoming samples, the europium anomaly is a distinctive feature of these Appalachian Basin samples. The typical Appalachian Basin sample is 3 times more enriched than typical Wyoming and Idaho samples across the board.

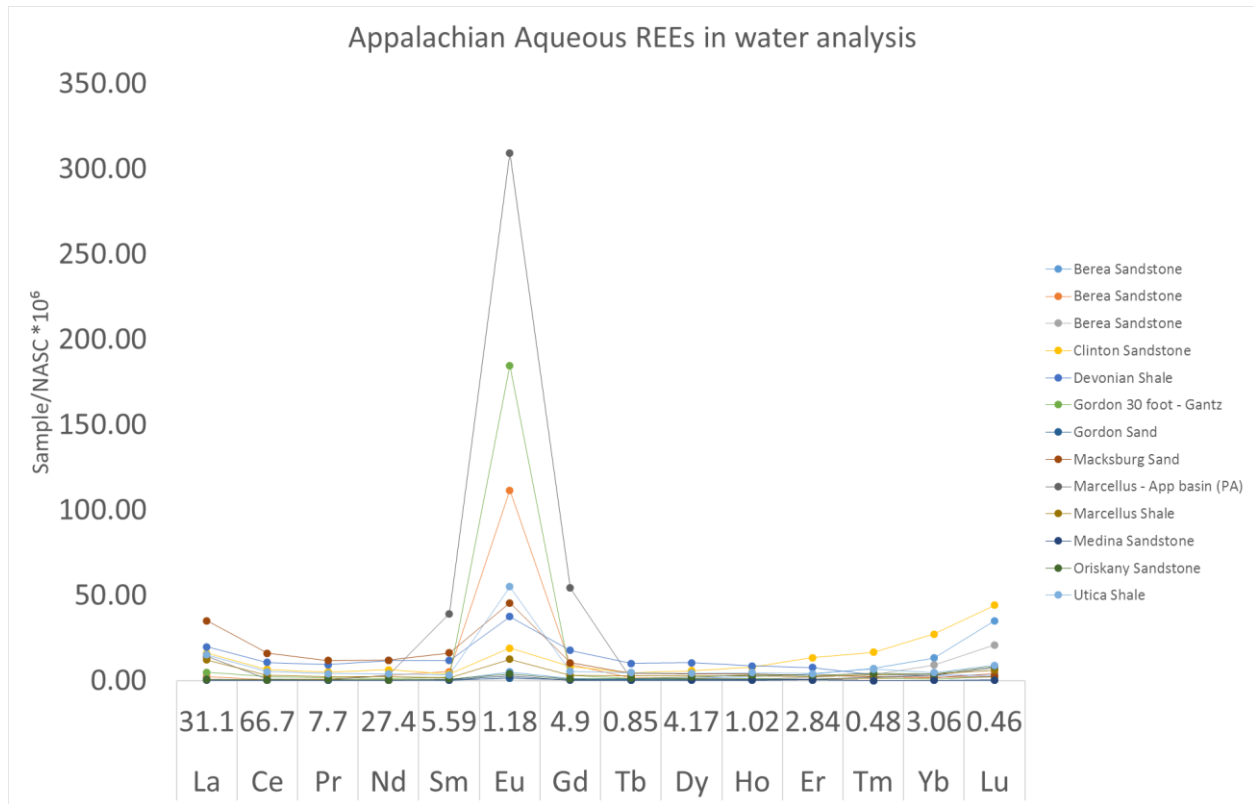


Figure 4.13: The Appalachian samples shown on a NASC-normalized REE diagram. The Appalachian is generally more enriched in all REEs. While some samples (Gordon Sand, Medina, and Oriskany Sandstones) never exceed the typical range for REEs in produced waters (10 on the y-axis) most samples have some form of LREE, HREE, or europium enrichment beyond the expected range. The Berea sandstone (blue and grey lines) samples that have detectable but minor europium enrichment have significant HREE enrichment. Conversely, the Berea sandstone (orange line) with extreme europium enrichment has minor HREE enrichment. An asymmetry in some of the Sm-Gd rider peaks suggests a process analogous to the PRB acts on most of these samples. Note that the scale runs from 0 to 350 times the shifted NASC, which is the largest anomaly recorded in this project.

The Appalachian samples are sodium-chloride type. Due to their significant TDS (averaging ~150,000 mg/L) many other major ions are present in significant concentrations. The pH is near-neutral, averaging 6.6 units. This average is distorted by the outlier pH of 4.6 found in one of the Berea sandstones (orange line in Figure 4.13). The acidic pH of that Berea sample could be the direct cause of its europium enrichment, but if so, further work is needed to explain why HREEs weren't similarly affected.

2.8 Produced Waters of the Williston Basin, North Dakota

Samples from the Williston basin partition into two distinct groups of typical LREE concentrations, and elevated LREE concentrations. Most samples have significant europium anomalies with balanced Sm-Gd riders. However there are exceptions to this both in the low-europium samples and in a minority of peaks with unbalanced riders.

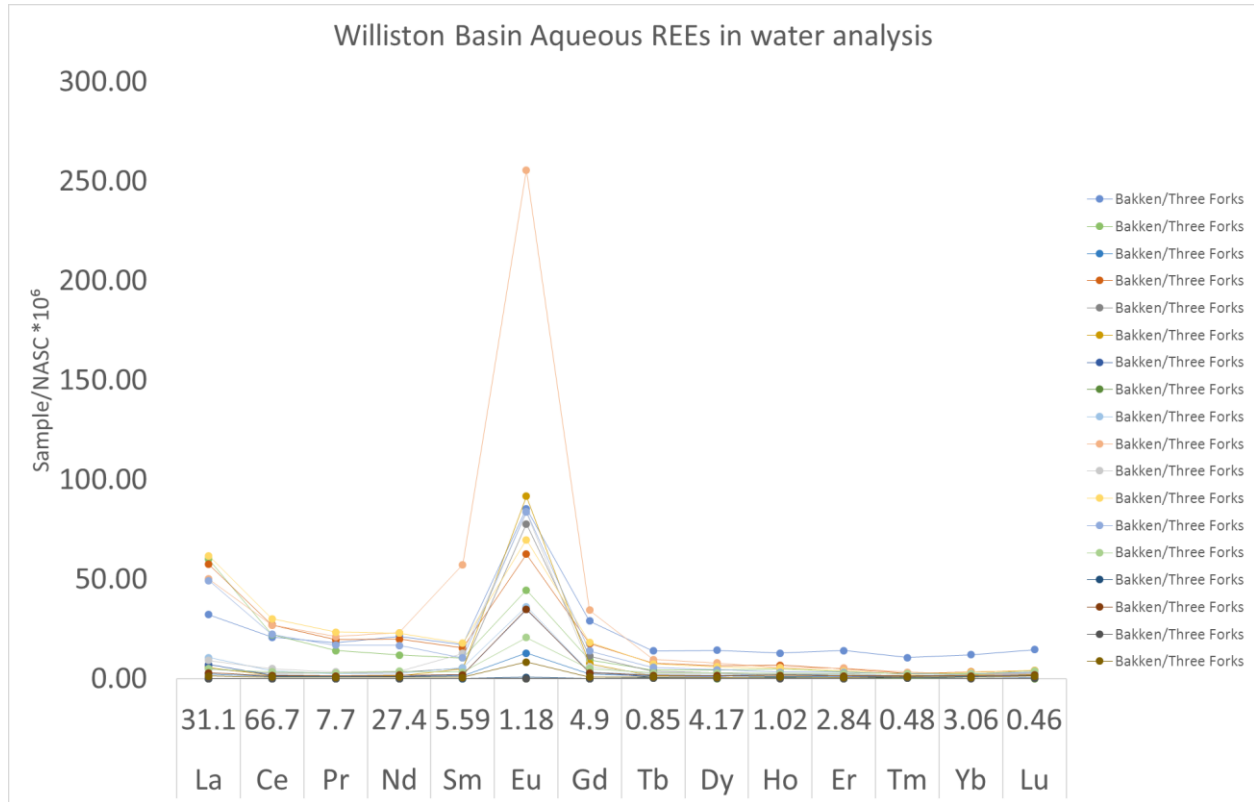


Figure 4.14: The Williston Basin sample set shown on a NASC-normalized plot. The Williston Basin contains two distinct groups of waters defined by an elevation of LREEs or lack thereof. The most significant peak (orange) appears to have unbalanced rider peaks different from all other samples, with Sm over Gd rather than Gd over Sm. However, the samarium was most likely boosted by the LREE enrichment, so this unbalanced style is less severe than it appears.

The Williston Basin, produces hydrocarbons from horizontal wells fracked in the Bakken Shale. These wells are the most saline in this study with an average TDS of over 310,000 mg/L and no significant outliers. As with most wells of such high salt content their water type is sodium-chloride, and other major ions are significant. Due to sample limitations, bicarbonate was not measured in these samples, so the TDS could be even higher. The pH is slightly acidic, averaging 7.2 units with no outliers.

Shortly after REE analysis, the researchers performed bivariate analysis to learn if the high and low LREE groups correlated to any other analyses' concentration. Because no correlation was discovered, either the cause of this behavior is multi-component or depends upon on some other parameters that were not measured for these brine waters. The conclusion of Chapter 6's advanced statistical techniques suggests that a multi-component analysis does not explain the behavior, and an unknown variable dictates REE concentration.

The unbalanced riders reflect the enrichment of gadolinium in excess of what would be expected from its nearest reliable neighbors samarium and terbium (europium is highly variable for unrelated redox reasons, and therefore not a suitable point for comparison). The gadolinium enrichment was observed in select Appalachian waters, and all PRB waters. The extensive cretaceous marine influence in the PRB is well established. Similar marine influence could have existed in Paleozoic marine shales such as the Bakken, Marcellus, and Utica.

2.9 Produced Waters of the Permian Basin, Texas

The Permian basin contains three units of interest, the Leonardian carbonates, the Wolfcamp-Cline shales, and the Pennsylvanian carbonates. Unlike the water samples from carbonate reservoirs in Wyoming that less Europium than expected, carbonate-hosted waters from the Permian basin have significant europium. Further, the two high-europium Leonardian samples also contain high concentrations of barium (more than any other carbonate in this study), but the importance of this co-variance is unclear.

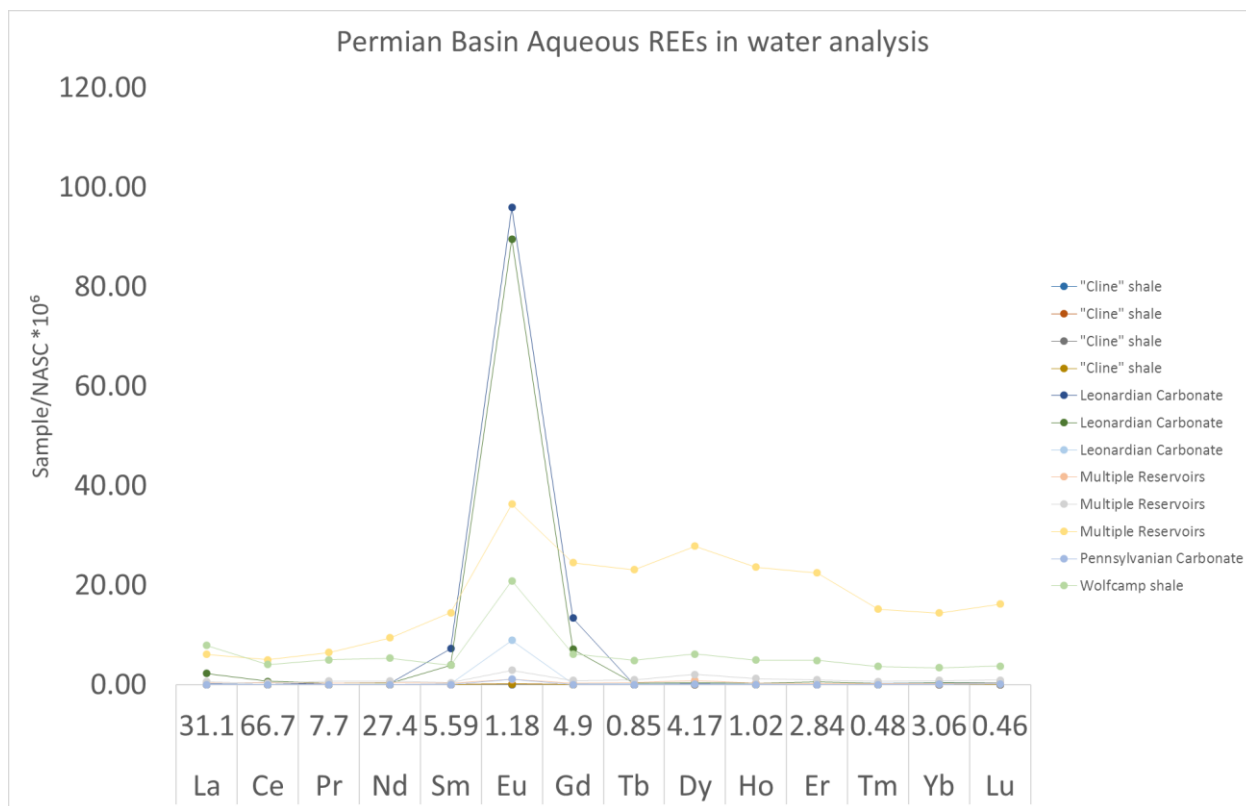


Figure 4.15: A NASC-normalized REE diagrams for the Permian Basin. Two Leonardian Carbonates have pronounced Eu enrichment with rider peaks typical of PRB-style gadolinium enrichment. The Cline samples have comparatively low TDS and are almost devoid of REEs, causing them to plot almost exactly on the zero of this graph. The yellow “Multiple Reservoirs” sample shows HREE enrichment, as does the Wolfcamp sample, to a lesser degree.

The Permian basin samples are sodium chloride type. The Cline shale samples have an average TDS of 45,000 mg/L but the other samples average 130,000 mg/L. The pH of the Permian basin waters is slightly basic, averaging 7.3 units.

The Permian basin samples contain many patterns with gadolinium enrichment. This enrichment is seen as a rider peak on the side of the europium peak. These enrichments occur most often in samples that also have high europium, such as the Leonardian, Wolfcamp, and “Multiple Reservoirs” samples.

3. NEW OPTIONS FOR AQUEOUS REE NORMALIZATION

Section 2 of this chapter presented all REEs as NASC-Normalized values. NASC-normalization is traditional, and allows comparison to many sedimentary rocks, such as Chapter 5. However, because REEs occur in water at much lower concentrations (ng/kg) than they occur in rocks (mg/kg), the NASC-normalized values require multiplication by 10⁶ to be easily read. When comparison to rocks is not necessary, water-based normalizations such as the North Pacific Deep Water (NPDW) normalization can be used to avoid the 10⁶ multiplication. The NPDW was introduced by Alibo and Nozaki, 1999. It was later explicitly standardized in Nozaki, 2001.

REE	La	Ce	Pr	Nd	Sm	Eu	Gd	Tb	Dy	Ho	Er	Tm	Yb	Lu
ng/kg	5.38	0.56	0.72	3.43	0.68	0.19	1.07	0.18	1.36	0.39	1.33	0.21	1.45	0.26

Table 4.4: The concentrations reported by Nozaki (2001) for North Pacific Deep Water (NPDW) converted to ng/kg. These values are suitable for normalization of REEs dissolved in water. However, due to well established cerium behavior in the ocean’s water column, these values introduce a cerium anomaly into all continental waters because continental waters do not exhibit that cerium behavior.

NPDW has many advantages for REE normalization because it reflects the concentration of REEs in the ocean. These advantages include; (1) providing a conceptually meaningful baseline because most readers have a rough sense of ocean water’s absolute salt content, (2) allowing a rough comparison to Ocean Mining (Rothe, 1985) because any REE with sample/NPDW greater than 1 indicates a concentration greater than the bulk ocean, and (3) removing many artifacts that are inherent to the variable dissolution of REEs.

Although NPDW normalization carries the above benefits it has a major drawback when applied to continental waters because it introduces a positive Ce anomaly. Ce in the ocean follows a natural process of oxidation, adsorption, and isolation in sea-floor sediments (Alibo and Nozaki, 1999). This results in depletion of oceanic cerium, and causes nearly all non-ocean waters to appear comparatively enriched in cerium. This drawback of a distracting cerium peak partially motivated development of the Wyoming Basin Produced Waters (WBPW) normalization.

3.1 How the WBPW Normalization was made

Aqueous REE concentrations of 38 exemplar Wyoming water samples were statistically assessed to fit a single peak Gaussian function to each REE (Figure 4.16). The Gaussian mean of each REE was taken as the Wyoming Basin Produced Waters (WBPW) normalization. The normalization was limited to just the Wyoming samples that lacked unique features, had good reservoir control, and good quality of their analysis.

The statistical assessment had two parts. First a log-histogram was formed from the measurements of aqueous REEs in each of the 38 selected samples. Second, single-peak Gaussian Probability Density Functions (PDF) were fitted to these histograms to identify the mean concentration and variation from the mean. (Ganshin, 2017) While the confidence interval is informative and shows the greater precision in HREEs, it was not reflected in the normalization, but could be added under later work.

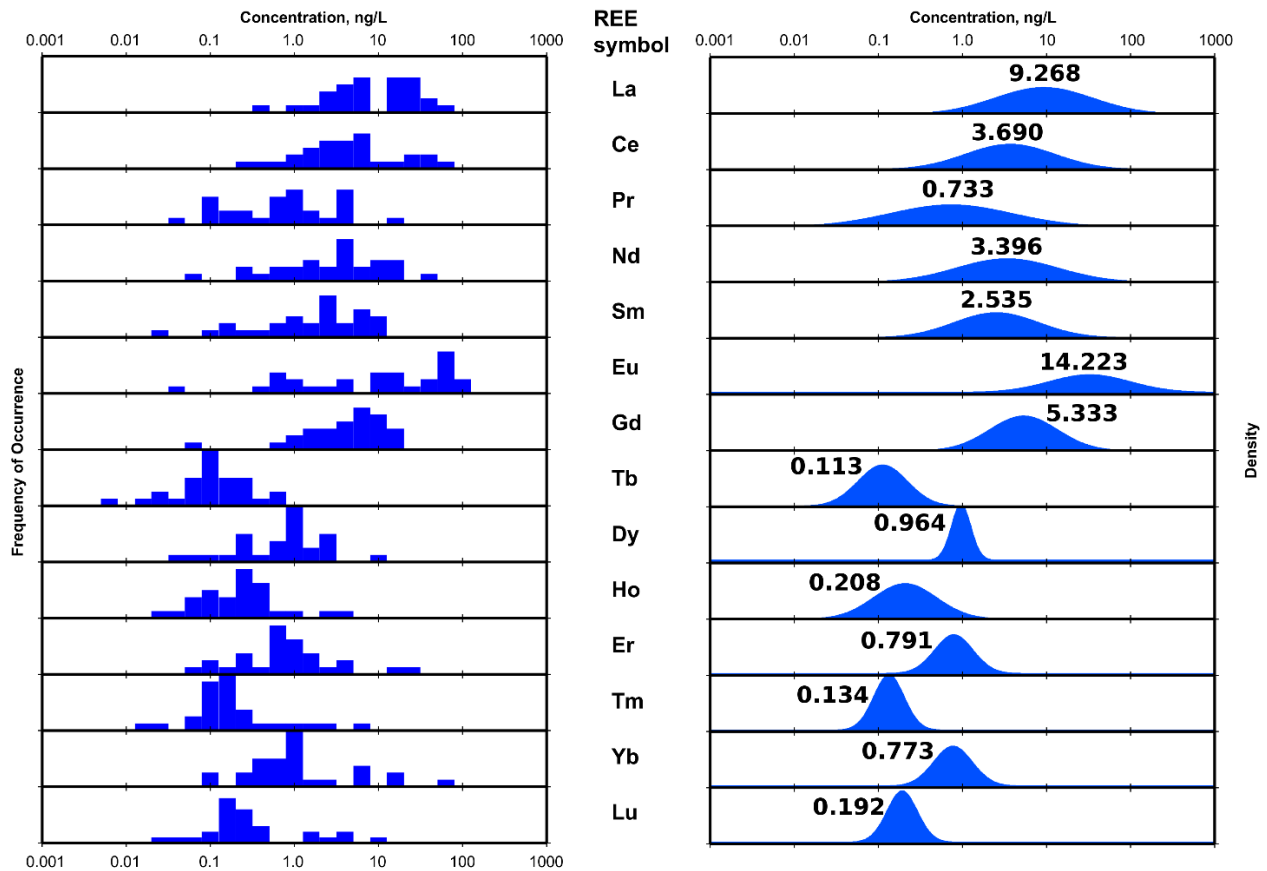


Figure 4.16: Empirical concentration log-histograms of Rare Earth Elements (REE) measured in 38 Wyoming samples (left) and the corresponding theoretical probability density functions (PDF's) obtained by fitting empirical distributions to a mono-peak Gaussian function, (right). The numbers indicate the theoretical peak (mean) concentrations (Ganshin, 2017).

The features visible in the PDF show both the Oddo–Harkins rule, and the fractionation of LREEs over HREEs. By choosing a normalization that reflects both of these their distracting effect on the REE patterns of the waters can be removed. Such a distraction-free normalization is more amenable to interpretation and identification of anomalies caused by local conditions. Future collections are expected to improve this normalization.

REE	La	Ce	Pr	Nd	Sm	Eu	Gd	Tb	Dy	Ho	Er	Tm	Yb	Lu
ng/kg	9.27	3.69	0.733	3.40	2.53	14.2	5.33	0.133	0.964	0.208	0.791	0.134	0.773	0.192

Table 4.4: The concentrations reported by Nye et al. (2018) for Wyoming Basin Produced Water (WBPW). These values are suitable for normalization of REEs dissolved in continental groundwater, especially waters reduced by interaction with hydrocarbons.

3.2 Features of the Normalization

As shown in Figure 4.17, we propose a new normalization to ease comparison of REEs in groundwater. Generally the LREEs were more variable and lower confidence, while the HREEs were better constrained. Also, as mentioned above the Oddo–Harkins rule and the LREE/HREE fractionation that is found in every terrestrial normalization is also present in ours.

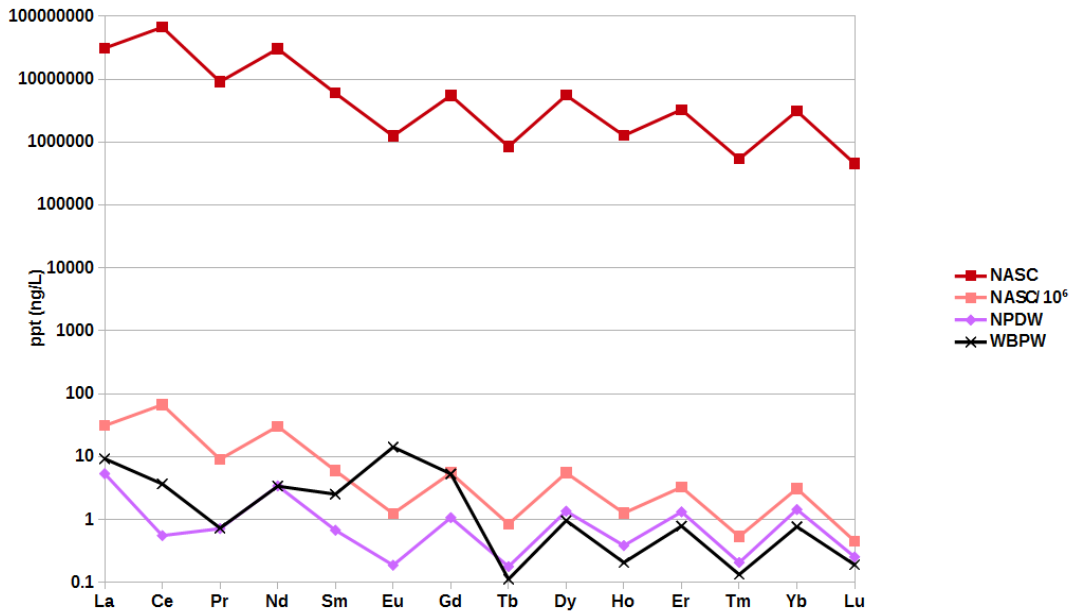


Figure 4.17: Chart of the absolute concentration in ppt (ng/L) of the North American Shale Composite (NASC in red), which has a pattern distinct from the North Pacific Deep Water (NPDW in purple). This can be seen by shifting NASC down by six orders of magnitude (pink). This difference in pattern is apparent in the Ce/Ce* concentrations, and also in the overall slope of the lines from LREEs to HREEs. The Wyoming Basin Produced Waters (WBPW in black) matches on-shore basin groundwater better than the other normalizations. This normalization is distinct from both NASC and NPDW in Ce/Ce* behavior, and especially in MREE behavior. The HREEs are similar to the existing normalizations.

This normalization has the benefit of removing distracting effects from the data and showing truly anomalous REE behavior, rather than all behavior that is different from the ocean (NPDW) or shale (NASC). In addition the excellent constraint on the sample collection exceeds that exercised for NASC which was compiled from 40 samples some of which had an unknown origin, and at least some of which were not even from North America (Grommet et al, 1984). Because NASC is an accepted and useful standard despite these shortcomings, WBPW could be as influential since it has about the same number of samples already, and has known locations for all its samples.

4. CONCLUSION

This section of the project discovered three significant findings: 1) that continental waters sampled for this study have two primary modes of samarium and gadolinium enrichment: balanced, and gadolinium-favored; 2) that positive cerium anomalies are rare but present in about 10% of the samples, mostly from geothermal sources; 3) that significant europium enrichment indicates a sub-surface water, but lack of such enrichment is not diagnostic of sample origin.

4.1 Balanced and unbalanced samarium-gadolinium rider peaks

First, a europium anomaly with balanced samarium-gadolinium rider peaks is the most common pattern of enrichment in produced waters. A significant minority of samples from parts of the Williston, Appalachian, and Permian Basins, and all of the Powder River Basin have unbalanced rider peaks where gadolinium is more enriched than samarium. Some groundwaters with low concentrations of all REEs, such as the Kevin Dome samples appear to lack all anomalies, although some have europium anomalies when sufficiently scrutinized. The reason for these two distinct modes of middle REE behavior is unknown.

4.2 Cerium anomalies and oxidation-induced water-rock fractionation

Second, the vast majority (89.7%) of samples have a negative cerium anomaly. Only 24 samples (10.7%) have the only positive cerium anomaly. Of those 24 samples with positive anomalies, 14 samples are from the ESRP, 1 sample is from Kevin Dome, 7 samples are from Wyoming basins, and 2 samples are from the Permian basin. The europium and cerium anomalies suggest that the two REEs with multiple naturally occurring oxidation states fractionate in different ways than the rest of the REEs. Europium fractionates into the water, and cerium tends to remain in the host reservoir rocks (Nye et al., 2017).

REE	Eu/Eu*	Ce/Ce*	LREE/HREE
ESRP	7.54	0.66	7.46
Kevin Dome	2.56	0.71	3.09
Wind River	22.15	0.69	17.26
Powder River	9.97	0.41	20.41
Green River	28.75	0.83	22.30
Washakie	48.93	0.41	5.00
Appalachian	13.30	0.69	36.93
Williston	8.24	0.78	80.20
Permian	11.85	0.75	17.53

Table 4.5: Averaged enrichment (>1) and depletion (<1) indices for Eu, Ce, and Light to Heavy REEs by basin. The largest europium anomalies are in the WRB. Significant Eu anomalies exist in the PRB also. Anomalies were calculated by: Eu/Eu^* , Ce/Ce^* , and La/Yb where: $Eu^* = \sqrt{(Sm_{NASC} \times Gd_{NASC})}$ and $Ce^* = \sqrt{(La_{NASC} \times Pr_{NASC})}$ after Taylor and McLennan, 1995.

4.3 Europium anomalies in association with oil and gas production

Third, significant europium enrichment occurs only in subsurface waters associated with oil and gas production. However, for an unknown reason, some subsurface produced waters can have insignificant europium enrichment. The result is that europium enrichment indicates a subsurface oil and gas water, but the absence of significant europium enrichment does not indicate any particular origin.

4.4 Basin-specific conclusions

Two models for two basins were developed as a result of the Wyoming sample's data analysis. These models attempt to explain two distinctive features in the Wind River Basin and the Powder River Basin.

4.4.1 Model for Wind River Basin enrichment, depletion, and hydraulic system

As above the Wind River Basin samples with a significant positive europium anomaly occur in samples from the Fort Union Formation (Figure 4.9) which are immature, young, continental sandstones containing significant Oil and Gas fields. A possible explanation for this positive anomaly comes from europium's two natural oxidation states. In nature, Eu can exist in divalent or trivalent state. In reducing conditions the easily dissolved divalent state is more common than the trivalent state (Sverjensky, 1984). Because of this behavior water-rock reactions in a reducing environment will enrich Eu over other redox-insensitive REEs. Such a reducing environment could be provided by hydrocarbons in the Fort Union Formation.

The opposite case, of a negative Eu anomaly, occurs in one sample from the Madison Limestone which is the deepest sample in the Wind River Basin. This sample's low europium content is caused in part by the host limestone containing very low concentrations of all REEs (see chapter 5). The limestone's REE deficiency was probably exacerbated by hydrothermal leaching which removed europium from the fluid-exposed parts of the Madison. This explanation depends upon hot, basement water passing through the Madison, leaching what little Eu there was, and leaving behind a rock surface with even less europium than the unreacted Madison. An intact rock sample from the Madison that exhibits europium leaching along its fractures would support this model, but if that fracture leaching were absent, this model is invalid.

A challenge to the above model is that units that trap natural gas should also trap water, yet the model suggests water escapes the Madison. Neelson et al., (2009) explained how this apparent contradiction resolves. Hydrothermal leaching could persist into the present day without allowing gas to escape the Madison because in units below the base of the Meeteetse Formation, the gas and water flow and storage systems are independent (Neelson et al. 2009). This explanation is especially attractive because the escape conduit (such as the faults identified by WSGS, 2015) that allowed water to leave the Madison could terminate in the Cody and help explain the HREE enrichment of that formation.

The other feature of the Madison sample is its HREE enrichment, which could have been sourced from the underlying basement. Basement rocks in the Wind River Basin have typical REE concentrations (Chapter 5) and a very large volume. Minor leaching would not noticeably lower the basement REE concentrations, and would provide a concentration of HREEs high enough to significantly elevate the HREE concentration of the Madison water. Because REEs do not dissolve readily (with the exception of Eu²⁺) this process may be slow allowing minor leaching to continue indefinitely.

The Cody sample with similar HREE enrichment might have received its HREEs through a similar process, with transport along one of the deep Wind River Basin faults that connect the Cody to the basement. (WSGS, 2015) However, it is unclear how HREEs could be transported in solution for well over a vertical mile, only to then concentrate and stall out in the Cody. A model to explain this behavior must not only offer a process for how the HREEs concentrated in the Cody, but also why that process wouldn't have occurred in any of the many formations between the Cody and the Madison.

4.4.2 Model for Cannonball Sea involvement in the Powder River Basin

In produced water samples with high europium content there are frequently small “rider” peaks on either side for samarium and gadolinium. However in the PRB the europium is below the level these riders are normally seen (compare with the high europium WRB samples). Further, the gadolinium rider is much larger than the samarium rider. This suggests that the gadolinium anomaly is not only significant but also caused by a unique variable not found in other regions. Nye et al., 2018 considered that this unique distinction was indicative of the marine influence of the marine origin of the sediments. Cannonball Sea arm. That work suggested that cretaceous marine shales in South Dakota or maybe even the entire area associated with the Western Interior Seaway could be responsible for the gadolinium peak.

4.5 Support for conclusions by other authors

This work also supports some previously established findings from other researchers. These findings include: 1) the concentrations of REEs in these brines are within the expected ranges for filtered natural water samples with near-neutral pH (e.g., Wood, 2002; Nelson et al., 2004) and 2) That continental groundwater may present a broad range of LREE-HREE ratios requiring site-specific evaluation.

CONTRIBUTIONS AND ACKNOWLEDGMENTS

GN and CN drafted this chapter manuscript, figures, and interpreted the data in this chapter. GN performed all aqueous REE extraction and measurement. CN compiled edits and conceived of the WBPW Normalization. All authors reviewed the chapter manuscript. Contributors include: The authors of chapter 2 who collected the water samples used in this chapter. Yuri Ganshin who developed and performed the computations to produce the WBPW Normalization. Tom Moore, who provided review and edits. Matt Johnson who provided an explanation for fluid behavior in the WRB's Madison formation. Funding for this work was provided by U.S. Department of Energy, Geothermal Technologies Office under Award DE-EE0007603. The authors would like to thank our DOE project managers Holly Thomas and Josh Mengers and also our Technical Monitoring Team for their support, advice, and insight.

REFERENCES

- Anders, M.H., Rodgers, D.W., Hemming, S.R., Saltzman, J., Divenere, V.J., Hagstrum, J.T., Embree, G.F., and Walter, R.C., 2014. A fixed sublithospheric source for the late Neogene track of the Yellowstone hotspot: Implications of the Heise and Picabo volcanic fields. *Journal of Geophysical Research: Solid Earth*, 119 (4), 2871–2906.
- Blackwell, D.D., 1989. Regional implications of heat flow of the Snake River Plain, northwestern United States. *Tectonophysics*, 164, 323-343.
- Cannon, C., Wood, T., Neupane, G., McLing, T., Mattson, E., Dobson, P. and Conrad, M., 2014. Geochemistry sampling for traditional and multicomponent equilibrium geothermometry in southeast Idaho. *GRC Transactions*, 38, 425-431.
- Dobson, P.F., Kennedy, B.M., Conrad, M.E., McLing, T., Mattson, E., Wood, T., Cannon, C., Spackman, R., van Soest, M. and Robertson, M., 2015. He isotopic evidence for undiscovered geothermal systems in the Snake River Plain. *PROCEEDINGS, Fortieth Workshop on Geothermal Reservoir Engineering, Stanford University, Stanford, California, January 26-28, 2015, SGP-TR-204*.
- Ganshin, Yuri. 2017. Personal communication.
- Grommet P.L., Dymek R. F., Haskin L.A., and Korotev R.L. (1984). The “North American shale composite”: Its compilation, major and trace element characteristics. *Geochimica et Cosmochimica Acta*, 48, pp. 2469-2482
- Mann, L.J., 1986. Hydraulic properties of rock units and chemical quality of water for INEL-1: a 10,365-foot deep test hole drilled at the Idaho National Engineering Laboratory, Idaho (No. IDO-22070). Geological Survey, Water Resources Division, Idaho Falls, ID (USA).
- Mattson, E.D., Conrad, M., Neupane, G., McLing, T., Wood, T. and Cannon, C., 2016. Geothermometry mapping of deep hydrothermal reservoirs in southeastern Idaho. Final Project Report No. INL/EXT-16-39154. Idaho National Laboratory (INL), Idaho Falls, ID, United States, p. 340.
- McLing, T.L., Smith, R.W., and Johnson, T.M., 2002. Chemical characteristics of thermal water beneath the eastern Snake River Plain. *Special Papers Geological Society of America*, 205-212.

- McLing, T., Smith, W., & Smith, R. (2014). Utilizing Rare Earth Elements as Tracers in High TDS Reservoir Brines in CCS Applications. *Energy Procedia*, 63, 3963-3974.
- Nealson, P.H., Trainor, P.K., and Finn, T.M., 2009, "Gas Oil, and water production in the Wind River Basin, Wyoming" U.S. Geological Survey Scientific Investigations Report 2008-5225, 24 p.
- Nelson, D. T., 2005, Rare Earth Elements as a Natural Tracer of Ground Water Flow in the Eastern Snake River Plain Aquifer, Idaho. M.S. Thesis: University of Idaho, Moscow, Idaho.
- Nelson, B.J., Wood, S.A. and Osiensky, J.L., 2004. Rare earth element geochemistry of groundwater in the Palouse Basin, northern Idaho–eastern Washington. *Geochemistry: Exploration, Environment, Analysis*, 4(3), 227-241.
- Neupane, G., Mattson, E.D., McLing, T.L., Palmer, C.D., Smith, R.W. and Wood, T.R., 2014. Deep geothermal reservoir temperatures in the Eastern Snake River Plain, Idaho using multicomponent geothermometry. PROCEEDINGS, Thirty-Ninth Workshop on Geothermal Reservoir Engineering Stanford University, Stanford, California, February 24-26, 2014 SGP-TR-202.
- Nozaki Y. Rare Earth Elements and their Isotopes in the Ocean. *Encyclopedia of Ocean Science*, Academic Press, (2001), pp. 2354-2366. <http://dx.doi.org/10.1006/rwos.2001.0284>.
- Nye, C., Quillinan, S., Neupane, G. and McLing, T., 2017. Aqueous rare earth element patterns and concentration in thermal brines associated with oil and gas production, Wyoming. PROCEEDINGS, 42nd Workshop on Geothermal Reservoir Engineering Stanford University, Stanford, California, February 13-15, 2017, SGP-TR-212.
- Nye, C., Bagdonas D., and Quillinan S. (2018) "A New Wyoming Basin Produced Waters REE Normalization and its Application" PROCEEDINGS, 43rd Workshop on Geothermal Reservoir Engineering. Stanford University, Stanford, California, February 12-14, 2018. Available at: https://pangea.stanford.edu/ERE/db/IGAstandard/record_detail.php?id=28263
- Pierce, K.L., and Morgan, L.A., 1992. The track of the Yellowstone hot slood: Volcanism, faulting, and uplift: *Geological Society of America Memoir*, 179, 1–52.
- Rodgers, D.W., Ore, H.T., Bobo, R.T., McQuarrie, N., and Zentner, N., 2002. Extension and subsidence of the eastern Snake River Plain, Idaho. *Tectonic and Magmatic Evolution of the Snake River Plain Volcanic Province*. Idaho Geological Survey Bulletin, 30, 121-155.
- Rothe P., 'Marine geology: mineral resources of the sea', in J.G.Richardson (ed.), *Managing the Ocean: Resources, Research, Law* (Lomond Publications, Mt Airy, MD, 1985), p. 21.
- Stetzenbach, K.J., Amano, M., Kreamer, D.K., and Hodge, V.F., Testing the limits of ICP-MS: Determination of trace elements in ground water at the part-pertrillion level: *Ground Water*, v. 32 p. 976-985. 1994.
- Strachan, D.M. , Tymochowicz, S., Schubert, P., Kingston, K.M., Preconcentration of trace transition metals and rare earth elements from highly saline solutions, *Analytical Chimica Acta*, 220, 243-249. 1989.
- Whitehead, R.L., 1992. Geohydrologic framework of the Snake River Plain regional aquifer system, Idaho and eastern Oregon. Regional aquifer system analysis-Snake River Plain, Idaho. US Department of the Interior, US Geological Survey Professional Paper 1408-B.
- Wood, S. A. (2001). Behavior of rare earth element in geothermal systems: a new exploration/exploitation tool. Final Project Report (No. DOE/ID13575). University of Idaho, Moscow, Idaho, US 94 p.
- (WSGS) Wyoming State Geological Survey (2015). "Geologic Cross Sections, Wind River Basin, Wyoming". State Geologist: Thomas A. Drean. Accessed from: <http://www.wsgs.wyo.gov/docs/wsgs-web-wrb-xsec.pdf>

Chapter 5: Rock Sample Analysis

Davin A. Bagdonas, Erin Phillips, J. Fred McLaughlin

Davin Bagdonas, Research Scientist, University of Wyoming, 1000 E. University Ave., Laramie, WY 82072
abags@uwyo.edu

Keywords: geothermal, rock, water-rock REE, hydrothermal, altered, Idaho, Wyoming

ABSTRACT

Researchers at the University of Wyoming have collected geothermal related rock samples from Wyoming basins and Idaho hydrothermal complex outcrops. These samples have been analyzed by optical microscopy methods, ICP-MS and –AES methods for geochemistry (major and trace elements), ion-exchange capacity, and X-ray Diffraction (XRD). These data have been used to understand REE concentration and relative abundances compared to the North American Shale Composite (NASC). The data have also been compared to the REEs in basin reservoirs where produced water samples have been collected. Naturally occurring hydrothermal systems have also been included in comparison to hydrothermal water samples collected in Idaho. Ion-exchange capacity and XRD mineralogy have also been used to identify the contribution to water chemistry of REE-bearing minerals within the rock systems. From this initial investigation, four primary basin reservoir types have been identified: shales, marine/delta sandstones, continental sandstones, and carbonates, all of which have predictable REE patterns. Additional samples of Idaho hydrothermal rocks exhibit a variety of REE behaviors, but within expectation of studied rock types. Distinct REE concentrations were found in reservoir rocks matching expected patterns of primary igneous and clastic sediments, clay dominated systems, organic-rich systems, and carbonate dominated systems. Many processes affect REE fractionation during the exchange of REEs from rocks to water, and complex relationships over geologic time periods make prediction difficult.

1. INTRODUCTION

This geological analysis was developed to complement the geochemical assessments of produced water and geothermal water samples. Specifically, this task was designed to test the influence of reservoir rock-type and corresponding mineralogy/geochemistry on the concentrations of REE found in oil and gas produced waters. There has been no direct investigation of REE reactions relative to rock-type in deep oil and gas brine prior to this investigation.

Based on geochemical trace element data, four primary REE concentration patterns can be described: (1) A primary igneous REE pattern including immature clastic sediment (sands and siltstones) patterns found at locations along basin margins, (2) Clay dominated patterns, (3) HREE-enriched patterns influenced by organic material abundances, and (4) Carbonate system patterns.

Correlation of REE concentrations in rocks to produced waters and naturally occurring hydrothermal systems are complex and difficult to predict. In this work we present the best inferences of these potential reactions, but acknowledge the difficulty of ascribing a single correlation to a single process. Many processes and factors affect REE fractionation during the exchange of REEs from rocks to water (or water to rock), including: (1) fluid history origin and host rock history interactions; (2) organic and nonorganic ligands within the water-rock system that occur over the entire history of a system; (3) migration of meteoric water input from basin margins to deep basin reservoirs; and (4) REE valence state preferences occurring in various geologic settings. Long and multi-event fluid histories over geologic time periods compound these complex relationships, making prediction more difficult.

2. DATA COLLECTION

2.1 Rock Sample Collection

Researchers at the University of Wyoming collected 83 rock samples representing target formations in 4 Wyoming basins (fig 5.1), and 18 samples representing various rock types occurring in natural geothermal systems across Idaho. All rock samples have been matched to lithologies from which water samples have been collected. Wyoming basin samples were selected from core available at the USGS Core Research Center (CRC) in Golden, Colorado. Core samples were chosen for the best representation of basin subsurface intervals (formation types) where water samples used in this investigation originated. When enough information about well perforation intervals was available the team attempted to match the sub-region of the formation that most closely matched this perforated interval from which the waters originated. The Idaho samples were selected from outcrops within or adjacent to active hydrothermal systems. These outcrops represent both intrusive and extrusive igneous systems, metamorphic rocks, and some sediments. From all samples, plugs were removed and later split into an aliquot for whole rock chemistry, ion-exchange, or XRD analysis, and a second aliquot for thin section analysis.

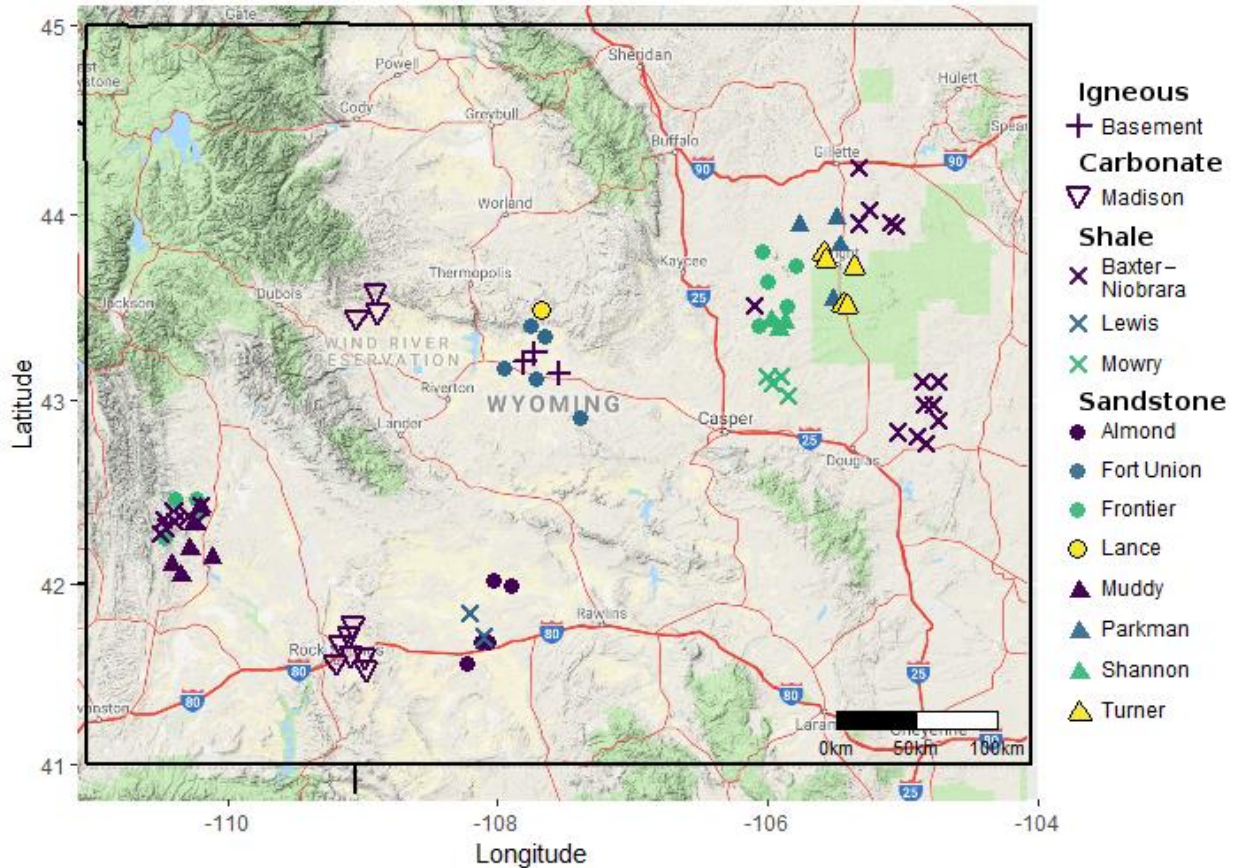


Figure 5.1: Sample locations and lithology of core samples collected to represent geothermal water samples in Wyoming. All samples shown here were collected at the USGS Core Research Center. Core is representative of the three major basins where produced water samples were collected, and correlates to sampled intervals. The contemporaneous Baxter (southwest, Wyoming) and Niobrara (northeast, Wyoming) have been combined for simplicity in the figure.

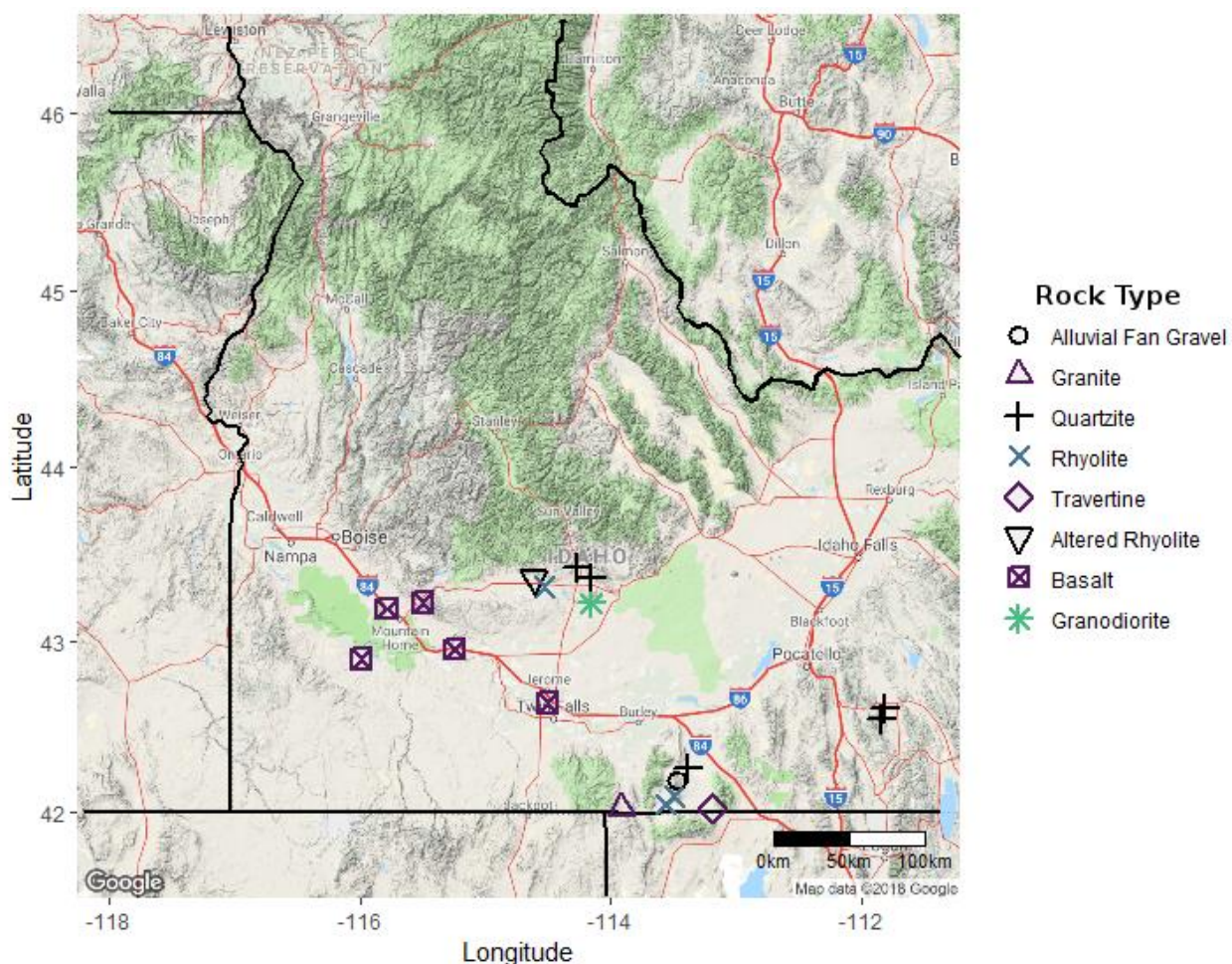


Figure 5.2: Sample locations and lithology of samples collected to represent geothermal water samples in Idaho.

2.2 Analysis of Rock samples

Samples were analyzed using optical microscopy methods common to thin section petrography. Mineralogy descriptions derived from optical microscopy methods helped guide selection of geochemical, ion-exchange capacity, and XRD sample analysis.

2.2.1 Geochemistry

Geochemistry of rock samples was analyzed (ALS, Reno, NV) by both ICP-AES and ICP-MS standard procedures for whole-rock geochemistry major oxide and trace element compositions, respectively (data available at <https://gdr.openei.org/submissions/953>, <https://gdr.openei.org/submissions/926>, and <https://gdr.openei.org/submissions/989>). To verify trace element geochemistry, including REEs, comparison with previously obtained data for similar formations in Wyoming basins was made. Measured REEs for each rock sample were plotted on standard REE spider-diagrams normalized to the North American Shale Composite (NASC) (figs 5.3, 5.4, 5.5, and 5.6). NASC is an appropriate choice because most samples are sandstones, shales, and related sediments. For consistency and direct comparison with sediments, igneous samples (figs 5.5 and 5.6) were also NASC normalized. NASC normalization was also appropriate as it was used for water REEs as in Chapter 4.

2.2.2 Cation Exchange Capacity Analysis

Cation exchange capacity (CEC) analysis was completed by Wyoming Analytical Laboratories (Laramie, WY). Analysis focused on four primary reservoir types representing major basin rock types in Wyoming: shales, marine sandstones, continental sandstones and carbonates (Table 5.1, below). Bulk samples, involving the combination of several plugs per formation were used to represent larger formation intervals.

Formation	Rock type represented
Fort Union	Continental sandstone
Sussex	Marine sandstone

Madison	Shallow marine carbonate
Mowry	Deep water marine shale

Table 5.1: Table of the rock samples used in this work and the four type lithologies they represent.

The Fort Union Formation and Sussex Formation were selected as representative of continental and marine sandstones, respectively. The Madison Formation was chosen as a carbonate example, and the Mowry Shale as the best fit for shale type in evaluated basins.

2.2.3 X-ray Diffraction Analysis

X-ray diffraction analysis was completed at the Wyoming State Geological Survey (Laramie, WY). Thirty-one CRC samples were selected that correspond to reservoirs investigated for water chemistry (table 5.2). Similar to CEC samples, these were selected as the representative examples of marine and continental sandstone, shales, and carbonate rocks. Samples were selected from pieces of core plugs that were analyzed via thin sections. They were then powdered and analyzed on a Rigaku MiniFlex II desktop diffractometer (30 kV, 15 mA, 0.02° step width, and 1.02 seconds/step scan speed). Raw XRD data were then processed through JADE for mineral identification based on merit of fit, with additional comparison and verification to mineral identification from thin sections.

3. ROCK SAMPLE RESULTS AND DISCUSSION

Rock samples were collected to represent best the intervals and formations where water data were collected in Wyoming basins (fig 1). These lithologies have been divided into subgroups of rock type, including shales, sandstones, carbonates, and in a few cases igneous basement rocks. Samples were evaluated for anomalous REE concentrations by plotting on Upper Continental Crust (UCC) or NASC normalized spider diagrams according to their rock type. Subsequently, all samples were NASC-normalized for comparison to each other.

3.1 Geochemistry (REEs)

Shales from Wyoming basins (fig 5.3) group around a sample/NASC value of 1. Shales are expected to produce this result when NASC-normalized. Four shale subgroups are apparent in the data: (1) Baxter Shale samples plot below NASC, (2) Lewis Shales are enriched in LREEs and depleted in HREEs relative to NASC; (3) Mowry Shales are enriched in total REEs relative to NASC; and (4) Niobrara Shales are mostly depleted in total REEs with some LREE abundances above NASC. Exceptions to this Niobrara Shale behavior include: a single sample exhibiting enrichment in every REE, another single sample exhibiting a significant depletion in LREEs relative to NASC, and final single sample enriched in all REEs, especially in HREEs, relative to NASC. This last Niobrara behavior is interpreted to be typical of organic shale behaviors and likely does not reflect mineral behavior or source mineral input. Those samples with negatively sloped REE patterns (LREEs>HREEs) like the Lewis Shale likely reflect clastic source and may be considered less evolved shales when compared with flat REE patterns.

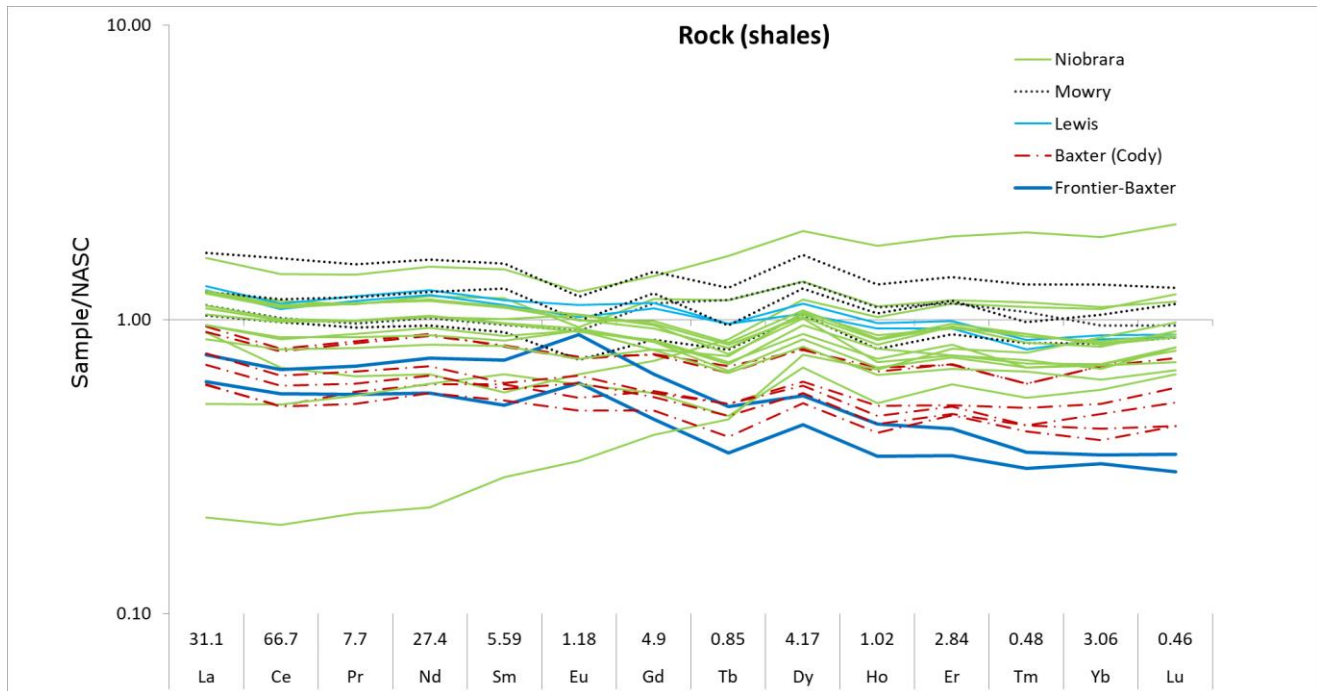


Figure 5.3: REE concentrations of shale samples collected at the Core Research Center normalized to the North American Shale Composite (NASC). Values for NASC from Gromet et al. (1984) are given on the X-axis in ppm. While most samples generally follow the NASC trend, some are enriched in HREE and nearly all Wyoming shales have a Dy and Gd anomaly.

Sandstones from Wyoming basins (figs 5.4 and 5.5) exhibit typical NASC normalized clastic sediment REE patterns, resulting in relative LREE enrichment over HREEs. The majority of evaluated samples including the Almond, Fort Union, Lance, Shannon,

Frontier, and Parkman Formations have total REE values of less than $NASC=1$. Only one Frontier sample shows relative total REE enrichment above $NASC=1$, while a few Muddy and Turner formation samples have slightly elevated concentrations of some LREEs compared to $NASC$. Both continental and marine sandstones in this work are seen to inherit with little to no modification the igneous REE pattern of their protoliths.

A different Frontier Formation sample exhibits a MREE hump that is relatively enriched compared to $NASC$ (fig 5.5). This hump may indicate hydrothermal deposition of REEs in a redox boundary of the sediment, or a mineral control that is different than other sandstone samples evaluated here. Additionally, a single Muddy Formation sample exhibits the highest LREE concentration and a steeper slope from LREEs decreasing to HREEs. This is likely indicative of mineral control on LREEs in this sample, similar to monazite or rhabdophane REE behavior.

The Madison Formation (fig 5.4) was the only carbonate formation assessed. All samples exhibit significant relative depletion in total REEs relative to $NASC$ and have no significant relative enrichment in LREE or HREEs. Within the Madison samples there are two groups of REE behaviors. Three of the ten samples have relatively flat REE $NASC$ normalized profiles while the remaining samples have variable saw-tooth patterns that are more depleted in total REEs. This difference may represent two groups of carbonates that have been in contact with different waters or have different rock/water interaction variables, although the saw-tooth could also be an analytical artifact.

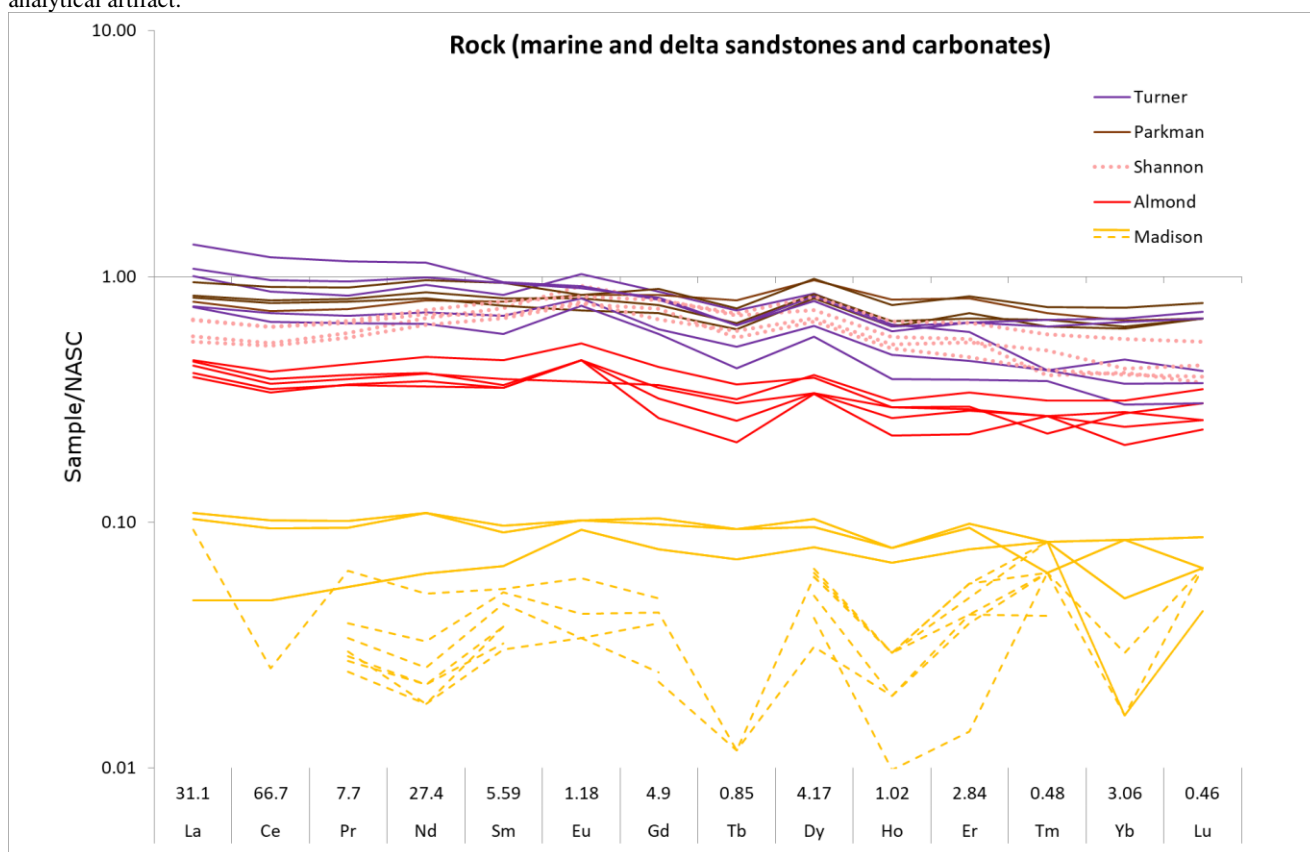


Figure 5.4: REE concentrations of marine and delta sandstones and carbonate samples collected at the Core Research Center normalized to the North American Shale Composite (Gromet et al., 1984). Normalizing values in ppm are provided in the X-axis; Y-axis is logarithmic and unit-less due to normalization. Note that most marine and delta sandstones are more enriched in LREE compared to HREE relative to $NASC$, and that carbonates have distinctly lower REE concentrations. Carbonate samples are divided into two groups; solid lines are distinctly flat whereas dashed lines are likely saw-tooth because of low values and associated analytical artifact.

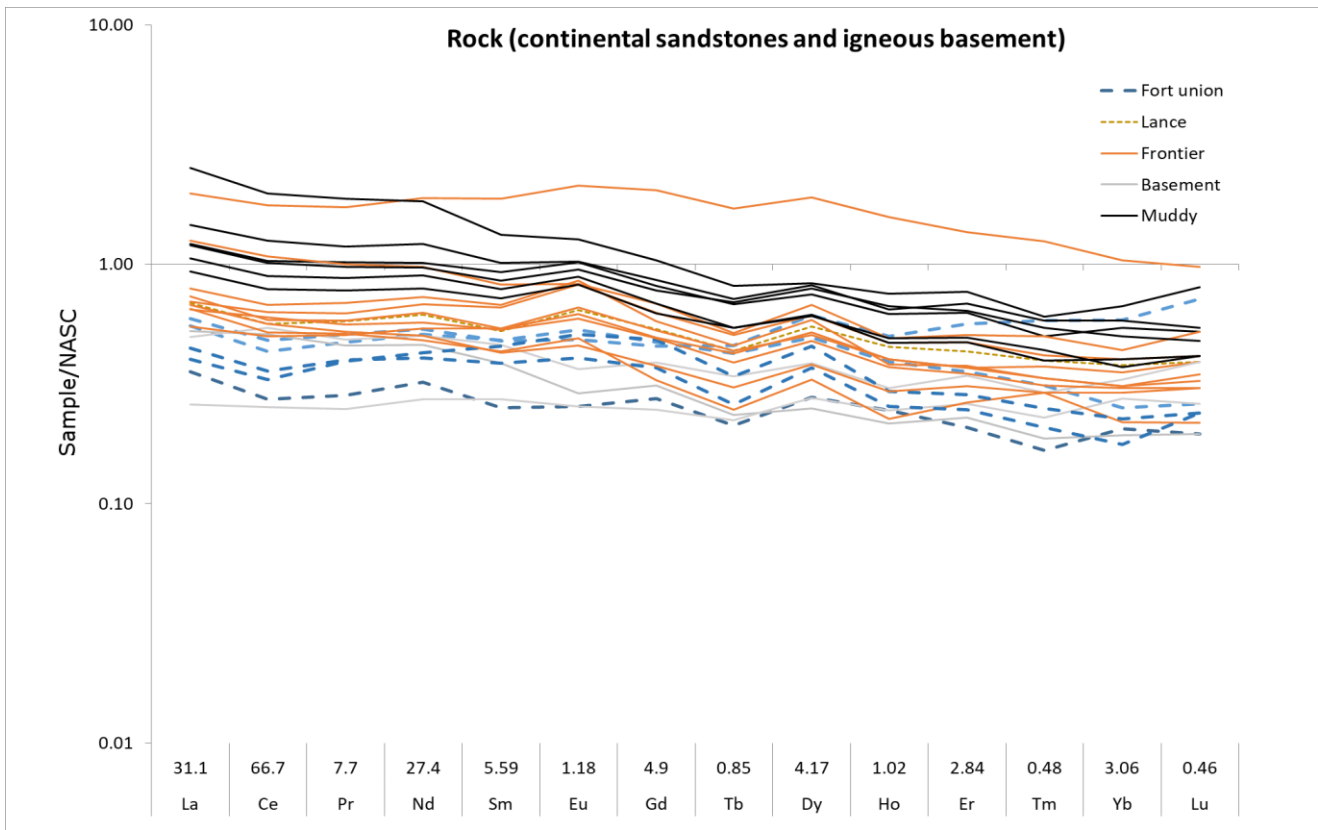


Figure 5.5: REE concentrations of continental sandstone and basement samples collected at the Core Research Center normalized to the North American Shale Composite (Gromet et al., 1984). Normalizing values in ppm are provided in the X-axis; Y-axis is logarithmic and unit-less due to normalization. Note that most sandstones are more enriched in LREE compared to HREE relative to NASC, and are similar to igneous basement rocks.

Several lithologies have been identified as hosts to Idaho water samples collected for this project (fig 5.2). These lithologies have been grouped into individual rock types for evaluation. All samples have been NASC normalized for comparison with other samples in this project. Diversity of rock types in this evaluation has resulted in a wide variety of REE behaviors discussed below (fig 5.6).

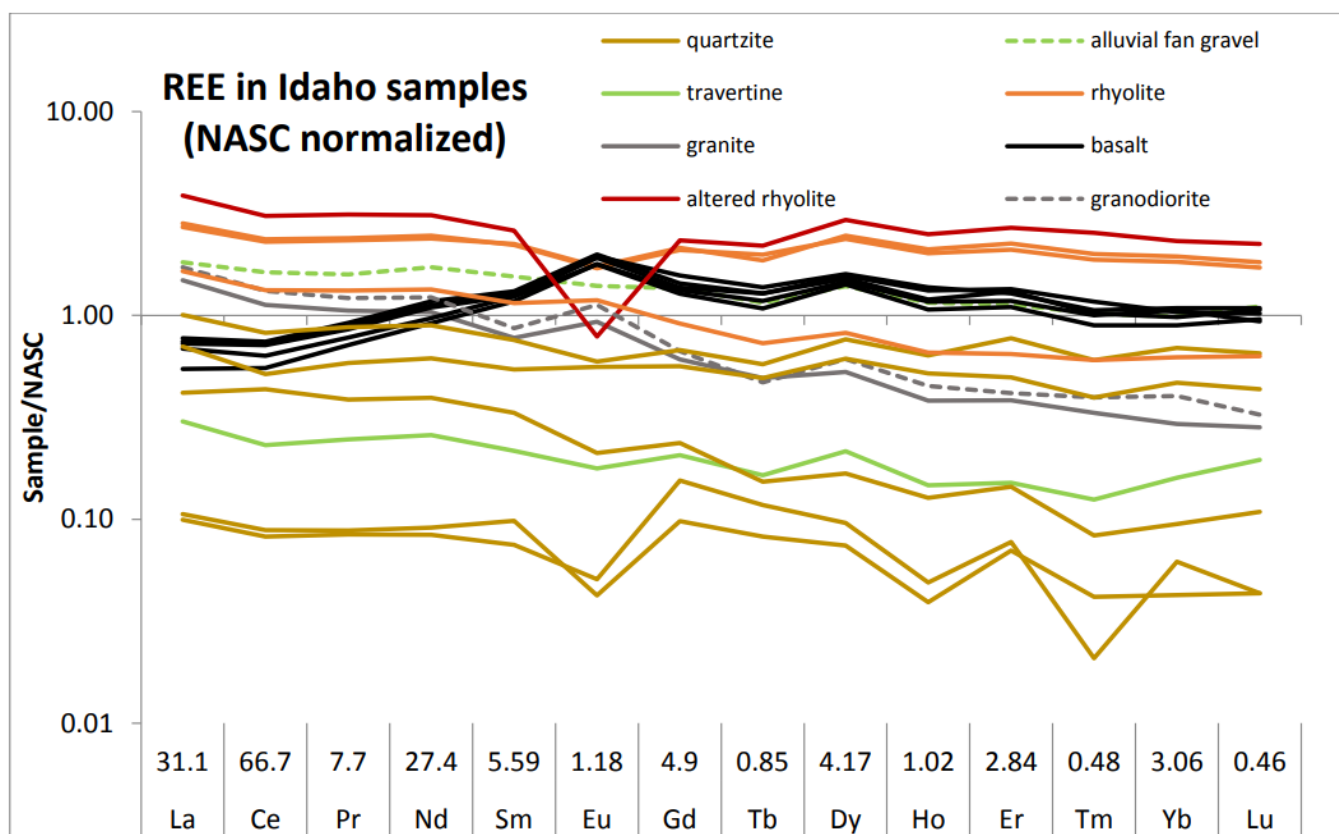


Figure 5.6 REE concentrations of Idaho rock samples collected in the field and normalized to NASC (Gromet et al., 1984). Normalizing values in ppm are provided in the X-axis; Y-axis is logarithmic and unit less due to normalization. REE concentrations of this sample set vary; notable observations include the low concentration of REE in quartzite samples and Eu-enriched and Eu-depleted rhyolites.

In general, basalt samples behave predictably. They cluster as a group and exhibit relative positive Eu anomalies and have slightly enriched HREEs when compared to LREEs. They are relatively enriched in total REEs compared to NASC. Despite variable hydrothermal involvement of these samples from relatively fresh to strongly altered, they behave as single group. This suggests that REEs have not been mobilized from the basalt samples, or water/rock interactions have been limited to an insignificant surface area.

Rhyolite samples in this investigation are less constrained, but form two individual REE profile types. A typical rhyolite REE behavior is seen with two samples, having relatively enriched total REE profiles and minor negative Eu anomalies. LREEs are slightly enriched compared to HREEs, resulting in a negatively sloped REE profile. The second variety of rhyolite REE profile is exhibited by an altered rhyolite sample. This sample is similar in composition to the typical rhyolites described above, but has undergone significant alteration from geothermal fluids. The result is a significant negative Eu anomaly that suggests Eu depletion by hydrothermal waters. The remaining REEs are relatively enriched when compared to the typical rhyolites. This is common when other whole-rock constituents or mineral species have been removed via hydrothermal alteration. The LREE and HREE relative enrichment is evidence of these species remaining in the host rhyolite.

Several sandstone/quartzite host rocks were evaluated. All quartzite samples are relatively depleted in total REEs when compared to NASC. The lowest concentrations of total REEs are exhibited by two hydrothermally altered samples that have a long water/rock interaction history. Unaltered samples were not found, so inferences of REE removal via hydrothermal alteration can only be suggested at this time. The significant negative Eu anomalies of the two depleted samples hint at hydrothermal alteration, but again, unaltered host rock will need to be evaluated before determination of this behavior. The remaining sandstone/quartzite samples are similar to typical sandstones evaluated elsewhere exhibiting relatively greater LREE concentrations compared to HREEs, resulting in a negatively sloped REE profile.

A single granite sample and single granodiorite sample were evaluated for REEs. They do not show evidence of hydrothermal loss or gain of REEs and can be considered typical in REE behavior. It is likely that hydrothermal waters sourced from these rocks have very little water/rock interaction and limited available surface area to contact. This is typical of jointing in basement type rocks where hydrothermal fluid is constrained to low-surface area conduits.

Alluvial fan deposits and travertine sourced from hydrothermal waters flowing through those deposits were also evaluated for REE behaviors. Results are inconclusive at this time, but initial observation suggests the travertine has relative depletion in total REEs when compared to both alluvial fan deposits and underlying rhyolites. REEs are likely not being removed from rock to enter the fluid in this particular system because the water's residence time in the alluvial fan and rhyolites is very short.

3.2 Cation Exchange Results

Four distinct reservoir types were selected for CEC analysis: a shale, two sandstones (one continental and one marine), and a carbonate. The Mowry Shale has the highest value of CEC of 8.66 meq/100 gm. The Sussex Formation (a marine sandstone that is similar to the Shannon Sandstone) has an ion-exchange capacity of 7.91meq/100 gm, while the Fort Union Formation (continental sandstone) has a lower 4.84 meq/100 mg. The Madison Formation had the lowest ion-exchange capacity of 0.58 meq/100 gm. The Mowry Shale has the highest CEC, meaning its minerals harbor the greatest physical potential to attract and exchange positively charged cations such as REEs; it has slightly elevated REE concentrations relative to the other three selected samples (fig. 5.3, 5.4 and 5.5). The Madison Limestone has the lowest CEC, meaning its potential for collecting and/or exchanging positively charged cations is relatively low, and it has distinctly low REE concentrations with respect to the sample set.

3.3 X-ray Diffraction

A diversity of primary minerals were identified using XRD analysis (table 5.2), and are listed by rock type. Minerals in carbonate rocks include calcite, dolomite, quartz and clay. Continental sandstones are more diverse with quartz and clay occurring in all samples. Na-feldspar occurs in the Frontier Formation and a single Muddy Sandstone, but is absent in the majority of continental sandstones, indicating more mature sediments or diagenesis resulting in feldspar to clay transitions. The single Fort Union Formation sample is the most diverse and includes dolomite, kaolinite, chlorite, and dickite, but lacks feldspars. This sample is mature and has undergone diagenetic alterations resulting in dolomite cementation and kaolinite/chlorite growth. Kaolinite occurs in three of the Muddy Sandstone samples, but without the presence of chlorite, and the inclusion of rutile in a single occurrence (likely within quartz grains). These three samples are in different geographic locations than other Muddy samples indicating kaolinite stability in some of the Muddy while lack thereof in other places. This difference may play a subtle role in REE behavior, but would require additional investigation to verify. Two marine sandstones were evaluated. The Parkman Sandstone is less mature, cemented with dolomite and calcite, and has kaolinite in the matrix. In contrast, the Turner Sandstone is mature, having only quartz and some minor clay. Shale samples include the Baxter, Mowry, and Niobrara Shales, some of which contain biotite and muscovite. Calcite and dolomite occur in both the Baxter and Niobrara Shales, but are lacking in the Mowry Shale. Kaolinite occurs in all shales, while dickite occurs in a single Mowry sample.

CRC Sample ID	Depth (ft)	Formation	Rock Type	Na-Plagioclase	Quartz	Biotite	Muscovite	Clay	Calcite	Dolomite	Pyrite	Kaolinite	Chlorite	Dickite	Rutile
D037	7496	Madison	carbonate		X			X	X	X					
D037	7593	Madison	carbonate		X			X	X	X					
S462	7428	Fort Union	continental sandstone		X			X		X		X	X	X	
B209	6189	Frontier	continental sandstone	X	X			X	X						
E173	12232	Frontier	continental sandstone	X	X			X					X		
A110	7680	Muddy	continental sandstone		X			X				X			
A110	7663	Muddy	continental sandstone		X			X				X			
A606	7770	Muddy	continental sandstone		X			X				X			X
A650	7717	Muddy	continental sandstone		X			X							
A650	7732	Muddy	continental sandstone		X			X						X	
C548	8001	Muddy	continental sandstone		X			X							
D780	7632	Muddy	continental sandstone		X			X				X			
D839	8200	Muddy	continental sandstone	X	X			X							
A029	7317	Parkman	marine sandstone	X	X			X	X	X		X			
E124	10113	Turner	marine sandstone		X			X							
D904	454.5	Baxter	shale	X	X	X		X	X	X					
R567	2423	Mowry	shale	X	X		X	X			X	X	X		
R567	2475	Mowry	shale	X	X	X	X	X			X	X	X		
R571	2330	Mowry	shale		X			X				X		X	
W075	10646	Mowry	shale		X			X				X	X		
A648	6146	Niobrara	shale		X			X	X			X			
E815	9140	Niobrara	shale	X	X		X	X		X	X	X			
E815	9202	Niobrara	shale	X	X			X	X	X					

Table 5.2: Table of minerals found during the XRD investigation. The category “Clay” includes more clay minerals than shown. Because the samples were not glycolated these clays were identified in general rather than being subdivided into exact minerals. Minerals that were included in the search but not found in the preliminary investigation were: Ca-Plagioclase, Alkali feldspar, Pyroxene, Amphibole, Gypsum, Halite, Illite, Zircon, and Hematite.

4. CONCLUSION

1) Based on geochemistry data of trace elements of basin rock samples, four primary REE patterns have been recognized: (1) A primary igneous REE pattern including immature clastic sediment (sands and siltstones) patterns reflective of detrital source compositions from locations along basin margins, with REE profiles reflecting igneous REE-bearing host minerals (LREE-enriched, Eu-negative anomaly, and reduced HREE concentrations); (2) Clay dominated patterns with MREE enrichments on NASC normalized plots (having an abundance of ion-exchange favorable Si-Al sheets); (3) HREE-enriched patterns influenced by organic material abundances; (4) A carbonate systems pattern with overall lower REE concentrations than all other sediments, exhibiting a flat pattern across all REE species.

2) In some cases, NASC normalized patterns for a single sample may represent more than one REE influence/pattern type. For example, a single organic shale can exhibit both MREE- and HREE-enrichments due to a combination of organics and clays and still exhibit a

relative LREE-enrichment reflecting an origin of continental derived sediment. Another example is sandstone that exhibits a steeper than normal profile from LREEs to HREEs. This type of REE pattern is indicative of a greater than average LREE-bearing mineral concentration, like igneous sourced monazite, being present within a “lag deposit” of a sediment.

3) CEC appears to not have a correlation to the REE concentration in subsurface reservoirs, though this sample set is too limited for definitive conclusions. In short, shales tend to have larger CEC values, while carbonates have the least. Sandstones vary depending on their primary geochemical makeup wherein the volume and type of clay minerals might be the most pertinent variable. CEC was suggested for investigation as it was hypothesized to be a potentially simple prospecting REE technique. However, CEC requires relatively large sample volumes and involves a destructive analytical process, which are two factors that are typically avoided for core-based analytical techniques.

4) XRD analysis supports mineralogical observations from core and thin section; targeted reservoirs vary by maturity, mineralogy and clay content. All samples had some amount of clay and quartz, though these were only in trace quantities in carbonate samples. Reservoir samples with greater clay volumes, specifically marine shales, typically exhibit higher concentrations of MREE to HREE. Shale samples that do contain biotite or muscovite often contain pyrite, and can include chlorite. This is indicative of reduced shales, often with an abundance of organic materials and sulfur. Despite the organic nature of these shales, they do not appear to have increased REE concentrations, grouping around NASC (fig 5.3). Sandstone samples, which are predominantly quartz, exhibit the LREE enrichment that is similar to basement/granitic samples. The single Frontier Formation sample (CRC# E173), which exhibits an anomalous total REE enrichment (fig 5.5), appears to be slightly less mature based on inclusion of Na-feldspars, but otherwise has no indication of a primary mineral derived REE enrichment. Trace minerals, likely occurring within lag type deposits in immature sandstones are expected to greatly vary the REE concentrations within a formation depending on sample location. Nearly all of the samples were mature sediments, and lack minerals that are more abundant in first generation sediments (calcic plagioclase, pyroxene, etc.). This is correlative to the lack of an observed Eu anomaly in all sediments.

5) Correlation of REE concentrations in all rocks studied in this project to fluids in contact with those rocks is complex and difficult to predict. Initial description of potential relationships of water-rock interaction in regard to basin samples is described in Nye, et al. (2018). Essentially, a diversity of processes must play a role in REE exchange between water and hot reservoir rock. Many processes and factors affect REE fractionation during the exchange of REEs from rocks to water (or water to rock), including: (1) fluid history origin and host rock history interactions; (2) organic and nonorganic ligands within the water-rock system that occur over the entire history of a system; (3) meteoric water input on basin margins to deep basin reservoir end points; and (4) REE valence state preferences occurring in various geologic settings. Long fluid histories over geologic time periods compound these complex relationships, making prediction more difficult.

CONTRIBUTIONS AND ACKNOWLEDGMENTS

DB wrote this manuscript, collected and managed CRC/outcrop samples, and interpreted the data presented in this chapter. EP edited the manuscript and reviewed DB's interpretation. FM collected CRC samples, wrote the CEC section, wrote the X-ray Diffraction section, and conceived of the work presented in this chapter. All authors reviewed the chapter manuscript. Contributors include: Mackenzie Swift who prepared samples for XRD. Thomas Moore who prepared the maps of Figures 1 and 2. Funding for this work was provided by DOE EERE - Geothermal Technologies Program award number DE-EE0007603. The authors would like to thank our industry and landowner collaborators for site access and permission to sample. The USGS-CRC facility was invaluable for core samples. Wyoming State Geological Survey and Robert Gregory provided XRD facilities and interpretation.

REFERENCES

- Condie, K.C., 1991. Another look at rare earth elements in shales. *Geochimica et Cosmochimica Acta*, 55(9), pp.2527-2531.
- Condie, K.C., 1993. Chemical composition and evolution of the upper continental crust: contrasting results from surface samples and shales. *Chemical geology*, 104(1-4), pp.1-37.
- Gromet, L.P., Haskin, L.A., Korotev, R.L. and Dymek, R.F., 1984. The “North American shale composite”: its compilation, major and trace element characteristics. *Geochimica et Cosmochimica Acta*, 48(12), pp.2469-2482.
- Nye, C., Quillinan S., Neupane G., and McLing T. L.: Aqueous Rare Earth Element Patterns and Concentration in Thermal Brines Associated With Oil and Gas Production, *Proceedings*, 42nd Workshop on Geothermal Reservoir Engineering. Stanford University, Stanford, CA (2017). SGP-TR-212.
- Nye, C., Bagdonas, D.A., and Quillinan, Q.: A New Wyoming Basin Produced Waters REE Normalization and Its Application, *Proceedings*, 43rd Workshop on Geothermal Reservoir Engineering. Stanford University, Stanford, CA (2018). SGP-TR-213.

Chapter 6: Predicting Rare Earth Element Potential in Produced and Geothermal waters of the United States: Application of Emergent Self-Organizing Maps

Mark A. Engle

U.S. Geological Survey, University of Texas at El Paso, Dept. of Geological Sciences, 500 West University Ave., El Paso, Texas 79968

Keywords: Critical Minerals, Compositional Data Analysis, Neural Networks, Brines

ABSTRACT

This chapter presents findings from the application of emergent self-organizing map (ESOM) techniques in the multi-dimensional interpretation and prediction of rare earth element (REE) abundance in produced and geothermal waters in the United States. Rare earth elements and other ion concentrations in produced and geothermal waters generated as part of Chapter 4, along with other publicly available data, were utilized to examine relationships between variables in a multi-dimensional visualization provided by the ESOM algorithm. The ESOM algorithm organizes data based on their multivariate similarity (i.e., shortest distance) and maps them to neurons, each of which is associated with a codebook vector with values for every parameter in the dataset. Visualization of the variables in the ESOM trained using the input data shows that REE are distributed very similarly, with the exception of Eu, and that no single parameter appears to control their distribution. Prediction was performed by mapping new points onto a trained ESOM and assigning missing values from the codebook vector from the most similar neuron (i.e., the one with the smallest distance between itself and the data points). The data were then back transformed into the original units. Cross-validation was performed, using a random sample of the starting data that were not used in the training of the ESOM. Comparison of REE concentrations predicted from the ESOM versus those reported by the laboratory for the cross-validation samples, shows that predictions are generally good within an order of magnitude. Using the same approach, the U.S. Geological Survey Produced Waters Database, Version 2.3 (which includes both data from produced and geothermal waters) was mapped to the ESOM and predicted values were generated for samples that contained enough variables to be effectively mapped. Results show that in general, produced and geothermal waters are predicted to be enriched in REEs by an order of magnitude or more relative to seawater, with maximum predicted enrichments in excess of 1000-fold for some elements. The largest average predicted enrichments in produced and geothermal waters relative to North Pacific Deep Water were observed in light REEs (La to Gd), with generally less enrichment in the heavy REEs (Tb to Lu). Cerium and Eu exhibited the highest predicted potentials due to Ce depletion in seawater and release of Eu from reservoir materials during weathering and diagenetic reactions. The economic worth of the two most valuable REEs, Dy and Tb, are estimated to be significantly less than typical costs required to dispose of the waste brines remaining after REE removal. Spatial mapping of the resulting predictions indicates that predicted REE potential is high across many geologic basins in the United States and that REEs are typically spatially co-associated. The controlling factors were not determined from ESOM analysis, but based on the information currently available REE content in produced and geothermal waters is not obviously controlled by lithology, reservoir temperature, or salinity.

1. INTRODUCTION

Chapter 4 presents the most comprehensive dataset currently available on rare earth element (REE) concentrations in produced and deep geothermal waters in the United States. As information about REEs in produced waters generated during oil and gas production and geothermal fluids is significantly lacking, any insight gleaned on the abundance and distribution in waters from other

geologic basins informs the potential for future exploration and comparison of various possible REE sources. In an attempt to provide further insight, the objectives of this chapter are to leverage additional information from this dataset in two ways: 1) examine patterns in the distribution of REEs in produced and geothermal waters through the use of multivariate data analysis techniques and 2) develop and implement a technique allowing for the estimation of REE potential in produced and geothermal waters of the United States.

The technique selected to complete both objectives of this chapter is the emergent self-organizing map (ESOM), a type of neural network. Neural networks are mathematical algorithms that are meant to identify patterns in data and are helpful for data classification and clustering. The ESOM is a subclass of the more general self-organizing map (SOM) algorithm. SOM is an unsupervised system (meaning that group classification is not known to the algorithm) of competitive learning used to sort multivariate data based on similarity (e.g., distance) and structure. The result is typically a 1- or 2-dimensional “map” that captures the variability and patterns in the training data, the dataset used to generate the SOM. The SOM is not a literal cartographic map of sample or data location in the physical world; rather, it is a representation of structure of the input samples and the associated parameters. Competitive learning refers to the process that neurons, which make up the map, “compete” for each sample, allowing for similar data to form into clusters. The SOM is particularly useful for working with high dimensional datasets that can be more easily interpreted in a lower dimensional visualization, much like principal component analysis (PCA) or cluster analysis. However, the SOM algorithm is much more relaxed than PCA and operates on data with missing variables and, unlike cluster analysis, allows for visualization of both samples and parameters from the same mapping. Additionally, the SOM allows for mapping of new data onto a pre-existing map, which is potentially useful for statistical modeling. Unsurprisingly, the SOM is increasingly used for a variety of data analysis topics in the earth sciences (Dickson and Giblin, 2007; Lacassie et al., 2004; Liu and Weisberg, 2005; Sun et al., 2009; Žibret and Šajn, 2010). Creation of the SOM begins with generating a lattice of neurons that make up the map, typically arranged in a rectangular or hexagonal geometry. Associated with each neuron is a codebook vector whose length matches the number of dimensions in the dataset being mapped. The size of the map is selected arbitrarily but a traditional SOM is usually rather small, typically smaller than the number of samples in the dataset. For instance, Sun et al. (2009) used a 3x3 map for a training dataset of nearly 3,000 samples. The ESOM is nearly identical to the SOM except that it contains hundreds or thousands of neurons (many more than the number of data used in its creation). This variation in design has been shown to prove more successful in ordering of data and separation of groups with extremely complex geometries (Ultsch, 2007). As a tool for predicting missing or unknown values in a large dataset from a smaller, more complete dataset, the ESOM is ideal because it provides a larger range in available predicted values.

For the purposes of this chapter, the intent was to apply the information gained on REE distribution from a relatively small dataset (the input dataset) to a database that covers a much larger geographic area, through application of the ESOM. One such large dataset is the U.S. Geological Survey Produced Waters Geochemical Database (Version 2.3; herein referred to as the USGS database), which is publicly available and downloadable (available at: <https://eerscmap.usgs.gov/pwapp/>) containing geochemical and related data for roughly 115,000 water samples collected from deep, geologic reservoirs in the United States (Blondes et al., 2017). Notably, the database includes data for 689 geothermal wells taken from the Nevada Bureau of Mines Great Basin Geothermal Database (U.S. Department of Energy Geothermal Data Repository Submission 696). While the U.S. Geological Survey Produced Waters Geochemical Database is a useful tool for a variety of studies, it contains no data on the concentration of REEs. The USGS database also contains a significant proportion of missing parameters for most samples. Thus, it represents significant challenges for

application in any standard estimation or modeling technique (e.g., multivariate regression). Moreover, the input dataset used to create a predictive model (those of Chapter 4) contains subpopulations on account of inclusion of data from a broad range of geologic settings. Traditionally, statistical modeling requires pre-segregation of all subpopulations which would mathematically inhibit the ability to perform the mathematical functions required (Varmuza and Filzmoser, 2009). However, the ESOM algorithm does not contain these limitations, making it an ideal approach for the analysis at hand. The allowance for samples with missing values increases estimation uncertainty, but such samples cannot even be utilized in traditional statistical modeling methods.

As a final comment, the vast majority of data utilized in this section are compositional, meaning that they are relative parts (i.e., concentration data). As such, special care was taken to apply proper techniques of so-called compositional data analysis (CoDA) to prevent the development of spurious or induced correlations (Martín-Fernández et al., 2018). Brines are particularly prone to such issues and have been previously shown to generate unrealistic results or results which lack internal consistency if CoDA methods are not utilized (Engle and Rowan, 2013; Engle and Rowan, 2014; Engle et al., 2016).

2. METHODS AND DATA

2.1 Description of Input Data

The water quality parameters, REE concentrations, and concentration of other dissolved constituents including ions, for 105 samples from this current study were combined with 119 unique samples (no field duplicates or laboratory replicates) of shallow geothermal groundwater and springs in the Eastern Snake River Plain analyzed by Idaho National Laboratory (Table 5.1), downloaded from the U.S. Department of Energy Geothermal Data Repository (Neupane and McLing, 2017; Quillinan et al., 2017). Produced and geothermal waters used as input data come from a broad spatial area of the U.S. and cover a large span of salinities (<1,000 to >300,000 mg/L total dissolved solids [TDS]) and origin.

Table 6.1. Table describing source and number of water samples used in the input dataset for the REE prediction potential modeling.

Water Type	Area/Basin	Sample Collector/Source of Data	Number of samples
Produced/Formation Water	Wind River Basin	Univ. Wyoming	17
Produced/Formation Water	Powder River Basin	Univ. Wyoming	10
Produced/Formation Water	Washakie Basin	Univ. Wyoming	6
Produced/Formation Water	Green River Basin	Univ. Wyoming	6
Produced/Formation Water	Williston Basin	U.S. Geol. Survey	18
Produced/Formation Water	Appalachian Basin	U.S. Geol. Survey	13
Produced/Formation Water	Permian Basin	U.S. Geol. Survey	12
Produced/Formation Water	Kevin Dome	Idaho Nat'l Lab.	23
Geothermal Waters	Eastern Snake River Plain	Idaho Nat'l Lab.	119

2.2 Processing of Input Data

Sixty quantitative parameters and constituents are present in the input data. However approximately 44% of the data in these 60 parameters are either missing (i.e., not measured or reported; 38%) or censored (6%). Censored data are those in which the value is above or below a certain threshold; in this case censored data correspond to concentrations below the method or instrument detection limits (i.e., nondetects). To minimize errors caused by inclusion of constituents with few data, all constituents with >50% missing data were removed from the input model. In addition, NO₃ was

removed as it is not generally present in produced and formation waters, specific conductance and total dissolved solids were removed as they are highly correlated with the sum of major ions already in the dataset, and oxidation-reduction potential was removed as it is not known to be a reliable measurement in brines. The final list of 34 parameters for the input dataset includes (Table 6.2):

- 1) Water quality parameters – pH and reservoir temperature
- 2) Major, minor, and trace constituents – Al, alkalinity as HCO_3 , As, B, Ba, Br, Ca, Cl, F, K, Li, Mg, Na, Si, SO_4 , Sr, and U
- 3) REEs – Sc, La, Ce, Pr, Nd, Sm, Eu, Gd, Tb, Dy, Ho, Er, Tm, Yb, and Lu

All 34 parameters except for temperature were converted to units of mg/L (an activity coefficient of 1 was assumed for hydrogen in the conversion of pH).

The resulting dataset contains 5.6% censored data and 7.5% missing data. Missing concentration and pH data were assumed to be missing completely at random (MCAR). Censored data are also missing, but not at random as their value is below a certain threshold (typically the method detection limit or reporting limit). Of the 427 censored values in the dataset, 337 were present in just 7 constituents: Al, As, Ba, Br, F, Mg, and SO_4 . As a parsimonious approach, the remaining censored values were converted to MCAR. While the ESOM algorithm does not strictly require imputation of missing values during the initial training, the implementation that was utilized does not operate with null values. Given the relatively low percentage of missing data, a choice was made to impute them. Notably in later steps involving the larger USGS database, samples comprised primarily by MCAR values were easily handled without imputation. Values for MCAR elements in the input dataset were imputed from a k nearest neighbor (k NN) imputation algorithm using Aitchison distances (Hron, Templ, and Filzmoser, 2010). Subsequently, censored data were imputed with values below the detection limit from an expectation-maximization partial least squares regression approach using isometric log-ratio (ilr) transformed data (Hron et al., 2010). Detection limits for each sample varied based on the amount of dilution and the relevant method detection limit. To simplify imputation of censored data, they were split into those with Cl concentrations above and below 1000 mg/L because at high salinity, detection limits are lower due to increased need for sample dilution prior to analysis. Based on detection limits provided for each sample set, dilution factors for the samples, and method detection limits for each element, simplified detection limits were selected for two sub-populations (above and below 1000 mg Cl/L) and were used as upper maximum bounds for censored data imputation (Table 6.3). The remaining censored data (only 1.2% of the data) were converted to missing data.

Given its role in reaction kinetics and thermodynamics, specific attention was given to reservoir temperature. In the case of produced waters, estimated temperatures within the reservoirs were used where available. In the case of the geothermal waters, the sample temperatures were used but assumed to be minimum values due to cooling during travel to and at the surface. Comparison between reported reservoir temperature and the Li-Mg chemical geothermometer estimated temperature (Kharaka and Mariner, 1989) suggests that the available reservoir temperatures are consistent with the Li-Mg chemical geothermometer (Figure 6.1). Any missing reservoir temperatures from the produced water samples were estimated from the Li-Mg chemical geothermometer calculated value. In the case of surface geothermal waters, it was assumed that they have travelled from depth and the Li-Mg chemical geothermometer is a more accurate temperature for reactions that control their composition. For this reason, temperatures for geothermal waters were replaced by those estimated from the Li-Mg geothermometer.

Table 6.2. List of parameters used in the input dataset indicating units, and relative proportion of present, censored, and missing data.

Constituent	Units	% Present	% Censored	% Missing
Water Quality Parameters				
Reservoir Temp.	°C	71.4%	0.0%	28.6%
pH	pH units	90.2%	0.0%	9.8%
Major, minor, and trace constituents				
Al	mg/L	44.2%	45.5%	10.3%
Alkalinity as HCO ₃	mg/L	74.1%	0.0%	25.9%
As	mg/L	61.6%	18.3%	20.1%
B	mg/L	92.4%	3.1%	4.5%
Ba	mg/L	87.1%	5.4%	7.6%
Br	mg/L	41.5%	47.3%	11.2%
Ca	mg/L	99.6%	0.4%	0.0%
Cl	mg/L	96.9%	0.4%	2.7%
F	mg/L	71.9%	15.2%	12.9%
K	mg/L	98.7%	1.3%	0.0%
Li	mg/L	88.8%	2.7%	8.5%
Mg	mg/L	95.5%	4.5%	0.0%
Na	mg/L	99.1%	0.0%	0.9%
Si	mg/L	87.2%	2.2%	9.8%
SO ₄	mg/L	84.4%	14.3%	1.3%
Sr	mg/L	92.0%	0.4%	7.6%
U	ng/L	51.3%	0.0%	48.7%
Rare Earth Elements				
Sc	ng/L	57.6%	0.0%	42.4%
La	ng/L	97.8%	2.2%	0.0%
Ce	ng/L	98.2%	1.8%	0.0%
Pr	ng/L	96.4%	3.6%	0.0%
Nd	ng/L	96.0%	4.0%	0.0%
Sm	ng/L	98.7%	1.3%	0.0%
Eu	ng/L	99.1%	0.9%	0.0%
Gd	ng/L	97.8%	2.2%	0.0%
Tb	ng/L	96.9%	2.7%	0.4%
Dy	ng/L	99.6%	0.4%	0.0%
Ho	ng/L	98.7%	1.3%	0.0%
Er	ng/L	98.7%	1.3%	0.0%
Tm	ng/L	97.8%	2.2%	0.0%
Yb	ng/L	98.2%	1.8%	0.0%
Lu	ng/L	97.8%	1.8%	0.4%

Table 6.3. Maximum detection limits used in the imputation of censored data. All results in units of mg/L.

Element	Samples with Cl \geq 1000 mg/L	Samples with Cl < 1000 mg/L
Al	0.5	0.01
As	0.006	0.001
Ba	5	0.05
Br	50	5
F	5	0.5
Mg	1	1

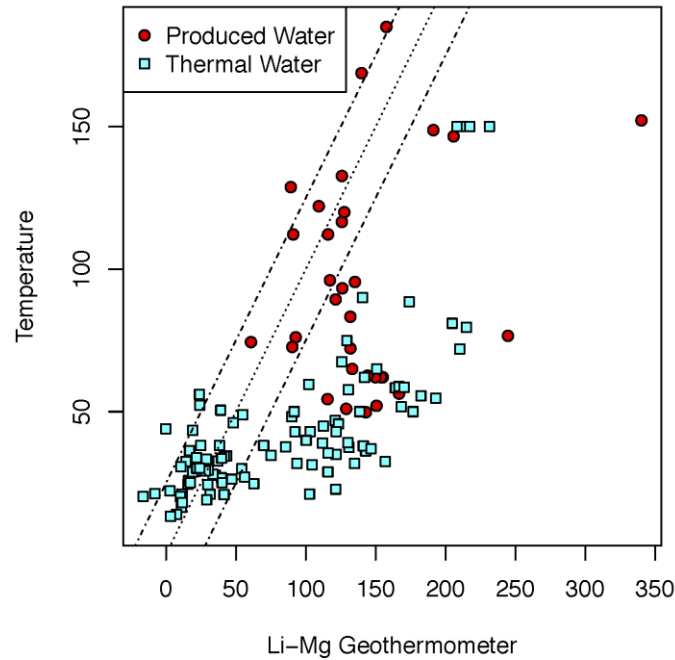


Figure 6.1. Reservoir and surface temperatures from produced and geothermal waters, respectively, from the input dataset versus temperatures estimated using the Li-Mg geothermometer (Kharaka and Mariner, 1989). All temperatures in units of °C. Dotted line shows 1:1 line and dashed-dotted lines show 25°C offsets from the 1:1 line.

2.3 Applying Principles of Compositional Data Analysis

Of the parameters in the input dataset, the clear majority are so-called compositional data, meaning they are relative parts; all concentration data are compositional. Compositional data lie within a lower dimensional subspace in positive Real space, called the simplex. Despite being part of positive Real space, data within the constraints of the simplex do not follow the standard rules of Euclidean geometry. Thus, all measures based on distances and angles (e.g., correlation, similarity, etc.) using compositional data may be incorrect using standard data analysis methods. Recently, Martín-Fernández et al. (2018) developed a specific scheme for treatment of compositional data in SOM and that approach is used here. Specifically in the case of brines, previous workers have shown that large variations in salinity may produce apparent co-associations between elements which are mathematically induced and in some cases completely spurious (Engle et al., 2016; Engle and Blondes, 2014; Engle and Rowan, 2013). To avoid such problems compositional data defined as $\mathbf{x}=(x_1, \dots, x_D)$ consisting of D -parts (e.g., constituents) were converted to $D-1$ isometric log-ratio coordinates which follow rules of Euclidean geometry (Egozcue et al., 2003), using:

$$z_{ij} = \sqrt{\frac{D-j}{D-j+1}} \ln \frac{\sqrt[D-j]{\prod_{l=j+1}^D x_{il}}}{x_{ij}} \quad \text{for } j=1, \dots, D-1 \quad (\text{Hron et al., 2010}) \quad (1).$$

Due to the presence of a geometric mean in the numerator of the Formula 1, missing data in the pre-transformed data can generate significant data loss in the coordinates; the geometric mean of a set of samples with missing values cannot be calculated. The USGS database contains a significantly higher proportion of missing data than the input dataset (Table 6.4). To minimize data loss, all non-REE constituents with >99% of values missing were removed from the input dataset (Al, As, Th, and U). Of the remaining compositional parameters, the data were re-ordered according to the proportion of

missing data in each row (REEs, F,...,Cl) and then converted to ilr coordinates using Formula 1. Table 6.5 provides a singular binary partition of the ilr-transformation denoting the compositional parameters in the numerator (shown by + symbols) and the denominator (shown by – symbols) for Formula 1. Re-ordering of the variables in this manner reduces the number of missing data in that the likelihood of having all the elements to calculate the geometric mean in the numerator of the transformation increases as the number of missing elements goes down. By using this approach, conversion of the input data to ilr coordinates increased the number of blank cells only modestly, from 2.38% to 3.51%.

Because the version of the ilr transformation used in this case is designed with a focus on minimizing data loss rather than trying to maximize the interpretative ability of the coordinates, all results (z_i) produced using these coordinates were back transformed ($ilr^{-1}(z_i)$) into the original units using:

$$x_{i1} = \exp\left(-\sqrt{\frac{D-1}{D}}z_{i1}\right) \quad (2),$$

$$x_{ij} = \exp\left(\sum_{l=1}^{j-1} \frac{1}{\sqrt{(D-l+1)(D-l)}}z_{il} - \sqrt{\frac{D-j}{D-j+1}}z_{ij}\right), \text{ for } j=2,\dots,D-1 \quad (3),$$

$$x_{iD} = \exp\left(\sum_{l=1}^{D-1} \frac{1}{(D-l+1)(D-l)}z_{il}\right), \quad (4),$$

following Hron et al. (2010).

Table 6.4 Number of concentration data present from the USGS Produced Waters Geochemical Database (Version 2.3).

Constituent	Number of Data	% Present
pH	86,630	75%
Al	680	0.6%
Alkalinity as HCO ₃	1,691	1.5%
As	493	0.4%
B	4,618	4.0%
Ba	12,498	11%
Br	6,548	5.7%
Ca	107,478	94%
Cl	108,646	95%
F	1,127	1.0%
K	31,550	27%
Li	6,126	5.3%
Mg	103,240	90%
Na	96,432	84%
Si	3,708	3.2%
SO ₄	93,104	81%
Sr	7,812	6.8%
Th	0	0.00%
U	21	<0.01%
Rare Earth Elements		
Sc	0	0.0%

Engle

La	0	0.0%
Ce	0	0.0%
Pr	0	0.0%
Nd	0	0.0%
Sm	0	0.0%
Eu	0	0.0%
Gd	0	0.0%
Tb	0	0.0%
Dy	0	0.0%
Ho	0	0.0%
Er	0	0.0%
Tm	0	0.0%
Yb	0	0.0%
Lu	0	0.0%

Table 6.5. Singular binary partition used in the transformation of compositional variables to ilr-coordinates. For each coordinate, compositional parameters used in the numerator are shown by + and those used in denominator are shown by -.

Constituent	z1	z2	z3	z4	z5	z6	z7	z8	z9	z10	z11	z12	z13	z14	z15	z16	z17	z18	z19	z20	z21	z22	z23	z24	z25	z26	z27	z28	z29
Sc	-																												
Nd	+	-																											
Pr	+	+	-																										
Tb	+	+	+	-																									
Lu	+	+	+	+	-																								
La	+	+	+	+	+	-																							
Gd	+	+	+	+	+	+	-																						
Tm	+	+	+	+	+	+	+	-																					
Ce	+	+	+	+	+	+	+	+	-																				
Yb	+	+	+	+	+	+	+	+	+	-																			
Sm	+	+	+	+	+	+	+	+	+	+	-																		
Ho	+	+	+	+	+	+	+	+	+	+	+																		
Er	+	+	+	+	+	+	+	+	+	+	+	-																	
Eu	+	+	+	+	+	+	+	+	+	+	+	+	-																
Dy	+	+	+	+	+	+	+	+	+	+	+	+	+	-															
F	+	+	+	+	+	+	+	+	+	+	+	+	+	+	-														
Alkalinity as HCO3	+	+	+	+	+	+	+	+	+	+	+	+	+	+	+	-													
Si	+	+	+	+	+	+	+	+	+	+	+	+	+	+	+	+	-												
B	+	+	+	+	+	+	+	+	+	+	+	+	+	+	+	+	+	-											
Br	+	+	+	+	+	+	+	+	+	+	+	+	+	+	+	+	+	+	-										
Li	+	+	+	+	+	+	+	+	+	+	+	+	+	+	+	+	+	+	+	+	-								
Ba	+	+	+	+	+	+	+	+	+	+	+	+	+	+	+	+	+	+	+	+	+	-							
Sr	+	+	+	+	+	+	+	+	+	+	+	+	+	+	+	+	+	+	+	+	+	+	-						
SO4	+	+	+	+	+	+	+	+	+	+	+	+	+	+	+	+	+	+	+	+	+	+	+	-					
Hplus	+	+	+	+	+	+	+	+	+	+	+	+	+	+	+	+	+	+	+	+	+	+	+	+	-				
K	+	+	+	+	+	+	+	+	+	+	+	+	+	+	+	+	+	+	+	+	+	+	+	+	+	-			
Mg	+	+	+	+	+	+	+	+	+	+	+	+	+	+	+	+	+	+	+	+	+	+	+	+	+	+	-		
Ca	+	+	+	+	+	+	+	+	+	+	+	+	+	+	+	+	+	+	+	+	+	+	+	+	+	+	+	-	
Cl	+	+	+	+	+	+	+	+	+	+	+	+	+	+	+	+	+	+	+	+	+	+	+	+	+	+	+	+	-
Na	+	+	+	+	+	+	+	+	+	+	+	+	+	+	+	+	+	+	+	+	+	+	+	+	+	+	+	+	+

2.4 Univariate and Multivariate Outlier Investigation and Detection

While non-linear data analysis methods like ESOM are often minimally impacted by outliers, utilization of univariate and multivariate investigation and outlier analysis are good standards of practice before applying any multivariate data analysis techniques. To examine for potentially problematic data (poor imputation methods, invalid analytical results, or erroneous entries), univariate and multivariate outlier analysis methods were applied to the ilr-transformed data. Univariate investigation included generation of an exploration data analysis plot of Reimann et al. (2008) for each ilr coordinate and subsequent inspection. The plots (e.g., Figure 6.2) include a density trace, a histogram, a 1-dimensional scatter plot, a Tukey box plot (left panel), and an empirical cumulative density function plot (right panel) which allow for examination of normality, multiple populations, and extreme values. Multiple populations were observed for ilr coordinates z_{16} (Figure 6.2; F in the denominator), z_{24} (SO₄ in the denominator), and z_{27} (Mg in the dominator), and likely represent clear geochemical differences between geothermal and produced waters. Visual examination of the EDA plots for all ilr-transformed data showed no evidence of significant outliers or extreme univariate values.

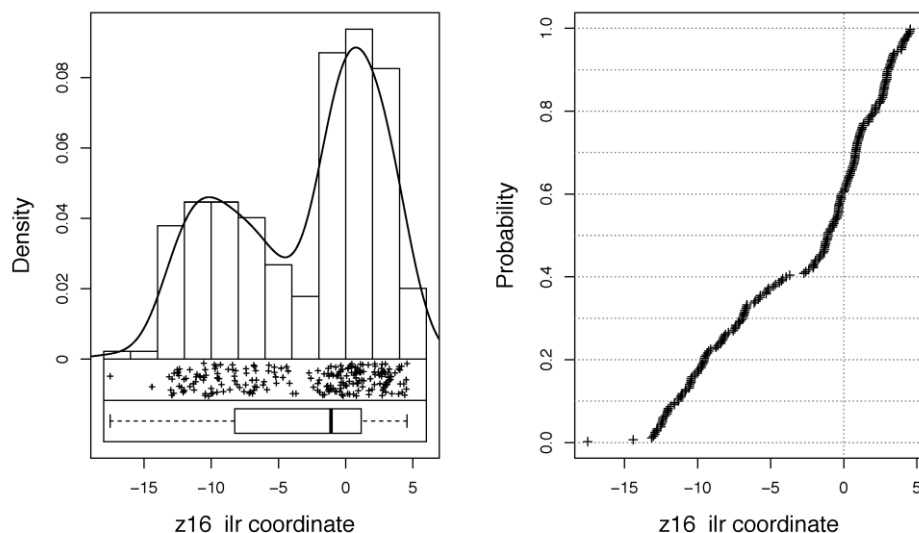


Figure 6.2. Exploratory data analysis for ilr coordinate z_{16} showing evidence of two populations representing higher and lower relative F abundances between geothermal and produced waters, respectively.

Given specific sensitivity to the REE data, multivariate outlier examination was focused there. An adaptive chi-square distance threshold of minimum covariance determinant-based Mahalanobis distance of ilr coordinates (Filzmoser et al., 2012) was applied to complete cases of the REE data in the input dataset. Results summarizing this analysis are shown as part of a principal component (PC) biplot in Figure 6.3, accounting for 70.8% of the variance in the dataset. Here the dataset appears to be smoothly clustered except for 4 samples, LC-31, PRB-12, MD-7, and MS-51. All three are red indicating that they contain high median REE relative abundances on average. The samples also plot as large crosses indicating that they are considered multivariate outliers based on an adaptive threshold based on robust Mahalanobis distances. Examination of the concentration data for these samples shows elevated Er and Yb in LC-31 (28.4 and 65.6 ng/L, respectively) but examination for PRB-12, MD-7, and MS-51 show no obvious extreme REE values suggesting their classification as outliers is a result multivariate patterns. Because the ESOM algorithm is non-linear and the analytical reports from Idaho National Laboratory indicated no obvious analytical problems with these samples, the data were kept in the dataset. Interpretation of the elemental data, shown as rays plotting away from the geometric mean of the dataset (0,0), indicate similarity among the light REEs (La to Gd), and among the heavy REEs (Tb to Lu) with Sm, Eu, and Gd exhibiting intermediate behavior. Europium exhibits a much longer ray indicating high log-ratio variance compared to the other REEs. Similarly, the length of the link created by connecting the rays for Eu and any other REE is longer than that for any other pairs of REEs, suggesting that Eu is the least likely to vary proportionally with the other REEs. These findings are consistent with the unique behavior of Eu relative to other REEs due to its multiple oxidation states.

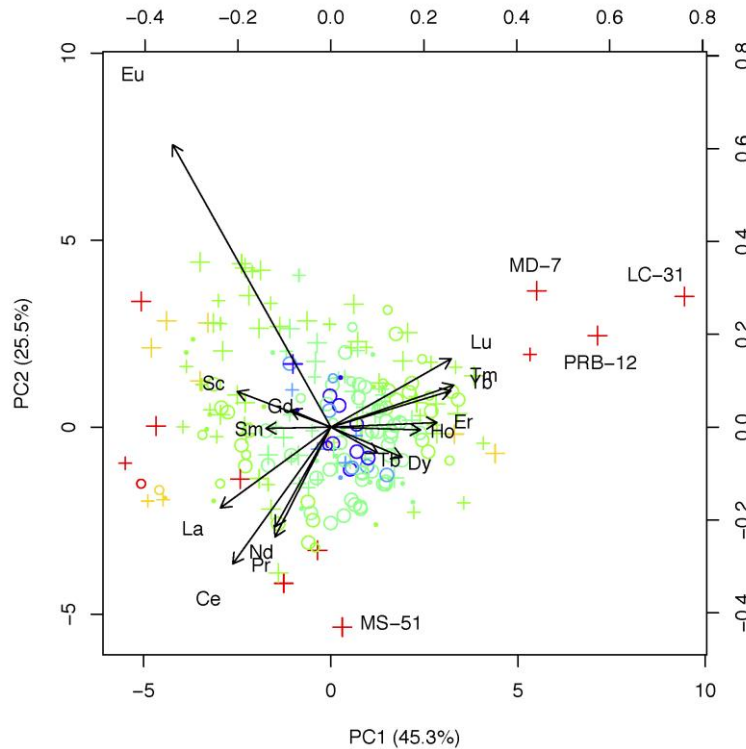


Figure 6.3. Results from multivariate outlier detection of REE data in the input dataset. Colors indicate the median REE concentration of the observations (warmer colors equal high median, cooler colors equal lower median). Symbols indicate quartiles of robust Mahalanobis distance, ranging from the lowest values (large circles) to the high values (large crosses).

2.4 Model Cross-Validation

Cross-validation methods were applied in an attempt to quantify uncertainty through the application of the ESOM to estimate REE values in unknown samples. Rows from the input dataset were randomly split between the training dataset (85% of rows; $n=190$) and the cross-validation dataset (15% of rows, $n=34$). The former was used to train the ESOM model and is the basis for all prediction. The latter was used to check the ability of the ESOM model to accurately predict REE concentrations for “blind” samples. The cross-validation data were mapped to trained ESOM (described in the next section) to generate predicted REE concentrations. The predicted concentrations were compared against the known REE concentrations for cross-validation dataset, allowing for calculation of model error.

2.5 Creation of a Trained Emergent Self-Organizing Map

As the ESOM algorithm relies on distance as its metric of similarity, the ilr -transformed data (\mathbf{z}) (except for temperature, which was kept in its original units) were normalized by the mean and the sample standard deviation of each coordinate ($\hat{\mathbf{z}}$):

$$\hat{z}_{ij} = \frac{z_{ij} - \bar{z}_j}{s_j} \quad (5),$$

where \bar{z}_j is the arithmetic mean of the j th coordinate and s_j is the sample standard deviation of the j th coordinate. Normalization provides an equal “weight” of every single coordinate and prevents individual ilr coordinates from having an unusually large impact on mapping. Data produced from ESOM results can be un-normalized through the inverse transformation:

$$z_{ij} = \hat{z}_{ij} s_j + \bar{z}_j \quad (6).$$

The values for \bar{z}_j and s_j from the training dataset also are used for normalization of the data mapped onto the trained ESOM in later steps. Data for temperature, which is not compositional, were also normalized using Formula 5. The mean and standard deviation of the reservoir temperature and ilr-transformed data are provided in Table 6.6.

Table 6.6. Mean and standard deviation (std. dev.) of variables in the training dataset. These values are used in conjunction with Formula 6 to un-normalize data applied to the ESOM.

Variable	Mean	Std. Dev.
Temp	92.707	52.220
z1	-6.857	1.295
z2	-6.606	1.485
z3	-8.181	1.495
z4	-10.015	1.435
z5	-10.354	1.518
z6	-7.515	1.529
z7	-9.132	1.358
z8	-11.687	1.612
z9	-8.728	1.823
z10	-10.862	1.750
z11	-11.573	1.706
z12	-13.279	1.877
z13	-12.916	2.082
z14	-13.429	1.651
z15	-14.451	2.283
z16	-2.984	5.466
z17	5.150	1.599
z18	2.224	2.452
z19	-2.340	2.131
z20	-0.096	1.688
z21	-1.637	1.647
z22	-4.278	4.478
z23	-1.422	1.695
z24	1.433	3.347
z25	-13.341	2.203
z26	-1.202	1.233
z27	-3.098	2.665
z28	-1.244	2.070
z29	-0.349	0.960

The ESOM lattice applied here consists of 82 x 50 neurons (4,100 total), which greatly outnumbers the 190 samples in the training dataset. In addition, unlike the SOM, the ESOM is typically created so

that the top of the map is connected to the bottom and the right-hand side connected to the left, as if one has unpeeled the outer layer from a donut and laid it out flat on a table.

Starting with our normalized data for temperature and the ilr coordinates ($\hat{\mathbf{z}}$) (a total of m columns), a codebook vector of length m was created for each neuron and filled with random values. The SOM algorithm was then run as follows (modified from Sun et al., 2009):

- 1) An input vector $\hat{\mathbf{z}}_i$ is selected at random from the training dataset and the Euclidean distances between it and all codebook vectors for all the neurons on the map are computed. Note that the Euclidean distance of ilr-transformed variables is equal to the Aitchison distance of untransformed compositional data.
- 2) The input vector $\hat{\mathbf{z}}_i$ is assigned to the codebook vector of the neuron that is closest to it. This neuron is known as the best matching unit (BMU). A Gaussian function is used to define the neighborhood of nearby neurons around the BMU. With each iteration of the algorithm, radius of the neighborhood decreases.
- 3) The codebook vectors of those neurons within the neighborhood are re-weighted to be more similar to \mathbf{x}_i using one of several possible functions. Typically, codebook vectors of neurons closer to BMU are more heavily re-weighted than those more distal. The amount of re-weighting (learning weight) also decreases over time.
- 4) The next input vector, $\hat{\mathbf{z}}_{i+1}$, is randomly selected and steps 1–3 are repeated. Once all the input vectors have been mapped (1 epoch), they are removed from the map and the process is repeated starting back at step 1. The learning is continued for a set number of epochs. Because the neighborhood and re-weighting function both decrease with each epoch, the map stabilizes with an increasing number of iterations.

The exact parameters applied in the generation of the ESOM shown here are provided in Table 5.7. All ESOM calculations were made using Version 3.1 of the Umatrix package in R. In the example presented here, weights for a neuron's codebook vector at the next step in the iteration (\mathbf{W}_{t+1}) are calculated from the corresponding weight at time t (\mathbf{W}_t) via:

$$\mathbf{W}_{t+1} = \mathbf{W}_t + N_t L_t (\mathbf{X}_{it} - \mathbf{W}_t) \quad (7),$$

where L_t is the learning rate at time t , and N_t is the neighborhood function.

The neighborhood function is defined as:

$$N_t = \exp\left(\frac{\|r_c - r_i\|}{2\sigma_t^2}\right) \quad (8),$$

where the numerator is the Euclidean distance between the codebook vector of the BMU (r_c) and that of any random neuron in the neighborhood (r_i), and σ_t is the radius of neighborhood at time t . Both L_t and σ_t decrease linearly throughout the run (Table 6.7). This decrease in L_t and σ_t ensure that in the early stages of the process, changes in the map are dramatic but near the end of the run, they become less and less impactful and the map starts to stabilize. When the trained ESOM is created (i.e., after algorithm has run through its defined number of epochs), the final weights from the codebook vectors for all the neurons in the ESOM are un-normalized using Formula 6 and the mean and standard deviation from Table 6.6. For all compositional variables, the weights are converted from ilr coordinates back into the original variables using the inverse transformation (Formulas 2-4). Note that these back-transformed data are in units of proportion. Compositional data analysis does not

distinguish between units of scale because corresponding data are of the same equivalence class (Aitchison, 1986).

Table 6.7 Parameters used in the ESOM algorithm.

Parameters	Method or setting
Number of rows in map	82
Number of columns in map	50
Number of training epochs	24
Initialization method	Uniform random values from mean \pm 2 standard deviations
Shape	Toroidal
Neighborhood function	Gaussian
Starting neighborhood radius	24
Ending neighborhood radius	1
Neighborhood cooling function	Linear
Starting learning rate	0.5
Ending learning rate	0.1
Learning rate cooling function	Linear

2.6 Rare Earth Element Potential Using the Trained Emergent Self-Organizing Map

In attempt to gain insight into potential for REE concentrations across a broader area than the original input dataset analyzed as part of this investigation, data from the USGS database were mapped to the trained ESOM. The USGS database contains no data on REEs and contains missing values for many constituents (As summarized in the documentation for Blondes et al., 2017). Using the same parameters as those used to create the trained ESOM using the training dataset, the compositional data from the USGS database were converted to ilr coordinates using Formula 1 using the same singular binary partition (Table 6.5). The ilr coordinates and reservoir temperature data, estimated using the Li-Mg chemical geothermometer, were normalized using the mean and standard deviation from the training dataset (Formula 5). In a balance between retaining enough data to be effective and requiring enough non-missing parameters to be meaningful, all data containing fewer than 7 of the ilr-variables were removed from the analysis, shrinking the total dataset from roughly 115,000 to 3,688 data points. If a larger cutoff is used, the number of points drops precipitously; only 826 samples (~0.7% of the total database) contain non-missing data for more than 8 ilr coordinates. The normalized and transformed data in this abridged version of the USGS database were mapped to the trained ESOM by finding the neuron whose codebook vector has the shortest distance to the input vector \hat{z}_i for each sample (i.e., the BMU). The missing values for each input vector were then taken from the corresponding element in the codebook vector of the respective BMU. The resulting data were un-normalized (formula 6) using the mean and standard deviation from the training dataset (Table 6.6), and the compositional parameters were back-transformed into the original variables (Formulas 2-4). The resulting compositional data are proportional; to convert them back into units of mg/L, each row was multiplied by the sum of the compositional data in the original dataset. This technique of imputing missing geochemical data by mapping them onto a SOM and using the values from the codebook vector of the BMU has previously been shown to work effectively (Dickson and Giblin, 2007).

3. RESULTS

3.1 Trained Emergent Self-Organizing Map

Arrangement of the training data using the ESOM algorithm shows that geothermal waters were distinguished from produced waters based on their multivariate geochemical structure (Figure 6.4). Samples from the Washakie and Wind River Basins showed some overlap with those from the

Williston and a portion of samples from the Appalachian Basin. Samples from the Permian and Appalachian basins showed less similarity among themselves than the other sampling areas.

The U*-matrix map (Figure 6.5) displays the U-heights, the sum of all distances between each neuron and its nearest neighbors, scaled by the Pareto Density Estimation for each neuron within in the trained ESOM (Ultsch, 2003). In this visualization of the data, features mapped as “mountain ranges” can be thought of as boundaries between clusters of data while those that appear as “valleys” represent the center of data clusters. Thus, the data from the Eastern Snake River Plain (see Figure 6.4. for BMUs for the training dataset) appear as their own cluster, distinct from the produced waters which plot around them. Similarly, samples from the Kevin Dome region in Montana also appear as their own cluster. Several of the Permian Basin samples, noted by features with a sink-hole appearance around several of the samples in the lower left corner of the map, suggest these samples are dissimilar to most other samples in the dataset. However for the most part, the produced water samples generally tended to overlap among basins. This is not surprising because similar processes tend to dominate the composition of produced waters, regardless of geographic location (Kharaka and Hanor, 2014).

Patterns in the relative distribution of the constituents used in the training dataset can be examined through visualization of the back-transformed weights from the codebook vectors of the trained ESOM (Figure 6.6). Mapped compositional parameters are in units of mass proportion and have been rescaled over the range [0,1]. In the case of reservoir temperature, the map was simply been rescaled over the range [0,1]. Comparison of mapped weights for Pr (a light REE) and Yb (a heavy REE) demonstrate that the REEs are distributed similarly among the samples in the training dataset. This is remarkable given that samples come from both geothermal and hydrocarbon waters and cover a diverse range of geologic systems (Table 6.1). Because the *ilr*-coordinates in this analysis were normalized (Formula 5) the apparent co-association between the REEs is likely not simply an artifact due to them exhibiting a larger log-ratio variance than the other constituents included in the input dataset. Europium, which unlike the other REEs exhibits both 2+ and 3+ oxidation states, shows a somewhat different pattern in its mapped weights, which is expected given its unique geochemical behavior relative to the other REEs. Maps for weights of reservoir temperature, Cl (a proxy for salinity), and H (a proxy for pH) suggest that none appear to independently control REE distribution among the samples. Of the remaining elements, two that most closely follow the patterns of the REE weight are F and Si. Thermodynamic calculations suggest that F can be an important ligand for REEs in F-rich, high temperature aqueous systems (Migdisov et al., 2016). Comparison of the weights for the REEs versus an overlay of the F and reservoir temperature maps do not overlap well, suggesting that if F complexation does play a role in controlling REE abundances, it is not limiting. Similarly, Si concentrations in deep geothermal and hydrocarbon reservoirs are strongly controlled by temperature-dependent reactions with silica polymorphs (Fournier et al, 1974; Kharaka and Mariner, 1989). However, comparison of the mapped weights for Si versus reservoir temperature suggests that Si may not be entirely temperature-controlled in these systems. Alternatively, Si may be supply-limited in non-clastic or mafic systems. In this scenario, the positive relationship between REE abundances and Si may indicate the significant role that specific clastic- or felsic-rich reservoirs play as the source for REEs. Relationships between REE concentrations and source rocks are examined in detail in Chapter 5.

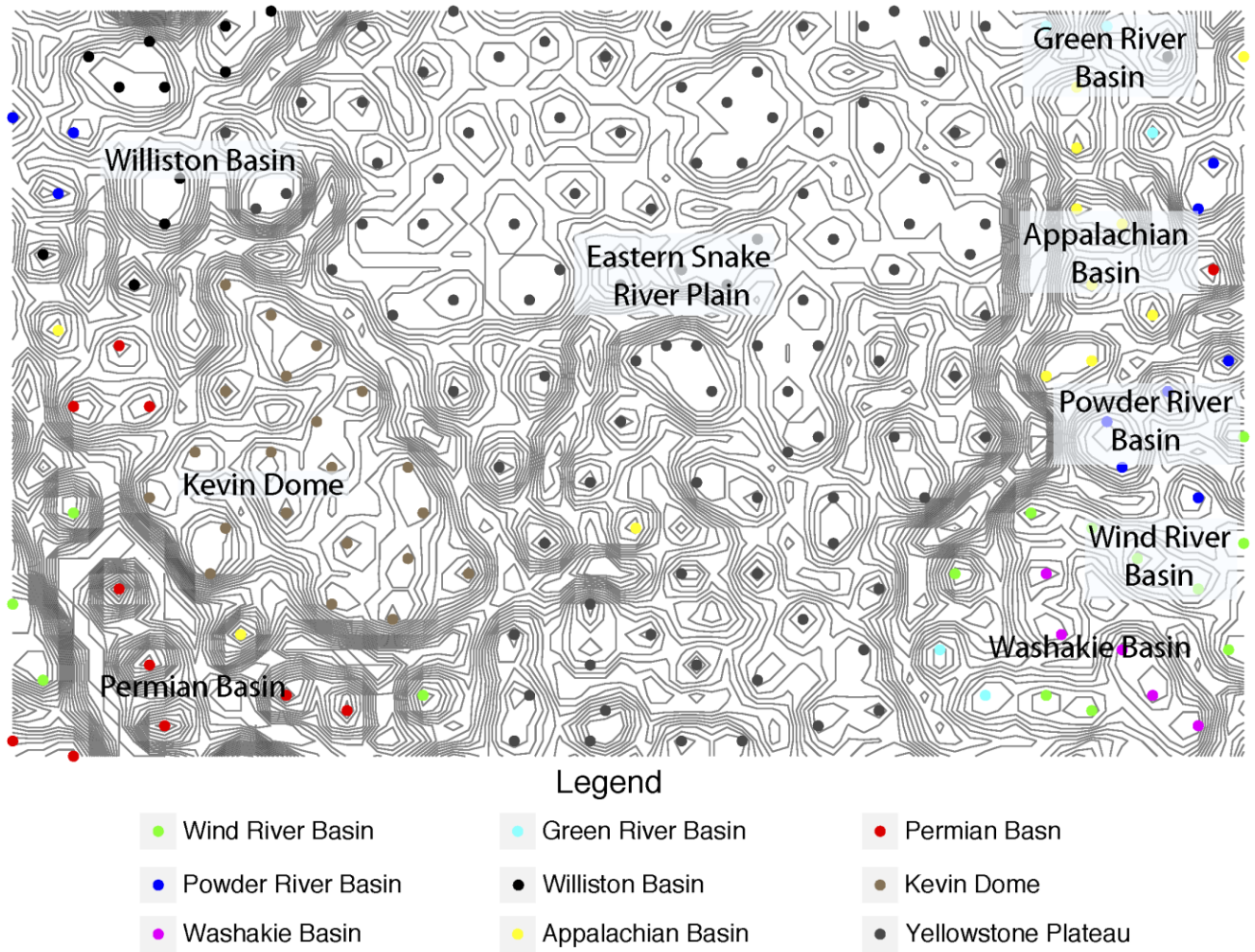


Figure 6.4. Foreground: Visualization of BMUs for the input data on the trained ESOM. Background: Contours of U-heights, the distance of each neuron and its neighbors. Points color-coded to indicate general sampling location.

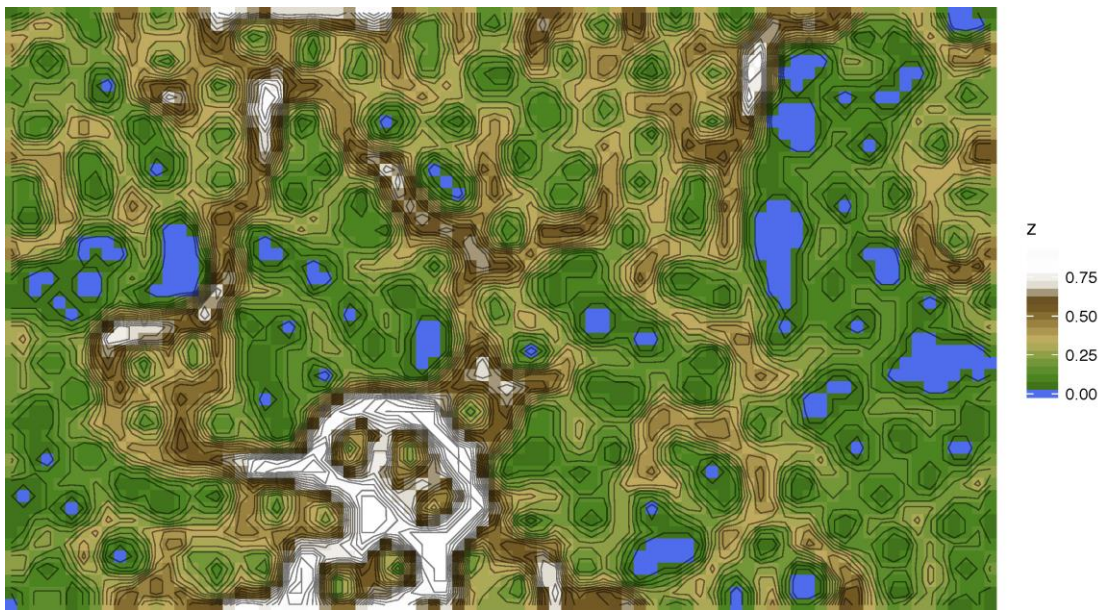


Figure 6.5. U*-matrix visualization of the ESOM created from the training dataset. Compare with Figure 6.4 for location of BMU of the training set.

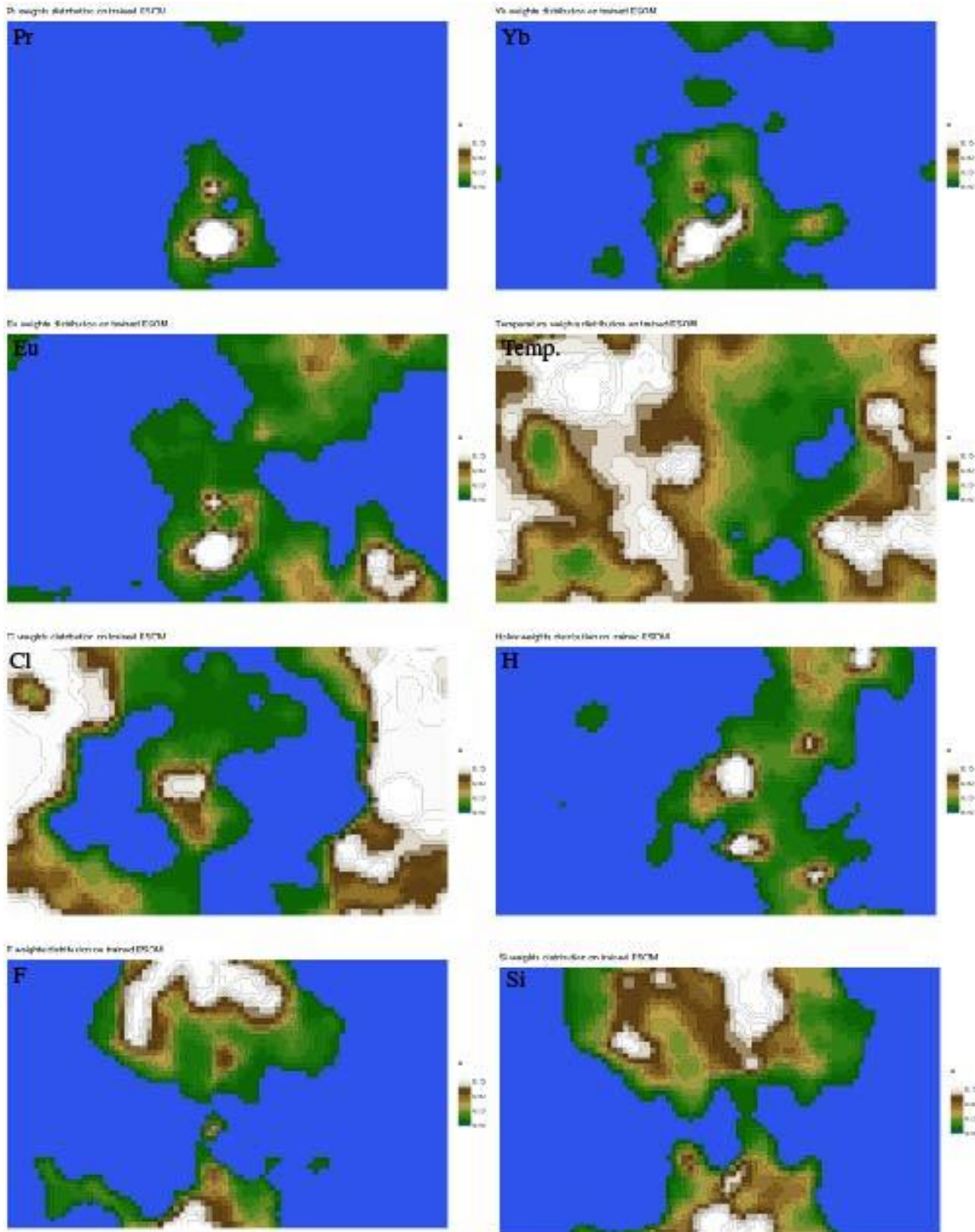


Figure 6.6. Visualizations of weights from the codebook vectors of the trained ESOM for Pr (proxy light REE), Yb (proxy heavy REE), Eu, estimated reservoir temperature, Cl, H, F, and Si. All compositional variables in units of proportion or reported ions by maps and rescaled over the range [0,1] for mapping. Temperature in units of °C and rescaled over the range [0,1] for mapping.

3.2 Cross-Validation Results

Each ilr-transformed (except for temperature) and normalized data point in the cross-validation set was mapped to the neuron on the trained ESOM with the smallest distance to itself (analogous to the BMU during the ESOM training). The REE values from these neurons were then assigned to each data point. All data were then un-normalized (Formula 6; Table 6.6), and the compositional parameters were back-transformed (Formulas 2-4). The resulting data are proportional; to convert them back into units of mg/L each row was multiplied by the sum of the compositional data in the original dataset. Cross-validation performance (CV_{error}) was determined by normalizing the data to seawater (NPDW-North Pacific Deep Water) (Alibo and Nozaki, 1999) and then taking the ratio of the ESOM-predicted values to the known values (Figure 6.7):

$$CV_{error} = \frac{\frac{x_{ESOM}}{x_{NPDW}}}{\frac{x_{known}}{x_{NPDW}}} \quad (8),$$

where x_{ESOM} is the concentration of a given REE as predicted from the ESOM, x_{known} is the concentration of a given REE from the input database, and x_{NPDW} is the concentration of the given REE in NPDW (Alibo and Nozaki, 1999). Results suggest that even for this simple model built using fewer than 200 data points for training, the ESOM can generally predict REE concentrations within an order of magnitude. Results were modestly better for La and Ce (i.e., smaller spread) and, in general, results tended to under-predict concentrations, especially for Eu and Tb, suggesting the estimates are conservative.

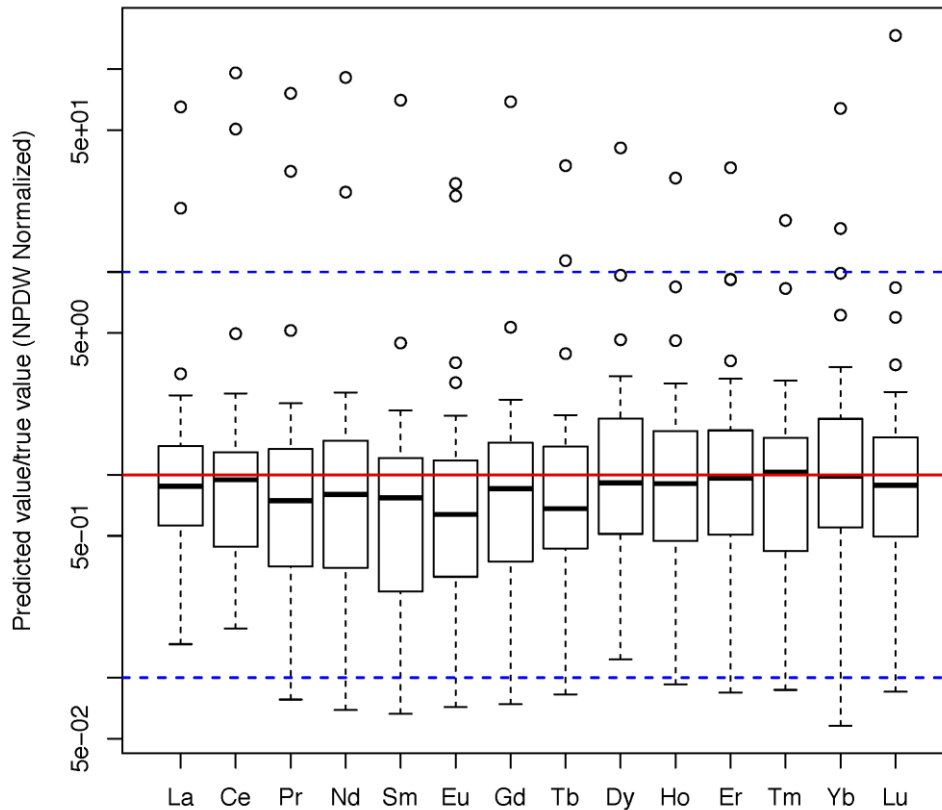


Figure 6.7. Prediction results for REEs in the cross-validation dataset. Red line ($y=1$) indicates perfect prediction and blue dashed lines ($y=0.1, 10$) indicate under- and over-prediction of NPDW-normalized data by an order of magnitude, respectively.

3.3 Rare Earth Element Potential Prediction

In general, results from REE concentration prediction for the abridged USGS database show that produced and deep geothermal waters of the United States are enriched in REEs compared to seawater (Figure 6.8). The markedly high predicted enrichments in Ce and Eu are likely due to depletion of these elements in seawater due to Ce oxidation and scavenging in the upper seawater column (Alibo and Nozaki, 1999) and release of Eu from feldspars into associated formation waters present in clastic reservoirs during weathering and diagenetic reactions. In general, the largest average predicted enrichments in produced and geothermal waters relative to NPDW were observed in light REEs (La to Gd), with generally less enrichment in the heavy REEs (Tb to Lu).

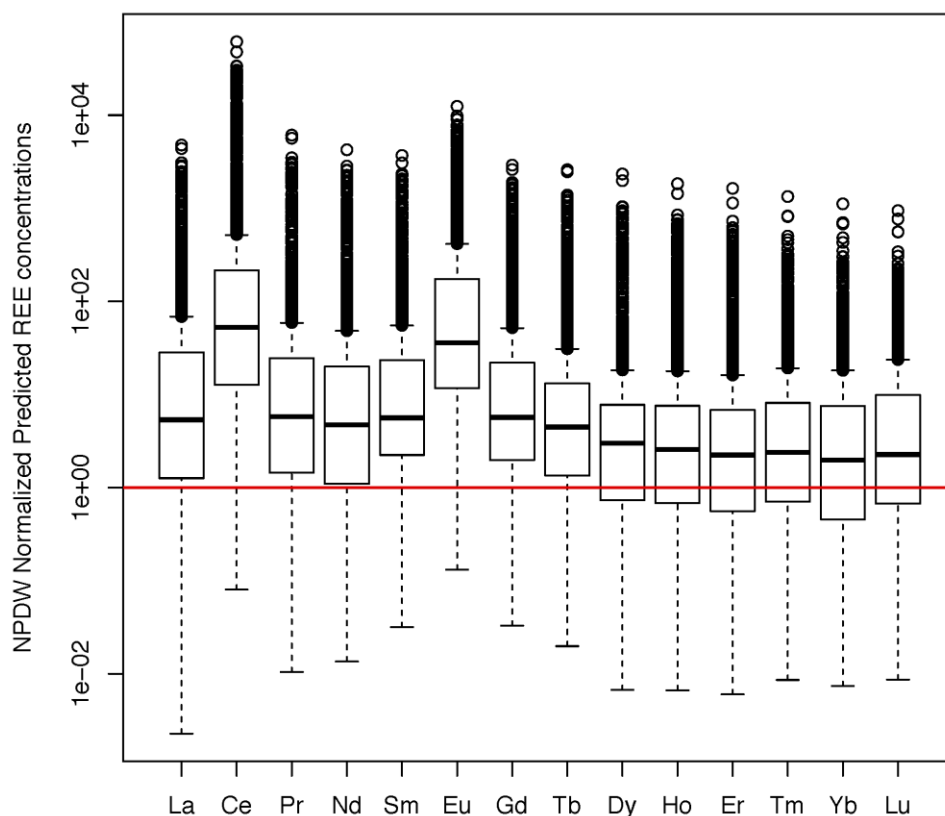


Figure 6.8. Predicted REE concentrations in produced and geothermal waters from the abridged USGS database relative to seawater (NPDW normalization).

Comparison of ESOM weights shows that similar patterns are observed for light REEs other than Eu versus heavy REEs, with Eu behaving independently due to its 2+ and 3+ redox states. To understand spatial controls and patterns on predicted REE concentrations from the ESOM model, maps were created showing predicted NPDW-normalized concentrations (i.e., predicted potential). Praseodymium was used as a surrogate for light REE behavior, Yb was used as a surrogate for heavy REE behavior, and Eu was also mapped due to its individual behavior. The data were categorized into low, medium, high, and highest categories based on the relative magnitude of the predicted potential values. Categorical ranges were developed for each surrogate individually (Table 6.8), to account for variations in the ranges of predicted potential (Figure 6.8). Note that 290 samples in the abridged USGS dataset did not contain latitude and longitude information and could not be mapped.

Maps of predicted mineral potential for Pr, Yb, and Eu are largely similar with the highest values focused primarily in the Permian Basin (southeast New Mexico and west Texas), Anadarko Basin (Oklahoma), Texas-Louisiana Salt Basin, Appalachian Basin (eastern Ohio and western Pennsylvania), Illinois Basin (southern Illinois and southern Indiana), and a few points spread out among basins in northwest New Mexico and eastern Utah. In general these basins exhibit some of the higher salinity values within the United States and all, except those in northwest New Mexico and eastern Utah, contain rocks and produced waters of marine origin (Hanor, 1994; Kharaka and Hanor, 2014). Notable differences for Eu include highest predicted potential also in the Michigan and Williston (North Dakota and Montana) basins. These areas produce some of the most saline waters in the United States with maximum total dissolved solids exceeding 400,000 mg/L, locally (Hanor, 1994). In terms of reservoir lithology, samples associated with the 25 highest predicted Pr and Yb potential largely overlap and include clastic sandstone and shale reservoirs (e.g., Clinton sandstone of the Appalachian Basin, Wilcox and Bromide sands of the Anadarko Basin, and Yeso, Artesia, and

Canyon groups of the Permian Basin) and carbonate reservoirs (Smackover Formation of the Texas-Louisiana Salt Basin, Ste. Genevieve limestone of the Illinois Basin, and Hunton Group of the Anadarko Basin). Also, no consistent trends with depth (a proxy for temperature) were observed with depths ranging from ~900 ft to over 15,000 ft, which agrees with the ESOM weight maps showing no clear relationship between temperature and relative REE proportion (Figure 6.6). TDS values also range substantially in the 25 samples with the highest predicted Pr and Yb potentials, from ~51,000 to 353,000 mg/L, suggesting that salinity does not appear to serve as a control. Slightly different patterns are observed with respect to Eu; the 25 samples with highest predicted Eu mineral potential are all very saline (range = 145,000 to 341,000 mg/L; median = 258,000 mg/L) but of variable depth (~2,200 to ~13,000 ft below ground surface). Reservoir lithologies are similar to those with predicted high Pr and Yb potential with the addition of a few carbonate reservoirs (Ellenburger and San Andres/Grayburg in the Permian Basin, carbonate portions of the Salina formation in the Michigan Basin, Charles formation in the Williston Basin, and Mississippi Chat in the Anadarko Basin). This finding does not immediately identify lithology as the sole control on predicted REE potential in such waters. Maps for the remaining REEs are provided in the chapter Appendix for comparison.

Table 6.8. Ranges in predicted REE potential for Pr, Yb, and Eu used in Figures 5.9 to 5.11. The categories were also used for the remaining REES, which are mapped in the chapter Appendix.

Category	Pr and LREEs	Yb and HREEs	Eu
Highest	>= 500	>= 125	>= 2500
High	100-499	50-124	1000-2499
Medium	10-99	1-49	100-999
Low	<10	<1	<100

These findings indicate that predicted REE potential is high across many oil and gas producing basins in the United States and is not obviously controlled by lithology, reservoir temperature, or salinity (except for perhaps Eu). However, the strong co-association among most of the REEs except for Eu (Figure 6.6) suggests that samples that contain elevated concentration of any single REE also likely contain elevated concentrations of most, if not all, remaining REEs. This knowledge potentially reduces the analytical effort required in potential future geochemical prospecting because analysis of only one of two REEs is likely to provide acceptable results. Similar observations of co-association have been reported for REE accumulations in other media, including seafloor muds (Takaya et al., 2018). Co-association of the REEs also informs approaches to extraction because potentially economic sources would necessitate processes to separate the REEs from one another. To that effect, efforts to improve extraction and separation of REEs from geological sources are on going.

In terms of possible economic benefit, the U.S. Geological Survey summarizes information on values for many mineral commodities (U.S. Geological Survey, 2018). Their 2017 estimates suggest that Dy and Tb are by far the most individually economic REEs at roughly \$180-\$190 per kg for Dy₂O₃ and \$470-\$480 per kg for Tb₂O₃. Assuming 100% removal of both Dy and Tb from produced or geothermal water samples, none of the samples is predicted to be worth more than a \$0.01/barrel (1 barrel = 42 gallons). However, such calculations are made entirely from mathematically estimated results and should be taken with extreme caution. At a minimum mineral commodity values would need to exceed the disposal costs of the remaining waste brine. Disposal costs for brines within the United States are not well quantified and vary by region, but generally span the range of roughly \$0.10 to more than \$4.00 per barrel (Ray, 2016).

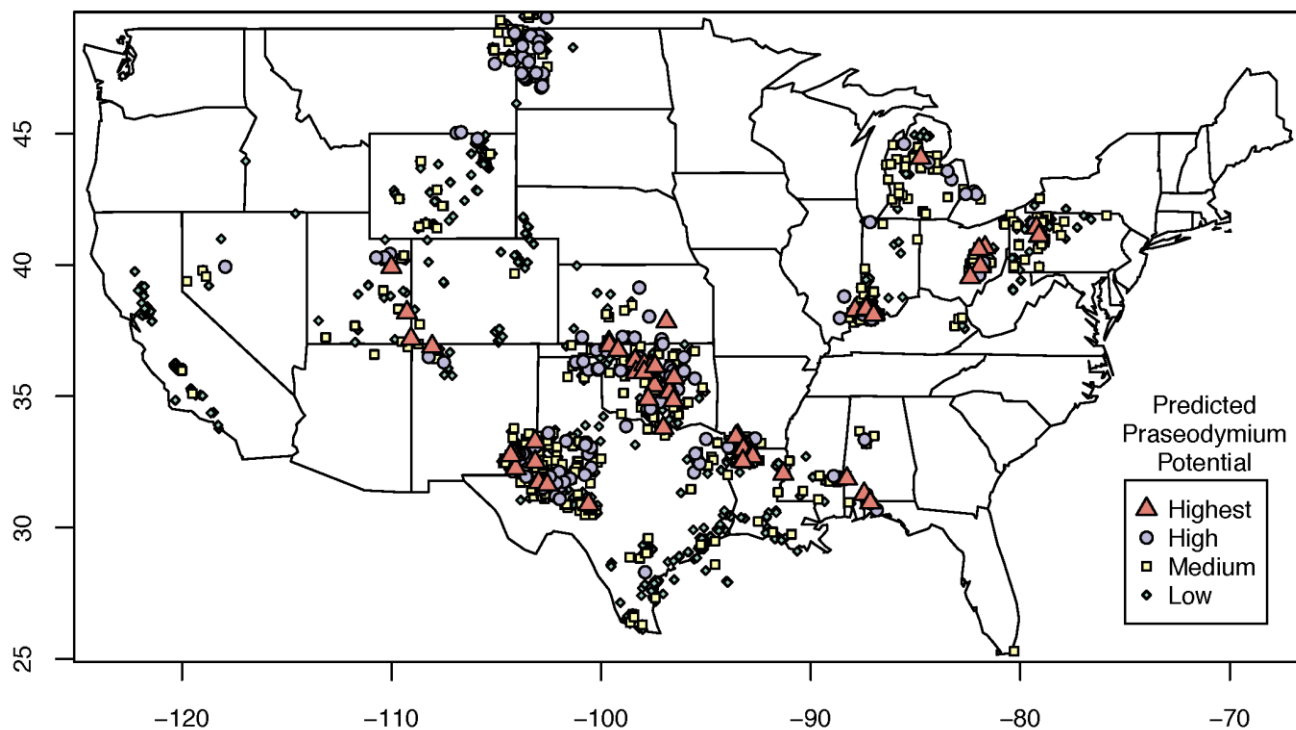


Figure 6.9. Predicted Pr potential of produced and geothermal waters.

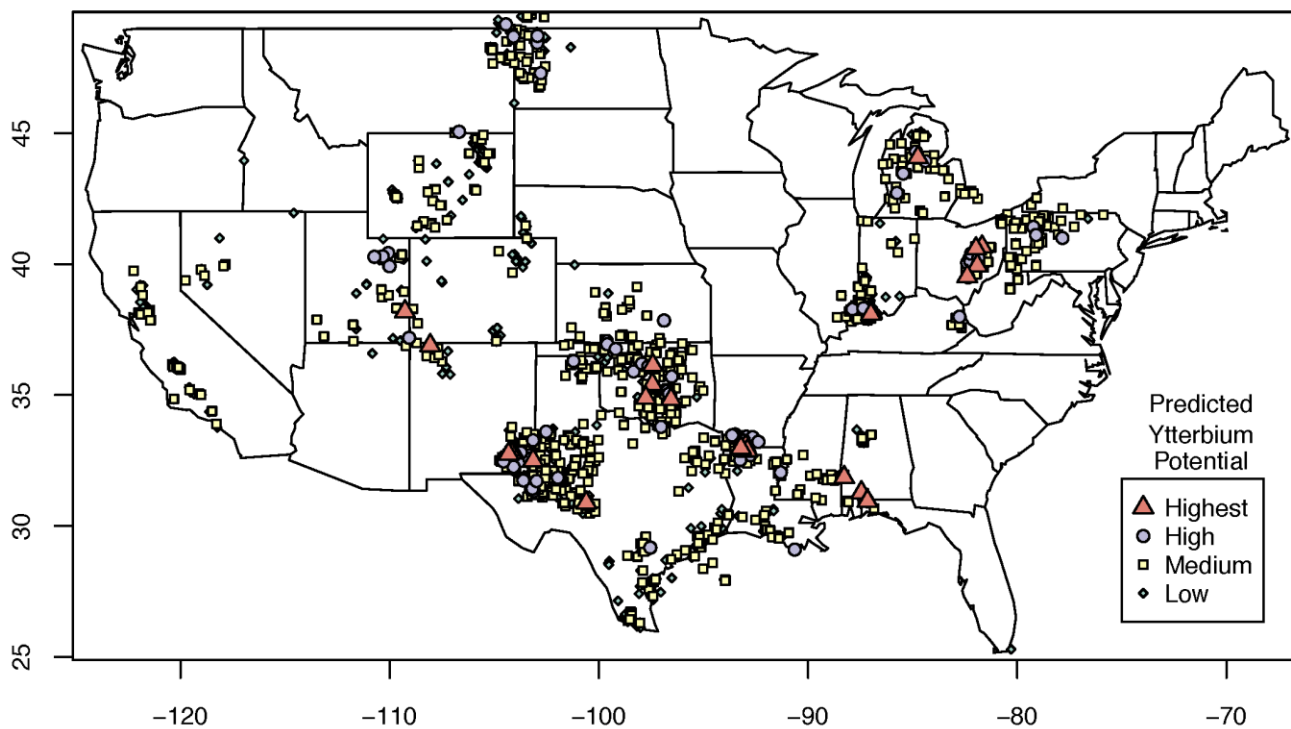


Figure 6.10. Predicted Yb potential of produced and geothermal waters.

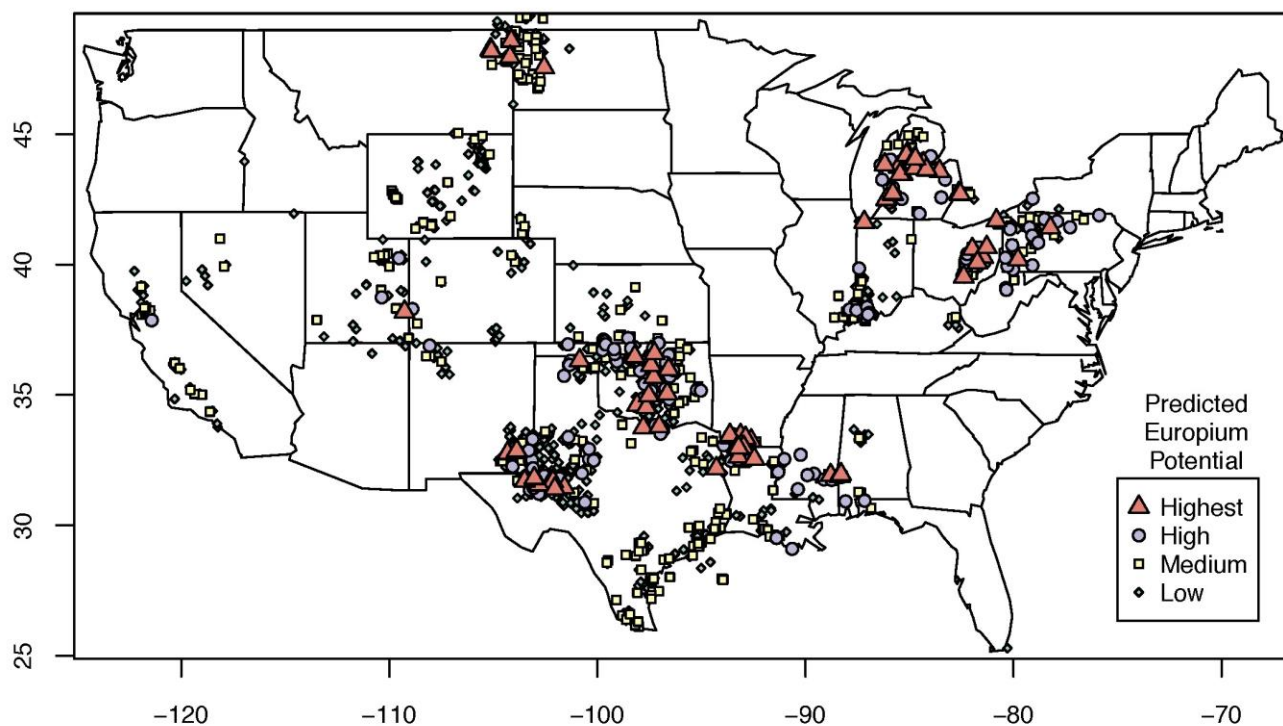


Figure 6.11. Predicted Eu potential of produced and geothermal waters.

4. SUMMARY

With respect to the two main objectives of this chapter, the following bullets capture the primary findings from this research:

Controls on REE concentration in produced and geothermal waters based on ESOM mapping:

Except for Eu, concentrations of REEs in produced and geothermal waters are strongly co-associated with one another and no single parameter used in the model serves as a strong pathfinder or predictor of REEs. Co-associations between high relative abundances of REEs and F were observed in some cases, suggesting a role for REE-F complexation, but F concentration does not appear to be limiting. Co-associations between Si and REEs were also observed and may suggest that specific clastic- or felsic-rich reservoirs may serve as a lithologic source.

Cross-validation modeling: For data which are chemically similar to samples used in the training dataset, NPDW-normalized predicted REE concentrations are typically accurate within an order of magnitude.

Predicted REE potential of produced and geothermal waters of the United States: In general, produced and geothermal waters are predicted to be enriched in REEs by an order of magnitude or more relative to seawater, with maximum predicted enrichments in excess of 1000-fold for some elements. The largest average predicted enrichments in produced and geothermal waters relative to NPDW were observed in light REEs (La to Gd), with generally less enrichment in the heavy REEs (Tb to Lu). Cerium and Eu exhibited the highest predicted potentials due to Ce depletion in seawater and release of Eu from reservoir materials during weathering and diagenetic reactions. The economic worth of the two most valuable REEs, Dy and Tb, is estimated to be significantly less than typical costs required to dispose of the waste brines remaining after REE removal.

Spatial patterns in predicted REE potential: Predicted REE potential is high across many geologic basins in the United States and the REEs are typically spatially co-associated, but based on the information currently available, are not obviously controlled by lithology, reservoir temperature, or salinity.

In terms of future work, new produced and geothermal water data containing REE concentrations can be added to the input dataset used here, to generate an even more robust ESOM. In turn, this can allow for better examination on the controlling variables for REEs in waters from deep sedimentary basins. Moreover, the trained ESOM and a table containing the predicted REE potential of samples in the USGS database created as part of this work are available as a digital download through the U.S. Department of Energy Geothermal Data Repository. Other datasets in need of REE prediction can be mapped to the ESOM to predict values using the methods described here. With increasing data and more flexible techniques such as the ESOM, methods to estimate resource commodities will only improve.

DISCLAIMER

Any use of trade, firm or product names is for descriptive purposes only and does not imply endorsement by the U.S. Government.

CONTRIBUTIONS AND ACKNOWLEDGMENTS

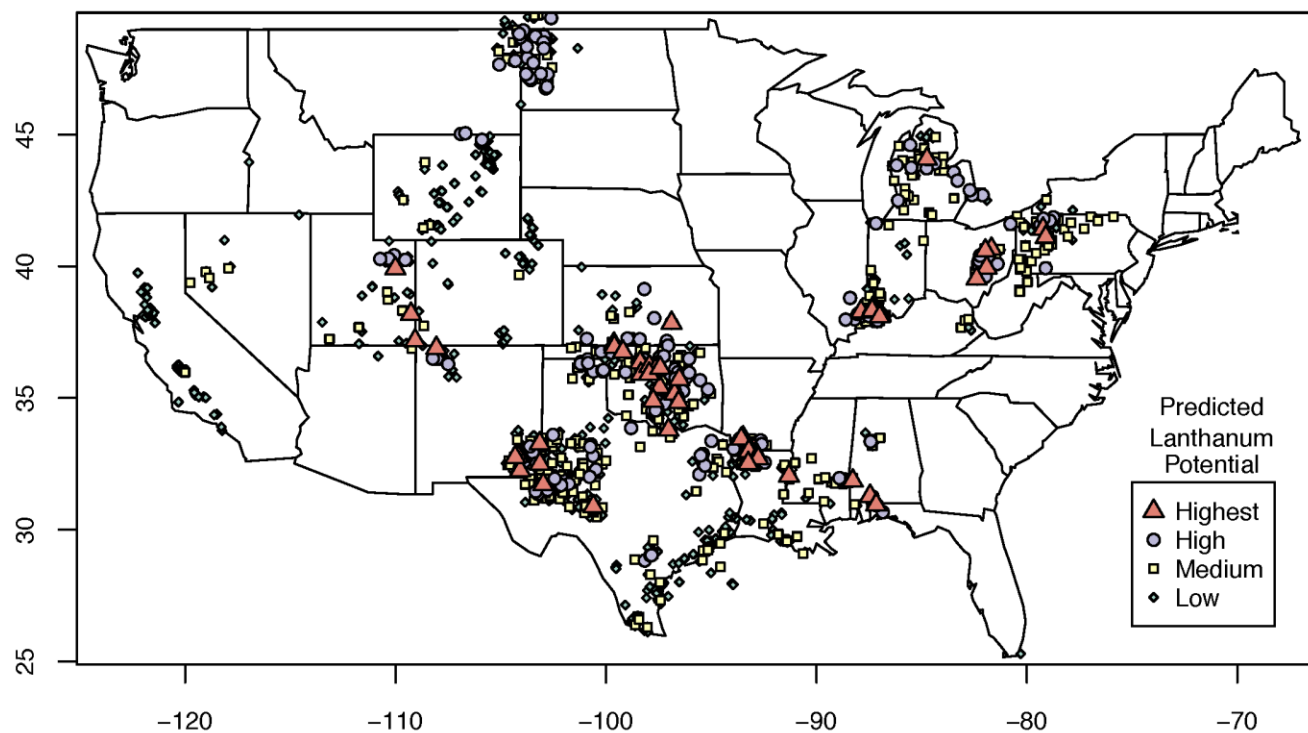
Mark Engle conceived this approach, performed all data analysis, created all figures and tables, and wrote and revised this report. Funding for this work was provided by U.S. Department of Energy, Geothermal Technologies Office under Award DE-EE0007603 and the U.S. Geological Survey Energy Resources Program. The author would like to thank our DOE project managers Holly Thomas and Josh Mengers and also our Technical Monitoring Team for their support, advice, and insight. Josep Antoni Martín-Fernández (University of Girona) provided thoughtful discussion and led development of CoDA techniques with the SOM. Madalyn Blondes and Ricardo Olea (both USGS) provided helpful feedback and suggestions on an earlier version of this chapter.

REFERENCES

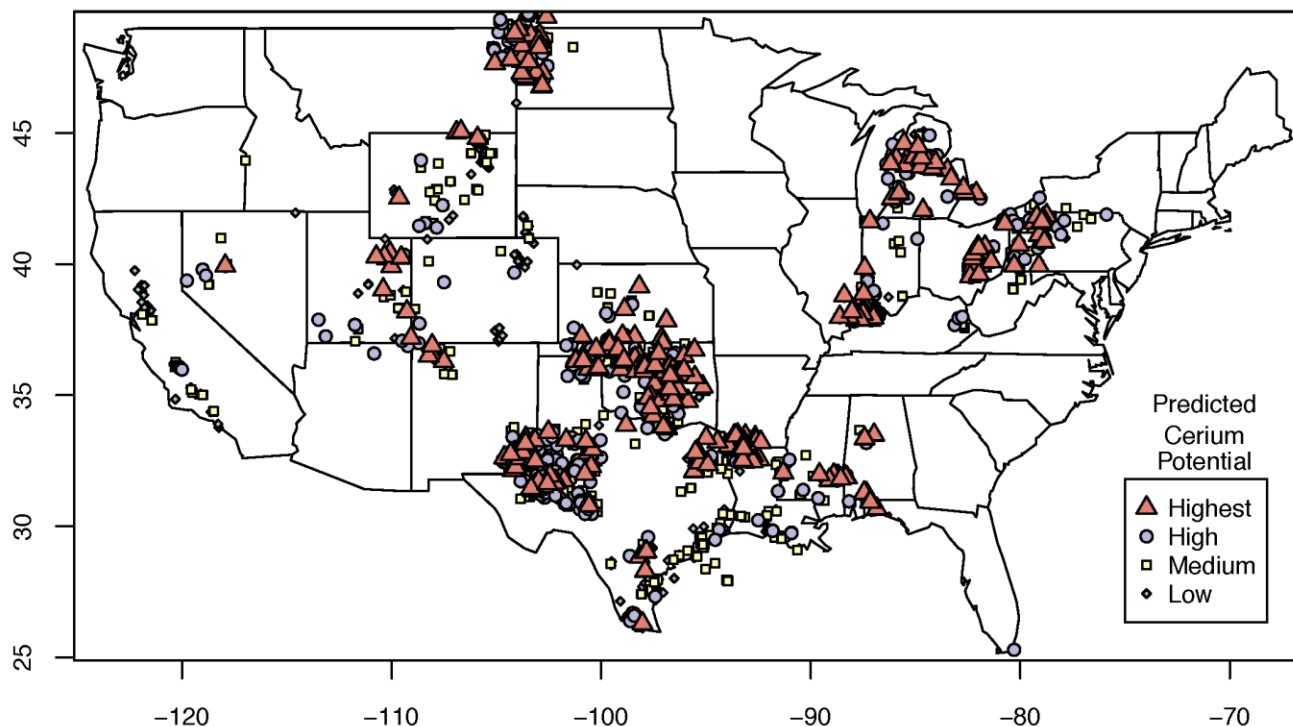
- Aitchison, J.: The statistical analysis of compositional data. Reprinted in 2003 with additional material by Blackburn Press: Chapman and Hall, (1986), 416 p.
- Alibo, D. S., and Nozaki, Y.: Rare earth elements in seawater: particle association, shale-normalization, and Ce oxidation. *Geochimica et Cosmochimica Acta*, **63**(3-4), (1999), 363–372.
- Blondes, M. S., Gans, K. D., Engle, M. A., Kharaka, Y. K., Reidy, M. E., Saraswathula, V., et al.: U.S. Geological Survey National Produced Waters Geochemical Database, version 2.3. U. S. Geological Survey, (2017). Retrieved from <https://eerscmap.usgs.gov/pwapp/>
- Dickson, B. L., and Giblin, A. M.: An evaluation of methods for imputation of missing trace element data in groundwaters. *Geochemistry: Exploration, Environment, Analysis*, **7**(2), (2007), 173–178.
- Egozcue, J., Pawłowsky-Glahn, V., Mateu-Figueras, G., and Barceló-Vidal, C.: Isometric logratio transformations for compositional data analysis. *Mathematical Geology*, **35**(3), (2003), 279–300.
- Engle, M. A., and Blondes, M. S.: Linking compositional data analysis with thermodynamic geochemical modeling: Oilfield brines from the Permian Basin, USA. *Journal of Geochemical Exploration*, **141**, (2014), 61–70.
- Engle, M. A., and Rowan, E. L.: Interpretation of Na-Cl-Br systematics in sedimentary basin brines: Comparison of concentration, element ratio, and isometric log-ratio approaches. *Mathematical Geosciences*, **45**, (2013), 87–101.
- Engle, M. A., and Rowan, E. L.: Geochemical evolution of produced waters from hydraulic fracturing of the Marcellus Shale, northern Appalachian Basin: A multivariate compositional data analysis approach. *International Journal of Coal Geology*, **126**, (2014), 45–56.
- Engle, M. A., Reyes, F. R., Varonka, M. S., Orem, W. H., Ma, L., Ianno, A. J., et al.: Geochemistry of formation waters from the Wolfcamp and “Cline” shales: Insights into brine origin, reservoir connectivity, and fluid flow in the Permian Basin, USA. *Chemical Geology*, **425**, (2016), 76–92.
- Filzmoser, P., Hron, K., and Reimann, C.: Interpretation of multivariate outliers for compositional data. *Computers & Geosciences*, **39**, (2012), 77–85.
- Fournier, R. O., White, D. E., and Truesdell, A. H.: Geochemical indicators of subsurface temperature-Part 1, basic assumptions. *Journal of Research of the U.S. Geological Survey*, **2**(3), (1974), 259–262.
- Hanor, J. S.: Origin of saline fluids in sedimentary basins, In Parnell, J. (ed.), *Geofluids: Origin, Migration and Evolution of Fluids in*

- Sedimentary Basins*, Geological Society Special Publication, 78, (1994), 151–174).
- Hron, K., Templ, M., and Filzmoser, P.: Imputation of missing values for compositional data using classical and robust methods. *Computational Statistics and Data Analysis*, **54**(12), (2010), 3095–3107.
- Kharaka, Y. K., and Hanor, J. S. Deep Fluids in Sedimentary Basins, Chapter 7.14, in *Treatise on Geochemistry*, 2nd ed., Elsevier, (2014), 471–515.
- Kharaka, Y. K., and Mariner, R. H.: Chemical geothermometers and their application to formation waters from sedimentary basins. In Naeser, N. D. and McCulloh, T. H. (Eds.), *Thermal History of Sedimentary Basins*, Springer Verlag, (1989), 99–117.
- Lacassie, J. P., Roser, B., Solar, J. R. D., and Herve, F.: Discovering geochemical patterns using self-organizing neural networks: A new perspective for sedimentary provenance analysis. *Sedimentary Geology*, **165**, (2004), 175–191.
- Liu, Y. and Weisberg, R.H.: Patterns of ocean current variability on the West Florida Shelf using the self-organizing map, *Journal of Geophysical Research*, **110**(C6), (2005), C06003, 12 p..
- Martín-Fernández, J. A., Engle, M. A., Ruppert, L. F., and Olea, R. A.: Advances in self-organizing maps for their application to compositional data. *Stochastic Environmental Research and Risk Assessment*, (2018), in review.
- Migdisov, A., Williams-Jones, A. E., Brugger, J., and Caporuscio, F. A.: Hydrothermal transport, deposition, and fractionation of the REE: Experimental data and thermodynamic calculations. *Chemical Geology*, **439**, (2016), 13–42.
- Neupane, G., and McLing, T.: Soda Geyser Geochemistry [dataset], U.S. Department of Energy Geothermal Data Repository, Submission 937, (2017), <http://doi.org/10.15121/1367546>.
- Quillinan, S., Nye, C. W., Neupane, G., and McLing, T.: Rare Earth Element Concentration of Wyoming Thermal Waters Update [dataset], U.S. Department of Energy Geothermal Data Repository, Submission 931, (2017), <http://doi.org/10.15121/1364771>.
- Ray, S.: National evaluation for development and exploration potential of mineral commodities in produced waters, M.S. Thesis, University of Texas at El Paso, El Paso, Texas, (2016), 218 p.
- Reimann, C., Filzmoser, P., Garrett, R., and Dutter, R.: Statistical data analysis explained: Applied environmental statistics with R, Wiley Publishing, (2008), 343 p.
- Sun, X., Deng, J., Gong, Q., Wang, Q., Yang, L., and Zhao, Z.: Kohonen neural network and factor analysis based approach to geochemical data pattern recognition. *Journal of Geochemical Exploration*, **103**(1), (2009), 6–16.
- Takaya, Y., Yasukawa, K., Kawasaki, T., Fujinaga, K., Ohta, J., Usui, Y., et al.: The tremendous potential of deep-sea mud as a source of rare-earth elements. *Scientific Reports*, **8**:5763, (2018), 1–8.
- U.S. Geological Survey: Mineral commodities summary 2018, U. S. Geological Survey, (2018), 200 p.
- Ultsch, A.: U*-Matrix: A tool to visualize clusters in high dimensional data., Department of Mathematics and Computer Science Technical Report No. 36, University of Marburg, Germany, (2003), 10 p.
- Ultsch, A.: Emergence in Self Organizing Feature Maps. *Proceedings*, Workshop on Self-Organizing Maps (WSOM '07), Bielefeld, Germany, (2007), 1–7.
- Varmuza, K., and Filzmoser, P.: Introduction to Multivariate Statistical Analysis in Chemometrics, CRC Press, (2009), 321 p.
- Žibret, G., and Šajn, R.: Hunting for geochemical associations of elements: Factor analysis and self-organising maps. *Mathematical Geosciences*, **42**(6), (2010), 681–703.

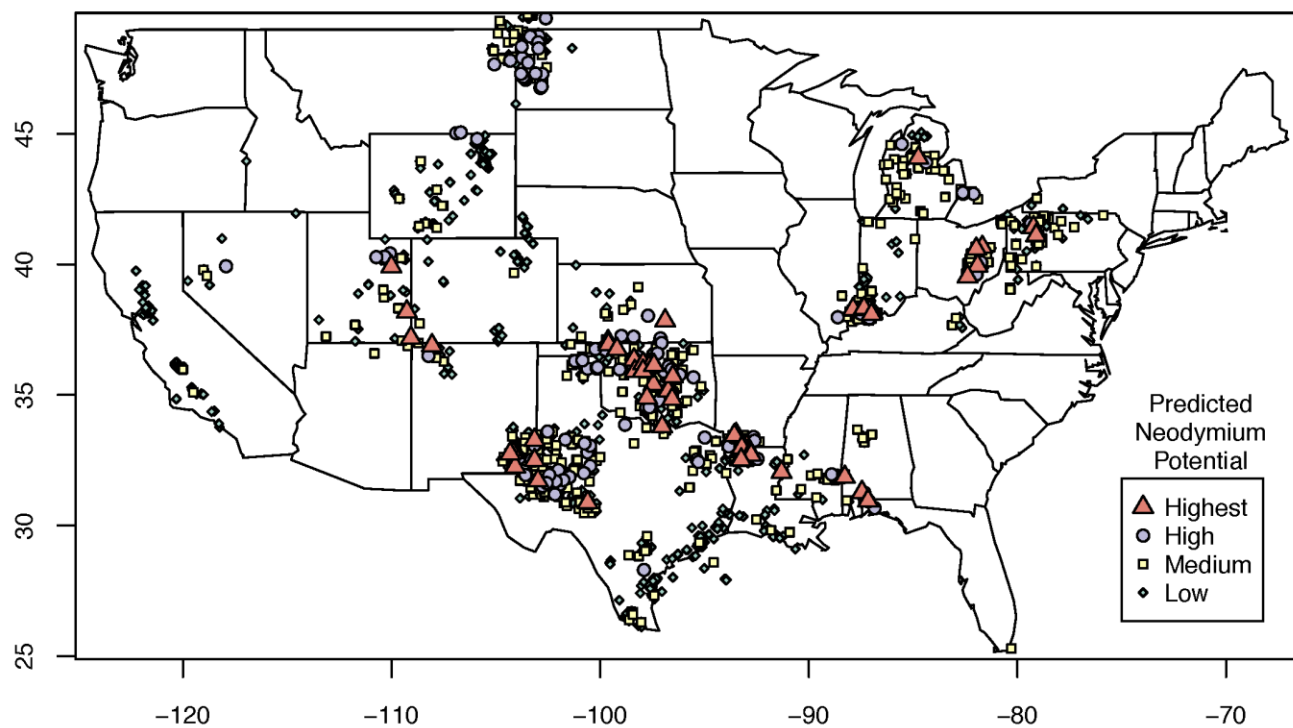
APPENDIX



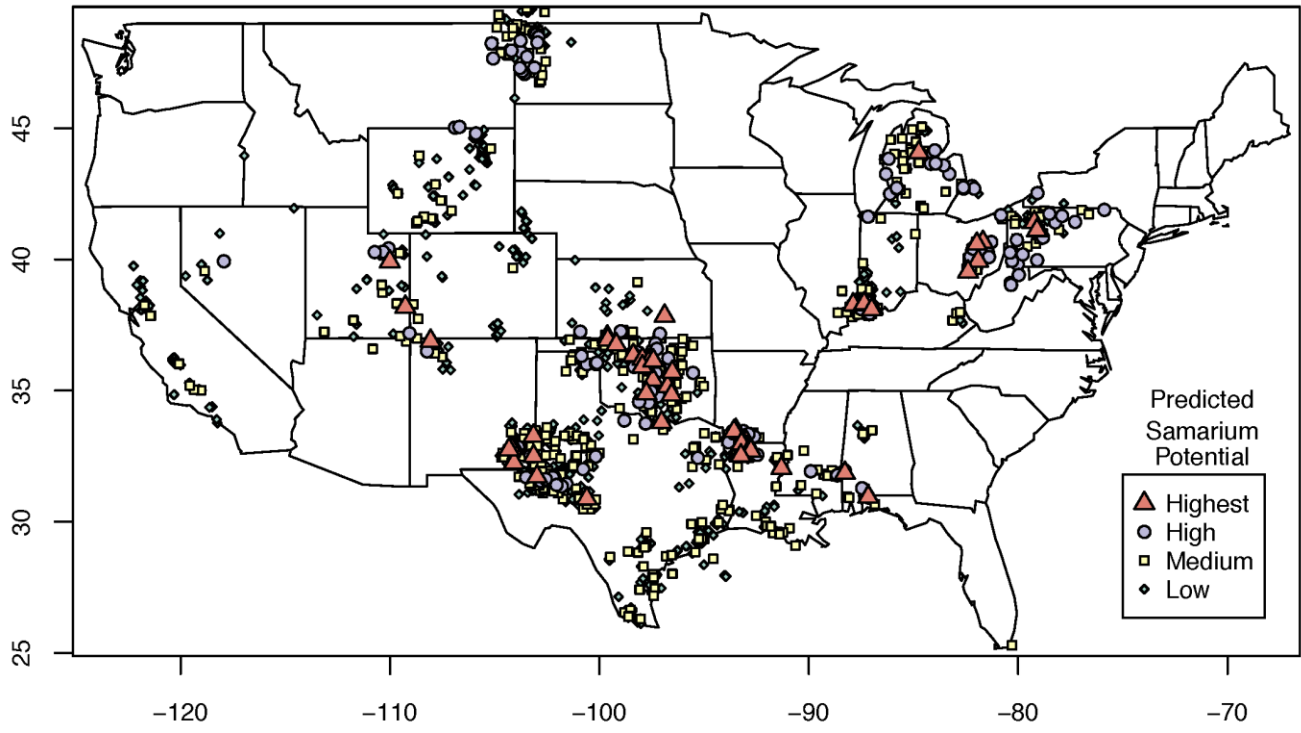
Appendix Figure 6.1. Predicted La potential of produced and geothermal waters.



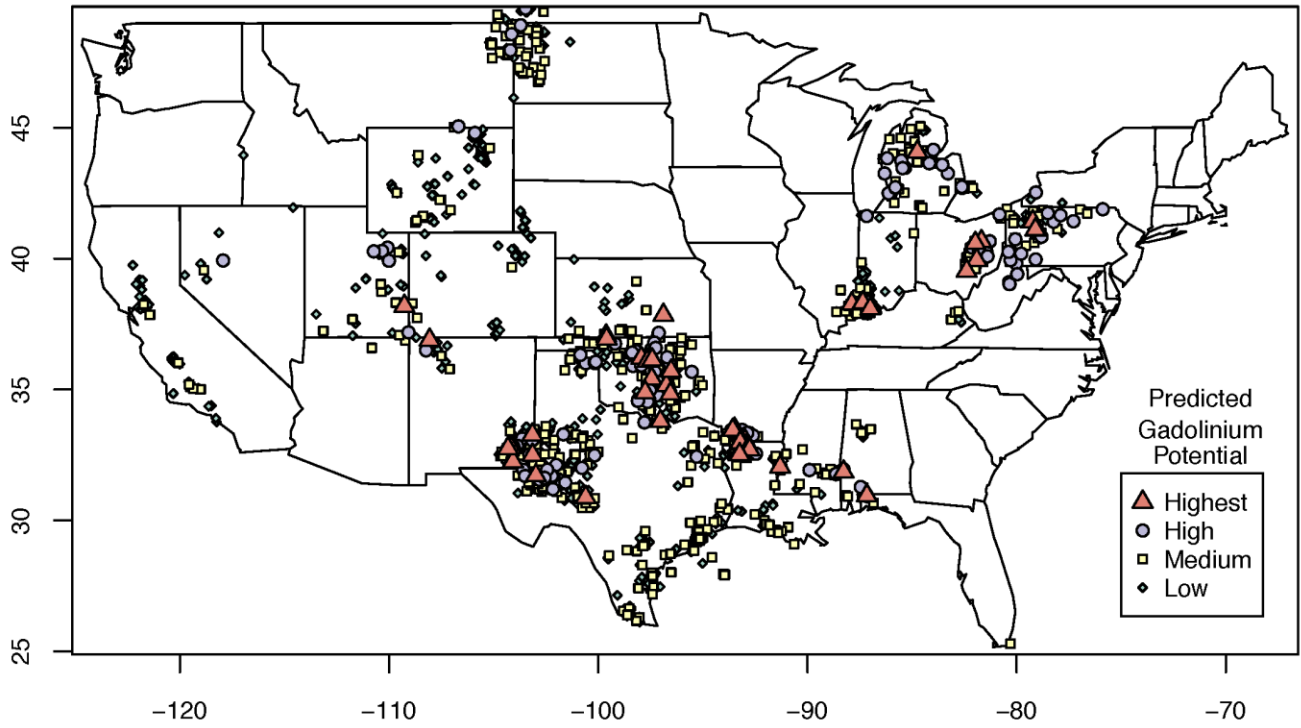
Appendix Figure 6.2. Predicted Ce potential of produced and geothermal waters.



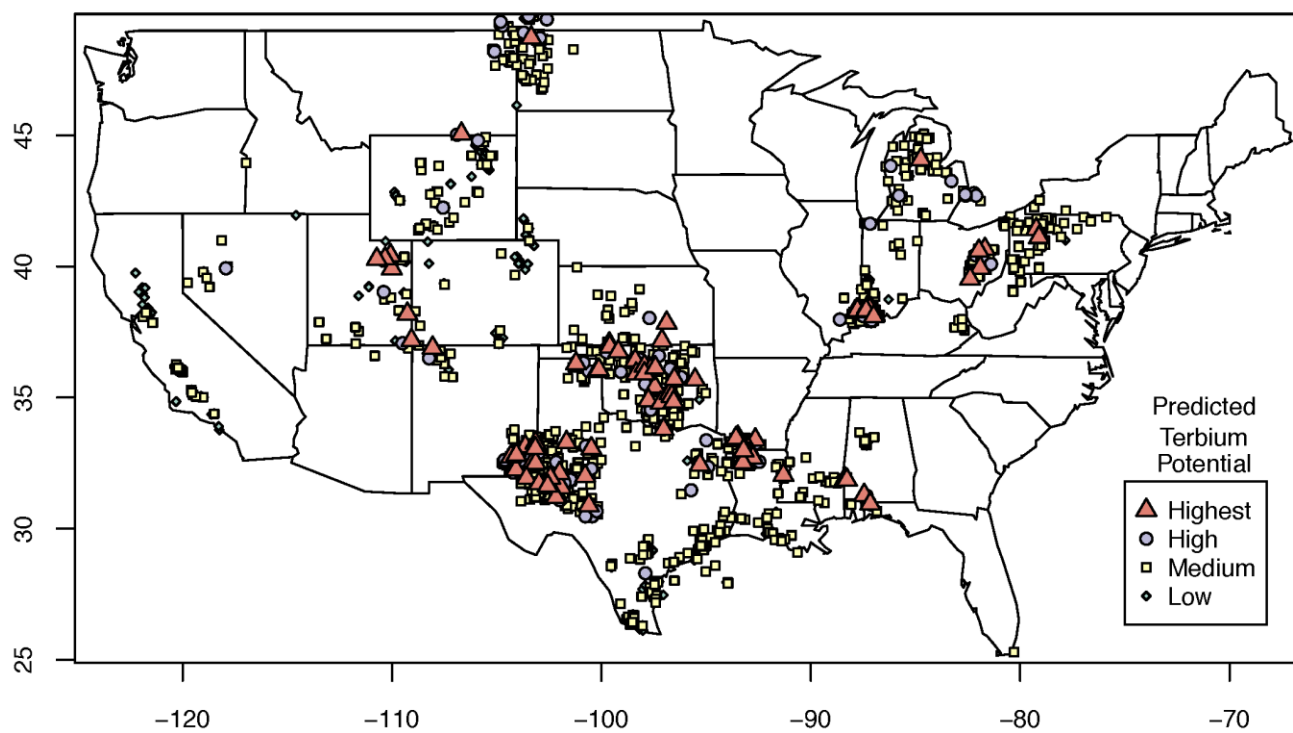
Appendix Figure 6.3. Predicted Nd potential of produced and geothermal waters.



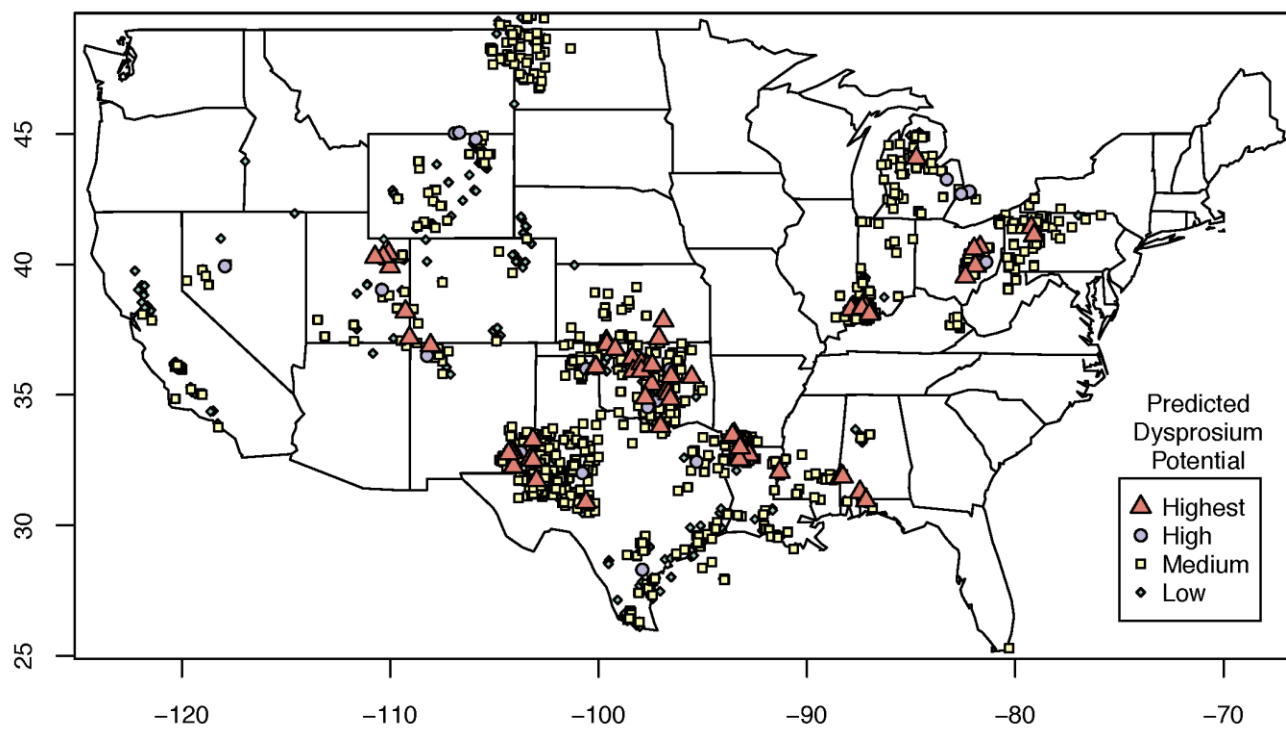
Appendix Figure 6.4. Predicted Sm potential of produced and geothermal waters.



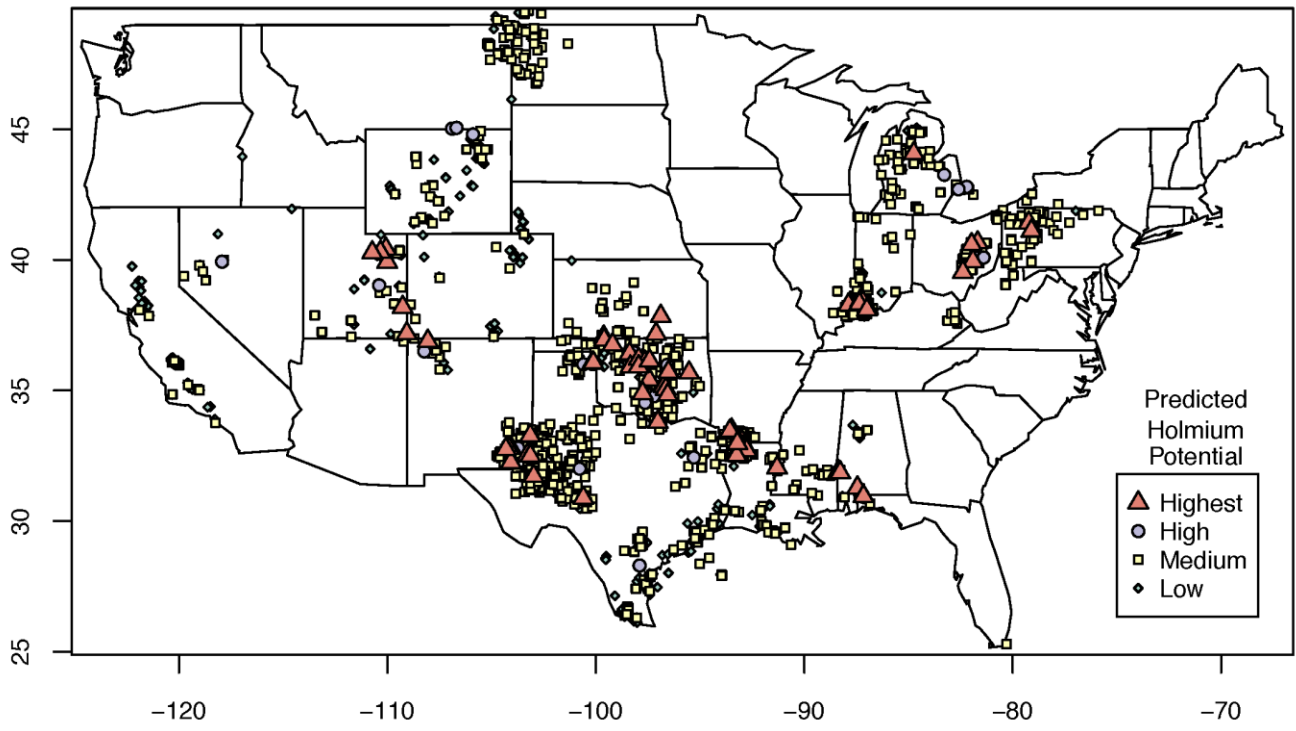
Appendix Figure 6.5. Predicted Gd potential of produced and geothermal waters.



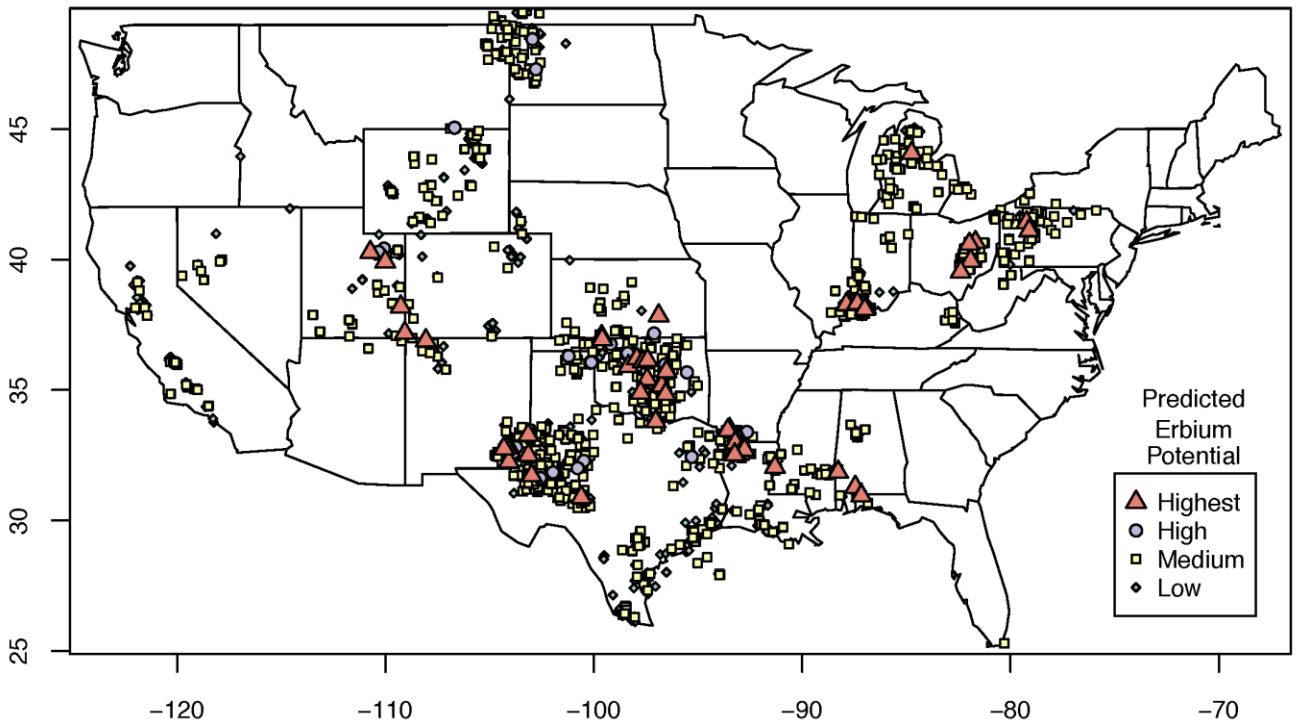
Appendix Figure 6.6. Predicted Tb potential of produced and geothermal waters.



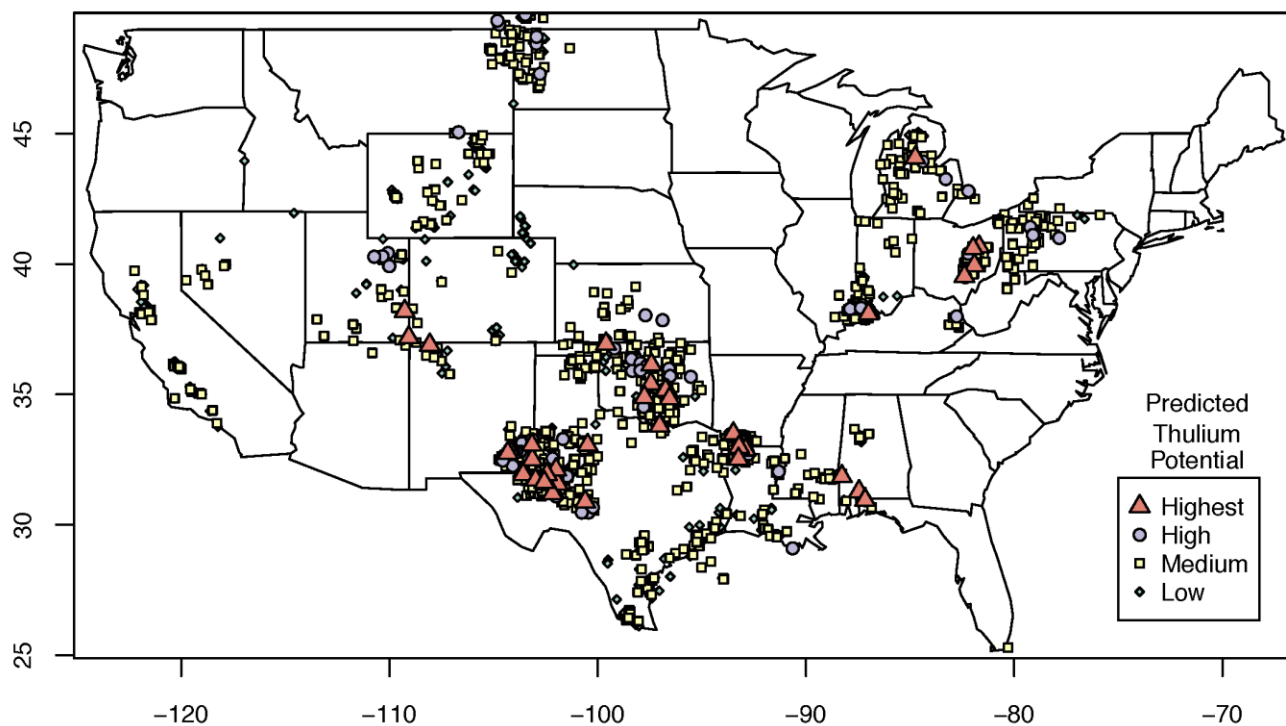
Appendix Figure 6.7. Predicted Dy potential of produced and geothermal waters.



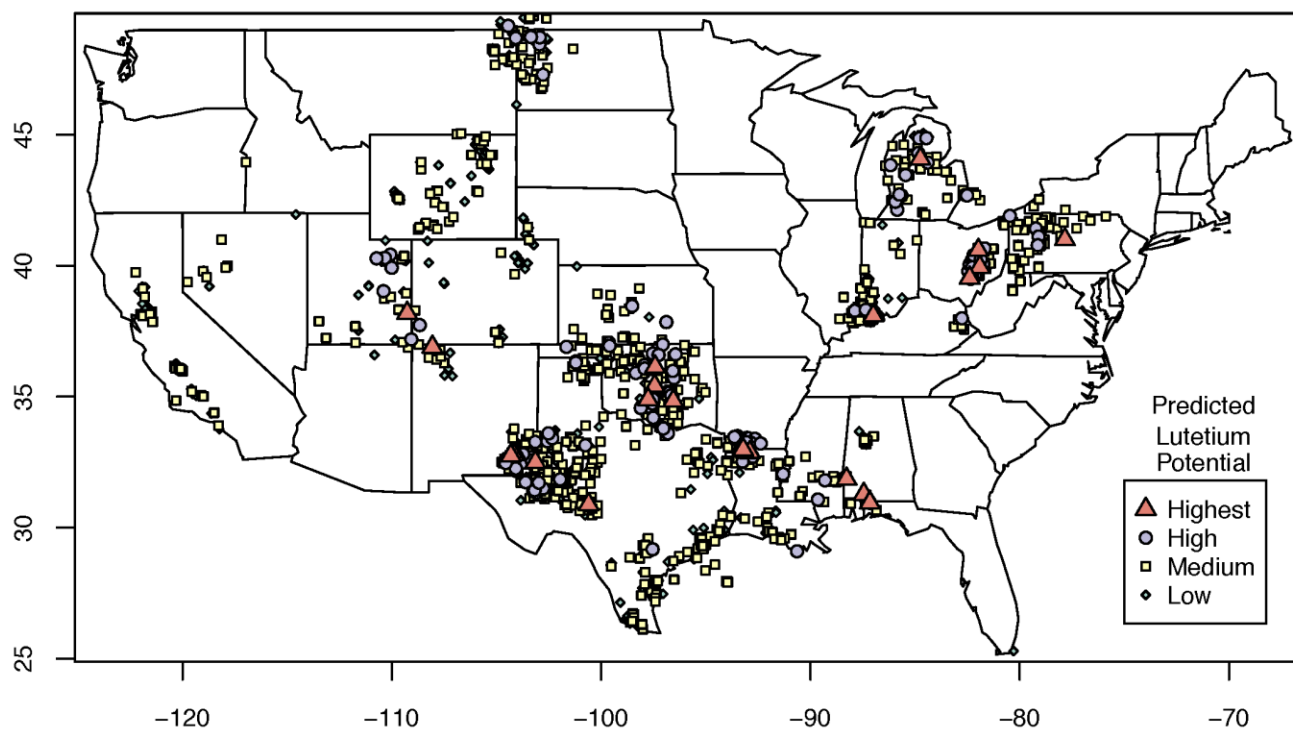
Appendix Figure 6.8. Predicted Ho potential of produced and geothermal waters.



Appendix Figure 6.9. Predicted Er potential of produced and geothermal waters.



Appendix Figure 6.10. Predicted Tm potential of produced and geothermal waters.



Appendix Figure 6.11. Predicted Lu potential of produced and geothermal waters.

Chapter 7: Technology Screening

Jonathan Brant, Mahdi Shahabadi

Jonathan Brant, Director, University of Wyoming, Department of Civil and Architectural Engineering, 1000 E. University Avenue,
 Laramie, WY 82071

E-mail Address: jbrant1@uwyo.edu

Keywords: Adsorption; Membrane Separation; Nanofiltration; Rare Earth Element; Solvent-Solvent Extraction

ABSTRACT

Though technologically possible, economic recovery of REEs from brines at the nano- to micro-gram per liter concentrations presents a unique set of challenges. This chapter presents a variety of separation technologies at differing levels of maturity that may be able to overcome some of these challenges, such as adsorption, solvent extraction, and membrane separation. Adsorption and solvent extraction have advantages like reusability and selectivity toward particular elements, but literature on their application for dilute solutions is sparse. On the other hand, nanofiltration has a confirmed ability to concentrate REEs in dilute streams, such as geothermal brines. Due to its promise, we carried out rough cost analyses for nanofiltration processes. Our review concludes that the most important obstacles to applying these extraction technologies arise from achieving finished REE concentrations and relative purities that warrant such financial investment, as well as with making the processes selective for the targeted elements.

Knowledge gaps in literature that must be addressed in order to further the development of treatment schemes aimed at REE recovery include understanding the transformation (physical and chemical) of REEs in brine mixtures during separation, acquisition of REE separation data using brine mixtures and different separation processes, and development of new “smart” adsorbents that can be deployed in, or receive, brine mixtures representative of geothermal brines and other complex mixtures.

1. REVIEW OF PROCESSES FOR RECOVERING RARE EARTH ELEMENTS (REES) FROM GEOTHERMAL BRINES

Rare earth elements (REEs) include the 15 different lanthanides, yttrium, and scandium. Based on their atomic number, REEs are divided into light rare earth elements (LREEs) and heavy rare earth elements (HREEs). LREEs include lanthanum (La), cerium (Ce), praseodymium (Pr), neodymium (Nd), promethium (Pm), and samarium (Sm). HREEs include europium (Eu), gadolinium (Gd), terbium (Tb), dysprosium (Dy), holmium (Ho), erbium (Er), thulium (Tm) Ytterbium (Yb), lutetium (Lu), scandium (Sc) and yttrium (Y). HREEs are less common and more valuable, in monetary terms, than LREEs (Ponou et al., 2014). Due to their remarkable chemical, electrical, metallurgical, magnetic, optical, and catalytic properties, REES are used in the manufacture of a wide variety of products like batteries, permanent magnets, automotive catalytic converters, fiber optics, lasers, and electronic devices (Ponou et al., 2014, Sadovsky et al., 2016).

Few concentrated deposits of REEs exist; however, the relative prevalence of low concentrations of REEs in the Earth’s crust results in their presence in formation waters. Previous studies have found that fluids generated through geothermal energy production may be enriched with REEs and represent a potentially untapped source of these critical materials (Callura et al., 2016). Results from a study done by Wood looking at REEs in geothermal waters are summarized in Table 1 (Wood, 2002). Unfortunately these concentrations often range from the nano-gram to micro-gram per liter level. At such low concentrations recovery of REEs is difficult to do economically and technologically. The technical challenge of REE separation from mixed brines centers on producing a product that is suitable for subsequent refining. This is problematic for many separation processes due to complexation reactions between the REE(s) and other materials in the brine solution. Despite this, and other, hurdles a number of efforts have focused on studying and developing new separation processes for REEs from brines, like that associated with geothermal systems. The importance and far ranging benefits associated with REE recovery from geothermal brines was recently covered in a review article authored by Smith et al. (2017).

Table 1.1: Summary of REE concentration data in geothermal source waters. All data was obtained from Wood (2002).

	Mean Concentration (ppt) ¹	Median Concentration (ppt)	Standard Deviation (ppt)	Number of Locations
Y	12430	25	62,869	551
Ce	9843	18	44,853	547
Nd	7775	12	29,897	423
La	4933	17	21,250	481
Gd	4648	5	21,774	484

Dy	2050	4	9,081	509
Sm	1964	3	7,736	366
Er	1505	3	6,480	449
Pr	1446	2	6,060	502
Yb	1397	3	6,204	463
Eu	1354	2	13,266	454

1. ppt = ng/L

2. REVIEW OF SEPARATION PROCESSES FOR REES IN MIXED BRINES

The separation of ionic materials, like REEs, from aqueous mixtures may be achieved using physical-chemical processes, such as adsorption, ion exchange, and non-porous membranes. Other types of processes, including biological processes, may also be used; however, these processes are limited in terms of their applicability to geothermal brines. The lack of pilot-scale and larger studies has resulted in a dearth of available economic data on REE separation processes, particularly when applied to relatively dilute feed streams. This lack of economic data of REE separation processes represents perhaps the most significant gap in the literature and the greatest need in terms of future research.

2.1 Adsorption Processes

Due to its non-toxicity, ability to regenerate the adsorbent, and ability to tailor the selectivity of an adsorbent for specific adsorbates adsorption process are considered as one of the best methods for REE recovery (Zhao, Repo et al. 2016, Iftekhar, Srivastava et al. 2017). Like ion exchange, adsorption processes must overcome a variety of challenges for REE recovery. Some of these challenges include competition between adsorbates for adsorption sites, relatively low concentrations of adsorbates in solution, and pretreatment prior to REE separation. While proven successful, the bulk of previous REE adsorption studies have used relatively simple electrolyte mixtures composed of a limited number of elements, thereby not exploring these practical challenges. Nevertheless, adsorption has been shown to be a viable method for removing REEs from aqueous mixtures. A summary of results from different REE adsorption studies is given in **Table 2**. Researchers have investigated different methods for improving the adsorption capacities of various adsorbents for REEs. To this end, much progress has been made in optimizing the selectivity and adsorption capacities of various adsorbents for different REEs. S. Iftekhar et al. studied Zn/Al layered double hydroxide (LDH) intercalated cellulose (CL) nanocomposite for selectively removing REEs from mixed ionic solutions (Iftekhar, Srivastava et al. 2017). Adsorption followed pseudo second order kinetics. Optimized specific adsorption capacities for Y^{3+} , La^{3+} and Ce^{3+} were 102.25, 92.51 and 96.25 mg/g, respectively. Kinetic experiments revealed that equilibrium was achieved in 10 min and the adsorbent was effective for up to five cycles. Borai et al. used three different adsorbents, including as Modified (H and Na forms) polymeric resins (hydrogels) abbreviated as MPRH and MPRNa, and silica composite (SC) for REE recovery from a multi-component solution containing La^{3+} , Ce^{3+} , Nd^{3+} and Eu^{3+} (Borai, Hamed et al. 2015). The SC adsorbent showed higher REE uptake. This was attributed to the high specific surface area of the porous silica. Also, REE exchange by all of the adsorbents followed the order $La^{3+} > Ce^{3+} > Nd^{3+} > Eu^{3+}$. Zhao et al. found the optimum adsorption by DTA- β -cyclodextrin in single adsorption studies, where a single adsorbate was in solution, followed the order $Eu^{3+} > Ce^{3+} > La^{3+}$. In multi-component adsorption studies, where more than one adsorbate was present in solution, a selectivity toward Eu^{3+} was observed and the adsorption followed the order $Eu^{3+} \gg Ce^{3+} > La^{3+}$ (Zhao, Repo et al. 2016). In a more recent study funded through the Department of Energy a new adsorbent (resin beads), named CRADA, was invented for recovering lanthanides from geothermal waters and is currently being examined for commercialization (Mayes, Halstenberg et al. 2018). Although the literature shows that adsorption is a viable method for recovering REEs from solution, it is lacking on data demonstrating its viability for mixed brines, like geothermal ones. In such applications, the aforementioned challenges have yet to be overcome, hindering the practical application of adsorption processes for REE recovery.

Table 1.2: Summary of results from adsorption studies investigating the selective recovery of various REEs from aqueous mixtures.

Ref.	Adsorbent	Isotherm Model ¹	Kinetic Model ²	Adsorption Capacity (mg/g)				
				Y^{3+}	La^{3+}	Ce^{3+}	Eu^{3+}	Nd^{3+}
(Iftekhar, Srivastava et al. 2017)	CL-Zn/Al LDH nanocomposite	L	PS2	102.25	92.51	96.25	-	-
(Zhu, Zheng et al. 2015)	HPC-g-PAA/APT granular	L	PS2	-	270	200	-	-
(Varshini, Das et al. 2015)	Biohydrogel modified with sporopollenin	L	PS2	-	-	333.3	-	-

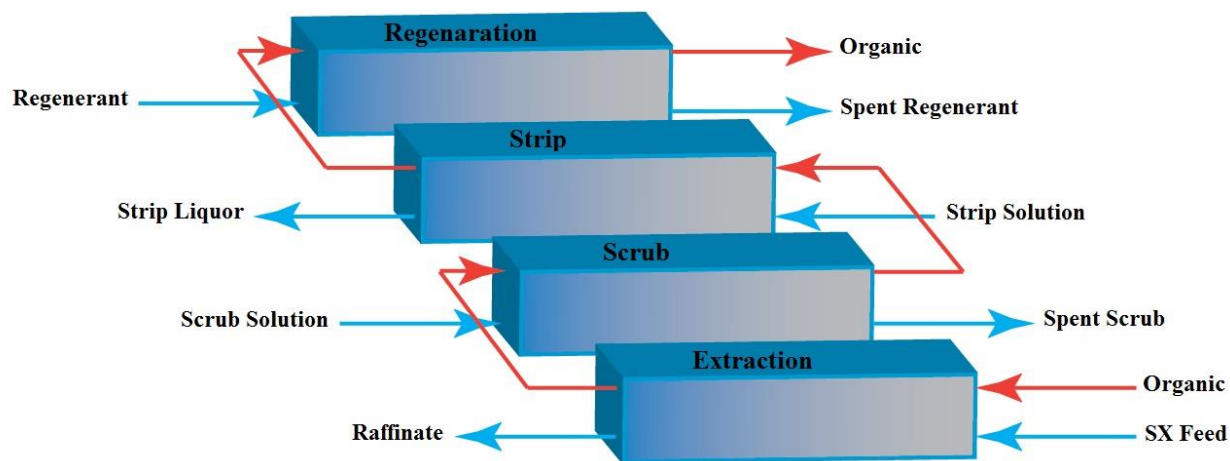
List Authors in Header, surnames only, e.g. Smith and Tanaka, or Jones et al.

(Varshini, Das et al. 2015)	Biohydrogel modified with xylan	F	PS2	-	-	200	-	-
(Anagnostopoulos and Symeopoulos 2013)	Malt spent rootlets	L	PS2	-	-	-	156	-
(Anagnostopoulos and Symeopoulos 2013)	Activated carbon	L	E	-	-	-	56	-
(Yao, Xiao et al. 2016)	Graphene oxide	L	PS2	-	-	-	142.8	-
(Hussien and Desouky 2014)	NaOH modified Pleurotus ostreatus	L	PS2	45.45	-	-	-	-
(Wang, Zhao et al. 2014)	Calcium alginate-poly glutamic acid hybrid gels	L	PS2	-	-	-	-	238
(Wang, Zhao et al. 2014)	Calcium alginate	L	PS2	-	-	-	-	194.73

- 1 L = Langmuir; F = Freundlich
- 2 PS2 = Pseudo second order; E = Elovich

2.2 Solvent Extraction Processes

Historically, ion exchange was the most practical method for the REE separation before the advent of industrial scale solvent extraction in the 1960s (Reddy, Kumar et al. 2009). Presently, solvent extraction is widely being used in commercial operations for REE separation from aqueous mixtures due to its ability to handle large volume of liquors (Peppard, Asanovich et al. 1953). In solvent extraction (**Figure 1.1**), the aqueous phase, which contains the REEs, is contacted with an organic phase. The organic phase is composed of an extractant, a solvent and modifiers all of which are organic compounds and immiscible in the aqueous phase. The extractant is the key component for extraction of specific element/s (REEs), while modifiers are added to the organic phase to modify its properties like pH and viscosity. Generally, there are three types of extractants for separating REEs: cation exchangers (or acidic extractants), solvation extractants (or neutral extractants), and anion exchangers (or basic extractants). The properties of the targeted element for recovery dictate the type(s) of extractants to be used. The REEs partition from the aqueous phase into the organic phase by forming organic-metal complexes. These complexes form through chemical reactions between the extractant and the metal, which is soluble in the organic phase. Impurities normally do not react with the extractant and thus, remain in the aqueous phase. Then the organic phase, containing the organic-metal complex, is separated from the aqueous phase (scrubbing step in **Figure 1.1**). The REE is then recovered and concentrated into another aqueous phase (strip liquor) with a high REE concentration by reversing the chemical reaction (stripping step in **Figure 2**). In the last step, regeneration, the organic phase is further purified to be reused in the extraction process. When selecting the extractant factors such as the composition of feed solution and the characteristics of the REE to be recovered must be considered. The advantages of solvent extraction are continuous operation, high treatment capacity, quick reaction rate and good separating effect; however, it needs large volumes of solvent (Ma, Zhao et al. 2017). The most important operating parameters affecting the extraction process are the concentration of the extractant agent, aqueous phase acidity, aqueous/organic volumetric ratio, contact time, and the stripping agent concentration (Abreu and Morais 2014).



Figur

e 1.1: Illustration of a solvent extraction process train for separating REEs from a liquid stream.

To date, the majority of research studies in the literature on multi-component REEs recovery and separation by solvent extraction are focused on the leach solutions obtained after processes like calcination and leaching. These processes are associated with hard rock mining operations, rather than water treatment systems. This focus is due to the relative immaturity of efforts centered on REE recovery from dilute solutions, like geothermal brines. A primary separation is often used for the separation of REEs from other substances. Di-(2-Ethylhexyl) phosphoric acid has been widely used for primary separation since the distribution coefficients of REEs as a group differ markedly from those of typical impurities in leach liquors (Xie, Zhang et al. 2014). For the secondary separation of REEs from each other, they are usually separated into two, three or sometimes four groups of solutions followed by subsequent separation of individual elements. There is a trade-off between process economics and REE selectivity. Higher selectivity lowers the number of stages, and hence capital and chemical inventory costs. For instance, cation exchangers usually possess higher selectivity than neutral and anionic exchangers; however, when using cation exchangers, a base is required to drive extraction, and acid is required for selectively washing the organic phase. Thereby, the reactive chemical requirement is greater with cation exchangers in comparison to neutral and anionic exchangers (Xie, Zhang et al. 2014). The secondary separation is much more challenging due to the chemical similarity of the REEs and a plant producing single REE products may contain hundreds of stages of mixers and settlers (Xie, Zhang et al. 2014).

Bastnesite ore is a primary source of REEs in China, the world's largest producer of REEs. During the refining process REEs are recovered from the leachate by solvent extraction using P204 (D2EHPA). The REEs are divided into two groups of La-Nd and Sm-Gd by preferential stripping and then they will be separated to individual REEs (Xie, Zhang et al. 2014). To reduce reagent consumption, modified separation processes have been tested at pilot-scale. For instance, Huang et al. used P204 or P507 to extract Th and most of Ce in the first step, then doing further extraction steps on the raffinate containing the remaining REEs to separate individual elements (Huang). One example of a commercial scale REE separation process is that from Molycorp Inc. (**Figure 1.2**). The Molycorp Inc. process is used to extract europium oxide from the leachate of Mountain Pass bastnesite (Xie, Zhang et al. 2014). In the first extraction step using 10 % D2EHPA in kerosene, REEs in the chloride solution are divided into two streams with Sm and all heavier REEs in the D2EHPA solution. Nd and lighter REEs partition into raffinate. It is quite easy to separate Nd and Sm as they are consecutive elements in any natural rare earth minerals, while they are not consecutive elements in the periodic table; promethium which is the intermediate element does not occur in nature. Moreover, the concentration of Sm and heavier REEs in bastnesite is much lower than the other REEs. So, they can be separated using a small volume of solvent. After removal of iron, Eu was separated from the solution using the same organic solution. Like other commercially available REE separation process, the Molycorp Inc. process is limited to treating relatively concentrated REE slurries in comparison to geothermal source waters. Nevertheless, the sequenced extraction process provides possible guidance for future development of REE separation systems for geothermal waters, as well as other dilute REE solutions.

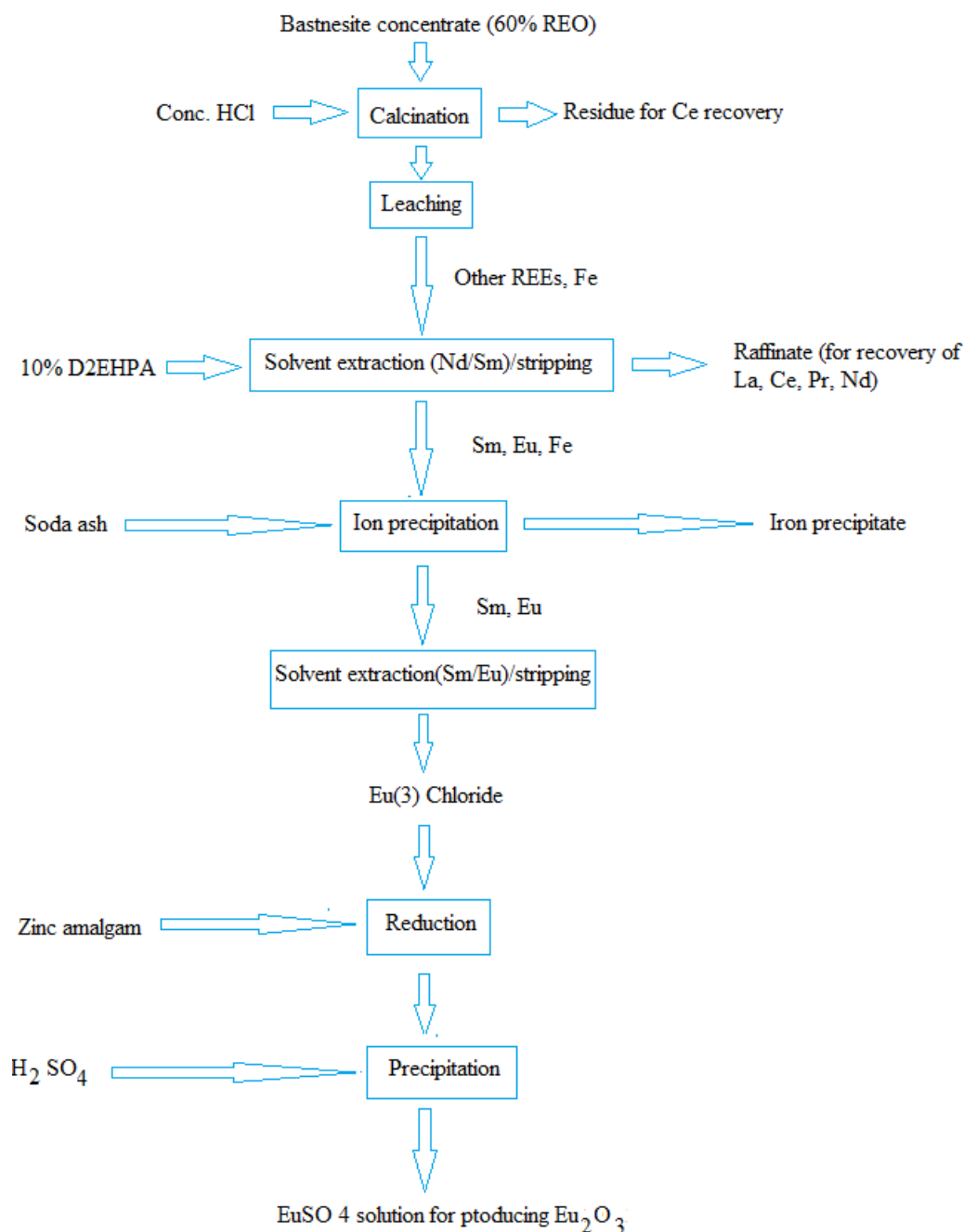


Figure 1.2: Illustration of the process train for separating europium oxide from bastnesite concentrate. This process train was developed by Molycorp Inc. (Xie, Zhang et al. 2014).

As previously addressed, the composition of feed is one of the key factors determining the organic phase. The chemistry of geothermal brines and the acidic leach solutions used in ore refining are different, which may result in the use of different chemicals for REEs recovery from brines by solvent extraction. However, the same strategies which has been industrialized for leach solutions can be utilized for brines with some modifications. Lab-scale solvent extraction experiments should be done to identify the differences and optimize the organic phase and configurations.

Work has been done to develop improved organic phases for extracting REEs from liquid mixtures, while also reducing their environmental footprint (Dong, Sun et al. 2015, Lu and Liao 2016, Wang, Huang et al. 2016, Ma, Zhao et al. 2017). One of the main issues in the extraction process is solvent saponification. Solvent saponification results in an increase in the efficiency by which the organic solvent extracts a target element, in this case an REE(s). This step is often used prior to the extraction step. A drawback to this process is the generation of large amounts of saponification wastewaters from acidic extractants. For instance, in the Chinese ion-adsorption REE mineral separation industry, HEH[EHP] is one of the most widely used extractants, which needs to be saponified for

REE separation. The saponified HEH[EHP] releases millions of gallons of saponification wastewater each year. To address this issue, Dong et al. made a new extractant named [N₁₈₈₈][EHEHP] with stronger extractability and similar separation factor for all the HREEs compared to those of the HEH[EHP]. Moreover, the results showed that the extracted Lu³⁺ by the new extractant could be fully stripped (Dong, Sun et al. 2015).

Wang et al. used a bi-functional ionic liquid, [N₁₈₈₈][CA12], for separating yttrium from HREEs via one-step process (Wang, Huang et al. 2016). These researchers achieved a yttrium purity of 99% because of the outstanding [N₁₈₈₈][CA12] extraction efficiency of HREEs and separation factor between yttrium and HREEs. Using [N₁₈₈₈][CA12] has many advantages over the conventional acidic extractants. First of all, [N₁₈₈₈][CA12] is low-cost and environment-friendly. No saponification steps were involved in the process. Moreover, water as a cheap and clean liquid can be used as the scrubbing and stripping reagents. The organic phase was also stable after the regeneration step and the extractability and separation performance of the organic phase showed no significant change after regeneration (Wang, Huang et al. 2016).

2.3 Membrane Separation Processes

Membrane processes represent a relatively new method for separating, or concentrating, REEs from relatively dilute streams like geothermal brines. In difference to the previously addressed processes, membrane processes may not be used to extract an REE from a mixture. Therefore, membrane processes must be paired with a more selective process like adsorption or ion exchange. Candidate membrane processes for concentrating REEs include nanofiltration (NF) and electrodialysis. In electrodialysis a membrane stack consisting of alternating cation and anion exchange membranes, an anode and a cathode is used to separate cations and anions using electrostatic interactions. Cations are attracted to the anode and anions to the cathode. The cation/anion exchange membranes allow like-charged ions to pass while retaining oppositely charged ions. By taking advantage of the tri-valent valence state of REEs and by tuning the strength of the electrical field ED may be used to selectively concentrate the REEs from concentrated brines as demonstrated by Takahashi (Takahashi, Miwa et al. 1993). System optimization may be achieved through careful membrane selection and design as manipulation of the feed solution chemistry, namely pH. NF is a pressure-driven process whose operation is akin to that of the more commonly used reverse osmosis (RO). Both NF and RO use semi-permeable membranes that reject salts and other dissolved solids, while allowing water to pass through. In RO, dissolved solids are rejected at an efficiency of $\geq 99\%$. In contrast, NF rejects polyvalent ions more efficiently than it does monovalent ions. This is due to the fact that ion rejection occurs through a combination of physical and electrostatic interactions, such as size exclusion, steric hindrance, Donnan equilibrium, and dielectric exclusion (Peeters, Mulder et al. 1999). Of these different mechanisms it is the electrostatic ones that may be manipulated through changes in solution chemistry in order to affect ion rejection. Ions with neutral charge are rejected due to size exclusion, while charged ions will be rejected or passed through due to either size exclusion (hydrated ionic radii) or electrostatic forces, with rejection increasing with increasing valency. Membrane surfaces are amphoteric and thus their surface charge may be manipulated through changes in solution pH. Presumably, as membrane surface charge changes so too will its rejection efficiency for ions of a given valency. In theory then, it would be possible to increase or decrease the rejection efficiency for an ion by manipulating the solution pH to change the magnitude and sign of the membrane surface charge. Operating below the isoelectric point for an NF membrane (a positively charged surface) will result in the permeation of cations and the rejection of anions (Luo and Wan 2013). Similarly, the magnitude of the ion valence will affect its permeation through the membrane. For example, as the pH approaches the isoelectric point for the membrane cations having a lower valence will begin permeating through the membrane while those having a higher valence will be rejected. Thus, by altering the surface charge for an NF membrane it would be possible to separate mono- and divalent cations from the produced water while rejecting or concentrating the tri-valent REEs and/or other precious elements. This concept was proven in an earlier study by Ricci et al. (Ricci, Ferreira et al. 2015) who studied the separation of metals and sulfuric acid from mine tailing wastewater using NF.

Murthy et al. studied the separation of cerium from a mixed wastewater using the NF-300 membrane (Murthy and Choudhary 2011). Cerium rejection increased with increasing in feed pressure (2-10 bar) and water flux across the membrane, and decreased with an increasing cerium concentration (10-80 mg/L of CeCl₃). The maximum Ce(III) rejection was found to be 94.37% and 90.03% for feed concentrations of 10 and 80 mg/L, respectively. In a separate study, Murthy et al. applied the NF-300 membrane to treat Nd(III) containing water (Murthy and Choudhary 2011). Rejection of Nd(III) ions was significantly affected by feed pH ranging from 46.22% for acidic medium and 90.12% for alkaline medium.

Micellar enhanced separation has been widely used for the removal of heavy metals by ultrafiltration (UF), which is a filtration process commonly used for separating organic macromolecules from water (Staszak, Konopczyńska et al. 2012). In difference to NF and ED, UF membranes do not inherently rejection salts, metals, and minerals in the dissolved phase. In the micellar enhanced UF process a surfactant is added to the aqueous mixture and once the critical micelle concentration (CMC) is reached, the surfactant monomers will assemble and aggregate to form large micelles (Puasa S.W 2011). Elements, such as REEs, become entrapped in the micelles, or adsorbed on the micelle surface, through electrostatic interactions. Because the micelles are larger than the nominal pore size of a given UF membrane, they are rejected, subsequently resulting in a concentrated stream of REEs. When using micellar enhanced process with NF, it would not be required to reach the CMC due to enhanced steric rejection. Murthy et al. used an anionic surfactant, sodium dodecyl sulfate, for separating Nd(III) from a mixed ionic solution (Murthy and Choudhary 2011). Rejection increased from 86.74% to 99.45% when increasing the surfactant concentration to 5 mg/L. Selective complexation step can be applied by using a water soluble chelating agent to form complexes with target ions, in this case REEs, with diameters larger than the membrane pore size. Murthy et al. used Ethylene diamine tetra acetic acid (EDTA) as the chelating agent for enhancing the separation of Nd(III) using NF (Murthy and Choudhary 2011). It was observed that Nd(III) rejection increased from 87% to 99% due to the formation of [Nd-EDTA]⁻ complexes. These researchers similarly used EDTA to increase the recovery of Ce(III) (Murthy and Choudhary 2011). The rejection for CeCl₃-EDTA feed solutions with the ratio of 2:1 increased from 90% to 99% at 10 bar and 16 L/min for 80 mg/ L cerium

List Authors in Header, surnames only, e.g. Smith and Tanaka, or Jones et al.

solution. This rather new and novel approach to separating REEs from aqueous mixtures represents a promising approach for REE recovery from geothermal brines. A remaining challenge in this area is selectively targeting the REE(s) in a complex mixture of elements and the subsequent refining step for the recovered REE(s).

3. CONCLUSION

Currently the best separation method overall is to concentrate the dilute geothermal brines by nanofiltration using positively charged membranes. This method can be further improved by appending an additional extraction method, or by modification of the details of the nanofiltration process.

Two potential modifications can be applied in the nanofiltration process to improve the permeate flux and subsequently reduce the energy costs are pore size and surface charge. While using membranes with bigger pores improves the permeate flux, REEs retention can be maintained by enhancing the positive charge of the membrane surface and/or entrapping REEs in micelles of a bigger size. Nanofiltration results in a concentrated mixture of REEs that needs to undergo further processes like adsorption, solvent extraction, etc. to selectively separate the elements.

CONTRIBUTIONS AND ACKNOWLEDGMENTS

JB and MS drafted this chapter manuscript and compiled edits. All authors reviewed the chapter manuscript. Contributors include: Savannah Bachman who conducted preliminary REE separation tests using nanofiltration (NF) membranes and analyzed associated and other water samples for REEs. Funding for this work was provided by U.S. Department of Energy, Geothermal Technologies Office under Award DE-EE0007603. The authors would like to thank our DOE project managers Holly Thomas and Josh Mengers and also our Technical Monitoring Team for their support, advice, and insight.

REFERENCES

- Abreu, R. D. and C. A. Morais (2014). "Study on separation of heavy rare earth elements by solvent extraction with organophosphorus acids and amine reagents." *Minerals Engineering* 61: 82-87.
- Anagnostopoulos, V. and B. Symeopoulos (2013). "Sorption of europium by malt spent rootlets, a lowcost biosorbent: effect of pH, kinetics and equilibrium studies." *Journal of Radioanalytical and Nuclear Chemistry* 295: 7-13.
- Borai, E. H., M. G. Hamed, A. M. El-kamash, T. Siyam and G. O. El-Sayed (2015). "Template polymerization synthesis of hydrogel and silica composite for sorption of some rare earth elements." *J Colloid Interface Sci* 456: 228-240.
- Callura JC, N.C., Perkins K, Washburn NR, Dzombak DA & Karamalidis AK (2016). "Selective Adsorption of Rare Earth Elements from Geothermal Brines." *Goldschmidt Abstracts*, 348.
- Dong, Y., X. Sun, Y. Wang and Y. Chai (2015). "The development of an extraction strategy based on EHEHP-type functional ionic liquid for heavy rare earth element separation." *Hydrometallurgy* 157: 256-260.
- Huang, X., Li, H., Xue, Xi., Zhang, G. "Development status and research progress in rare earth hydrometallurgy in China." *Journal of The Chinese Rare Earth Society* 24(2): 129-133.
- Hussien, S. S. and O. A. Desouky (2014). Biosorption studies on yttrium using low cost pretreated biomass of *Pleurotus ostreatus*. 4th International Conference on Radiation Sciences and Applications, ESRA. Taba, Egypt 139-150.
- Iftekhhar, S., V. Srivastava and M. Sillanpää (2017). "Synthesis and application of LDH intercalated cellulose nanocomposite for separation of rare earth elements (REEs)." *Chemical Engineering Journal* 309: 130-139.
- Lu, Y. and W. Liao (2016). "Extraction and separation of trivalent rare earth metal ions from nitrate medium by p-phosphonic acid calix[4]arene." *Hydrometallurgy* 165: 300-305.
- Luo, J. and Y. Wan (2013). "Effects of pH and salt on nanofiltration—a critical review." *Journal of Membrane Science* 438: 18-28.
- Ma, L., Z. Zhao, Y. Dong and X. Sun (2017). "A synergistic extraction strategy by [N1888][SOPAA] and Cyphos IL 104 for heavy rare earth elements separation." *Separation and Purification Technology* 174: 474-481.
- Mayes, R. T., P. Halstenberg, B. A. Moyer, A. Karamalidis and C. Noack (2018). *Selective Recovery of Critical Materials from Geothermal Fluid*. Oak Ridge, TN, Oak Ridge National Laboratory: 10.
- Murthy, Z. V. P. and A. Choudhary (2011). "Application of nanofiltration to treat rare earth element (neodymium) containing water." *Journal of Rare Earths* 29(10): 974-978.
- Murthy, Z. V. P. and A. Choudhary (2011). "Separation of cerium from feed solution by nanofiltration." *Desalination* 279(1-3): 428-432.
- Peeters, J. M. M., M. H. V. Mulder and H. Strathm (1999). "Streaming potential measurements as a characterization method for nanofiltration membranes." *Colloids and Surfaces A: Physicochemical and Engineering Aspects* 150: 247-259.
- Peppard, D. F., G. Asanovich, R. W. Atteberry, O. Dutemple, M. V. Gergel, A. W. Gnaedinger, G. W. Mason, V. H. Meschke, E. S. Nachtman and I. O. Winsch (1953). "Studies of the Solvent Extraction Behavior of the Transition Elements .2. Isolation of Gram Quantities of Th-230 (Ionium) from a Pitchblende Residue." *Journal of the American Chemical Society* 75(18): 4576-4578.

- Ponou J., L. P. Wang, G. Dodbiba, K. Okaya, T. Fujita, K. Mitsuhashi, T. Atarashi, G. Satoh, and M. Noda (2014). "Recovery of rare earth elements from aqueous solution obtained from Vietnamese clay minerals using dried and carbonized parachlorella." *Journal of Environmental Chemical Engineering*, 2(2): 1070-1081.
- Puasa S.W, R. M. S. a. S. A. S. A. K. (2011). An overview of Micellar – Enhanced Ultrafiltration in Wastewater Treatment Process. *International Conference on Environment and Industrial Innovation*. 12.
- Reddy, B. R., B. N. Kumar and S. Radhika (2009). "Solid-Liquid Extraction of Terbium from Phosphoric Acid Medium using Bifunctional Phosphinic Acid Resin, Tulsion CH-96." *Solvent Extraction and Ion Exchange* 27(5-6): 695-711.
- Ricci, B. C., C. D. Ferreira, A. O. Aguiar and M. C. S. Amaral (2015). "Integration of nanofiltration and reverse osmosis for metal separation and sulfuric acid recovery from gold mining effluent." *Separation and Purification Technology* 154: 11-21.
- Sadovsky D., A. Brenner, B. Astrachan, R. Gonen (2016). "Biosorption potential of cerium ions using Spirulina biomass." *Journal of Rare Earths*. 34(6): 644-652.
- Smith, Y.R., P. Kumar, and J.D. McLennan (2017). "On the Extraction of Rare Earth Elements from Geothermal Brines." *Resources-Basel*, 6(3).
- Staszak, K., B. Konopczyńska and K. Prochaska (2012). "Micellar Enhanced Ultrafiltration as a Method of Removal of Chromium(III) Ions from Aqueous Solutions." *Separation Science and Technology* 47(6): 802-810.
- Takahashi, H., K. Miwa and K.-i. Kikuchi (1993). "Separation of light rare-earth elements from rare-earth mixture solution by use of electro dialysis with complexing agents." *Int. J. of The Soc. of Mat. Eng. for Resources* 1(1): 132-139.
- Varshini, J. S. C., D. Das and N. Das (2015). "Recovery of cerium (III) from electronic industry effluent using novel biohydrogel: batch and column studies." *Der Pharmacia Lettre* 7: 166–179.
- Wang, F., J. Zhao, X. Wei, F. Huo, W. Li, Q. Hu and H. Liu (2014). "Adsorption of rare earths (III) by calcium alginate–poly glutamic acid hybrid gels." *Journal of Chemical Technology and Biotechnology* 89: 969–977.
- Wang, Y. L., C. Huang, F. J. Li, Y. M. Dong, Z. Y. Zhao and X. Q. Sun (2016). "The development of sustainable yttrium separation process from rare earth enrichments using bifunctional ionic liquid." *Separation and Purification Technology* 162: 106-113.
- Wood, S. A. (2002) "Behavior of Rare Earth Element In Geothermal Systems; A New Exploration/Exploitation Tool." (No. DOE/ID13575), University of Idaho (US).
- Xie, F., T. A. Zhang, D. Dreisinger and F. Doyle (2014). "A critical review on solvent extraction of rare earths from aqueous solutions." *Minerals Engineering* 56: 10-28.
- Yao, T., Y. Xiao, X. Wu, C. Guo, Y. Zhao and X. Chen (2016). "Adsorption of Eu(III) on sulfonated graphene oxide: Combined macroscopic and modeling techniques." *Journal of Molecular Liquids* 215: 443-448.
- Zhao, F., E. Repo, Y. Meng, X. Wang, D. Yin and M. Sillanpaa (2016). "An EDTA-beta-cyclodextrin material for the adsorption of rare earth elements and its application in preconcentration of rare earth elements in seawater." *J Colloid Interface Sci* 465: 215-224.
- Zhu, Y., Y. Zheng and A. Wang (2015). "A simple approach to fabricate granular adsorbent for adsorption of rare elements." *Int J Biol Macromol* 72: 410-420.

Chapter 8: Conclusions

Scott Quillinan, Charles Nye, Ghanashyam Neupane, Timothy Bartos, Jonathan Brant, J. Fred McLaughlin, Travis McLing

Scott Quillinan, Director of Research and Communications, University of Wyoming, 1000 E. University Ave., Laramie, WY 82072
scottyq@uwyo.edu

Keywords: REE enrichment, critical minerals

ABSTRACT

This study sampled and analyzed water from around the United States. Activities that enhanced this work included the co-collection of rock samples, the statistical analysis of the data with an ESOM, and evaluation of extraction by three promising methods. These activities led to five conclusions (1) REEs sometimes occur in continental groundwater in excess of 1000-times their seawater concentrations. (2) REEs exist as a trace (ng/L) component in all analyzed samples. (3) The traditional distinction of light (Z=57-64) and heavy (Z=65-71) REEs in rock-mineral chemistry applies to aqueous chemistry. (4) REE content is not significantly controlled by lithology, reservoir temperature, nor salinity. (5) REE concentration, both in sampled basins and neural network predictions of potential, appears to be spatially co-associated, with the basin mattering more than formation.

These conclusions suggest that future work study three questions. (1) What is the spatially-dependent variable that controls REE concentration? (2) Does the output of the ESOM change significantly as input samples are grown in both number and spatial extent? (3) Compared with next-gen analytical techniques, under what metrics does the current method for aqueous REE analysis perform well, and under what metrics is it surpassed? Some of these questions are being investigated in new projects that grew from this work, others would benefit from government support.

1. CONCLUSIONS OF THIS STUDY.

The study has five main conclusions. (1) REEs sometimes occur in continental groundwater in excess of 1000-times their seawater concentrations. (2) REEs exist as a trace (ng/L) component in all analyzed samples. (3) The traditional distinction of light and heavy REEs in rock-mineral chemistry applies to aqueous chemistry. The team identifies an unambiguous, and observationally substantiated, break of light and heavy REEs in natural aqueous systems between Gadolinium and Terbium. (4) REE content is not significantly controlled by lithology, reservoir temperature, nor salinity. (5) REE concentration, both in sampled basins and neural network predictions of potential, appears to be spatially co-associated. These five conclusions have advanced the scientific understanding of REEs in subsurface geothermal systems.

1.1 REEs can exceed seawater Concentrations by three orders of magnitude

Seawater has been suggested as a feedstock for valuable materials since before Davies (1964). The idea has been through a sequence of revivals, pilots, and in some cases economical operation such as magnesium (Lieberman, 2000) and bromide (Matthai et al. 1957) extraction plants in the United States. A common threshold for assessing the promise of an aqueous mineral resource is to compare it to seawater because the minerals dissolved in seawater are a functionally inexhaustible resource and ocean water mining technologies are direct competitors to the techniques used for continental water mining. If a resource fails to have concentrations greater than seawater it is unlikely to be economically viable barring a significant extra-market benefit, such as serving as a value-added revenue stream to geothermal energy operators.

REEs in produced waters pass this minimum check on economic viability because they can exceed seawater concentrations by three orders of magnitude. However, this only means that these waters are relatively superior to the ocean, not that they are economic in absolute terms. Further, challenges such as removal of unwanted chemical species could neutralize this benefit. A final detail that could significantly affect the economics of REE extraction is the distinctive REE ratios seen in the WBPW (Chapter 4). The WBPW shows that europium makes up a much greater fraction of the REEs in these waters than one would expect based on established REE proportions in rock. This detail could be a blessing or a curse depending on market demand for europium. A site-specific analysis of REE proportions is almost certainly essential to any assessment of economic viability, and could allow commercial operations to secure only the most attractive REEs (LREEs, HREEs, and specific elements depending on market conditions).

1.2 REEs occur in at least ng/L concentration in all continental groundwaters.

Every sample that was analyzed by INL, with the exception of the field blanks, contained measureable concentrations of REEs. This suggests that as in rocks, aqueous REEs are not rare so much as diluted in a large volume. The ubiquity of REEs in groundwater suggests that the process that places REEs into solution is non-unique, and can occur anywhere in the subsurface. While brines in some locations seem clearly more concentrated than others, no brine is devoid of REEs. The dilute ubiquity of REEs suggests that under extreme enough economic drivers, any country could compete in the REE market. The ubiquity of REEs may allow cultivation of higher concentrations if, as suggested below, the variable that controls their concentration can be isolated and manipulated. In that pursuit

negative evidence and positive evidence would both be beneficial. Discovery of a location with less than measurable (0.1 ng/L) concentrations of REEs would advance scientific understanding nearly as much as finding an area of anomalously high concentration.

1.3 Natural Aqueous Behavior Suggests Distinctive Behavior between Light and Heavy REEs, matching Atomic Numbers 57-64 and 65-71

Distribution and behavior of REEs fall neatly into two groups, the LREEs and the HREEs. The well-defined divide in behavior between Gd and Tb on the principle component diagram of Chapter 6 (Figure 6.3) supports these categories. While the REEs are remarkable for their similar chemical behavior, the details of their electron orbital filling may explain the observed difference between Gd and Tb. Gd is the Lanthanide with the greatest multiplicity under Hund’s Rule (Hund, 1925). Gadolinium’s eight unpaired electrons deviate from what a simple orbital filling order would predict by occupying the 5*d* orbital before the 4*f* is full. This deviation is partially because the total pairing energy is nearly the same as the difference in energy between the 4*f* and 5*d* orbitals in the [Xe]6*s*²4*f*⁷5*d*¹ configuration. The result is a larger gadolinium ionic radius more like the LREEs than the HREEs (Wolfram, 2018).

This difference in behavior is also visible with conventional normalized REE plots. As the WBPW normalization (Figure 4.17) shows, a break between LREE and HREEs occurs between gadolinium and terbium. It is important to note that by-and-large the REEs behave similarly to one another compared to other constituents found in produced and geothermal waters. This distinction is only apparent in detail, and most processes that affect one REE affect all other REEs.

1.4 Lithology, temperature, and salinity do not have a significant relationship to REE concentration

The ESOM’s output was compared with temperature and salinity but there was no significant relationship. The rocks were grouped into as shown in Table 5.1 however these lithologies also had no significant relationship. The possibility of a particular rock having a relationship to a particular water as described in Nye et al. (2018) remains, but requires understanding of each particular water-rock system and invocation of location-specific processes. Such descriptions are difficult to reduce to single parameters that allow easy comparison to the ESOM’s groupings. This is part of the reason the lithology was used for comparison in Chapter 6 rather than the exact rocks.

1.5 REE concentrations are often spatially co-associated

From the limited sample set available, samples from a single basin tend to exhibit REE concentrations of the same relative magnitude and there are significant differences between the various basins. This suggests there is a variable (or variables) that controls REE concentration, and that, in turn, the unknown variable is spatially controlled.

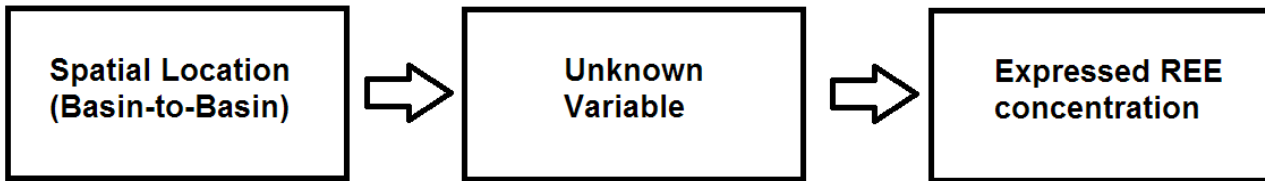


Figure 8.1: The sequence of causes that must exist, but is currently not known, to result in the observed spatial trends.

The expected candidate variables mentioned above in subsection 1.4 of this chapter do not appear to be the dominant controlling mechanisms of REE behavior, but the presence of a basin-to-basin trend suggests a controlling variable, or variables exist. The variable, or variables that do explain the basin-to-basin trend are of key interest for future work as in subsection 2.1 below.

The team suggests the following possible unknown variables, which were not tested in this study: (1) the rock types previously encountered on the water’s recharge flow path rather than the present reservoir, (2) anthropogenic introduction of REEs or (3) in-situ microbial extraction/concentration. It is also possible that a combination of variables produces the observed REE behavior. For example: neither marine shales nor horizontal well-construction on their own produce high aqueous REE concentrations, but when both occur together they might. This particular pair of variables has not been supported with observations during this study.

Originally the team considered that many basins could be grouped together, and that only the Powder River Basin was anomalous. This view changed because the collection of new samples from more basins, and the ESOM output revealed that basin-by-basin control is the norm, and it is not only the Powder River Basin that is anomalous.

List Authors in Header, surnames only, e.g. Smith and Tanaka, or Jones et al.

2. OPPORTUNITIES FOR FUTURE WORK.

The conclusions of this work suggest that future work is needed in three areas. (1) The spatially-dependent variable that controls REE concentration should be found. (2) The sample set used for training the ESOM should be grown in both number and spatial extent. (3) A comparison should be performed between the current method for aqueous REE analysis and next-gen analytical techniques. Some of these topics are being investigated in new projects that grew from this work.

2.1 Hunt for the unknown variable

This work established that REE behavior is not significantly correlated to TDS, Temperature, nor Lithology, but that REE behavior is spatially associated. This basin-by-basin trend supports the conclusion that REE concentration is non-random, and must be correlated to some unknown variable. More work is needed to discover what this unknown variable is, and why some basins, but not others, have high REE concentrations.

One option for this unknown variable is the minor components of the lithology, such as the organic fraction. This work searched for an association of major lithology components to aqueous REE concentration, but found no significant relationship. However, it remains possible that a minor component of the lithology, such as the organic fraction, could be responsible. While clastic sediments and igneous rocks are well understood, the effects of organic material on aqueous REEs need more research. Organics are well established as a good complexing agent, and strong reducing agent. Their interaction with water requires more work to understand the combined and sometimes conflicting effects of mixed clastic-organic packages on REE behavior. Clays, especially those with high ion-exchange capacities are similarly problematic.

Another option is the depositional history is more important than the unit deposited. Our interpretation of the marine Gd signature in the PRB suggests that the Cretaceous shale packages of North and South Dakota should have the same Gd behavior because they have similar histories under the Cannonball Sea “arm” (Blakey, 2014). If the Cannonball Sea sediments in these areas show the same Gd signature then this anomaly could be related to that event. However, if they do not show that anomaly then the entire Western Interior Seaway may be responsible for this phenomenon. While the researchers have a sample from the Bakken, shallower shale packages are not yet part of the collection, and their collection is of great interest.

Similar to depositional history, the hydrologic history of a basin may be the variable. Numerous “flushing” events have occurred in most basins, and are often associated with glaciations, which are in turn are sometimes detectable with Stable Isotope studies (Bowen, 2002). Most chemical species quickly re-equilibrate after these flushing events, but due to the lack of data on REE behavior in natural systems, it is possible that REEs do not re-equilibrate as quickly. If so, basins that have had more thorough or more recent flushing events could have different REE expressions that are out of equilibrium.

Further work should seek to rule out these candidates for the unknown spatially-associated variable or to find support for them.

2.2 Bigger sample set that includes ESOM-identified target areas and post-use waters

As with most datasets that prove resistant to interpretation, future work should prioritize expanding the dataset presented here. By adding more samples, the effect of anomalous individual samples will be reduced and the big-picture trends that affect REE behavior will begin to emerge. The ESOM’s output suggests that the geothermal produced waters of Oklahoma, northern Louisiana, southern Illinois, and the Utah-Colorado boarder should be targeted first due to their high predicted potential as REE resources. While these ESOM-identified target areas are the most likely to facilitate a better interpretation, new samples from any location might provide the evidence for a breakthrough revealing the key component of REE behavior.

Other waters that have been used for their intended purpose and then directed towards disposal could be a REE resource. These waters are typically rejected due to high salinity or unique chemistry unsuited to their continued use. Example waters include; the concentrate produced by water purification plants, cooling water that has been concentrated by evaporation with each re-cycle, water used for industrial processes such as the Solvay trona-production process, and the water used to transport coal power station ash to holding ponds. Each of these, and other post-use waters, has a different chemistry and assumedly different REE patterns. If enough post-use waters are tested, the law of averages dictates that at least one will be enriched in the most valuable REEs, and prove readily extractable. Figure 8.2 shows some data from a different project sampling industrial reject water sources. In this case, Power Station combined-ash holding ponds have more HREEs than one would expect. The sample named “Site 23” shows that by selecting the correct part of the pond a recovery operation could acquire a feedstock with significant concentration of HREEs, in an otherwise low TDS water. This expansion of the sample set into other basins will not only control noise, and maybe reveal a link to REE concentration.

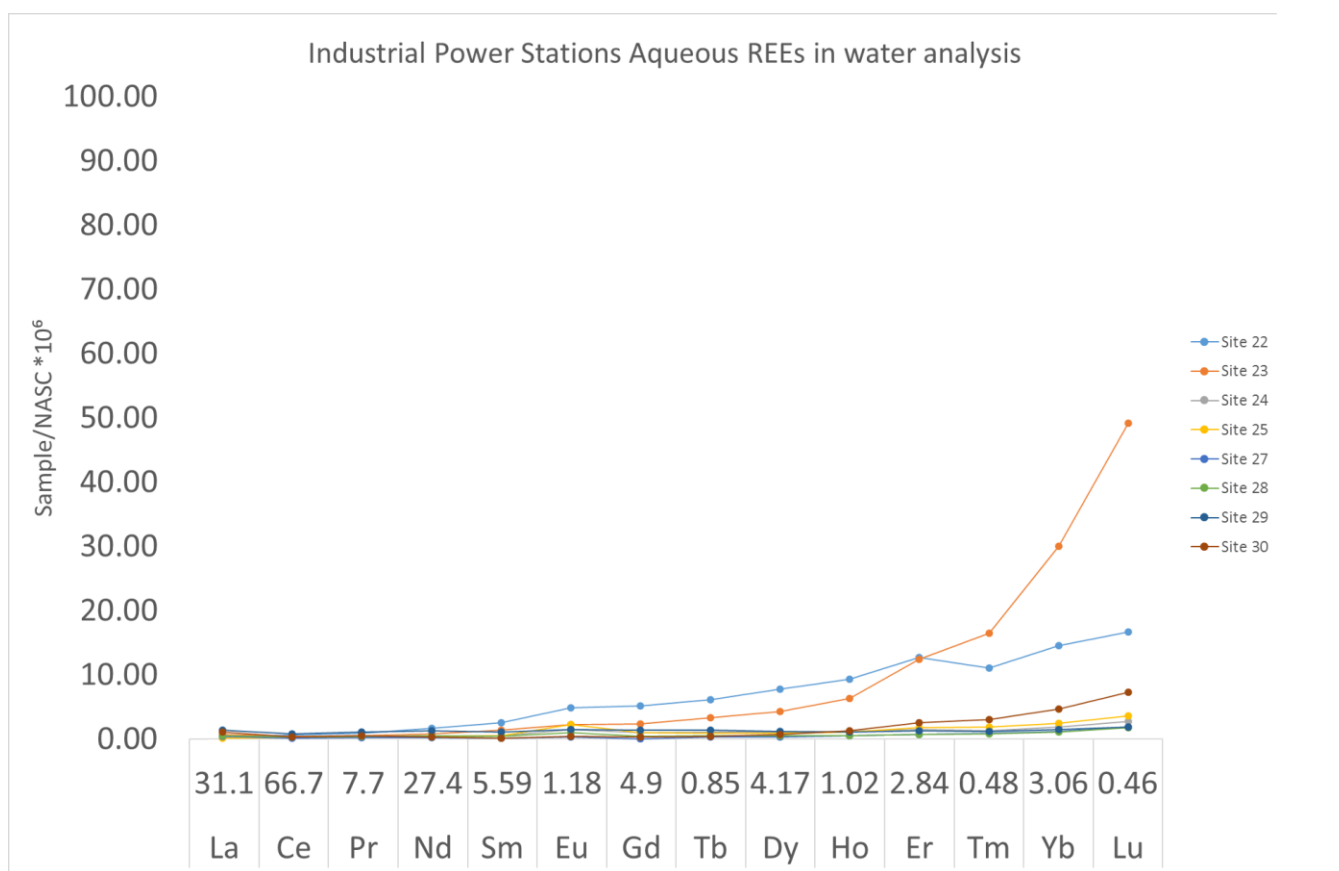


Figure 8.2: The REE content of water in industrial power station ash holding ponds. These eight samples are from two plants in Wyoming. .

2.3. Comparison and validation of new analytical techniques

In the last year next-gen analytical methods have reached the market, and some manufacturers claim they can directly measure REEs at the ng/L level without the interferences that normally render that approach unfeasible. This is an extreme claim given the long-standing historical difficulties of direct measurement, and requires cautious optimism. An option for future work is to perform a comparative analysis with a next-gen ICP-MS, such as the Agilent 8900 Triple Quadrupole, and the current pre-concentration method. Such a comparison would reveal, under realistic conditions, what areas the next-gen methods are superior, and which areas the current method is superior. This would allow other researchers to correctly choose either these next-gen methods or the current method based on the details of their work on REEs in natural systems.

3. CONCLUSION

Initial findings suggest that more work is needed to understand the dominant controls on REE concentration in geothermal and produced waters, but general characterization of REE concentrations in natural geothermal groundwater now exists. From this limited data it is not currently clear whether economic concentrations of REEs exist in these systems, but it is clear that continental groundwater offers a potentially much more abundant source than seawater. A serious geochemical exploration program would be needed to find and characterize the upper end of REE concentration in these systems. Despite uncertainty, this report presents the first step in this answering these questions. This study has shown new discoveries that enhance the scientific community's understanding of REE behavior in natural systems. It is important to keep researching REEs in natural systems, because although many questions are now answered, many more questions remain.

CONTRIBUTIONS AND ACKNOWLEDGMENTS

CN drafted this chapter manuscript and compiled edits. Authors of the respective chapters conceived of the work presented in this chapter. All authors reviewed the chapter manuscript. Funding for this work was provided by U.S. Department of Energy, Geothermal Technologies Office under Award DE-EE0007603. The authors would like to thank our DOE project managers Holly Thomas and Josh Mengers and also our Technical Monitoring Team for their support, advice, and insight.

REFERENCES

Bowen, G. J. and B. Wilkinson (2002). Spatial distribution of d18O in meteoric precipitation. *Geology*, April 2002, v. 30, no. 4, p. 315-318.

List Authors in Header, surnames only, e.g. Smith and Tanaka, or Jones et al.

- Davies, R.V., J. Kennedy, K.M. Hill, R.W. McIlroy, R. Spence, (1964). Extraction of Uranium from Sea Water. *Nature*, Volume 203, 1964, Pages 1110–1115. <http://dx.doi.org/10.1038/2031110a0>
- Miessler, G.L. and D.A. Tarr, *Inorganic Chemistry* (Prentice-Hall, 2nd edn 1999) ISBN 0138418918.
- Hund, F. (1925). Zur Deutung verwickelter Spektren, insbesondere der Elemente Scandium bis Nickel. Berlin 1925 in: *Zeitschrift für Physik*. 33. S.345-371,Abb. Accessed from: <https://link.springer.com/content/pdf/10.1007/BF01328319.pdf>
- Liberman, Marvin B (2000). The Magnesium Industry in Transition Anderson School at UCLA, Los Angeles, CA. Accessed from: <http://www.anderson.ucla.edu/faculty/marvin.lieberman/publications/MagnesiumIndustryTransition2001.PDF>
- Matthai, H. F. William Back, R. P. Orth, and Robert Brennan. (1957) Geological Survey Circular 378. Water Resources of the San Francisco Bay area California. <https://pubs.usgs.gov/circ/1957/0378/report.pdf>
- Nye, C., Bagdonas, D.A., and Quillinan, Q.: A New Wyoming Basin Produced Waters REE Normalization and Its Application, *Proceedings*, 43rd Workshop on Geothermal Reservoir Engineering. Stanford University, Stanford, CA (2018). SGP-TR-213.
- Wolfram Research, Inc. (2018) (www.wolfram.com), Mathematica Online, Champaign, IL. Accessed via: Periodic Table Table, Theodore Gray (2018) <http://periodictable.com/Properties/A/AtomicRadius.html>

Appendices

1. APPENDIX TABLES

The three appendix tables reproduced in this report start on the next page. In order, these three tables are: (1) the Sample List, (2) the Aqueous Geochemistry, and (3) the Aqueous Rare Earth Element Concentration. The Sample List table contains the metadata for the samples including location, formation, and field parameters. The Aqueous Geochemistry table provides the concentration of major and minor aqueous analytes, grouped respectively. Please note that the data spans two sets of 10 pages due to the large number of elements and ions measured during this work. The Aqueous Rare Earth Element Concentration table contains the trace aqueous REE concentrations for each sample. Again, please note that the data spans two sets of 15 pages.

2. ESOM DATA

“Codebook vectors from a trained emergent self-organizing map displaying multivariate topology of geochemical and reservoir temperature data from produced and geothermal waters of the United States” can be found at DOI: <https://doi.org/10.5066/P9376ALD> (Engle, M.A.,2018)

This data matrix contains the codebook vectors for a 82 x 50 neuron Emergent Self-Organizing Map which describes the multivariate topology of reservoir temperature and geochemical data for 190 samples of produced and geothermal waters from across the United States. Variables included are coordinates derived from reservoir temperature and concentration of Sc, Nd, Pr, Tb, Lu, Gd, Tm, Ce, Yb, Sm, Ho, Er, Eu, Dy, F, alkalinity as bicarbonate, Si, B, Br, Li, Ba, Sr, sulfate, H (derived from pH), K, Mg, Ca, Cl, and Na converted to units of proportion. The concentration data were converted to isometric log-ratio coordinates (following Hron et al., 2010), where the first ratio is Sc serving as the denominator to the geometric mean of all of the remaining elements (Nd to Na), the second ratio is Nd serving as the denominator by the geometric mean of all of the remaining elements (Pr to Na), and so on, until the final ratio is Na to Cl. Both the temperature and log-ratio coordinates of the concentration data were normalized to a mean of zero and a sample standard deviation of one.

This data matrix is provided to allow users to map new sample sources to the ESOM using a minimum distance measurement (such as Euclidean distance) through an algorithm such as a k-nearest neighbor. Any data sets used in this way need to be isometrically log-ratio transformed and standardized using the exact same formulation of the training dataset used to create this matrix. This case can be useful both for instances of data classification or for non-linear estimation. In the case of the latter, missing values (i.e., those in need of estimation) can be imputed from the codebook vector for the best match unit (i.e., the neuron with the smallest multivariate distance to the point being estimated). The imputed value can then convert back into the original units through the inverse of data standardization and for concentration data, the inverse of the isometric log-ratio transformation (Hron et al., 2010). Note that for concentration data, the results are in units of proportion and can be converted back into the original units by multiplying each row by the sum of the compositional data in the original dataset.

3. MEMBRANE RECOVERY COST TOOL

These excel files were used to assess the practicality/economics associated with using membrane processes (NF, RO) to recover REEs from brines. There was no or very limited data for adsorption or solvent extraction technologies for dilute REE brines so those technologies could not be assessed. This tool was developed by the Center of Excellence in Produced Water Management (CEPWM) at University of Wyoming.

4. ROCK GEOCHEMISTRY

Rock geochemistry of major oxides and trace elements compositions are available at <https://gdr.openei.org/submissions/953>, <https://gdr.openei.org/submissions/926>, and <https://gdr.openei.org/submissions/989>. The sample preparation and analysis were performed at ALS of Reno, Nevada. All data post-processing and interpretation were performed at University of Wyoming as described in Chapter 5.

5. COMMON-SCALE PLOTS OF AQUEOUS REE GEOCHEMISTRY

The REE-diagrams at the end of the appendix are similar to those in Chapter 4, except that they have been set to the same axis to allow easy comparison between basins. The top of each diagram is equal to one 10,000th of the element’s concentration in NASC. Samples that exceed this level are indicated, as is their value above the top of the diagram. The final diagram is the industrial waters reproduced from Chapter 8.

Quillinan et al., 2018, Sample List

Sample ID	Formation	Area	Lithology	Type	Temperature[C]	pH	Lattitude	Longitude
MD-2	Fort Union	Wind River	Sandstone	Produced Water	11	9.6	43.177	-107.661
MD-3	Upper Fort Union	Wind River	Coal	Produced Water	36.0	7.2	43.181	-107.679
MD-4	Fort Union	Wind River	Sandstone	Produced Water	25.2	7.3	43.161	-107.652
MD-5	NA	Wind River	NA	Produced Water	29.6	7.0	43.164	-107.561
MD-6	NA	Wind River	NA	Produced Water	35.3	10.0	43.164	-107.561
MD-7	Fort Union	Wind River	Sandstone	Produced Water	65.4	7.6	43.174	-107.543
MD-8	Fort Union-Lance	Wind River	Sandstone	Produced Water	52.1	7.3	43.182	-107.504
PRB-10	Niobrara	Powder River Basin	Carbonate	Produced Water	16.7	7.3	43.767	-105.478
PRB-11	Turner	Powder River Basin	Sandstone	Produced Water	34.6	6.9	43.695	-105.506
PRB-12	Parkman	Powder River Basin	Sandstone	Produced Water	52.3	7.9	43.708	-105.509
PRB-13	Turner	Powder River Basin	Sandstone	Produced Water	53.4	6.8	43.693	-105.508
PRB-14	Parkman	Powder River Basin	Sandstone	Produced Water	50.4	7.7	43.693	-105.518
PRB-15	Mowry	Powder River Basin	Shale	Produced Water	40.0	7.0	43.560	-105.930
PRB-16	Niobrara	Powder River Basin	Carbonate	Produced Water	40.0	6.5	43.561	-105.945
PRB-17	Shannon	Powder River Basin	Sandstone	Produced Water	34.0	6.9	43.561	-105.943
PRB-18	Frontier	Powder River Basin	Shale	Produced Water	34.0	6.6	43.575	-105.994
PRB-19	Frontier	Powder River Basin	Shale	Produced Water	44.0	6.7	43.575	-105.994
LC-31	Madison	Wind River	Carbonate		20	6.5	43.278	-107.607

Quillinan et al., 2018, Sample List

Sample ID	Formation	Area	Lithology	Type	Temperature[C]	pH	Lattitude	Longitude
WA-33			Shale/Sands					
	Lewis-Almond	Washakie	tone	Produced Water	15.9	7.5	41.738	-108.135
WA-34	Almond	Washakie	Sandstone	Produced Water	15.7	7.8	41.748	-108.111
WA-35			Shale/Sands					
	Lewis-Almond	Washakie	tone	Produced Water	18.8	7.1	41.822	-108.020
WA-36	Almond	Washakie	Sandstone	Produced Water	23.4	6.9	41.835	-108.037
WA-37	Almond	Washakie	Sandstone	Produced Water	17.9	6.8	41.726	-107.979
WA-40			Shale/Sands					
	Lewis-Almond	Washakie	tone	Produced Water	26.2	6.6	41.417	-108.050
LB-42		Green River						
	Maddison	Basin	Dolomite	Produced Water	18.6	6.1		
LB-43		Green River						
	Frontier/Baxter	Basin	tone	Produced Water	5.5	4.9	42.330	-110.315
LB-44		Green River						
	Muddy	Basin	Sandstone	Produced Water	8	5.0	42.288	-110.319
LB-45		Green River						
	Frontier/Baxter	Basin	tone	Produced Water	9.1	8.4	42.261	-110.307
LB-46		Green River						
	Frontier	Basin	Shale	Produced Water	9.9	5.8	42.383	-110.247
LB-47		Green River						
	Frontier	Basin	Shale	Produced Water	10.8	5.8	42.402	-110.296
MS-50	Mesa-Verde	Wind River		Produced Water	54	7.9	43.288	-107.614
MS-51	Lower Fort							
	Union	Wind River		Produced Water	55	7.0	43.286	-107.624
MS-52	Lower Fort							
	Union	Wind River		Produced Water	31	6.8	43.283	-107.624
MS-54	Lance	Wind River	Shale	Produced Water	63.1	7.7	43.291	-107.625
MS-55	Gather-Station	Wind River		Produced Water	37.8	7.3	43.293	-107.624
MS-56	Lance	Wind River	Shale	Produced Water	6.71	NR	43.301	-107.621
MS-57	Lower Fort							
	Union	Wind River	Sandstone	Produced Water	33.7	6.8	43.291	-107.655

Quillinan et al., 2018, Sample List

Sample ID	Formation	Area	Lithology	Type	Temperature[C]	pH	Lattitude	Longitude
MS-58	Cody	Wind River	Shale	Produced Water		6.8	43.306	-107.743
MS-59	Cody	Wind River	Shale	Produced Water	24.5	6.8	43.304	-107.738
WB-MT-8-14-1	Bakken/Three Forks	Williston	Carbonate	Produced Water	NR	7.2	48.156389	-103.628056
WB-ND-8-14-2	Bakken/Three Forks	Williston	Carbonate	Produced Water	NR	7.2	48.156389	-103.628056
WB-ND-8-14-3	Bakken/Three Forks	Williston	Carbonate	Produced Water	NR	7.4	48.156389	-103.628056
WB-ND-8-14-4	Bakken/Three Forks	Williston	Carbonate	Produced Water	NR	7.1	48.156389	-103.628056
WB-ND-8-14-5	Bakken/Three Forks	Williston	Carbonate	Produced Water	NR	7.2	48.156389	-103.628056
WB-ND-8-14-6	Bakken/Three Forks	Williston	Carbonate	Produced Water	NR	7.3	48.156389	-103.628056
WB-ND-8-14-7	Bakken/Three Forks	Williston	Carbonate	Produced Water	NR	7.3	48.156389	-103.628056
WB-ND-8-14-8	Bakken/Three Forks	Williston	Carbonate	Produced Water	NR	7.3	48.156389	-103.628056
WB-ND-8-14-9	Bakken/Three Forks	Williston	Carbonate	Produced Water	NR	7.2	48.156389	-103.628056
WB-ND-8-14-10	Bakken/Three Forks	Williston	Carbonate	Produced Water	NR	7.3	48.156389	-103.628056
WB-ND-8-14-11	Bakken/Three Forks	Williston	Carbonate	Produced Water	NR	7.4	48.156389	-103.628056
WB-ND-8-14-12	Bakken/Three Forks	Williston	Carbonate	Produced Water	NR	7.2	48.156389	-103.628056
WB-ND-8-14-14	Bakken/Three Forks	Williston	Carbonate	Produced Water	NR	NR	48.156389	-103.628056
1A (BS-101)	Bakken/Three Forks	Williston	Carbonate	Produced Water	NR	NR	48.156389	-103.628056

Quillinan et al., 2018, Sample List

Sample ID	Formation	Area	Lithology	Type	Temperature[C]	pH	Lattitude	Longitude
2A (BS-107)	Bakken/Three Forks	Williston	Carbonate	Produced Water	NR	NR	48.156389	-103.628056
3A(BS-112)	Bakken/Three Forks	Williston	Carbonate	Produced Water	NR	NR	48.156389	-103.628056
4A (BS-116)	Bakken/Three Forks	Williston	Carbonate	Produced Water	NR	NR	48.156389	-103.628056
5A (BS-120)	Bakken/Three Forks	Williston	Carbonate	Produced Water	NR	NR	48.156389	-103.628056
GR1 Dup	Oriskany Sandstone	Appalachian	Sandstone	Produced Water	NR	7.3	40.000000	-81.800000
6 HD Dup	Utica Shale	Appalachian	Sandstone	Produced Water	NR	6.8	40.900000	-80.400000
6 HM	Marcellus Shale	Appalachian	Shale	Produced Water	NR	7.2	40.900000	-80.400000
Sc.01.14.14	Berea							
ST	Sandstone	Appalachian	Sandstone	Produced Water	NR	6.7	39.600000	-81.600000
BE.01.14.14	Clinton							
.ST	Sandstone	Appalachian	Sandstone	Produced Water	NR	7.0	39.500000	-81.900000
CM-1	Gordon 30 foot - Gantz	Appalachian	Sandstone	Produced Water	NR	6.2	39.600000	-81.300000
DC-1	Devonian Shale	Appalachian	Shale	Produced Water	NR	6.6	39.500000	-81.100000
RS-1	Berea							
	Sandstone	Appalachian	Sandstone	Produced Water	NR	4.6	39.400000	-81.400000
CC-1								
	Macksburg Sand	Appalachian	Sandstone	Produced Water	NR	7.0	39.416667	-81.450000
D-5	Medina							
	Sandstone	Appalachian	Sandstone	Produced Water	NR	7.0	39.416667	-81.450000
MA-2	Marcellus - App basin (PA)	Appalachian	Shale	Produced Water	NR	NR	39.896389	-80.186389
LS #20	Berea							
	Sandstone	Appalachian	Sandstone	Produced Water	NR	6.7	39.416667	-81.450000
NH #1	Gordon Sand	Appalachian	Sandstone	Produced Water	NR	6.7	39.416667	-81.450000

Quillinan et al., 2018, Sample List

Sample ID	Formation	Area	Lithology	Type	Temperature[C]	pH	Lattitude	Longitude
14-TX-7B	Leonardian Carbonate	Permian	Carbonate	Produced Water	NR	7.6	31.193889	-101.458889
14-TX-8B	Leonardian Carbonate	Permian	Carbonate	Produced Water	NR	7.1	31.193889	-101.458889
14-TX-9B	Leonardian Carbonate	Permian	Carbonate	Produced Water	NR	7.6	31.193889	-101.458889
14-TX-23B	"Cline" shale	Permian	Shale	Produced Water	NR	7.7	31.863889	-101.481111
14-TX-24B	"Cline" shale	Permian	Shale	Produced Water	NR	7.1	31.863889	-101.481111
14-TX-25B	"Cline" shale	Permian	Shale	Produced Water	NR	7.7	31.863889	-101.481111
14-TX-26B	"Cline" shale	Permian	Shale	Produced Water	NR	7.7	31.863889	-101.481111
14-TX-27B	Pennsylvanian Carbonate	Permian	Carbonate	Produced Water	NR	7.1	31.863333	-102.365556
14-TX-28B	Multiple Reservoirs	Permian	Carbonate	Produced Water	NR	7.1	31.863333	-102.365556
14-TX-41B	Wolfcamp shale	Permian	Shale	Produced Water	NR	7.0	31.260000	-100.820833
14-TX-48B	Multiple Reservoirs	Permian	Carbonate	Produced Water	NR	7.2	31.260000	-100.820833
14-TX-49B	Multiple Reservoirs	Permian	Carbonate	Produced Water	NR	7.2	31.260000	-100.820833
Kohles and Kohles Well	Kevin Dome, Montana, Site #							
	1	Kevin Dome	NR	Produced Water	NR	7.8	48.870733	-111.722150
Kohles and Kohles Well	Kevin Dome, Montana, Site #							
	1	Kevin Dome	NR	Produced Water	NR	NR	48.870733	-111.722150
Paul George Mule Well	Kevin Dome, Montana, Site #							
	2	Kevin Dome	NR	Produced Water	NR	8.5	48.869285	-111.718250
Paul George Mule Well	Kevin Dome, Montana, Site #							
	2	Kevin Dome	NR	Produced Water	NR	NR	48.869285	-111.718250

Quillinan et al., 2018, Sample List

Sample ID	Formation	Area	Lithology	Type	Temperature[C]	pH	Lattitude	Longitude
Paul George Kitty Well	Kevin Dome, Montana, Site # 3	Kevin Dome	NR	Produced Water	NR	8.5	48.868014	-111.719550
Paul George Kitty Well	Kevin Dome, Montana, Site # 3	Kevin Dome	NR	Produced Water	NR	8.1	48.868014	-111.719550
Paul George Kitty Well	Kevin Dome, Montana, Site # 3	Kevin Dome	NR	Produced Water	NR	NR	48.868014	-111.719550
Paul George Reservoir	Kevin Dome, Montana, Site # 4	Kevin Dome	NR	Produced Water	NR	8.8	48.868632	-111.718512
Paul George Reservoir	Kevin Dome, Montana, Site # 4	Kevin Dome	NR	Produced Water	NR	NR	48.868632	-111.718512
Kearn's Well	Kevin Dome, Montana, Site # 5	Kevin Dome	NR	Produced Water	NR	7.8	48.859463	-111.709110
Kearn's Well	Kevin Dome, Montana, Site # 5	Kevin Dome	NR	Produced Water	NR	NR	48.859463	-111.709110
Paul George House Well	Kevin Dome, Montana, Site # 6	Kevin Dome	NR	Produced Water	NR	8.0	48.867922	-111.719909
Paul George House Well	Kevin Dome, Montana, Site # 6	Kevin Dome	NR	Produced Water	NR	NR	48.867922	-111.719909
Pace Well	Kevin Dome, Montana, Site # 7	Kevin Dome	NR	Produced Water	NR	6.7	48.844358	-111.724396

Quillinan et al., 2018, Sample List

Sample ID	Formation	Area	Lithology	Type	Temperature[C]	pH	Lattitude	Longitude
Pace Well	Kevin Dome, Montana, Site # 7	Kevin Dome	NR	Produced Water	NR	NR	48.844358	-111.724396
Kleinert Farms Fishing Pond	Kevin Dome, Montana, Site # 9	Kevin Dome	NR	Produced Water	NR	9.1	48.882283	-111.719767
Kleinert Farms Fishing Pond	Kevin Dome, Montana, Site # 9	Kevin Dome	NR	Produced Water	NR	NR	48.882283	-111.719767
Kleinert Farms Fishing Pond	Kevin Dome, Montana, Site # 9	Kevin Dome	NR	Produced Water	NR	NR	48.882283	-111.719767
Wallewein Reservoir South End	Kevin Dome, Montana, Site # 10	Kevin Dome	NR	Produced Water	NR	NR	48.846256	-111.698621
Kearn's Reservoir	Kevin Dome, Montana, Site # 12	Kevin Dome	NR	Produced Water	NR	7.7	48.862667	-111.706367
Kearn's Reservoir	Kevin Dome, Montana, Site # 12	Kevin Dome	NR	Produced Water	NR	NR	48.862667	-111.706367
Nagy Well	Kevin Dome, Montana, Site # 13	Kevin Dome	NR	Produced Water	NR	NR	48.893322	-111.706413
Alme Well	Kevin Dome, Montana	Kevin Dome	NR	Produced Water	NR	NR	48.899837	-111.758113
Wood Well	Unknown	ESRP	NR	Thermal Waters	NR	7.7	43.452888	-111.997716

Quillinan et al., 2018, Sample List

Sample ID	Formation	Area	Lithology	Type	Temperature[C]	pH	Lattitude	Longitude
Heise Hot Springs	Unknown	ESRP	NR	Thermal Waters	NR	6.3	43.642830	-111.687680
Lidy HS1	Unknown	ESRP	NR	Thermal Waters	NR	7.2	44.145580	-112.554940
Lidy HS2	Unknown	ESRP	NR	Thermal Waters	NR	7.2	44.141660	-112.552400
Green Cyn HS	Unknown	ESRP	NR	Thermal Waters	NR	7.2	43.792110	-111.440090
Sturm_W	Unknown	ESRP	NR	Thermal Waters	NR	8.7	44.093250	-111.435340
Condie HS Green	Unknown	ESRP	NR	Thermal Waters	NR	7.0	43.332775	-113.917904
House W Eckert	Unknown	ESRP	NR	Thermal Waters	NR	7.1	43.602339	-113.242139
Office W Campbell	Unknown	ESRP	NR	Thermal Waters	NR	9.5	42.699400	-114.910400
Well1	Unknown	ESRP	NR	Thermal Waters	NR	8.0	42.644970	-114.787060
Well2	Unknown	ESRP	NR	Thermal Waters	NR	8.0	42.644320	-114.782940
Miracle HS Well	Unknown	ESRP	NR	Thermal Waters	NR	9.5	42.694570	-114.855920
Driscol Well	Unknown	ESRP	NR	Thermal Waters	NR	8.6	42.544789	-114.948551
Spring	Unknown	ESRP	NR	Thermal Waters	NR	8.7	42.543480	-114.948969
CSI Well2	Unknown	ESRP	NR	Thermal Waters	NR	8.8	42.583180	-114.474960
Comore Loma 6	Unknown	ESRP	NR	Thermal Waters	NR	6.7	43.442444	-111.904836
Comore Loma 5	Unknown	ESRP	NR	Thermal Waters	NR	6.9	43.437740	-111.930180
Blackhawk Well2	Unknown	ESRP	NR	Thermal Waters	NR	6.6	43.431420	-111.945010
Blackhawk Well1	Unknown	ESRP	NR	Thermal Waters	NR	6.8	43.431420	-111.944690
RRG1	Unknown	ESRP	NR	Thermal Waters	NR	7.1	42.102070	-113.384340
RRG2	Unknown	ESRP	NR	Thermal Waters	NR	6.9	42.110420	-113.375190

Quillinan et al., 2018, Sample List

Sample ID	Formation	Area	Lithology	Type	Temperature[C]	pH	Lattitude	Longitude
RRG7	Unknown	ESRP	NR	Thermal Waters	NR	6.3	42.083594	-113.358653
RRG4	Unknown	ESRP	NR	Thermal Waters	NR	7.1	42.097870	-113.385410
Indian HS	Unknown	ESRP	NR	Thermal Waters	NR	7.2	42.725890	-112.873810
Grush Diary	Unknown	ESRP	NR	Thermal Waters	NR	9.2	42.236669	-113.369706
RRG USGS W	Unknown	ESRP	NR	Thermal Waters	NR	8.1	42.107989	-113.392061
RRG Crook Well	Unknown	ESRP	NR	Thermal Waters	NR	8.3	42.096561	-113.378000
Milford Sweat	Unknown	ESRP	NR	Thermal Waters	NR	7.3	43.364140	-113.789430
Magic RLW Runoff	Unknown	ESRP	NR	Thermal Waters	NR	8.6	43.327770	-114.399410
Elk Creek HS1	Unknown	ESRP	NR	Thermal Waters	NR	9.1	43.423410	-114.628570
Elk Creek HS2	Unknown	ESRP	NR	Thermal Waters	NR	9.1	43.423220	-114.628650
Barron Well Wardrop	Unknown	ESRP	NR	Thermal Waters	NR	8.0	43.292410	-114.910020
HS1 Magic RLW	Unknown	ESRP	NR	Thermal Waters	NR	9.4	43.382900	-114.932240
Prince	Unknown	ESRP	NR	Thermal Waters	NR	6.8	43.327770	-114.399410
Albert HS1	Unknown	ESRP	NR	Thermal Waters	NR	9.1	43.129660	-115.338410
Oakley WS Richard	Unknown	ESRP	NR	Thermal Waters	NR	9.3	42.173340	-113.861630
Austin W Marsh Creek	Unknown	ESRP	NR	Thermal Waters	NR	9.0	42.085330	-113.939840
W	Unknown	ESRP	NR	Thermal Waters	NR	8.2	42.476630	-113.507700
Sliger Well Banbury HS	Unknown	ESRP	NR	Thermal Waters	NR	9.4	42.703990	-114.856990
W	Unknown	ESRP	NR	Thermal Waters	NR	9.2	42.688410	-114.826800

Quillinan et al., 2018, Sample List

Sample ID	Formation	Area	Lithology	Type	Temperature[C]	pH	Lattitude	Longitude
Banbury HS	Unknown	ESRP	NR	Thermal Waters	NR	9.2	42.688410	-114.826800
Johnston Well	Unknown	ESRP	NR	Thermal Waters	NR	9.3	43.002940	-115.192220
Leo Ray Hill	Unknown	ESRP	NR	Thermal Waters	NR	8.7	42.668510	-114.824360
Leo Ray Road	Unknown	ESRP	NR	Thermal Waters	NR	8.4	42.667780	-114.826730
Hensley W	Unknown	ESRP	NR	Thermal Waters	NR	9.6	42.705010	-114.857010
Latty HS	Unknown	ESRP	NR	Thermal Waters	NR	9.3	43.110250	-115.312580
Laib W	Unknown	ESRP	NR	Thermal Waters	NR	7.6	42.946320	-115.494230
CSI W1	Unknown	ESRP	NR	Thermal Waters	NR	8.8	42.580500	-114.470890
Lary	Unknown	ESRP	NR	Thermal Waters	NR	9.2	42.597550	-114.400180
Anderson Pristine S	Unknown	ESRP	NR	Thermal Waters	NR	9.2	42.613900	-114.487990
TF High School	Unknown	ESRP	NR	Thermal Waters	NR	7.8	42.572560	-114.451750
Anderson CG W	Unknown	ESRP	NR	Thermal Waters	NR	9.1	42.577500	-114.288700
Butte City W	Unknown	ESRP	NR	Thermal Waters	NR	7.4	43.608270	-113.244320
Quidop S1	Unknown	ESRP	NR	Thermal Waters	NR	6.7	43.025830	-112.025510
Quidop S2 (ID 58)	Unknown	ESRP	NR	Thermal Waters	NR	6.6	43.037170	-112.004270
Yandell Warm Springs	Unknown	ESRP	NR	Thermal Waters	NR	7.3	43.114480	-112.166600
Skaggs Ranch	Unknown	ESRP	NR	Thermal Waters	NR	7.7	42.437580	-113.434320
Durfee Hot Springs	Unknown	ESRP	NR	Thermal Waters	NR	8.8	42.100080	-113.633540
Basin Cemetery	Unknown	ESRP	NR	Thermal Waters	NR	7.9	42.223330	-113.791670

Quillinan et al., 2018, Sample List

Sample ID	Formation	Area	Lithology	Type	Temperature[C]	pH	Lattitude	Longitude
Wybenga Dairy	Unknown	ESRP	NR	Thermal Waters	NR	7.5	42.482160	-113.973410
David Bosen Well	Unknown	ESRP	NR	Thermal Waters	NR	6.7	42.139440	-111.937090
Schwendiman Well	Unknown	ESRP	NR	Thermal Waters	NR	7.6	43.877170	-111.558900
Clyde W Cinder Block Well	Unknown	ESRP	NR	Thermal Waters	NR	7.5	43.885660	-111.559490
Newdale City W Spackman Well	Unknown	ESRP	NR	Thermal Waters	NR	7.4	43.901270	-111.509670
Fort Hall Thermal W Riverdale Resort	Unknown	ESRP	NR	Thermal Waters	NR	7.3	43.883080	-111.618600
Downata H.S.	Unknown	ESRP	NR	Thermal Waters	NR	7.2	43.858400	-111.678700
Lava H.S.	Unknown	ESRP	NR	Thermal Waters	NR	7.9	42.978130	-112.416540
Hailey H.S.	Unknown	ESRP	NR	Thermal Waters	NR	7.2	42.164644	-111.837271
Frenchman's Bend H.S.	Unknown	ESRP	NR	Thermal Waters	NR	7.2	42.387505	-112.085967
Worswick H.S.	Unknown	ESRP	NR	Thermal Waters	NR	6.4	42.619780	-112.006091
Wolf H.S.	Unknown	ESRP	NR	Thermal Waters	NR	9.1	43.505166	-114.354989
Tindall Well North	Unknown	ESRP	NR	Thermal Waters	NR	8.7	43.641204	-114.490743
Bruneau H.S. well	Unknown	ESRP	NR	Thermal Waters	NR	9.3	43.563605	-114.799356
	Unknown	ESRP	NR	Thermal Waters	NR	9.5	43.337230	-115.044302
	Unknown	ESRP	NR	Thermal Waters	NR	8.6	42.794755	-115.871111
	Unknown	ESRP	NR	Thermal Waters	NR	8.4	42.790227	-115.719751

Quillinan et al., 2018, Sample List

Sample ID	Formation	Area	Lithology	Type	Temperature[C]	pH	Lattitude	Longitude
Lower Indian Bathtub H.S.	Unknown	ESRP	NR	Thermal Waters	NR	8.0	42.767291	-115.727055
Piranha well	Unknown	ESRP	NR	Thermal Waters	NR	7.7	42.830371	-115.894187
Ward well #1	Unknown	ESRP	NR	Thermal Waters	NR	8.5	42.854627	-115.947241
Shane Ward well	Unknown	ESRP	NR	Thermal Waters	NR	8.0	42.848043	-115.973935
Irwin well #1	Unknown	ESRP	NR	Thermal Waters	NR	8.6	42.822249	-115.861240
Comore Loma 7	Unknown	ESRP	NR	Thermal Waters	NR	7.2	43.438817	-111.911418
Rush Warm Springs 1	Unknown	ESRP	NR	Thermal Waters	NR	6.7	43.364911	-113.882168
Hawley Warm Springs	Unknown	ESRP	NR	Thermal Waters	NR	6.9	43.657882	-111.712868
Elkhorn Warm Springs	Unknown	ESRP	NR	Thermal Waters	NR	7.1	43.654338	-111.701418
Doug Mills Hot Well	Unknown	ESRP	NR	Thermal Waters	NR	6.1	42.083773	-112.276451
Charles Crittenden	Unknown	ESRP	NR	Thermal Waters	NR	6.5	42.070424	-112.267056
Ashton Warms Springs	Unknown	ESRP	NR	Thermal Waters	NR	8.5	44.090630	-111.459264
Warm River Springs 1	Unknown	ESRP	NR	Thermal Waters	NR	6.8	44.098133	-111.368144
Site 14	Unknown	ESRP	NR	Thermal Waters	NR	7.8	43.726215	-112.776256
USGS 7	Unknown	ESRP	NR	Thermal Waters	NR	6.6	43.820682	-112.745256

Quillinan et al., 2018, Sample List

Sample ID	Formation	Area	Lithology	Type	Temperature[C]	pH	Lattitude	Longitude
500m Spring Mountain Home AFB	Unknown	ESRP	NR	Thermal Waters	NR	6.6	42.655598	-111.646005
#1 Mountain Home AFB	Unknown	ESRP	NR	Thermal Waters	NR	8.1	43.070264	-115.883444
#2 Gonsales Thermal Well	Unknown	ESRP	NR	Thermal Waters	NR	8.4	43.026920	-115.894100
SVR-5 Barron Heating Well (Grandpa Barron Well)	Unknown	ESRP	NR	Thermal Waters	NR	7.9	43.302483	-114.908981
Strom Well 2015	Unknown	ESRP	NR	Thermal Waters	NR	8.0	43.302470	-114.900780
SVR-4 Grandpa Barron Spring	Unknown	ESRP	NR	Thermal Waters	NR	8.7	43.291780	-114.911620
Higgs Well, SVR-9	Unknown	ESRP	NR	Thermal Waters	NR	9.5	43.292210	-115.076930
Soda Geyser Site #6	Unknown	ESRP	NR	Thermal Waters	NR	8.2	43.313520	-114.900490
Soda Geyser Site #5	Unknown	ESRP	NR	Thermal Waters	NR	6.8	43.283450	-114.915990
	Unknown	ESRP	NR	Thermal Waters	NR	7.9	43.280170	-114.877700
	Unknown	ESRP	NR	Thermal Waters	NR	7.5	42.658194	-111.607824
	Unknown	ESRP	NR	Thermal Waters	NR	7.4	42.658092	-111.606445

Quillinan et al., 2018, Sample List

Sample ID	Formation	Area	Lithology	Type	Temperature[C]	pH	Lattitude	Longitude
Soda Geyser Site #4	Unknown	ESRP	NR	Thermal Waters	NR	7.2	42.657991	-111.605487
Soda Geyser Site #3	Unknown	ESRP	NR	Thermal Waters	NR	7.1	42.657517	-111.605414
Soda Geyser Site #2	Unknown	ESRP	NR	Thermal Waters	NR	6.6	42.657483	-111.605337
Soda Geyser Site #1	Unknown	ESRP	NR	Thermal Waters	NR	6.4	42.657365	-111.605292
Soda Geyser Site #0	Unknown	ESRP	NR	Thermal Waters	NR	6.4	42.657293	-111.605241
Soda_Geyse r	Unknown	ESRP	NR	Thermal Waters	NR	6.4	42.657300	-111.605200
Soda Creek near Mammoth	Unknown	ESRP	NR	Thermal Waters	NR	6.6	42.721921	-111.625400
Soda Creek near Ocatagon	Unknown	ESRP	NR	Thermal Waters	NR	7.2	42.659929	-111.602778
Sulphure Spring	Unknown	ESRP	NR	Thermal Waters	NR	6.3	42.645125	-111.506180
Steamboat Spring filtered	Unknown	ESRP	NR	Thermal Waters	NR	6.5	42.655080	-111.642000
Pavilion Well	Unknown	ESRP	NR	Thermal Waters	NR	NR	42.655800	-111.643700
Mammoth Spring	Unknown	ESRP	NR	Thermal Waters	NR	5.8	42.713531	-111.623617

Quillinan et al., 2018, Sample List

Sample ID	Formation	Area	Lithology	Type	Temperature[C]	pH	Lattitude	Longitude
Hooper Spring	Unknown	ESRP	NR	Thermal Waters	NR	5.7	42.679000	-111.603700
Octagon Spring	Unknown	ESRP	NR	Thermal Waters	NR	5.9	42.659943	-111.602736
Lovers Delight	Unknown	ESRP	NR	Thermal Waters	NR	5.9	42.664720	-111.600980
Outhouse Spring	Unknown	ESRP	NR	Thermal Waters	NR	6.4	42.655520	-111.644130

Quillinan et al., 2018; Aqueous Geochemistry

Sample ID	Alkalinity as CaCO ₃	Br (mg/L)	Ca (mg/L)	Cl ⁻ (mg/L)	Mg (mg/L)	K (mg/L)	Na (mg/L)	SO ₄ (mg/L)	Al (mg/L)	As (mg/L)	Ba (mg/L)	B (mg/L)
MD-2	4500.0	3.0	1.0	633.0	ND	40.0	2590.0	ND	ND	ND	0.5	7.3
MD-3	3410.0	15.0	16.0	1190.0	13.0	57.0	3510.0	5.0	ND	ND	23.5	3.8
MD-4	3390.0	11.0	18.0	1550.0	3.0	27.0	2480.0	4.0	ND	ND	7.4	9.1
MD-5	2550.0	17.0	22.0	2040.0	3.0	23.0	2500.0	ND	0.2	ND	5.9	11.2
MD-6	4950.0	134.0	3.0	19600.0	ND	183.0	23200.0	19700.0	0.0	0.1	0.1	82.7
MD-7	1930.0	13.0	17.0	2030.0	2.0	17.0	2200.0	15.0	ND	ND	3.5	10.1
MD-8	2020.0	15.0	20.0	2060.0	2.0	18.0	2160.0	ND	ND	ND	4.3	11.8
PRB-10	268.0	196.0	734.0	20100.0	72.0	95.0	13000.0	NR	ND	0.2	83.9	22.9
PRB-11	267.0	355.0	2290.0	35600.0	180.0	208.0	22300.0	ND	ND	0.3	246.0	15.7
PRB-12	NR	71.8	83.0	8620.0	9.0	115.0	5100.0	NR	ND	ND	8.9	9.8
PRB-13	323.0	349.0	2340.0	37800.0	171.0	1170.0	20100.0	ND	ND	0.3	204.0	19.0
PRB-14	1440.0	89.0	60.0	11100.0	13.0	258.0	5970.0	ND	ND	ND	14.4	11.2
PRB-15	425.0	293.0	1680.0	33000.0	98.0	76.0	15900.0	ND	ND	0.2	42.1	30.5
PRB-16	256.0	558.0	814.0	44600.0	74.0	79.0	13700.0	ND	ND	0.2	65.1	29.8
PRB-17	519.0	714.0	386.0	45900.0	56.0	119.0	17000.0	ND	ND	0.3	177.0	17.7
PRB-18	219.0	261.0	1770.0	24300.0	72.0	181.0	13200.0	ND	ND	0.2	113.0	13.6
PRB-19	223.0	398.0	2560.0	31200.0	127.0	245.0	15500.0	ND	0.4	0.2	145.0	11.0
LC-31	1830.0	ND	2.0	8350.0	ND	56.0	379.0	ND	0.5	0.3	0.2	10.1
WA-33	2070.0	28.0	23.0	2630.0	4.0	32.0	2520.0	260.0	0.0	ND	2.2	12.4
WA-34	2460.0	17.0	8.0	1760.0	2.0	25.0	2170.0	243.0	0.0	ND	2.2	5.9
WA-35	1900.0	49.0	30.0	4970.0	7.0	32.0	3440.0	253.0	0.0	ND	15.3	14.6
WA-36	954.0	48.0	70.0	6440.0	ND	35.0	414.0	184.0	ND	ND	3.3	16.2
WA-37	2190.0	42.0	34.0	4530.0	7.0	29.0	3510.0	348.0	0.0	ND	7.5	16.8
WA-40	1190.0	15.0	5.0	1930.0	1.0	37.0	1780.0	283.0	ND	ND	1.0	13.9
LB-42	187.0	1.0	8.0	474.0	2.0	47.0	320.0	32.0	ND	0.1	ND	6.4
LB-43	276.0	ND	46.0	1620.0	7.0	69.0	1150.0	ND	0.1	ND	5.7	1.1
LB-44	472.0	5.0	49.0	2270.0	12.0	45.0	1690.0	10.0	ND	ND	4.1	1.6
LB-45	1881.0	12.0	2.0	1830.0	ND	25.0	1950.0	ND	ND	ND	2.6	3.9
LB-46	103.0	17.0	800.0	12400.0	65.0	121.0	6040.0	ND	0.2	ND	106.0	2.6
LB-47	181.0	8.0	211.0	4920.0	25.0	79.0	2990.0	ND	ND	ND	11.1	3.4
MS-50	1095.6	64.9	34.0	6787.0	2.0	74.0	3890.0	ND	ND	ND	9.5	93.4

NR= Not reported

ND=Not detected

Quillinan et al., 2018; Aqueous Geochemistry

Sample ID	Alkalinity as CaCO ₃	Br (mg/L)	Ca (mg/L)	Cl ⁻ (mg/L)	Mg (mg/L)	K (mg/L)	Na (mg/L)	SO ₄ (mg/L)	Al (mg/L)	As (mg/L)	Ba (mg/L)	B (mg/L)
MS-51	2244.0	26.4	21.0	3157.0	4.0	32.0	2860.0	ND	ND	ND	10.3	11.8
MS-52	1639.0	24.2	13.0	2827.0	4.0	19.0	2830.0	16.5	ND	ND	4.5	25.5
MS-54	2189.0	19.8	13.0	2277.0	1.0	15.0	2120.0	16.5	ND	ND	5.1	20.0
MS-55	1738.0	37.4	22.0	4202.0	2.0	43.0	2960.0	ND	ND	ND	7.2	48.1
MS-56	784.3	14.3	9.0	1628.0	1.0	9.0	1410.0	7.7	ND	ND	1.8	12.2
MS-57	1683.0	20.9	11.0	2519.0	3.0	13.0	1680.0	13.2	ND	ND	2.6	11.0
MS-58	352.0	116.6	104.0	11990.0	6.0	201.0	6090.0	ND	ND	ND	36.7	79.7
MS-59	610.5	40.7	29.0	3410.0	3.0	23.0	2340.0	ND	ND	ND	6.0	30.5
WB-MT-8-14-1	NR	760.0	19700.0	199000.0	1440.0	6780.0	97900.0	192.0	0.8	NR	22.9	515.0
WB-ND-8-14-2	NR	758.0	19200.0	188000.0	1250.0	6740.0	88200.0	193.0	<0.54	NR	22.0	455.0
WB-ND-8-14-3	NR	708.0	19700.0	173000.0	1300.0	6420.0	78700.0	235.0	<0.54	NR	27.2	462.0
WB-ND-8-14-4	NR	851.0	23500.0	204000.0	1350.0	8540.0	93200.0	201.0	<0.54	NR	17.1	535.0
WB-ND-8-14-5	NR	859.0	23800.0	202000.0	1390.0	8220.0	91100.0	189.0	<0.54	NR	19.6	541.0
WB-ND-8-14-6	NR	799.0	20300.0	176000.0	1270.0	7370.0	77500.0	308.0	<0.54	NR	17.7	522.0
WB-ND-8-14-7	NR	877.0	23100.0	192000.0	1300.0	8700.0	85000.0	254.0	<0.54	NR	21.2	569.0
WB-ND-8-14-8	NR	934.0	23800.0	200000.0	1320.0	8930.0	88800.0	217.0	<0.54	NR	12.5	584.0
WB-ND-8-14-9	NR	914.0	23300.0	196000.0	1260.0	8810.0	86900.0	237.0	<0.54	NR	51.2	575.0
WB-ND-8-14-10	NR	813.0	21900.0	203000.0	1310.0	8220.0	94100.0	210.0	<0.54	NR	18.8	527.0
WB-ND-8-14-11	NR	847.0	18100.0	159000.0	1220.0	5610.0	72400.0	185.0	<0.54	NR	25.3	373.0
WB-ND-8-14-12	NR	713.0	19100.0	170000.0	1210.0	6570.0	76200.0	191.0	<0.54	NR	34.2	415.0
WB-ND-8-14-14	NR	683.0	17600.0	157000.0	1070.0	5830.0	69800.0	184.0	<0.54	NR	18.5	374.0
1A (BS-101)	NR	744.0	19600.0	201000.0	1350.0	6810.0	96900.0	192.0	NR	NR	NR	NR
2A (BS-107)	NR	770.0	19800.0	199000.0	1360.0	6920.0	95600.0	189.0	NR	NR	NR	NR
3A(BS-112)	NR	732.0	19500.0	198000.0	1410.0	6500.0	96000.0	239.0	NR	NR	NR	NR
4A (BS-116)	NR	612.0	19200.0	177000.0	1380.0	6580.0	97900.0	216.0	NR	NR	NR	NR
5A (BS-120)	NR	691.0	19200.0	201000.0	1390.0	6520.0	97400.0	226.0	NR	NR	NR	NR
GR1 Dup	NR	775.0	9990.0	100000.0	2240.0	1020.0	44300.0	81.6	< 0.4	ND	2.2	26.8

NR= Not reported

ND=Not detected

Quillinan et al., 2018; Aqueous Geochemistry

Sample ID	Alkalinity as CaCO ₃	Br (mg/L)	Ca (mg/L)	Cl ⁻ (mg/L)	Mg (mg/L)	K (mg/L)	Na (mg/L)	SO ₄ (mg/L)	Al (mg/L)	As (mg/L)	Ba (mg/L)	B (mg/L)
6 HD Dup	NR	1500.0	19400.0	132000.0	2350.0	1060.0	51200.0	20.9	< 0.04	< 0.006	2260.0	NR
6 HM	NR	1370.0	19500.0	139000.0	2250.0	775.0	56300.0	21.2	< 0.04	< 0.006	128.0	NR
Sc.01.14.14 ST	NR	662.0	11600.0	91600.0	2520.0	161.0	39300.0	<4.00	< 0.22	0.1	44.0	0.6
BE.01.14.14.ST	NR	3300.0	28900.0	190000.0	3680.0	1820.0	58300.0	169.0	< 0.22	0.3	1.6	21.3
CM-1	NR	402.0	8870.0	82300.0	2100.0	173.0	36500.0	5.5	< 0.4	< 0.006	117.0	1.7
DC-1	NR	18.7	68.9	2640.0	28.5	7.4	1640.0	8.6	< 0.02	ND	0.4	0.3
RS-1	NR	433.0	5820.0	59500.0	1470.0	159.0	27400.0	14.1	< 0.4	ND	171.0	1.3
CC-1	54.3	186.0	3310.0	27600.0	735.0	51.9	13700.0	1230.0	< 0.077	ND	0.1	0.2
D-5	9.0	3010.0	32300.0	186000.0	4040.0	1990.0	62000.0	135.0	< 0.22	0.1	2.9	14.4
MA-2	NR	979.0	13800.0	92300.0	1260.0	221.0	39100.0	<60	NR	NR	3720.0	20.3
LS #20	8.0	662.0	11600.0	91600.0	2520.0	161.0	39300.0	<4.00	< 0.22	0.1	44.0	0.6
NH #1	7.3	692.0	10700.0	92300.0	2070.0	152.0	33900.0	<4.00	< 0.22	ND	126.0	< 2.5
14-TX-7B	128.8	755.0	1440.0	82400.0	370.0	400.0	47400.0	<300	NR	NR	411.2	39.6
14-TX-8B	314.9	758.0	1470.0	83300.0	345.0	360.0	48100.0	<300	NR	NR	376.0	31.0
14-TX-9B	473.2	691.0	1650.0	71200.0	317.0	520.0	39600.0	<300	NR	NR	<20	40.9
14-TX-23B	926.8	920.0	659.0	22000.0	84.7	129.0	13600.0	<300	NR	NR	<20	36.7
14-TX-24B	918.6	930.0	687.0	22400.0	88.7	126.0	13700.0	<300	NR	NR	<20	37.8
14-TX-25B	696.3	585.0	649.0	19700.0	94.3	133.0	12400.0	<300	NR	NR	<20	31.9
14-TX-26B	570.0	1220.0	3360.0	54900.0	430.0	212.0	30600.0	<300	NR	NR	<20	31.6
14-TX-27B	634.0	219.0	1730.0	31200.0	274.0	<125	18200.0	1050.0	NR	NR	<20	32.4
14-TX-28B	460.1	376.0	5740.0	79600.0	1110.0	649.0	44000.0	965.0	NR	NR	<20	40.8
14-TX-41B	279.7	642.0	6250.0	84900.0	849.0	351.0	46200.0	905.0	NR	NR	<20	38.7
14-TX-48B	354.3	568.0	3780.0	75700.0	541.0	364.0	43100.0	706.0	NR	NR	<20	38.8
14-TX-49B	320.7	554.0	3630.0	73600.0	517.0	374.0	42600.0	584.0	NR	NR	<20	40.8
Kohles and Kohles Well	394.6	NR	125.0	69.0	242.0	3.0	1030.0	2550.0	nd	nd	0.0	2.0
Kohles and Kohles Well	NR	<50	92.6	56.7	201.4	5.1	734.7	2050.0	nd	nd	0.0	1.8
Paul George Mule Well	693.0	NR	30.0	69.0	312.0	16.0	1400.0	2760.0	nd	nd	0.1	1.6

NR= Not reported

ND=Not detected

Quillinan et al., 2018; Aqueous Geochemistry

Sample ID	Alkalinity as CaCO ₃	Br (mg/L)	Ca (mg/L)	Cl ⁻ (mg/L)	Mg (mg/L)	K (mg/L)	Na (mg/L)	SO ₄ (mg/L)	Al (mg/L)	As (mg/L)	Ba (mg/L)	B (mg/L)
Paul George Mule Well	NR	<50	27.5	46.1	268.5	24.3	1350.0	1967.0	nd	nd	0.0	1.6
Paul George Kitty Well	343.9	NR	5.0	60.0	3.0	2.0	1170.0	1670.0	nd	nd	0.0	1.6
Paul George Kitty Well	819.7	NR	4.0	35.0	2.0	2.0	1080.0	1320.0	nd	nd	0.0	1.5
Paul George Kitty Well	NR	<50	6.4	46.3	3.5	3.9	1081.7	1377.0	nd	nd	0.0	1.6
Paul George Reservoir	269.3	NR	198.0	234.0	905.0	27.0	3140.0	9560.0	nd	nd	0.0	2.0
Paul George Reservoir	NR	<50	291.3	304.0	1400.5	73.7	3787.5	11885.0	0.1	ND	0.0	2.2
Kearn's Well	207.2	NR	249.0	48.0	259.0	9.0	101.0	1420.0	nd	nd	0.0	0.1
Kearn's Well	NR	<50	38.1	15.2	41.3	27.8	12.5	50.0	nd	nd	0.0	0.1
Paul George House Well	341.8	NR	19.0	5.0	15.0	4.0	534.0	533.0	nd	nd	0.0	1.4
Paul George House Well	NR	<50	27.0	25.0	24.4	5.6	430.6	441.0	nd	nd	0.0	1.4
Pace Well	223.7	NR	460.0	103.0	292.0	5.0	221.0	2240.0	nd	nd	0.0	0.3
Pace Well	NR	<50	625.8	117.0	370.2	6.6	263.9	2187.0	nd	nd	0.0	0.3
Kleinert Farms Fishing Pond	111.9	NR	201.0	64.0	299.0	18.0	447.0	2270.0	0.1	nd	0.0	0.0
Kleinert Farms Fishing Pond	NR	<50	192.6	42.2	265.9	25.0	333.4	1480.0	nd	ND	0.0	0.1
Kleinert Farms Fishing Pond	NR	<50	232.9	48.9	290.9	24.3	405.6	1642.0	nd	ND	0.0	0.1
Wallewein Reservoir South End	NR	<50	277.9	794.0	1194.0	53.9	3127.0	12048.0	nd	ND	0.0	1.6
Kearn's Reservoir	274.5	NR	295.0	162.0	930.0	47.0	1540.0	6800.0	nd	nd	0.0	2.0

NR= Not reported

ND=Not detected

Quillinan et al., 2018; Aqueous Geochemistry

Sample ID	Alkalinity as CaCO ₃	Br (mg/L)	Ca (mg/L)	Cl ⁻ (mg/L)	Mg (mg/L)	K (mg/L)	Na (mg/L)	SO ₄ (mg/L)	Al (mg/L)	As (mg/L)	Ba (mg/L)	B (mg/L)
Kearn's Reservoir	NR	<50	406.6	188.0	1273.5	77.9	1713.4	6934.0	nd	ND	0.0	1.9
Nagy Well	NR	<50	120.6	25.0	108.2	7.7	93.0	373.0	nd	nd	0.0	0.3
Alme Well	NR	<50	305.7	47.5	286.2	4.2	262.2	1516.0	nd	nd	0.0	0.3
Wood Well	218.0	NR	80.1	17.9	21.1	4.7	20.4	43.1	0.0	NR	NR	0.2
Heise Hot Springs	816.8	ND	487.7	2267.5	93.8	206.2	1539.7	712.3	0.1	ND	4.5	0.1
Lidy HS1	109.2	ND	66.2	7.3	15.6	13.2	25.4	101.9	0.0	ND	0.1	0.1
Lidy HS2	135.5	ND	64.2	6.9	16.3	13.5	27.6	98.3	0.0	ND	0.1	0.1
Green Cyn HS	113.2	ND	144.2	0.9	33.8	4.5	5.0	314.2	NR	ND	0.0	0.0
Sturm_W	54.8	ND	3.2	3.3	0.0	0.9	33.2	5.8	0.0	ND	0.0	0.0
Condie HS	260.8	ND	61.1	14.0	11.5	22.5	62.4	33.5	0.0	ND	0.3	0.3
Green House W	236.5	ND	77.8	22.2	27.7	9.4	33.8	57.5	NR	ND	0.2	0.1
Eckert Office W	66.7	0.8	5.7	46.5	0.7	4.2	112.8	90.9	0.0	ND	0.2	0.0
Campbell Well1	119.3	0.4	23.5	23.1	3.0	7.7	57.5	40.5	0.0	ND	0.1	0.0
Campbell Well2	105.1	0.4	26.7	20.0	3.5	8.0	55.9	31.8	0.0	ND	0.1	0.0
Miracle HS Well	76.8	ND	0.8	31.7	0.0	1.9	128.2	33.7	0.0	0.1	0.3	<LOD
Driscoll Well	78.8	0.8	11.2	53.3	0.4	1.4	149.4	188.0	0.0	ND	0.1	0.0
Driscoll Spring	80.9	3.0	11.1	53.6	0.8	1.9	146.6	186.6	0.0	ND	0.1	0.0
CSI Well2	105.1	<LOD	4.5	26.4	0.2	3.3	94.9	46.8	0.0	ND	0.2	0.0
Comore Loma 6	184.0	ND	50.8	126.1	15.2	16.0	96.7	32.2	0.0	ND	0.2	0.2
Comore Loma 5	208.2	ND	52.0	120.3	18.5	15.8	89.7	25.6	0.0	ND	0.2	0.2
Blackhawk Well2	224.4	ND	77.4	204.9	22.1	17.3	124.4	37.0	0.0	ND	0.3	0.2
Blackhawk Well1	222.4	ND	75.3	196.5	21.0	16.7	122.2	39.1	0.0	ND	0.3	0.2

NR= Not reported

ND=Not detected

Quillinan et al., 2018; Aqueous Geochemistry

Sample ID	Alkalinity as CaCO ₃	Br (mg/L)	Ca (mg/L)	Cl ⁻ (mg/L)	Mg (mg/L)	K (mg/L)	Na (mg/L)	SO ₄ (mg/L)	Al (mg/L)	As (mg/L)	Ba (mg/L)	B (mg/L)
RRG1	28.3	0.1	59.9	956.1	0.2	39.9	567.7	58.4	0.1	ND	0.3	0.0
RRG2	31.5	ND	52.5	979.9	0.1	37.9	418.2	63.7	0.1	ND	0.2	0.0
RRG7	27.3	ND	199.2	2197.1	0.1	150.3	1258.2	59.3	0.1	ND	0.5	0.1
RRG4	36.8	0.4	59.8	790.4	0.1	38.8	542.5	59.3	0.1	ND	0.2	0.0
Indian HS	184.4	ND	80.8	216.3	19.5	11.5	126.0	19.8	0.0	ND	0.1	0.3
Grush Diary	234.5	ND	0.9	69.0	0.1	2.5	164.0	24.0	0.1	ND	0.1	0.0
RRG USGS W	78.8	0.5	70.7	976.5	0.1	24.8	621.5	56.5	0.0	ND	0.3	0.0
RRG Crook Well	29.3	1.1	157.7	1679.7	0.3	35.9	1186.9	56.5	0.1	ND	0.5	0.1
Milford Sweat	208.2	ND	66.5	6.6	13.7	8.5	43.0	49.9	0.0	0.1	0.2	0.1
Magic RLW Runoff	588.0	ND	13.2	79.1	1.3	20.9	333.0	52.9	0.0	ND	1.2	0.1
Elk Creek HS1	76.8	ND	2.3	23.2	0.0	1.7	90.2	42.6	0.0	ND	0.3	0.0
Elk Creek HS2	74.8	ND	2.3	23.1	0.0	1.6	91.2	42.6	0.0	ND	0.3	0.0
Barron Well	149.6	ND	16.9	9.5	0.6	3.0	156.2	210.9	0.0	ND	0.2	0.0
Wardrop HSI	159.7	ND	1.2	5.1	0.3	0.9	56.0	11.5	0.1	ND	0.0	0.0
Magic RLW	582.3	ND	22.3	74.1	1.4	19.8	310.5	50.3	0.0	ND	1.2	0.2
Prince Albert HSI	86.9	ND	0.3	2.6	0.0	2.7	55.3	8.4	0.0	ND	0.0	0.0
Oakley WS	89.0	ND	2.2	52.6	0.0	2.2	85.7	21.4	0.0	ND	0.1	0.0
Richard Austin W	169.8	ND	2.1	16.2	0.1	1.9	106.0	22.8	0.0	ND	0.1	0.0
Marsh Creek W	103.1	ND	9.1	51.8	0.4	4.3	107.8	50.3	0.0	ND	0.1	0.0
Sliger Well	175.9	ND	0.9	50.4	0.0	1.6	136.4	30.1	0.1	0.1	0.5	0.0
Banbury HS W	206.2	ND	0.9	16.9	0.0	1.6	96.8	23.5	0.0	ND	0.2	0.0
Banbury HS	139.5	ND	1.0	16.8	0.0	1.6	94.9	23.5	0.0	ND	0.2	0.0
Johnston Well	97.0	ND	2.4	5.9	0.0	1.3	77.4	10.3	0.0	ND	0.3	0.0
Leo Ray Hill	116.3	0.0	5.9	14.0	0.2	3.4	61.7	31.3	0.0	ND	0.1	0.0
Leo Ray Road	115.2	0.0	7.6	11.7	0.5	4.1	56.4	24.8	0.0	ND	0.1	0.0
Hensley W	192.1	0.0	1.9	51.9	0.0	1.6	121.6	33.1	0.0	0.1	0.6	0.0

NR= Not reported

ND=Not detected

Quillinan et al., 2018; Aqueous Geochemistry

Sample ID	Alkalinity as CaCO ₃	Br (mg/L)	Ca (mg/L)	Cl ⁻ (mg/L)	Mg (mg/L)	K (mg/L)	Na (mg/L)	SO ₄ (mg/L)	Al (mg/L)	As (mg/L)	Ba (mg/L)	B (mg/L)
Latty HS	89.0	ND	0.2	2.7	0.0	1.9	53.9	11.5	0.0	ND	0.0	0.0
Laib W	733.9	ND	9.4	66.2	0.6	9.8	291.7	10.4	0.2	ND	2.2	0.1
CSI W1	127.4	ND	4.0	25.8	0.2	3.0	86.3	45.4	0.0	ND	0.2	0.0
Lary Anderson	155.7	ND	1.2	21.1	0.0	2.2	118.1	36.3	0.0	ND	0.3	0.0
Pristine S	127.4	ND	1.3	26.7	0.0	2.1	109.3	30.8	0.0	ND	0.3	0.0
TF High School	133.4	ND	39.9	37.5	9.0	4.9	55.4	76.0	0.0	ND	0.1	0.0
Anderson CG W	204.2	ND	1.5	34.4	0.0	3.1	126.5	37.4	0.0	0.1	0.5	0.0
Butte City W	319.4	ND	51.6	19.8	20.9	7.5	32.5	49.4	0.0	ND	0.2	0.1
Quidop S1	511.5	ND	165.4	23.3	55.8	23.0	28.4	223.9	0.0	ND	0.1	0.0
Quidop S2 (ID 58)	588.3	ND	199.5	15.2	69.0	34.1	33.8	344.9	0.4	ND	0.1	0.1
Yandell Warm Springs	220.4	ND	72.5	16.3	26.3	3.9	13.5	90.4	0.0	ND	0.0	0.0
Skaggs Ranch	149.6	0.0	27.7	20.4	2.0	3.9	32.6	14.5	0.0	ND	0.0	0.1
Durfee Hot Springs	89.0	0.0	8.2	59.2	0.4	3.3	84.3	28.2	0.0	ND	0.1	0.0
Basin Cemetery	101.1	ND	18.3	47.4	2.4	2.0	58.0	21.0	0.0	ND	0.1	0.0
Wybenga Dairy	95.0	ND	25.0	13.1	1.1	8.7	20.9	15.7	0.0	ND	0.1	0.1
David Bosen Well	483.2	6.2	206.9	7128.9	18.5	794.9	4523.3	49.2	0.1	0.1	5.6	3.2
Schwendiman Well	136.5	ND	26.9	13.7	6.9	5.5	39.3	25.2	0.0	ND	0.1	0.0
Clyde W	151.6	ND	24.7	15.4	7.3	5.3	45.6	23.0	0.0	ND	0.1	0.0
Cinder Block Well	150.6	ND	18.2	12.2	3.5	5.0	52.2	17.2	0.0	ND	0.2	0.0
Newdale City W	208.2	ND	27.6	24.9	4.7	8.1	70.9	29.7	0.0	ND	0.2	0.1
Spackman Well	157.7	ND	37.2	5.8	13.7	3.0	11.6	12.9	0.0	ND	0.1	0.0
Fort Hall Thermal W	185.0	NR	55.4	NR	21.3	7.1	29.3	NR	NR	ND	0.1	0.1

NR= Not reported

ND=Not detected

Quillinan et al., 2018; Aqueous Geochemistry

Sample ID	Alkalinity as CaCO ₃	Br (mg/L)	Ca (mg/L)	Cl ⁻ (mg/L)	Mg (mg/L)	K (mg/L)	Na (mg/L)	SO ₄ (mg/L)	Al (mg/L)	As (mg/L)	Ba (mg/L)	B (mg/L)
Riverdale Resort	408.4	<5	23.3	295.0	8.6	16.5	345.0	11.1	< 0.01	ND	0.6	0.0
Downata H.S.	234.5	<5	40.0	18.9	14.3	8.7	20.1	17.9	< 0.01	ND	0.1	0.2
Lava H.S.	416.5	<5	102.3	197.7	31.7	37.4	157.5	96.2	< 0.01	ND	0.5	0.1
Hailey H.S.	96.0	<5	2.8	4.4	0.0	3.8	71.7	37.3	0.0	< 0.001	0.1	0.0
Frenchman's Bend H.S.	80.9	<5	3.9	5.4	0.3	1.7	63.1	36.5	0.1	ND	0.1	0.0
Worswick H.S.	69.8	<5	1.0	5.2	0.0	2.7	73.2	32.4	0.1	ND	0.1	0.0
Wolf H.S.	89.0	<5	1.4	3.0	0.0	2.3	52.4	6.5	0.1	ND	0.0	0.0
Tindall Well North	80.9	<5	8.1	10.2	0.2	7.8	56.4	24.3	< 0.01	ND	0.1	0.0
Bruneau H.S. well	103.1	<5	9.2	9.7	0.8	5.8	50.8	16.6	< 0.01	ND	0.1	0.0
Lower Indian Bathtub H.S.	82.9	<5	6.0	9.9	0.4	5.4	56.8	17.3	< 0.01	ND	0.1	0.0
Piranha well	79.9	<5	5.8	9.3	0.2	7.1	51.9	19.7	< 0.01	ND	0.1	0.0
Ward well #1	97.0	<5	5.1	8.4	0.1	9.0	52.8	30.7	< 0.01	ND	0.1	0.0
Shane Ward well	105.1	<5	29.3	10.8	2.1	10.4	56.5	82.1	< 0.01	ND	0.1	0.0
Irwin well #1	56.6	<5	5.8	9.2	0.2	6.4	50.3	17.7	< 0.01	ND	0.1	0.0
Comore Loma 7	220.4	<5	36.6	26.3	9.7	6.1	23.7	13.4	< 0.01	ND	0.1	0.1
Rush Warm Springs 1	230.5	<5	48.0	13.4	9.8	14.5	47.4	27.4	< 0.01	ND	0.2	0.2
Hawley Warm Springs	176.9	<5	39.0	6.2	9.7	3.2	9.7	6.0	< 0.01	ND	0.0	0.1
Elkhorn Warm Springs	111.2	<5	40.3	5.1	9.1	3.3	10.5	7.6	< 0.01	ND	0.0	0.1
Doug Mills Hot Well	424.6	<5	269.2	4224.3	50.3	181.5	2312.2	88.9	< 0.01	ND	1.2	0.5

NR= Not reported

ND=Not detected

Quillinan et al., 2018; Aqueous Geochemistry

Sample ID	Alkalinity as CaCO ₃	Br (mg/L)	Ca (mg/L)	Cl ⁻ (mg/L)	Mg (mg/L)	K (mg/L)	Na (mg/L)	SO ₄ (mg/L)	Al (mg/L)	As (mg/L)	Ba (mg/L)	B (mg/L)
Charles Crittenden	469.1	<5	290.5	4831.8	57.7	213.7	2463.5	85.8	< 0.01	0.1	1.2	0.5
Ashton Warms Springs	69.8	<5	<1	<5	0.1	1.4	31.6	3.2	< 0.01	ND	0.0	0.0
Warm River Springs 1	152.6	<5	10.5	6.5	1.3	0.7	21.8	8.1	< 0.01	ND	0.0	0.0
Site 14	210.3	<5	40.2	9.9	14.5	3.8	NR	24.4	<0.001	NR	0.0	0.1
USGS 7	149.6	<5	29.3	9.4	9.5	5.5	NR	16.2	<0.001	NR	0.1	0.0
500m Spring	1985.4	<5	998.0	4.7	147.0	35.2	12.1	867.0	<0.001	0.1	<0.150	0.0
Mountain Home AFB #1	50.5	<5	13.1	3.1	4.3	3.4	14.2	8.6	<0.01	<0.01	0.0	0.0
Mountain Home AFB #2	70.8	<5	21.8	12.6	6.7	3.7	14.9	20.3	<0.01	<0.01	0.0	0.0
Gonsales Thermal Well	209.3	<5	1.9	13.3	<1	1.8	112.9	13.8	0.0	<0.01	0.3	<0.001
SVR-5	122.3	<5	1.3	8.6	<1	1.1	92.1	4.7	<0.01	<0.01	0.2	0.0
Barron Heating Well (Grandpa Barron Well)	175.9	<5	1.4	4.8	<1	1.4	59.3	4.4	0.0	<0.01	0.2	0.0
Strom Well 2015	81.9	<5	1.0	1.5	<1	<1	37.0	4.0	0.0	<0.01	0.0	<0.001
SVR-4	162.8	<5	1.1	6.8	<1	<1	68.4	5.9	<0.01	<0.01	0.2	0.0
Grandpa Barron Spring	45.5	<5	8.0	1.7	1.1	3.8	9.6	1.8	<0.01	<0.01	0.0	0.0
Higgs Well, SVR-9	61.7	<5	3.3	6.3	1.7	3.4	31.8	5.7	<0.01	<0.01	0.1	0.0
Soda Geyser Site #6	1344.5	<5	537.5	4.7	140.1	17.7	8.5	750.0	<0.01	ND	0.0	0.0
Soda Geyser Site #5	1742.8	<5	662.0	4.5	133.4	16.9	8.3	768.0	0.0	ND	0.0	0.0

NR= Not reported

ND=Not detected

Quillinan et al., 2018; Aqueous Geochemistry

Sample ID	Alkalinity as CaCO ₃	Br (mg/L)	Ca (mg/L)	Cl ⁻ (mg/L)	Mg (mg/L)	K (mg/L)	Na (mg/L)	SO ₄ (mg/L)	Al (mg/L)	As (mg/L)	Ba (mg/L)	B (mg/L)
Soda Geyser Site #4	1892.5	<5	769.3	4.4	99.6	12.4	4.4	779.0	0.0	ND	0.0	0.0
Soda Geyser Site #3	1886.3	<5	764.9	4.4	104.4	13.2	4.8	766.0	0.0	ND	0.0	0.0
Soda Geyser Site #2	2076.2	<5	777.6	4.4	79.2	9.8	2.8	823.0	0.1	ND	0.0	0.0
Soda Geyser Site #1	2062.2	<5	778.6	4.4	72.9	9.1	2.6	868.0	0.1	ND	0.1	0.0
Soda Geyser Site #0	2076.4	<5	781.0	4.4	68.9	8.7	2.3	750.0	0.1	ND	0.1	0.0
Soda_Geyser	1991.0	NR	963.5	5.0	187.2	23.8	13.2	762.0	0.2	NR	NR	nd
Soda Creek near Mammoth	377.0	NR	84.6	9.9	67.0	6.3	17.7	35.6	NR	NR	NR	nd
Soda Creek near Ocatagon	NR	NR	87.3	48.9	74.0	7.9	34.2	50.7	NR	NR	NR	0.1
Sulphure Spring	589.0	NR	196.4	NR	48.3	1.3	6.6	30.8	0.1	NR	NR	0.1
Steamboat Spring filtered	1853.0	NR	970.1	NR	196.7	26.7	12.2	878.9	0.1	NR	NR	NR
Pavilion Well	2009.0	NR	954.8	NR	196.5	27.6	12.5	919.2	0.3	NR	NR	NR
Mammoth Spring	722.0	NR	139.0	12.1	152.2	17.0	42.0	47.9	0.1	NR	NR	0.1
Hooper Spring	681.0	NR	125.8	11.8	132.3	12.8	33.0	53.5	0.1	NR	NR	0.1
Octagon Spring	1300.0	NR	579.7	14.8	181.6	21.6	31.2	409.9	0.1	NR	NR	nd
Lovers Delight	1071.0	NR	180.0	26.9	170.1	15.2	41.0	62.6	0.1	NR	NR	0.1
Outhouse Spring	1769.0	NR	990.7	5.6	199.2	26.5	12.0	880.6	0.2	NR	NR	NR

NR= Not reported

ND=Not detected

Quillinan et al., 2018; Aqueous Geochemistry

Sample ID	F ⁻ (mg/L)	Fe (mg/L)	Li (mg/L)	Mn (mg/L)	Mo (mg/L)	N as NH3 (mg/L)	P (mg/L)	SiO2 (mg/L)	Si (mg/L)	Sr (mg/L)
MD-2	1.3	0.3	2.5	ND	0.002	8.6	ND	NR	3.5	0.1
MD-3	1.0	0.2	3.8	0.025	ND	42.0	0.4	NR	27.7	0.8
MD-4	1.8	0.1	2.2	0.014	ND	9.9	0.1	NR	35.5	1.0
MD-5	1.8	0.1	1.8	0.011	ND	5.5	0.3	NR	39.1	1.2
MD-6	10.0	0.1	13.8	ND	ND	6.4	4.9	NR	164.0	0.1
MD-7	2.1	0.1	1.2	ND	ND	3.7	ND	NR	38.4	0.9
MD-8	2.0	0.1	1.4	0.016	ND	5.2	0.4	NR	35.7	1.1
PRB-10	NR	2.0	5.9	2.26	ND	NR	0.8	NR	6.0	64.0
PRB-11	0.5	12.7	14.6	0.53	ND	44.0	ND	NR	42.1	171.0
PRB-12	NR	4.5	0.8	0.21	ND	NR	19.2	NR	17.1	7.9
PRB-13	0.5	57.3	14.4	1.15	ND	49.0	ND	NR	47.5	164.0
PRB-14	1.9	0.4	0.9	0.08	ND	11.5	1.6	NR	22.7	12.3
PRB-15	1.0	1.6	8.9	0.85	ND	33.0	1.8	NR	73.3	111.0
PRB-16	1.0	25.0	6.7	0.51	ND	63.0	14.6	NR	68.6	84.9
PRB-17	0.8	5.6	5.1	0.19	ND	28.0	5.6	NR	37.7	87.8
PRB-18	0.7	0.9	10.2	0.476	ND	31.0	1.8	NR	55.0	135.0
PRB-19	0.5	26.6	11.1	1.4	ND	38.0	ND	NR	34.7	187.0
LC-31	6.6	ND	1.4	0.027	0.01	45.0	ND	NR	4.0	0.3
WA-33	6.0	ND	0.8	0.074	ND	NR	0.4	NR	21.0	4.0
WA-34	8.0	ND	0.8	0.025	0.004	NR	ND	NR	22.0	2.4
WA-35	13.0	ND	2.4	0.034	0.002	NR	0.2	NR	37.0	4.6
WA-36	12.0	ND	2.5	0.036	ND	NR	ND	NR	36.0	0.3
WA-37	13.0	0.3	1.7	0.05	0.002	NR	0.2	NR	39.0	0.7
WA-40	16.0	1.3	1.6	0.22	0.342	NR	ND	NR	43.0	1.6
LB-42	0.3	0.2	1.6	0.17	ND	NR	ND	NR	1.3	0.5
LB-43	ND	166.0	0.2	26.7	ND	NR	ND	NR	0.4	5.5
LB-44	ND	626.0	0.3	31.7	ND	NR	ND	NR	2.8	6.8
LB-45	2.0	2.2	0.3	0.022	0.003	NR	ND	NR	7.0	0.9
LB-46	ND	31.1	2.3	2.23	ND	NR	ND	NR	3.7	89.0
LB-47	ND	1.6	1.3	0.97	0.002	NR	ND	NR	5.0	24.5
MS-50	2.2	ND	10.6	0.014	0.003	NR	ND	NR	60.9	23.1

NR= Not reported

ND=Not detected

Quillinan et al., 2018; Aqueous Geochemistry

Sample ID	F ⁻ (mg/L)	Fe (mg/L)	Li (mg/L)	Mn (mg/L)	Mo (mg/L)	N as NH3 (mg/L)	P (mg/L)	SiO2 (mg/L)	Si (mg/L)	Sr (mg/L)
MS-51	2.0	0.2	1.3	0.035	0.002	NR	ND	NR	24.6	1.9
MS-52	2.0	0.1	1.9	0.007	ND	NR	ND	NR	45.3	1.0
MS-54	2.3	0.1	2.3	0.005	0.001	NR	2.6	NR	48.3	4.2
MS-55	2.2	0.1	5.4	0.01	ND	NR	1.9	NR	22.0	11.0
MS-56	1.4	ND	0.9	0.004	ND	NR	ND	NR	14.0	1.6
MS-57	1.1	ND	0.9	0.006	ND	NR	ND	NR	21.5	0.7
MS-58	5.5	3.0	13.2	0.332	0.003	NR	ND	NR	19.6	64.6
MS-59	2.2	0.1	2.4	0.156	0.042	NR	0.2	NR	25.9	3.9
WB-MT-8-14-1	4.2	NR	66.4	16.8	NR	1646.2	NR	NR	NR	1430.0
WB-ND-8-14-2	4.2	NR	50.7	21.1	NR	2414.9	NR	NR	NR	1580.0
WB-ND-8-14-3	3.2	NR	56.5	22.4	NR	2174.2	NR	NR	NR	1770.0
WB-ND-8-14-4	5.2	NR	71.2	27.9	NR	2686.7	NR	NR	NR	2010.0
WB-ND-8-14-5	3.6	NR	74.4	34.7	NR	2593.5	NR	NR	NR	2030.0
WB-ND-8-14-6	7.1	NR	62.7	19.4	NR	2632.3	NR	NR	NR	1850.0
WB-ND-8-14-7	6.6	NR	74.2	24.9	NR	2609.0	NR	NR	NR	1970.0
WB-ND-8-14-8	5.7	NR	75.1	26.5	NR	2772.1	NR	NR	NR	2070.0
WB-ND-8-14-9	6.3	NR	74.0	24.8	NR	2725.5	NR	NR	NR	2090.0
WB-ND-8-14-10	5.8	NR	73.3	28.6	NR	2554.7	NR	NR	NR	1870.0
WB-ND-8-14-11	4.2	NR	40.8	17.8	NR	2267.4	NR	NR	NR	1540.0
WB-ND-8-14-12	4.2	NR	53.3	20.6	NR	2383.8	NR	NR	NR	1630.0
WB-ND-8-14-14	3.8	NR	43.2	18.4	NR	2205.2	NR	NR	NR	1450.0
1A (BS-101)	4.4	NR	NR	NR	NR	1646.2	NR	NR	NR	NR
2A (BS-107)	5.1	NR	NR	NR	NR	1801.5	NR	NR	NR	NR
3A(BS-112)	4.4	NR	NR	NR	NR	1382.2	NR	NR	NR	NR
4A (BS-116)	4.7	NR	NR	NR	NR	1467.6	NR	NR	NR	NR
5A (BS-120)	4.5	NR	NR	NR	NR	1537.5	NR	NR	NR	NR
GR1 Dup	Below DL	163.0	86.7	1.9	< 0.02	197.2	NR	NR	< 40	792.0

NR= Not reported

ND=Not detected

Quillinan et al., 2018; Aqueous Geochemistry

Sample ID	F ⁻ (mg/L)	Fe (mg/L)	Li (mg/L)	Mn (mg/L)	Mo (mg/L)	N as NH ₃ (mg/L)	P (mg/L)	SiO ₂ (mg/L)	Si (mg/L)	Sr (mg/L)
6 HD Dup	3.4	197.0	57.8	12.2	< 0.002	295.1	NR	NR	< 40	4370.0
6 HM	Below DL	175.0	173.0	6.6	< 0.002	236.8	NR	NR	< 40	3890.0
Sc.01.14.14 ST	<2.00	51.4	2.5	8.7	0.1	NR	NR	NR	6.5	241.0
BE.01.14.14.ST	<2.00	132.0	49.2	38.4	0.2	NR	NR	NR	9.7	1150.0
CM-1	Below DL	110.0	4.3	9.4	< 0.02	24.8	NR	NR	< 40	151.0
DC-1	2.2	3.4	0.2	0.2	< 0.001	0.8	NR	NR	3.2	< 1
RS-1	Below DL	2.7	2.4	5.6	< 0.02	20.5	NR	NR	< 40	112.0
CC-1	NR	41.9	0.5	1.6	ND	NR	NR	NR	4.5	134.0
D-5	NR	190.0	58.0	50.7	0.2	NR	NR	NR	12.6	1070.0
MA-2	NR	184.0	96.2	5.5	NR	NR	NR	NR	NR	2720.0
LS #20	NR	51.4	2.5	8.7	0.1	NR	NR	NR	6.5	241.0
NH #1	NR	78.5	2.5	9.9	0.1	NR	NR	NR	5.5	179.0
14-TX-7B	NR	6.7	29.2	<0.5	NR	584.7	NR	NR	4.1	830.0
14-TX-8B	NR	11.2	35.1	<0.5	NR	588.6	NR	NR	6.7	859.0
14-TX-9B	NR	65.2	52.2	0.9	NR	807.6	NR	NR	8.7	1100.0
14-TX-23B	NR	206.8	19.7	2.9	NR	87.7	NR	NR	30.5	344.0
14-TX-24B	NR	183.0	19.5	2.7	NR	88.5	NR	NR	24.3	339.0
14-TX-25B	NR	28.7	17.9	0.9	NR	74.8	NR	NR	23.3	295.0
14-TX-26B	NR	160.0	32.6	3.1	NR	225.2	NR	NR	23.6	1700.0
14-TX-27B	NR	62.5	NR	1.7	NR	80.0	NR	NR	27.5	85.5
14-TX-28B	NR	3.4	NR	<0.5	NR	641.4	NR	NR	13.0	193.0
14-TX-41B	NR	49.2	28.9	1.1	NR	492.3	NR	NR	12.7	266.0
14-TX-48B	NR	39.7	25.7	1.1	NR	507.0	NR	NR	12.5	286.0
14-TX-49B	NR	54.4	24.9	1.3	NR	489.2	NR	NR	12.5	341.0
Kohles and Kohles Well	1.4	NR	3.0	NR	NR	NR	NR	NR	3.8	6.3
Kohles and Kohles Well	<5	NR	5.1	NR	NR	NR	NR	NR	4.6	4.3
Paul George Mule Well	3.1	NR	16.0	NR	NR	NR	NR	NR	2.2	1.1

NR= Not reported

ND=Not detected

Quillinan et al., 2018; Aqueous Geochemistry

Sample ID	F ⁻ (mg/L)	Fe (mg/L)	Li (mg/L)	Mn (mg/L)	Mo (mg/L)	N as NH ₃ (mg/L)	P (mg/L)	SiO ₂ (mg/L)	Si (mg/L)	Sr (mg/L)
Paul George Mule Well	<5	NR	24.3	NR	NR	NR	NR	NR	2.8	0.7
Paul George Kitty Well	1.0	NR	2.0	NR	NR	NR	NR	NR	2.8	0.9
Paul George Kitty Well	1.4	NR	2.0	NR	NR	NR	NR	NR	3.1	0.7
Paul George Kitty Well	<5	NR	3.9	NR	NR	NR	NR	NR	3.4	0.6
Paul George Reservoir	0.3	NR	27.0	NR	NR	NR	NR	NR	NR	6.8
Paul George Reservoir	<5	NR	73.7	NR	NR	NR	NR	NR	1.1	8.5
Kearn's Well	ND	NR	9.0	NR	NR	NR	NR	NR	3.9	2.7
Kearn's Well	<0.5	NR	27.8	NR	NR	NR	NR	NR	4.3	0.4
Paul George House Well	0.8	NR	4.0	NR	NR	NR	NR	NR	3.0	1.0
Paul George House Well	<5	NR	5.6	NR	NR	NR	NR	NR	3.6	1.1
Pace Well	0.2	NR	5.0	NR	NR	NR	NR	NR	4.2	3.5
Pace Well	<5	NR	6.6	NR	NR	NR	NR	NR	4.9	3.7
Kleinert Farms Fishing Pond	0.1	NR	18.0	NR	NR	NR	NR	NR	NR	2.3
Kleinert Farms Fishing Pond	<5	NR	25.0	NR	NR	NR	NR	NR	1.9	1.8
Kleinert Farms Fishing Pond	<5	NR	24.3	NR	NR	NR	NR	NR	0.5	1.9
Wallewein Reservoir South End	<5	NR	53.9	NR	NR	NR	NR	NR	0.6	5.1
Kearn's Reservoir	0.1	NR	47.0	NR	NR	NR	NR	NR	NR	8.2

NR= Not reported

ND=Not detected

Quillinan et al., 2018; Aqueous Geochemistry

Sample ID	F ⁻ (mg/L)	Fe (mg/L)	Li (mg/L)	Mn (mg/L)	Mo (mg/L)	N as NH3 (mg/L)	P (mg/L)	SiO2 (mg/L)	Si (mg/L)	Sr (mg/L)
Kearn's Reservoir	<5	NR	77.9	NR	NR	NR	NR	NR	2.0	9.2
Nagy Well	<5	NR	7.7	NR	NR	NR	NR	NR	5.2	3.7
Alme Well	<5	NR	4.2	NR	NR	NR	NR	NR	6.4	3.1
Wood Well	0.4	0.0	NR	NR	NR	NR	NR	14.5	9.2	NR
Heise Hot Springs	4.0	NR	2.5	NR	NR	NR	NR	33.6	21.5	5.5
Lidy HS1	4.6	NR	0.0	NR	NR	NR	nd	37.8	24.1	0.6
Lidy HS2	4.7	NR	0.0	NR	NR	NR	nd	34.2	21.8	0.6
Green Cyn HS	1.5	NR	0.0	NR	NR	NR	0.0	27.0	17.2	1.2
Sturm_W	2.1	NR	0.0	NR	NR	NR	NR	63.1	40.3	0.0
Condie HS	1.6	NR	0.1	NR	NR	NR	NR	29.5	18.8	0.9
Green House W	0.7	NR	0.0	NR	NR	NR	nd	31.6	20.2	0.7
Eckert Office W	12.2	NR	0.0	NR	NR	NR	0.0	52.0	33.2	0.0
Campbell Well1	2.2	NR	0.1	NR	NR	NR	nd	71.9	45.9	0.2
Campbell Well2	2.5	NR	0.1	NR	NR	NR	nd	69.4	44.3	0.2
Miracle HS Well	22.4	NR	0.0	NR	NR	NR	0.1	99.5	63.5	0.0
Driscoll Well	2.4	NR	0.2	NR	NR	NR	nd	45.5	29.1	0.1
Driscoll Spring	2.4	NR	0.2	NR	NR	NR	nd	48.4	30.9	0.1
CSI Well2	9.6	NR	0.0	NR	NR	NR	0.0	64.2	41.0	0.0
Comore Loma 6	0.4	NR	0.1	NR	NR	NR	NR	65.3	41.7	0.3
Comore Loma 5	0.3	NR	0.1	NR	NR	NR	NR	85.1	54.3	0.2
Blackhawk Well2	0.2	NR	0.1	NR	NR	NR	NR	83.7	53.4	0.4
Blackhawk Well1	0.3	NR	0.1	NR	NR	NR	NR	82.0	52.3	0.4

NR= Not reported

ND=Not detected

Quillinan et al., 2018; Aqueous Geochemistry

Sample ID	F ⁻ (mg/L)	Fe (mg/L)	Li (mg/L)	Mn (mg/L)	Mo (mg/L)	N as NH3 (mg/L)	P (mg/L)	SiO2 (mg/L)	Si (mg/L)	Sr (mg/L)
RRG1	9.1	NR	1.6	NR	NR	NR	NR	132.8	84.8	1.5
RRG2	9.5	NR	1.0	NR	NR	NR	NR	157.3	100.4	1.2
RRG7	6.0	NR	2.6	NR	NR	NR	NR	226.8	144.8	4.9
RRG4	7.2	NR	1.6	NR	NR	NR	NR	133.6	85.3	1.4
Indian HS	0.5	NR	0.1	NR	NR	NR	NR	20.4	13.0	2.1
Grush Diary	6.7	NR	0.1	NR	NR	NR	NR	73.0	46.6	0.0
RRG USGS W	7.0	NR	1.5	NR	NR	NR	NR	84.3	53.8	1.6
RRG Crook Well	6.1	NR	2.6	NR	NR	NR	NR	95.9	61.2	3.1
Milford Sweat	1.9	NR	0.0	NR	NR	NR	NR	24.6	15.7	0.4
Magic RLW Runoff	10.6	NR	1.2	NR	NR	NR	NR	109.4	69.8	0.6
Elk Creek HS1	15.1	NR	0.2	NR	NR	NR	NR	65.0	41.5	0.1
Elk Creek HS2	15.2	NR	0.2	NR	NR	NR	NR	65.3	41.7	0.1
Barron Well	7.1	NR	0.4	NR	NR	NR	NR	51.7	33.0	0.4
Wardrop HSI	3.4	NR	0.1	NR	NR	NR	NR	76.8	49.0	0.0
Magic RLW	9.9	NR	1.2	NR	NR	NR	NR	103.7	66.2	0.9
Prince Albert HSI	7.0	NR	0.0	NR	NR	NR	NR	110.1	70.3	0.0
Oakley WS	7.6	NR	0.0	NR	NR	NR	NR	79.2	50.5	0.1
Richard Austin W	2.4	NR	0.1	NR	NR	NR	NR	29.7	19.0	0.0
Marsh Creek W	13.2	NR	0.1	NR	NR	NR	NR	62.5	39.9	0.1
Sliger Well	24.2	NR	0.1	NR	NR	NR	NR	93.5	59.7	0.0
Banbury HS W	11.4	NR	0.0	NR	NR	NR	NR	103.4	66.0	0.0
Banbury HS	11.4	NR	0.0	NR	NR	NR	NR	102.8	65.6	0.0
Johnston Well	17.0	NR	0.0	NR	NR	NR	NR	40.9	26.1	0.0
Leo Ray Hill	3.4	NR	0.1	NR	NR	NR	NR	54.1	34.5	0.0
Leo Ray Road	3.4	NR	0.1	NR	NR	NR	NR	54.5	34.8	0.0
Hensley W	24.1	NR	0.0	NR	NR	NR	NR	83.3	53.2	0.0

NR= Not reported

ND=Not detected

Quillinan et al., 2018; Aqueous Geochemistry

Sample ID	F ⁻ (mg/L)	Fe (mg/L)	Li (mg/L)	Mn (mg/L)	Mo (mg/L)	N as NH3 (mg/L)	P (mg/L)	SiO2 (mg/L)	Si (mg/L)	Sr (mg/L)
Latty HS	6.8	NR	0.0	NR	NR	NR	NR	103.2	65.9	0.0
Laib W	1.7	NR	0.3	NR	NR	NR	NR	57.7	36.8	0.1
CSI W1	8.6	NR	0.0	NR	NR	NR	NR	60.9	38.9	0.0
Lary Anderson	15.8	NR	0.0	NR	NR	NR	NR	69.3	44.2	0.0
Pristine S	16.5	NR	0.0	NR	NR	NR	NR	71.6	45.7	0.0
TF High School	2.4	NR	0.0	NR	NR	NR	NR	59.1	37.7	0.2
Anderson CG W	23.4	NR	0.1	NR	NR	NR	NR	66.0	42.1	0.0
Butte City W	0.6	NR	0.0	NR	NR	NR	NR	33.2	21.2	0.6
Quidop S1	0.8	NR	0.1	NR	NR	NR	NR	16.1	10.2	1.8
Quidop S2 (ID 58)	0.8	NR	0.2	NR	NR	NR	NR	19.6	12.5	2.6
Yandell Warm Springs	0.6	NR	0.0	NR	NR	NR	NR	16.6	10.6	0.5
Skaggs Ranch	1.5	NR	0.0	NR	NR	NR	NR	44.1	28.1	0.1
Durfee Hot Springs	6.2	NR	0.1	NR	NR	NR	NR	67.9	43.3	0.1
Basin Cemetery	3.6	NR	0.0	NR	NR	NR	NR	40.2	25.7	0.2
Wybenga Dairy	0.7	NR	0.0	NR	NR	NR	NR	69.4	44.3	0.2
David Bosen Well	5.2	NR	6.1	NR	NR	NR	NR	95.1	60.7	20.4
Schwendiman Well	2.6	NR	0.1	NR	NR	NR	NR	61.5	39.3	0.1
Clyde W	3.2	NR	0.1	NR	NR	NR	NR	65.0	41.5	0.1
Cinder Block Well	4.2	NR	0.1	NR	NR	NR	NR	70.5	45.0	0.1
Newdale City W	5.0	NR	0.1	NR	NR	NR	NR	70.4	44.9	0.1
Spackman Well	0.5	NR	<0.000	NR	NR	NR	NR	29.6	18.9	0.1
Fort Hall Thermal W	NR	NR	0.0	NR	NR	NR	NR	50.0	31.9	0.3

NR= Not reported

ND=Not detected

Quillinan et al., 2018; Aqueous Geochemistry

Sample ID	F ⁻ (mg/L)	Fe (mg/L)	Li (mg/L)	Mn (mg/L)	Mo (mg/L)	N as NH3 (mg/L)	P (mg/L)	SiO2 (mg/L)	Si (mg/L)	Sr (mg/L)
Riverdale Resort	10.1	NR	0.2	NR	NR	NR	NR	77.6	49.5	0.2
Downata H.S.	<0.5	NR	0.0	NR	NR	NR	NR	29.9	19.1	0.3
Lava H.S.	0.7	NR	0.2	NR	NR	NR	NR	35.2	22.5	0.7
Hailey H.S.	8.3	NR	0.1	NR	NR	NR	NR	80.4	51.3	0.1
Frenchman's Bend H.S.	12.3	NR	0.2	NR	NR	NR	NR	87.2	55.6	0.1
Worswick H.S.	14.2	NR	0.2	NR	NR	NR	NR	96.3	61.4	0.1
Wolf H.S.	1.9	NR	0.0	NR	NR	NR	NR	63.9	40.8	0.0
Tindall Well North	12.5	NR	< 0.01	NR	NR	NR	NR	81.3	51.9	0.0
Bruneau H.S. well	8.7	NR	< 0.01	NR	NR	NR	NR	73.8	47.1	0.0
Lower Indian Bathtub H.S.	7.9	NR	< 0.01	NR	NR	NR	NR	77.4	49.4	0.0
Piranha well	10.6	NR	< 0.01	NR	NR	NR	NR	81.2	51.8	0.0
Ward well #1	7.5	NR	0.0	NR	NR	NR	NR	89.1	56.8	0.0
Shane Ward well	4.9	NR	0.0	NR	NR	NR	NR	82.5	52.6	0.1
Irwin well #1	10.9	NR	< 0.01	NR	NR	NR	NR	81.3	51.9	0.0
Comore Loma 7	<0.5	NR	0.0	NR	NR	NR	NR	48.6	31.0	0.2
Rush Warm Springs 1	1.5	NR	0.1	NR	NR	NR	NR	29.8	19.0	0.8
Hawley Warm Springs	0.7	NR	0.0	NR	NR	NR	NR	56.0	35.7	0.1
Elkhorn Warm Springs	0.8	NR	0.0	NR	NR	NR	NR	57.0	36.4	0.1
Doug Mills Hot Well	1.1	NR	2.0	NR	NR	NR	NR	40.7	25.9	8.3

NR= Not reported

ND=Not detected

Quillinan et al., 2018; Aqueous Geochemistry

Sample ID	F ⁻ (mg/L)	Fe (mg/L)	Li (mg/L)	Mn (mg/L)	Mo (mg/L)	N as NH3 (mg/L)	P (mg/L)	SiO2 (mg/L)	Si (mg/L)	Sr (mg/L)
Charles Crittenden	1.0	NR	2.2	NR	NR	NR	NR	35.6	22.7	8.9
Ashton Warms Springs	2.8	NR	0.0	NR	NR	NR	NR	113.0	72.1	0.0
Warm River Springs 1	2.6	NR	0.1	NR	NR	NR	NR	37.7	24.0	0.0
Site 14	<0.5	NR	0.0	NR	NR	NR	NR	32.7	20.8	0.2
USGS 7	1.7	NR	0.0	NR	NR	NR	NR	49.8	31.8	0.1
500m Spring	0.9	NR	0.2	NR	NR	NR	NR	36.0	23.0	4.3
Mountain Home AFB #1	<0.5	NR	0.0	NR	NR	NR	NR	19.2	12.3	0.0
Mountain Home AFB #2	<0.5	NR	0.0	NR	NR	NR	NR	20.6	13.1	0.1
Gonsales Thermal Well	11.8	NR	0.2	NR	NR	NR	NR	42.4	27.0	0.0
SVR-5	8.5	NR	0.1	NR	NR	NR	NR	31.0	19.8	0.0
Barron Heating Well (Grandpa Barron Well)	4.8	NR	0.0	NR	NR	NR	NR	23.9	15.2	0.0
Strom Well 2015	1.0	NR	0.0	NR	NR	NR	NR	15.3	9.8	0.0
SVR-4	6.3	NR	0.1	NR	NR	NR	NR	34.1	21.8	0.0
Grandpa Barron Spring	<0.5	NR	0.0	NR	NR	NR	NR	25.6	16.4	0.0
Higgs Well, SVR-9	2.4	NR	0.0	NR	NR	NR	NR	25.5	16.3	0.0
Soda Geyser Site #6	<0.5	NR	0.1	NR	NR	NR	NR	15.7	10.0	3.4
Soda Geyser Site #5	<0.5	NR	0.1	NR	NR	NR	NR	15.7	10.0	3.5

NR= Not reported

ND=Not detected

Quillinan et al., 2018; Aqueous Geochemistry

Sample ID	F ⁻ (mg/L)	Fe (mg/L)	Li (mg/L)	Mn (mg/L)	Mo (mg/L)	N as NH3 (mg/L)	P (mg/L)	SiO2 (mg/L)	Si (mg/L)	Sr (mg/L)
Soda Geyser Site #4	<0.5	NR	0.1	NR	NR	NR	NR	16.3	10.4	3.8
Soda Geyser Site #3	<0.5	NR	0.1	NR	NR	NR	NR	16.1	10.3	3.9
Soda Geyser Site #2	0.6	NR	0.1	NR	NR	NR	NR	16.0	10.2	3.9
Soda Geyser Site #1	0.7	NR	0.1	NR	NR	NR	NR	15.7	10.0	3.8
Soda Geyser Site #0	1.0	NR	0.1	NR	NR	NR	NR	15.9	10.2	3.8
Soda_Geyser	NR	4.7	NR	NR	NR	NR	NR	16.0	10.2	NR
Soda Creek near Mammoth	NR	NR	NR	NR	NR	NR	NR	21.7	13.8	NR
Soda Creek near Ocatagon	NR	0.2	NR	NR	NR	NR	NR	21.2	13.5	NR
Sulphure Spring	NR	NR	NR	NR	NR	NR	NR	6.9	4.4	NR
Steamboat Spring filtered	0.6	9.7	NR	NR	NR	NR	NR	16.0	10.2	NR
Pavilion Well	0.8	11.3	NR	NR	NR	NR	NR	16.3	10.4	NR
Mammoth Spring	NR	11.5	NR	NR	NR	NR	NR	44.5	28.4	NR
Hooper Spring	NR	7.2	NR	NR	NR	NR	NR	35.4	22.6	NR
Octagon Spring	NR	13.4	NR	NR	NR	NR	NR	29.5	18.8	NR
Lovers Delight	NR	9.6	NR	NR	NR	NR	NR	36.4	23.2	NR
Outhouse Spring	NR	11.3	NR	NR	NR	NR	NR	14.8	9.4	NR

NR= Not reported

ND=Not detected

Quillinan et al., 2018; Aqueous Rare Earth Element Concentration

Sample ID	Sc (ng/L)	Y (ng/L)	La (ng/L)	Ce (ng/L)	Pr (ng/L)	Nd (ng/L)	Sm (ng/L)	Eu (ng/L)	Gd (ng/L)	Tb (ng/L)
MD-2	3.57	NR	76.38	72.09	14.59	46.12	4.15	4.32	6.02	0.53
MD-3	1.58	NR	24.16	21.63	4.45	13.95	2.03	11.25	2.79	0.24
MD-4	22.24	NR	21.53	19.25	3.92	15.79	8.07	66.16	10.29	0.27
MD-5	0.16	NR	13.80	6.42	1.08	5.05	7.91	74.21	10.12	0.11
MD-6	0.89	NR	5.47	1.93	0.28	0.69	0.31	0.65	0.15	0.05
MD-7	5.71	NR	14.14	11.31	2.19	10.61	7.57	68.11	9.64	0.24
MD-8	1.00	NR	7.15	3.01	0.58	2.98	5.57	56.70	7.20	0.06
PRB-10	5.69	NR	19.34	3.42	0.47	1.65	1.14	15.94	19.34	0.05
PRB-11	1.49	NR	20.10	6.88	1.15	3.61	1.01	8.51	11.55	0.06
PRB-12	0.71	NR	3.33	1.68	0.30	0.86	0.14	0.92	1.18	0.02
PRB-13	2.14	NR	1.39	2.34	0.12	0.33	0.09	0.52	0.77	0.01
PRB-14	2.61	NR	0.83	0.56	0.09	0.22	0.35	0.71	1.15	0.07
PRB-15	3.90	NR	2.23	0.81	0.12	0.31	0.18	1.39	2.06	0.09
PRB-16	2.62	NR	16.73	4.49	0.75	2.05	0.79	3.10	5.40	0.18
PRB-17	2.29	NR	22.59	1.89	0.60	0.79	0.64	9.94	13.26	0.05
PRB-18	0.90	NR	7.32	0.89	0.17	0.68	0.31	4.25	6.52	0.03
PRB-19	0.67	NR	0.48	0.22	0.04	0.06	0.02	0.03	0.06	0.01
LC-31	8.17	NR	47.05	24.94	4.94	13.56	1.78	0.95	3.40	0.76
WA-33	ND	NR	2.63	3.37	1.00	4.03	2.91	41.05	3.83	0.11
WA-34	ND	NR	3.21	0.49	0.13	1.16	2.76	36.79	3.52	0.09
WA-35	ND	NR	2.00	3.08	0.97	5.01	12.33	120.10	15.31	0.11
WA-36	ND	NR	12.66	4.45	0.55	4.33	8.56	113.04	11.00	0.14
WA-37	ND	NR	4.78	1.78	0.20	1.88	3.93	53.31	5.10	0.09
WA-40	ND	NR	4.30	5.71	1.61	4.93	1.36	15.60	1.87	0.09
LB-42	ND	NR	5.76	7.74	1.30	3.43	0.80	0.36	1.67	0.20
LB-43	ND	NR	39.29	49.76	4.13	10.99	2.84	0.67	1.88	0.32
LB-44	ND	NR	28.59	37.42	3.51	10.49	2.40	18.90	3.55	0.31
LB-45	ND	NR	5.09	6.87	1.21	4.83	2.37	22.84	3.02	0.17
LB-46	ND	NR	15.62	18.38	0.92	2.00	0.48	6.82	0.78	0.06
LB-47	ND	NR	5.42	2.32	0.09	1.72	5.61	77.91	7.28	0.09

NR=Not Reported

Quillinan et al., 2018; Aqueous Rare Earth Element Concentration

Sample ID	Sc (ng/L)	Y (ng/L)	La (ng/L)	Ce (ng/L)	Pr (ng/L)	Nd (ng/L)	Sm (ng/L)	Eu (ng/L)	Gd (ng/L)	Tb (ng/L)
MS-50	1.20	2.32	0.77	1.39	0.13	0.66	0.17	2.34	0.23	0.04
MS-51	3.07	17.50	4.20	5.80	0.35	0.90	1.04	5.43	1.56	0.07
MS-52	1.43	15.65	2.59	5.20	0.57	2.76	0.73	6.48	0.97	0.18
MS-54	6.53	2.96	1.19	0.96	0.06	0.20	0.36	2.59	0.50	0.02
MS-55	3.50	3.68	1.41	2.41	0.21	1.33	0.25	0.75	0.60	0.07
MS-56	7.03	2.80	0.52	0.25	0.02	0.13	0.29	1.61	0.57	0.03
MS-57	4.87	1.97	0.33	0.22	0.04	0.10	0.17	0.53	0.26	NR
MS-58	5.86	169.16	0.99	1.64	0.09	0.45	0.17	0.63	0.68	0.47
MS-59	0.71	7.85	0.90	1.59	0.15	0.90	0.25	1.23	0.49	0.10
WB-MT-8-14-1	NR	NR	1000.21	1385.48	138.02	583.96	95.37	100.77	141.91	11.79
WB-ND-8-14-2	NR	NR	1864.78	1475.26	108.47	323.18	58.31	52.54	45.86	3.69
WB-ND-8-14-3	NR	NR	73.64	75.93	7.16	27.62	7.07	15.16	11.93	1.04
WB-ND-8-14-4	NR	NR	1784.03	1799.96	150.75	544.35	85.73	73.76	85.89	6.64
WB-ND-8-14-5	NR	NR	154.64	183.16	21.93	93.60	29.73	91.66	55.71	2.94
WB-ND-8-14-6	NR	NR	172.15	108.20	9.62	41.34	26.62	108.07	37.00	1.25
WB-ND-8-14-7	NR	NR	219.63	117.98	9.68	31.84	11.95	41.03	16.65	0.69
WB-ND-8-14-8	NR	NR	0.13	0.10	NR	NR	0.12	0.08	NR	0.10
WB-ND-8-14-9	NR	NR	328.86	251.85	18.35	68.93	29.95	42.71	16.56	1.66
WB-ND-8-14-10	NR	NR	1556.20	1794.74	162.06	631.56	320.05	301.44	168.10	8.16
WB-ND-8-14-11	NR	NR	283.82	332.68	25.54	95.63	70.24	98.65	30.10	1.97

NR=Not Reported

Quillinan et al., 2018; Aqueous Rare Earth Element Concentration

Sample ID	Sc (ng/L)	Y (ng/L)	La (ng/L)	Ce (ng/L)	Pr (ng/L)	Nd (ng/L)	Sm (ng/L)	Eu (ng/L)	Gd (ng/L)	Tb (ng/L)
WB-ND-8-14-12	NR	NR	1919.46	2006.28	179.95	624.73	98.96	82.21	88.96	6.23
WB-ND-8-14-14	NR	NR	1529.91	1480.15	129.24	454.52	57.90	98.95	68.20	4.76
1A (BS-101)	NR	NR	156.45	225.24	22.19	99.67	17.83	24.26	24.46	2.41
2A (BS-107)	NR	NR	1.30	2.21	0.34	0.53	NR	0.69	0.29	0.35
3A(BS-112)	NR	NR	88.35	101.01	10.31	49.05	10.79	41.12	14.32	1.36
4A (BS-116)	NR	NR	NR	1.24	0.07	NR	0.52	0.08	NR	0.13
5A (BS-120)	NR	NR	40.01	54.37	4.97	21.22	3.60	9.80	3.97	0.66
GR1 Dup	NR	NR	14.83	16.11	3.99	7.65	4.57	4.44	4.22	1.06
6 HD Dup	NR	NR	468.13	339.94	31.71	102.78	18.28	64.87	26.19	3.90
6 HM	NR	NR	373.46	192.25	16.08	58.01	8.51	14.75	14.18	2.31
Sc.01.14.14 ST	NR	NR	15.06	16.51	2.66	6.95	3.11	5.94	4.77	0.73
BE.01.14.14.ST	5.28	521.42	495.61	426.77	38.57	173.97	21.33	22.28	39.50	3.72
CM-1	NR	NR	146.52	156.17	12.18	26.72	9.53	217.90	14.82	0.98
DC-1	NR	NR	613.11	701.13	71.43	319.23	65.48	44.21	86.58	8.51
RS-1	NR	NR	72.60	34.20	4.80	77.34	29.00	131.61	45.99	1.26
CC-1	NR	NR	1086.12	1061.98	89.99	323.56	90.74	53.61	50.66	3.63
D-5	NR	NR	3.14	4.65	0.40	1.36	1.17	3.30	0.45	0.14
MA-2	NR	NR	439.17	42.55	4.37	79.84	218.59	364.90	265.42	0.97
LS #20	13.83	26.92	24.47	23.31	1.29	6.19	1.30	1.51	2.27	0.38
NH #1	NR	16.90	17.20	19.52	1.29	6.53	1.09	1.74	2.28	0.28
14-TX-7B	NR	NR	6.69	3.32	1.95	8.74	40.55	113.14	65.43	NR
14-TX-8B	NR	NR	69.28	41.52	2.28	8.34	21.89	105.70	34.78	0.22

NR=Not Reported

Quillinan et al., 2018; Aqueous Rare Earth Element Concentration

Sample ID	Sc (ng/L)	Y (ng/L)	La (ng/L)	Ce (ng/L)	Pr (ng/L)	Nd (ng/L)	Sm (ng/L)	Eu (ng/L)	Gd (ng/L)	Tb (ng/L)
14-TX-9B	NR	NR	1.72	3.63	0.24	2.53	1.12	10.46	0.87	0.13
14-TX-23B	NR	NR	NR	NR	NR	NR	NR	NR	NR	NR
14-TX-24B	NR	NR	NR	NR	NR	NR	0.17	0.16	0.10	NR
14-TX-25B	NR	NR	NR	NR	NR	NR	0.23	NR	0.26	NR
14-TX-26B	NR	NR	1.72	1.22	NR	NR	0.31	0.12	NR	NR
14-TX-27B	NR	NR	0.10	NR	NR	NR	NR	1.25	NR	NR
14-TX-28B	NR	NR	14.56	24.53	1.96	9.85	1.44	1.21	1.15	0.33
14-TX-41B	NR	NR	245.59	266.82	38.48	145.54	21.93	24.63	30.07	4.11
14-TX-48B	NR	NR	18.59	19.60	5.57	18.61	1.96	3.37	3.97	0.80
14-TX-49B	NR	NR	189.41	334.22	49.94	257.92	80.64	42.77	120.17	19.64
Kohles and Kohles Well	8.27	NR	8.03	12.37	2.23	10.88	2.75	1.44	4.13	0.70
Kohles and Kohles Well	15.92	NR	14.27	23.37	4.41	20.30	5.10	1.44	5.63	1.14
Paul George Mule Well	3.60	NR	1.88	2.15	0.41	2.01	0.60	1.02	0.75	0.12

NR=Not Reported

Quillinan et al., 2018; Aqueous Rare Earth Element Concentration

Sample ID	Sc (ng/L)	Y (ng/L)	La (ng/L)	Ce (ng/L)	Pr (ng/L)	Nd (ng/L)	Sm (ng/L)	Eu (ng/L)	Gd (ng/L)	Tb (ng/L)
Paul George Mule Well	2.69	NR	0.76	1.16	0.24	1.20	0.31	0.38	0.77	0.15
Paul George Kitty Well	3.69	NR	0.79	1.28	0.23	1.13	0.33	0.38	0.40	0.09
Paul George Kitty Well	3.02	NR	0.59	1.13	0.22	0.98	0.30	0.16	0.39	0.14
Paul George Kitty Well	3.12	NR	1.38	1.45	0.28	1.20	0.32	0.18	0.37	0.10
Paul George Reservoir	28.88	NR	9.35	18.43	3.08	15.95	4.69	1.49	6.32	1.17
Paul George Reservoir	56.28	NR	9.85	115.01	21.63	90.11	18.97	4.26	18.40	3.29
Kearn's Well	3.62	NR	6.80	8.48	1.67	7.66	1.83	1.07	2.15	0.35
Kearn's Well	2.27	NR	6.19	20.79	3.93	18.29	4.21	1.28	4.17	0.69
Paul George House Well	7.64	NR	0.65	0.95	0.20	0.85	0.26	0.26	0.29	0.09
Paul George House Well	8.89	NR	1.07	1.24	0.27	1.07	0.26	0.21	0.28	0.14
Pace Well	6.42	NR	2.53	2.57	0.44	2.01	0.37	0.21	0.46	0.07

NR=Not Reported

Quillinan et al., 2018; Aqueous Rare Earth Element Concentration

Sample ID	Sc (ng/L)	Y (ng/L)	La (ng/L)	Ce (ng/L)	Pr (ng/L)	Nd (ng/L)	Sm (ng/L)	Eu (ng/L)	Gd (ng/L)	Tb (ng/L)
Pace Well	15.32	NR	2.31	4.03	0.76	2.88	0.62	0.26	0.09	0.09
Kleinert Farms Fishing Pond	6.05	NR	4.62	5.07	0.97	3.58	0.60	0.20	0.93	0.22
Kleinert Farms Fishing Pond	11.53	NR	5.53	11.87	2.17	10.05	3.39	1.24	7.53	1.00
Kleinert Farms Fishing Pond	3.54	NR	7.07	7.53	1.44	5.12	0.97	0.29	0.51	0.24
Wallewein Reservoir South End	6.87	NR	2.89	6.94	1.31	6.98	2.23	0.82	3.09	0.65
Kearn's Reservoir	2.25	NR	5.08	9.74	2.02	5.62	0.82	0.44	1.17	0.25
Kearn's Reservoir	3.95	NR	11.11	23.71	4.39	20.61	5.86	1.85	10.46	1.94
Nagy Well	3.51	NR	0.85	0.83	0.19	0.69	0.19	0.19	0.24	0.08
Alme Well	12.44	NR	2.24	1.68	0.41	1.57	0.36	0.30	0.49	0.14
Wood Well	4.31	NR	7.69	1.88	2.13	5.49	2.00	3.65	2.91	1.38
Heise Hot Springs	27.18	NR	105.68	193.88	23.97	77.96	14.13	4.44	23.82	6.29
Lidy HS1	0.69	NR	1.10	1.20	0.15	0.71	0.25	0.76	0.36	0.05

NR=Not Reported

Quillinan et al., 2018; Aqueous Rare Earth Element Concentration

Sample ID	Sc (ng/L)	Y (ng/L)	La (ng/L)	Ce (ng/L)	Pr (ng/L)	Nd (ng/L)	Sm (ng/L)	Eu (ng/L)	Gd (ng/L)	Tb (ng/L)
Lidy HS2	1.07	NR	1.43	1.70	0.30	1.50	0.63	1.18	1.31	0.28
Green Cyn HS	1.31	NR	0.65	0.31	0.08	0.31	0.13	0.50	0.18	0.05
Sturm_W	0.09	NR	1.32	2.14	0.37	1.32	0.27	0.10	0.37	0.05
Condie HS	0.62	NR	2.91	0.78	0.17	0.85	0.35	1.67	0.66	0.10
Green House W	0.86	NR	2.25	1.46	0.31	1.08	0.29	0.71	0.38	0.05
Eckert Office W	1.06	NR	10.49	17.72	2.55	10.08	2.51	0.29	3.02	0.53
Campbell Well1	0.97	NR	1.20	0.15	0.33	1.97	0.69	0.17	1.19	0.27
Campbell Well2	0.69	NR	1.78	0.13	0.37	2.29	0.92	0.08	1.33	0.21
Miracle HS Well	0.49	NR	2.19	4.02	0.48	2.04	0.46	0.06	0.63	0.09
Driscoll Well	0.43	NR	2.48	7.99	0.75	2.79	0.46	0.62	1.02	0.25
Driscoll Spring	0.98	NR	2.76	8.40	0.82	2.62	0.66	0.72	1.06	0.22
CSI Well2	0.50	NR	1.26	1.11	0.40	1.63	0.43	0.05	0.75	0.09
Comore Loma 6	1.10	NR	5.54	1.54	0.69	3.13	0.94	2.83	1.91	0.33
Comore Loma 5	1.49	NR	2.58	1.53	0.33	1.40	0.53	2.77	0.87	0.09
Blackhawk Well2	1.47	NR	3.59	1.29	0.47	2.43	0.95	5.02	1.63	0.24
Blackhawk Well1	1.54	NR	2.17	0.85	0.18	0.92	0.58	4.53	0.98	0.10
RRG1	1.67	337.07	91.90	152.03	13.49	27.40	3.44	1.24	6.14	1.67
RRG2	0.90	NR	1.25	1.69	0.17	0.61	0.15	0.23	0.17	0.02

NR=Not Reported

Quillinan et al., 2018; Aqueous Rare Earth Element Concentration

Sample ID	Sc (ng/L)	Y (ng/L)	La (ng/L)	Ce (ng/L)	Pr (ng/L)	Nd (ng/L)	Sm (ng/L)	Eu (ng/L)	Gd (ng/L)	Tb (ng/L)
RRG7	1.29	2.50	3.78	2.93	0.27	0.95	0.15	0.86	0.21	0.04
RRG4	0.77	NR	1.42	0.70	0.10	0.30	0.12	0.27	0.15	0.01
Indian HS	1.59	NR	3.95	1.70	0.54	2.31	0.88	1.37	1.21	0.13
Grush Diary	0.33	NR	1.31	2.07	0.27	1.13	0.38	0.20	0.72	0.13
RRG USGS W	8.33	NR	6.71	9.29	1.88	6.47	1.02	1.07	1.07	0.11
RRG Crook Well	0.75	1.82	1.33	2.09	0.18	0.71	0.18	2.35	0.24	0.04
Milford Sweat	1.57	NR	1.68	1.02	0.27	1.15	0.34	1.99	0.42	0.03
Magic RLW Runoff	2.40	NR	5.09	5.43	1.01	4.12	1.10	2.30	1.56	0.33
Elk Creek HS1	2.37	NR	0.81	0.85	0.17	0.63	0.11	0.08	0.14	0.00
Elk Creek HS2	0.46	NR	4.24	3.43	0.63	2.35	0.37	0.18	0.36	0.03
Barron Well	1.17	NR	3.91	3.27	0.40	1.66	0.42	0.38	0.55	0.13
Wardrop HS1	0.73	NR	2.41	4.27	0.39	1.71	0.31	0.08	0.58	0.13
Magic RLW	2.14	NR	0.73	0.64	0.14	0.65	0.48	2.27	0.76	0.09
Prince Albert HSI	0.67	NR	6.71	13.63	1.58	7.92	1.72	0.19	1.70	0.31
Oakley WS	1.14	NR	0.88	2.06	0.27	1.13	0.09	0.03	0.18	0.03

NR=Not Reported

Quillinan et al., 2018; Aqueous Rare Earth Element Concentration

Sample ID	Sc (ng/L)	Y (ng/L)	La (ng/L)	Ce (ng/L)	Pr (ng/L)	Nd (ng/L)	Sm (ng/L)	Eu (ng/L)	Gd (ng/L)	Tb (ng/L)
Richard Austin W	0.43	NR	1.50	3.41	0.37	2.41	0.48	0.54	0.76	0.16
Marsh Creek W	8.81	NR	0.80	3.19	0.48	2.12	0.16	0.14	0.32	0.10
Sliger Well	0.60	NR	0.89	1.83	0.19	0.77	0.20	0.06	0.22	0.03
Banbury HS W	0.18	NR	1.62	2.58	0.51	2.15	0.43	0.08	0.60	0.09
Banbury HS	1.12	NR	1.24	1.19	0.24	0.91	0.19	0.05	0.25	0.02
Johnston Well	0.05	NR	5.52	5.99	1.17	4.20	0.70	0.09	0.93	0.16
Leo Ray Hill	--	NR	1.64	1.35	0.26	1.12	0.28	0.02	0.47	0.08
Leo Ray Road	--	NR	1.41	1.23	0.21	1.16	0.25	0.06	0.52	0.13
Hensley W	1.88	NR	25.13	37.90	7.07	30.26	6.24	0.62	6.14	0.97
Latty HS	0.79	NR	3.85	4.68	0.95	3.68	0.96	0.14	1.13	0.22
Laib W	58.12	NR	315.57	412.49	78.85	296.35	63.54	10.95	63.89	9.02
CSI W1	0.55	NR	1.23	1.46	0.36	1.77	0.44	0.07	0.61	0.07
Lary Anderson	0.30	NR	1.61	3.93	0.71	4.01	1.28	0.05	2.37	0.47
Pristine S	0.44	NR	1.87	3.02	0.71	3.10	0.65	0.06	0.92	0.12
TF High School	1.00	NR	2.24	4.36	1.10	5.02	0.95	0.92	1.26	0.17
Anderson CG W	8.00	NR	21.22	58.00	9.91	61.19	19.83	1.52	22.78	4.42
Butte City W	1.14	NR	1.53	0.73	0.22	0.96	0.37	0.83	0.47	0.04
Quidop S1	5.07	NR	2.01	3.30	0.50	2.45	0.82	0.59	1.06	0.20

NR=Not Reported

Quillinan et al., 2018; Aqueous Rare Earth Element Concentration

Sample ID	Sc (ng/L)	Y (ng/L)	La (ng/L)	Ce (ng/L)	Pr (ng/L)	Nd (ng/L)	Sm (ng/L)	Eu (ng/L)	Gd (ng/L)	Tb (ng/L)
Quidop S2 (ID 58)	1.62	NR	2.14	4.27	0.59	2.77	0.92	0.82	1.70	0.29
Yandell Warm Springs	0.06	NR	0.81	1.14	0.24	0.93	0.14	0.34	0.19	0.02
Skaggs Ranch	NR	NR	0.90	1.12	0.18	0.59	0.25	0.79	0.79	0.20
Durfee Hot Springs	NR	NR	1.06	2.51	0.29	1.05	0.31	0.31	0.39	0.06
Basin Cemetery	0.23	NR	1.72	0.48	0.19	0.47	0.17	0.24	0.19	0.11
Wybenga Dairy	NR	NR	0.67	0.46	0.17	0.45	0.32	1.74	0.36	0.12
David Bosen Well	52.40	64.12	82.50	166.55	20.30	74.94	11.22	11.10	18.29	5.45
Schwendi man Well	NR	NR	1.50	2.05	0.37	0.96	0.33	0.75	0.44	0.16
Clyde W Cinder Block Well	0.73	NR	1.27	1.77	0.25	0.94	0.18	0.97	0.31	0.04
Newdale City W	0.44	NR	3.33	2.31	0.69	3.12	0.74	1.55	1.36	0.28
Spackman Well	0.61	NR	3.30	2.18	0.63	2.88	0.65	0.30	1.04	0.19
Fort Hall Thermal W	0.06	NR	1.88	1.32	0.37	1.07	0.37	0.72	0.68	0.22

NR=Not Reported

Quillinan et al., 2018; Aqueous Rare Earth Element Concentration

Sample ID	Sc (ng/L)	Y (ng/L)	La (ng/L)	Ce (ng/L)	Pr (ng/L)	Nd (ng/L)	Sm (ng/L)	Eu (ng/L)	Gd (ng/L)	Tb (ng/L)
Riverdale Resort	NR	NR	0.97	2.16	0.72	2.01	0.45	0.89	0.63	0.30
Downata H.S.	NR	NR	1.58	2.17	0.50	1.36	0.54	2.31	0.83	0.10
Lava H.S.	NR	NR	1.37	2.31	0.76	2.46	0.56	3.36	0.90	0.14
Hailey H.S.	NR	NR	3.14	7.21	0.71	2.57	0.39	0.24	0.50	0.07
Frenchman's Bend H.S.	NR	NR	9.65	32.21	2.47	10.42	1.59	0.65	1.94	0.27
Worswick H.S.	NR	NR	0.48	0.87	0.14	0.32	0.11	0.12	0.22	0.05
Wolf H.S.	NR	NR	100.62	182.56	19.73	68.47	10.73	2.15	11.22	1.51
Tindall Well North	NR	NR	3.15	5.77	0.78	2.21	0.45	0.42	0.71	0.13
Bruneau H.S. well	NR	NR	2.24	0.54	0.29	0.28	0.13	0.19	0.19	0.05
Lower Indian Bathtub H.S.	NR	NR	1.34	0.94	0.17	0.27	0.07	0.17	0.22	0.05
Piranha well	NR	NR	0.96	0.75	0.21	0.40	0.13	0.29	0.23	0.05
Ward well #1	NR	NR	0.76	1.37	0.25	0.60	0.20	1.19	0.36	0.07
Shane Ward well	NR	NR	1.47	1.89	0.29	0.69	0.25	0.90	0.39	0.08
Irwin well #1	NR	NR	0.92	1.39	0.24	0.60	0.25	0.21	0.22	0.05

NR=Not Reported

Quillinan et al., 2018; Aqueous Rare Earth Element Concentration

Sample ID	Sc (ng/L)	Y (ng/L)	La (ng/L)	Ce (ng/L)	Pr (ng/L)	Nd (ng/L)	Sm (ng/L)	Eu (ng/L)	Gd (ng/L)	Tb (ng/L)
Comore Loma 7	1.05	11.08	7.02	3.45	1.12	3.32	0.55	2.23	0.86	0.14
Rush Warm Springs 1	NR	NR	1.73	2.09	0.29	1.19	0.36	4.09	0.73	0.15
Hawley Warm Springs	NR	NR	1.51	1.15	0.36	1.26	0.20	1.92	0.66	0.09
Elkhorn Warm Springs	NR	NR	1.51	0.93	0.26	0.97	0.24	2.58	0.42	0.05
Doug Mills Hot Well	NR	NR	16.43	25.33	2.25	9.33	2.42	7.70	3.77	0.63
Charles Crittenden	NR	NR	0.80	0.94	0.09	0.34	0.42	12.36	0.77	0.09
Ashton Warms Springs	NR	NR	23.60	46.01	5.40	17.02	3.02	0.40	3.63	0.66
Warm River Springs 1	NR	NR	2.53	3.45	0.56	1.85	0.44	0.20	0.71	0.21
Site 14	NR	NR	0.81	1.14	0.22	0.53	0.28	1.90	0.25	0.12
USGS 7	NR	NR	1.79	3.15	0.34	1.10	0.18	0.52	0.20	0.05
500m Spring	NR	NR	3.18	5.06	0.63	1.83	0.41	0.21	0.60	0.19
Mountain Home AFB #1	NR	NR	0.53	0.86	0.19	0.38	0.09	0.32	0.15	0.05

NR=Not Reported

Quillinan et al., 2018; Aqueous Rare Earth Element Concentration

Sample ID	Sc (ng/L)	Y (ng/L)	La (ng/L)	Ce (ng/L)	Pr (ng/L)	Nd (ng/L)	Sm (ng/L)	Eu (ng/L)	Gd (ng/L)	Tb (ng/L)
Mountain Home AFB #2	NR	NR	1.23	2.43	0.32	0.89	0.26	0.35	0.31	0.19
Gonsales Thermal Well	NR	NR	1.83	2.85	0.37	1.00	0.32	0.09	0.34	0.07
SVR-5 Barron Heating Well (Grandpa Barron Well)	NR 1.49	NR 5.10	2449.19 9.44	6458.96 14.45	450.87 1.52	1406.75 4.15	184.41 0.78	31.98 0.38	229.46 0.94	36.38 0.29
Strom Well 2015	NR	NR	12.16	42.50	1.73	5.09	0.74	0.07	0.90	0.13
SVR-4 Grandpa Barron Spring	NR NR	NR NR	501.05 13.77	1201.39 20.57	89.94 3.68	270.58 17.40	40.34 3.47	7.34 0.83	48.77 4.69	7.19 0.63
Higgs Well, SVR-9	0.73	8.65	5.52	9.25	1.10	4.04	0.74	0.64	0.98	0.19
Soda Geyser Site #6	NR	0.73	0.44	0.83	0.37	nd	0.01	0.04	0.08	0.05
Soda Geyser Site #5	NR	1.42	0.14	0.31	nd	nd	0.01	0.03	0.04	0.01
Soda Geyser Site #4	NR	9.27	0.72	1.12	0.05	0.11	0.09	0.20	0.13	0.16

NR=Not Reported

Quillinan et al., 2018; Aqueous Rare Earth Element Concentration

Sample ID	Sc (ng/L)	Y (ng/L)	La (ng/L)	Ce (ng/L)	Pr (ng/L)	Nd (ng/L)	Sm (ng/L)	Eu (ng/L)	Gd (ng/L)	Tb (ng/L)
Soda Geyser Site #3	NR	16.97	3.27	0.82	nd	0.67	0.01	0.03	0.11	0.04
Soda Geyser Site #2	0.44	30.01	8.96	10.33	5.13	7.43	3.81	2.65	4.35	4.12
Soda Geyser Site #1	0.51	49.59	9.70	10.90	3.27	8.04	1.81	2.12	2.55	2.42
Soda Geyser Site #0	0.56	50.26	13.22	13.93	2.17	6.74	1.35	1.73	3.23	2.79
Soda_Geyser	5.57	NR	12.94	12.17	2.31	9.00	1.47	0.59	2.08	0.33
Soda Creek near Mommoth	7.20	NR	5.79	2.60	0.89	3.98	0.67	0.52	1.17	0.20
Soda Creek near Ocatagon	15.12	NR	7.62	4.94	1.07	4.30	0.67	1.29	1.03	0.15
Sulphure Spring	38.80	NR	1595.29	1226.44	259.48	962.50	132.29	27.45	164.46	22.92
Steamboat Spring filtered	4.12	NR	6.34	7.15	1.36	6.61	1.58	0.95	2.30	0.36
Pavilion Well	23.92	NR	202.05	188.26	38.43	138.40	19.30	3.93	23.45	3.62
Mammoth Spring	58.72	NR	14.14	14.96	2.72	14.00	2.48	1.07	4.65	0.90

NR=Not Reported

Quillinan et al., 2018; Aqueous Rare Earth Element Concentration

Sample ID	Sc (ng/L)	Y (ng/L)	La (ng/L)	Ce (ng/L)	Pr (ng/L)	Nd (ng/L)	Sm (ng/L)	Eu (ng/L)	Gd (ng/L)	Tb (ng/L)
Hooper Spring	54.18	NR	17.42	21.61	3.80	21.06	4.47	2.02	7.50	1.23
Octagon Spring	147.21	NR	62.23	54.91	10.15	47.67	8.58	2.40	15.67	3.00
Lovers Delight	32.65	NR	20.46	17.38	3.14	14.95	2.52	1.08	4.75	0.84
Outhouse Spring	2.89	NR	8.77	10.99	1.93	8.73	1.76	0.71	2.75	0.47

NR=Not Reported

Quillinan et al., 2018; Aqueous Rare Earth Element Concentration

Sample ID	Dy (ng/L)	Ho (ng/L)	Er (ng/L)	Tm (ng/L)	Yb (ng/L)	Lu (ng/L)
MD-2	2.34	0.45	1.32	0.16	0.75	0.17
MD-3	1.22	0.25	0.63	0.07	0.43	0.06
MD-4	1.18	0.32	0.97	0.20	1.19	0.26
MD-5	0.55	0.15	0.47	0.13	0.63	0.21
MD-6	0.25	0.07	0.22	0.05	0.22	0.04
MD-7	0.91	0.24	0.61	0.16	0.74	0.19
MD-8	0.65	0.12	0.51	0.08	0.59	0.15
PRB-10	0.25	0.07	0.26	0.10	0.38	0.31
PRB-11	0.24	0.07	0.23	0.06	0.28	0.19
PRB-12	0.13	0.04	0.09	0.03	0.08	0.03
PRB-13	0.05	0.02	0.08	0.02	0.09	0.02
PRB-14	0.96	0.28	1.00	0.17	1.00	0.20
PRB-15	2.90	2.08	14.04	2.65	18.59	3.55
PRB-16	2.19	0.87	4.22	0.95	7.35	1.83
PRB-17	0.68	0.36	2.52	0.61	5.05	1.31
PRB-18	0.25	0.07	0.23	0.08	0.40	0.15
PRB-19	0.05	0.12	3.16	1.42	15.65	3.98
LC-31	10.41	4.49	28.42	7.57	65.65	9.53
WA-33	0.89	0.24	0.52	0.19	0.98	0.35
WA-34	0.21	0.09	0.14	0.09	0.22	0.09
WA-35	0.95	0.26	0.77	0.19	1.18	0.32
WA-36	1.39	0.44	1.74	0.32	2.44	0.45
WA-37	0.45	0.14	0.54	0.11	1.00	0.24
WA-40	1.08	0.16	0.92	0.29	5.06	2.23
LB-42	1.14	0.30	0.85	0.15	0.90	0.20
LB-43	2.31	0.59	1.97	0.25	1.53	0.26
LB-44	1.99	0.42	1.14	0.14	0.89	0.16
LB-45	1.22	0.23	0.73	0.12	0.95	0.19
LB-46	0.50	0.10	0.33	0.04	0.33	0.04
LB-47	0.09	0.09	0.09	0.09	0.32	0.12

NR=Not Reported

Quillinan et al., 2018; Aqueous Rare Earth Element Concentration

Sample ID	Dy (ng/L)	Ho (ng/L)	Er (ng/L)	Tm (ng/L)	Yb (ng/L)	Lu (ng/L)
MS-50	0.23	0.10	0.18	0.02	0.18	0.04
MS-51	0.64	0.25	1.22	0.22	1.45	0.23
MS-52	1.41	0.43	1.90	0.37	2.93	0.47
MS-54	0.07	0.02	0.08	0.01	0.10	0.02
MS-55	0.42	0.10	0.31	0.04	0.33	0.06
MS-56	0.09	0.02	0.08	0.01	0.07	0.02
MS-57	0.04	0.01	0.06	0.01	0.09	0.02
MS-58	14.82	12.50	95.68	20.49	165.05	26.48
MS-59	0.87	0.21	0.51	0.05	0.27	0.05
WB-MT-8-14-1	59.61	13.12	39.97	5.06	36.92	6.69
WB-ND-8-14-2	18.12	4.96	10.06	1.05	8.42	1.32
WB-ND-8-14-3	5.05	1.06	2.59	0.58	2.97	0.56
WB-ND-8-14-4	26.63	6.80	13.46	1.32	10.33	1.85
WB-ND-8-14-5	11.86	1.96	6.30	0.60	5.69	1.12
WB-ND-8-14-6	7.52	1.77	5.28	0.66	5.96	0.97
WB-ND-8-14-7	3.88	2.71	2.99	0.71	3.91	0.71
WB-ND-8-14-8	0.08	0.09	0.05	0.08	0.24	0.03
WB-ND-8-14-9	6.80	2.35	5.39	0.70	7.28	1.43
WB-ND-8-14-10	32.66	5.72	14.91	1.49	6.67	1.23
WB-ND-8-14-11	9.86	2.24	6.30	0.57	5.37	1.00

NR=Not Reported

Quillinan et al., 2018; Aqueous Rare Earth Element Concentration

Sample ID	Dy (ng/L)	Ho (ng/L)	Er (ng/L)	Tm (ng/L)	Yb (ng/L)	Lu (ng/L)
WB-ND-8-14-12	24.36	5.34	11.01	0.94	9.62	1.90
WB-ND-8-14-14	18.48	3.30	8.98	1.10	7.39	1.33
1A (BS-101)	11.66	2.55	7.29	1.24	6.79	1.74
2A (BS-107)	0.42	0.29	0.24	0.28	0.64	0.25
3A(BS-112)	6.17	1.58	3.69	0.63	3.92	0.83
4A (BS-116)	0.53	0.07	0.17	0.13	NR	0.07
5A (BS-120)	1.68	0.80	1.24	0.49	2.07	0.58
GR1 Dup	8.43	3.25	8.73	2.06	11.81	3.79
6 HD Dup	17.45	4.70	11.59	3.19	14.20	4.05
6 HM	10.62	2.81	5.89	1.69	11.61	2.83
Sc.01.14.14 ST	5.12	2.34	10.13	3.35	40.17	16.10
BE.01.14.14.ST	24.02	7.90	37.94	7.95	83.20	20.30
CM-1	3.76	1.22	2.39	0.79	2.61	1.06
DC-1	43.00	8.76	21.59	1.63	9.16	1.38
RS-1	5.20	0.88	2.30	0.62	4.85	1.96
CC-1	15.91	3.83	8.89	1.12	6.17	1.04
D-5	0.57	0.19	0.60	NR	0.54	0.13
MA-2	4.49	0.91	2.27	0.98	9.09	3.48
LS #20	2.15	0.73	5.44	1.68	27.68	9.56
NH #1	1.11	0.21	0.68	NR	0.45	0.07
14-TX-7B	0.61	0.07	0.12	0.08	0.47	0.19
14-TX-8B	1.90	0.28	1.43	0.15	1.32	0.19

NR=Not Reported

Quillinan et al., 2018; Aqueous Rare Earth Element Concentration

Sample ID	Dy (ng/L)	Ho (ng/L)	Er (ng/L)	Tm (ng/L)	Yb (ng/L)	Lu (ng/L)
14-TX-9B	0.31	0.22	0.19	0.12	0.85	0.17
14-TX-23B	0.13	0.05	NR	0.00	NR	NR
14-TX-24B	0.12	0.04	NR	0.02	NR	NR
14-TX-25B	NR	NR	0.03	NR	NR	0.01
14-TX-26B	0.16	NR	0.12	NR	0.16	0.03
14-TX-27B	0.13	NR	NR	NR	0.15	0.05
14-TX-28B	3.41	0.25	0.51	0.10	0.34	0.14
14-TX-41B	25.53	5.04	13.85	1.76	10.34	1.70
14-TX-48B	8.65	1.23	2.80	0.29	2.45	0.40
14-TX-49B	115.94	24.05	63.83	7.27	44.04	7.44
Kohles and Kohles Well	4.99	1.22	3.93	0.57	3.70	0.63
Kohles and Kohles Well	6.46	1.47	4.33	0.62	3.83	0.65
Paul George Mule Well	0.88	0.25	0.92	0.16	1.26	0.25

NR=Not Reported

Quillinan et al., 2018; Aqueous Rare Earth Element Concentration

Sample ID	Dy (ng/L)	Ho (ng/L)	Er (ng/L)	Tm (ng/L)	Yb (ng/L)	Lu (ng/L)
Paul George Mule Well	0.45	0.19	0.55	0.14	0.83	0.20
Paul George Kitty Well	0.90	0.28	1.14	0.20	1.60	0.30
Paul George Kitty Well	1.21	0.39	1.54	0.30	2.28	0.41
Paul George Kitty Well	1.12	0.32	1.43	0.25	2.05	0.38
Paul George Reservoir	8.66	2.17	8.03	1.26	9.29	1.65
Paul George Reservoir	19.25	4.20	13.06	1.82	13.29	2.24
Kearn's Well	2.14	0.51	1.59	0.23	1.45	0.24
Kearn's Well	4.05	0.75	2.13	0.29	1.75	0.28
Paul George House Well	0.70	0.21	0.72	0.12	0.82	0.15
Paul George House Well	0.63	0.23	0.70	0.16	0.77	0.17
Pace Well	0.47	0.11	0.30	0.04	0.23	0.04

NR=Not Reported

Quillinan et al., 2018; Aqueous Rare Earth Element Concentration

Sample ID	Dy (ng/L)	Ho (ng/L)	Er (ng/L)	Tm (ng/L)	Yb (ng/L)	Lu (ng/L)
Pace Well	0.68	0.23	0.53	0.14	0.49	0.16
Kleinert Farms Fishing Pond	1.42	0.39	1.27	0.20	1.21	0.21
Kleinert Farms Fishing Pond	6.23	1.59	4.80	1.00	5.65	1.12
Kleinert Farms Fishing Pond	1.26	0.34	0.95	0.18	0.90	0.18
Wallewein Reservoir South End	3.93	1.04	3.26	0.59	3.76	0.74
Kearn's Reservoir	1.27	0.32	0.80	0.14	0.44	0.13
Kearn's Reservoir	12.00	3.51	11.27	2.11	12.32	2.33
Nagy Well	0.50	0.19	0.60	0.11	0.70	0.15
Alme Well	0.66	0.20	0.49	0.11	0.33	0.11
Wood Well	4.17	2.03	4.83	1.97	6.40	2.26
Heise Hot Springs	47.88	11.50	33.19	5.05	30.53	4.51
Lidy HS1	0.46	0.11	0.37	0.05	0.33	0.04

NR=Not Reported

Quillinan et al., 2018; Aqueous Rare Earth Element Concentration

Sample ID	Dy (ng/L)	Ho (ng/L)	Er (ng/L)	Tm (ng/L)	Yb (ng/L)	Lu (ng/L)
Lidy HS2	2.21	0.48	1.38	0.17	1.04	0.11
Green Cyn HS	0.42	0.03	0.10	0.02	0.10	0.00
Sturm_W	0.44	0.12	0.33	0.07	0.33	0.05
Condie HS	0.97	0.28	0.94	0.14	0.76	0.14
Green House W	0.35	0.08	0.29	0.04	0.30	0.02
Eckert Office W	3.29	0.65	1.97	0.28	1.91	0.22
Campbell Well1	1.23	0.39	1.06	0.23	1.02	0.13
Campbell Well2	1.37	0.33	1.05	0.21	0.85	0.10
Miracle HS Well	0.55	0.12	0.31	0.06	0.37	0.07
Driscoll Well	1.42	0.28	0.79	0.10	0.52	0.05
Driscoll Spring	1.11	0.26	0.82	0.11	0.64	0.07
CSI Well2	0.64	0.15	0.38	0.05	0.29	0.05
Comore Loma 6	3.03	0.93	3.73	0.66	4.80	0.87
Comore Loma 5	0.78	0.23	0.84	0.15	1.15	0.18
Blackhawk Well2	2.31	0.67	2.60	0.45	3.18	0.56
Blackhawk Well1	1.37	0.36	1.55	0.28	2.10	0.37
RRG1	19.68	5.84	20.71	2.99	17.17	2.13
RRG2	0.10	0.01	0.06	0.01	0.04	nd

NR=Not Reported

Quillinan et al., 2018; Aqueous Rare Earth Element Concentration

Sample ID	Dy (ng/L)	Ho (ng/L)	Er (ng/L)	Tm (ng/L)	Yb (ng/L)	Lu (ng/L)
RRG7	0.15	0.03	0.08	0.01	0.06	0.01
RRG4	0.07	0.03	0.07	0.01	0.05	0.01
Indian HS	1.02	0.26	0.89	0.13	0.76	0.09
Grush Diary	1.14	0.20	0.53	0.06	0.27	0.05
RRG USGS W	0.73	0.14	0.42	0.07	0.35	0.07
RRG Crook Well	0.13	0.02	0.06	0.01	0.06	0.01
Milford Sweat	0.35	0.10	0.29	0.05	0.23	0.05
Magic RLW Runoff	2.06	0.61	1.97	0.36	1.70	0.35
Elk Creek HS1	0.09	0.03	0.07	0.03	0.04	0.03
Elk Creek HS2	0.22	0.05	0.14	0.04	0.09	0.03
Barron Well	1.19	0.19	0.66	0.11	0.80	0.13
Wardrop HS1	1.37	0.16	0.59	0.13	0.95	0.16
Magic RLW	0.89	0.21	0.64	0.10	0.53	0.09
Prince Albert HS1	2.25	0.46	1.33	0.19	1.28	0.15
Oakley WS	0.25	0.02	0.05	0.00	0.04	nd

NR=Not Reported

Quillinan et al., 2018; Aqueous Rare Earth Element Concentration

Sample ID	Dy (ng/L)	Ho (ng/L)	Er (ng/L)	Tm (ng/L)	Yb (ng/L)	Lu (ng/L)
Richard Austin W	1.04	0.19	0.58	0.08	0.39	0.06
Marsh Creek W	1.13	0.15	0.47	0.07	0.45	0.02
Sliger Well	0.26	0.04	0.11	0.02	0.12	NR
Banbury HS W	0.71	0.18	0.52	0.09	0.47	0.09
Banbury HS	0.23	0.07	0.17	0.05	0.21	0.06
Johnston Well	1.19	0.29	0.98	0.10	0.53	0.07
Leo Ray Hill	0.84	0.22	0.82	0.09	0.43	0.06
Leo Ray Road	1.27	0.38	1.39	0.15	0.95	0.13
Hensley W	5.79	1.12	3.29	0.48	3.29	0.45
Latty HS	1.59	0.36	1.08	0.18	1.02	0.17
Laib W	50.85	9.70	29.09	3.95	24.40	3.79
CSI W1	0.56	0.13	0.38	0.07	0.25	0.05
Lary Anderson	3.64	0.94	2.85	0.35	1.60	0.25
Pristine S	0.78	0.17	0.49	0.07	0.30	0.05
TF High School	1.29	0.33	1.10	0.18	1.11	0.25
Anderson CG W	28.21	5.56	16.38	2.25	18.11	1.98
Butte City W	0.33	0.07	0.24	0.04	0.27	0.01
Quidop S1	1.55	0.41	1.47	0.24	1.65	0.31

NR=Not Reported

Quillinan et al., 2018; Aqueous Rare Earth Element Concentration

Sample ID	Dy (ng/L)	Ho (ng/L)	Er (ng/L)	Tm (ng/L)	Yb (ng/L)	Lu (ng/L)
Quidop S2 (ID 58)	1.83	0.37	1.30	0.21	1.81	0.30
Yandell Warm Springs	0.19	0.04	0.19	0.02	0.14	0.01
Skaggs Ranch	3.13	1.20	4.94	0.78	5.11	0.87
Durfee Hot Springs	0.32	0.09	0.27	0.05	0.45	0.08
Basin Cemetery	0.27	0.10	0.21	0.09	0.21	0.10
Wybenga Dairy	0.29	0.14	0.27	0.12	0.21	0.11
David Bosen Well	13.12	3.20	5.77	0.74	15.19	3.78
Schwendi man Well	0.53	0.24	0.54	0.17	0.51	0.26
Clyde W Cinder Block Well	0.50	0.15	0.49	0.10	0.50	0.10
	0.64	0.22	0.50	0.17	0.46	0.16
Newdale City W	2.58	0.69	2.55	0.38	2.20	0.35
Spackman Well	1.57	0.45	1.61	0.28	2.22	0.41
Fort Hall Thermal W	1.52	0.52	1.73	0.34	1.71	0.33

NR=Not Reported

Quillinan et al., 2018; Aqueous Rare Earth Element Concentration

Sample ID	Dy (ng/L)	Ho (ng/L)	Er (ng/L)	Tm (ng/L)	Yb (ng/L)	Lu (ng/L)
Riverdale Resort	1.18	0.44	1.14	0.35	1.47	0.45
Downata H.S.	0.45	0.16	0.53	0.08	0.53	0.11
Lava H.S.	1.16	0.30	0.81	0.09	0.79	0.13
Hailey H.S.	0.38	0.13	0.21	0.06	0.41	0.07
Frenchman's Bend H.S.	1.88	0.38	1.17	0.11	1.05	0.38
Worswick H.S.	0.16	0.05	0.17	0.05	0.36	0.10
Wolf H.S.	8.57	1.65	5.35	0.58	3.96	0.55
Tindall Well North	0.61	0.15	0.26	0.05	0.36	0.09
Bruneau H.S. well	0.15	0.09	0.30	0.05	0.20	0.15
Lower Indian Bathtub H.S.	0.10	0.05	0.11	0.05	0.16	0.07
Piranha well	0.17	0.05	0.28	0.05	0.25	0.05
Ward well #1	0.26	0.07	0.27	0.05	0.31	0.06
Shane Ward well	0.25	0.15	0.61	0.07	0.28	0.12
Irwin well #1	0.19	0.05	0.15	0.05	0.20	0.05

NR=Not Reported

Quillinan et al., 2018; Aqueous Rare Earth Element Concentration

Sample ID	Dy (ng/L)	Ho (ng/L)	Er (ng/L)	Tm (ng/L)	Yb (ng/L)	Lu (ng/L)
Comore Loma 7	1.05	0.28	0.97	0.16	1.06	0.17
Rush Warm Springs 1	1.01	0.30	1.00	0.13	0.53	0.20
Hawley Warm Springs	0.32	0.10	0.22	0.05	0.15	0.09
Elkhorn Warm Springs	0.31	0.05	0.30	0.05	0.09	0.05
Doug Mills Hot Well	4.31	1.15	4.37	0.61	3.41	0.62
Charles Crittenden	0.27	0.09	0.20	0.09	0.36	0.09
Ashton Warms Springs	4.64	0.95	2.61	0.37	2.12	0.30
Warm River Springs 1	1.65	0.50	1.51	0.24	1.40	0.27
Site 14	0.18	0.15	0.23	0.10	0.23	0.20
USGS 7 500m Spring	0.11	0.05	0.07	0.05	0.09	0.05
1.09	0.34	0.92	0.19	0.91	0.28	
Mountain Home AFB #1	0.13	0.06	0.11	0.06	0.59	0.08

NR=Not Reported

Quillinan et al., 2018; Aqueous Rare Earth Element Concentration

Sample ID	Dy (ng/L)	Ho (ng/L)	Er (ng/L)	Tm (ng/L)	Yb (ng/L)	Lu (ng/L)
Mountain Home AFB #2	0.39	0.24	0.46	0.22	0.80	0.29
Gonsales Thermal Well	0.46	0.12	0.30	0.05	0.34	0.05
SVR-5	225.26	46.40	134.82	18.13	105.99	14.05
Barron Heating Well (Grandpa Barron Well)	1.43	0.41	1.09	0.25	1.69	0.45
Strom Well 2015	0.63	0.10	0.43	0.05	0.17	0.05
SVR-4	42.24	8.70	25.49	3.39	19.58	2.73
Grandpa Barron Spring	5.79	1.26	4.29	0.59	5.31	0.88
Higgs Well, SVR-9	1.36	0.34	1.22	0.20	1.35	0.23
Soda Geyser Site #6	0.10	0.06	0.09	0.04	0.10	0.05
Soda Geyser Site #5	0.05	0.02	0.08	0.01	0.27	0.02
Soda Geyser Site #4	0.34	0.21	0.64	0.20	0.95	0.28

NR=Not Reported

Quillinan et al., 2018; Aqueous Rare Earth Element Concentration

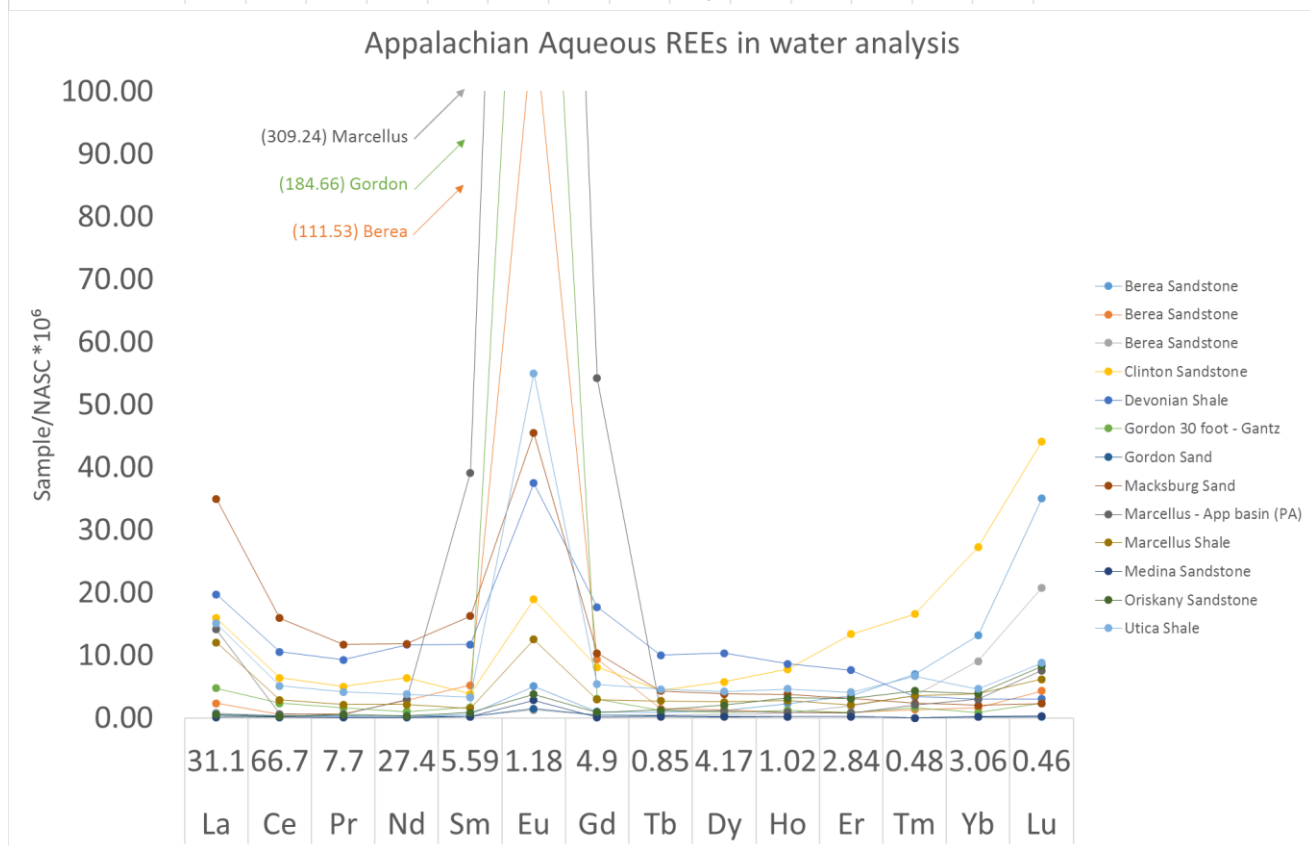
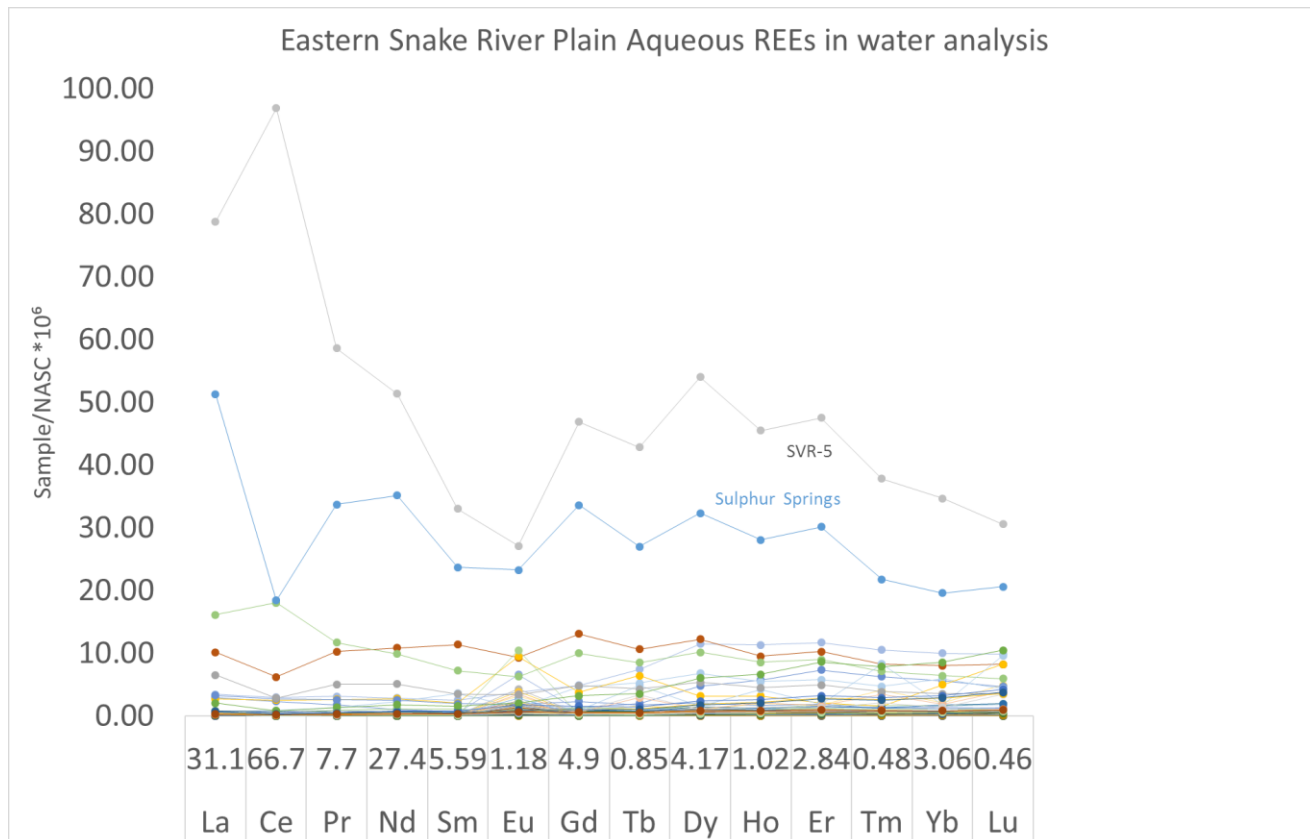
Sample ID	Dy (ng/L)	Ho (ng/L)	Er (ng/L)	Tm (ng/L)	Yb (ng/L)	Lu (ng/L)
Soda Geyser Site #3	0.76	0.20	0.97	0.17	1.43	0.21
Soda Geyser Site #2	6.41	4.29	5.28	3.96	5.42	4.41
Soda Geyser Site #1	4.66	2.13	4.58	1.64	5.59	1.79
Soda Geyser Site #0	3.98	1.45	3.70	0.99	4.02	1.58
Soda_Geysers	2.63	0.69	2.47	0.37	2.25	0.38
Soda Creek near Mommoth	1.88	0.54	2.08	0.34	2.29	0.47
Soda Creek near Ocatagon	1.41	0.37	1.39	0.24	1.55	0.33
Sulphure Spring	134.66	28.58	85.47	10.43	59.79	9.46
Steamboat Spring filtered	2.90	0.79	2.60	0.42	2.45	0.47
Pavilion Well	22.30	4.55	13.89	1.83	10.70	1.65
Mammoth Spring	7.74	2.18	7.93	1.23	8.58	1.62

NR=Not Reported

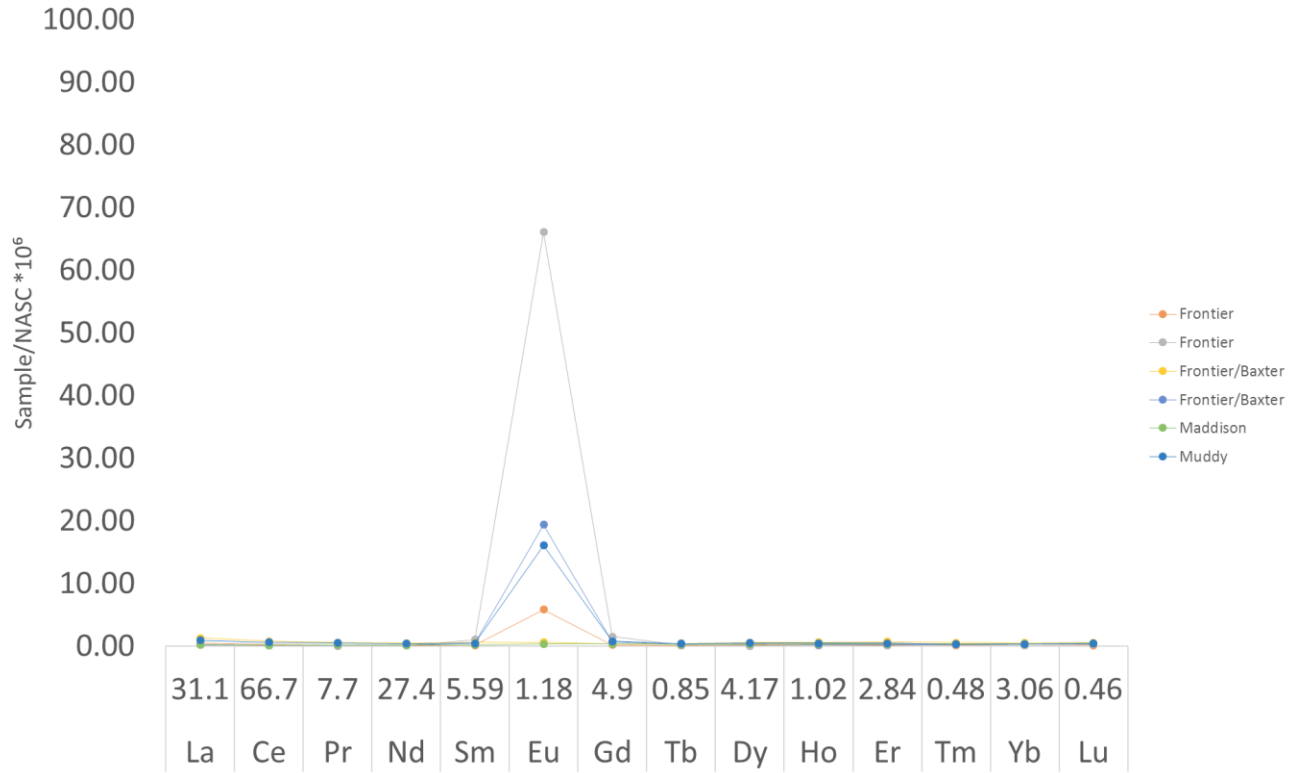
Quillinan et al., 2018; Aqueous Rare Earth Element Concentration

Sample ID	Dy (ng/L)	Ho (ng/L)	Er (ng/L)	Tm (ng/L)	Yb (ng/L)	Lu (ng/L)
Hooper Spring	9.71	2.60	9.14	1.39	9.86	1.95
Octagon Spring	25.08	6.72	24.31	3.75	26.09	4.80
Lovers Delight	7.21	2.06	7.67	1.20	8.81	1.71
Outhouse Spring	3.47	0.82	2.66	0.39	2.40	0.42

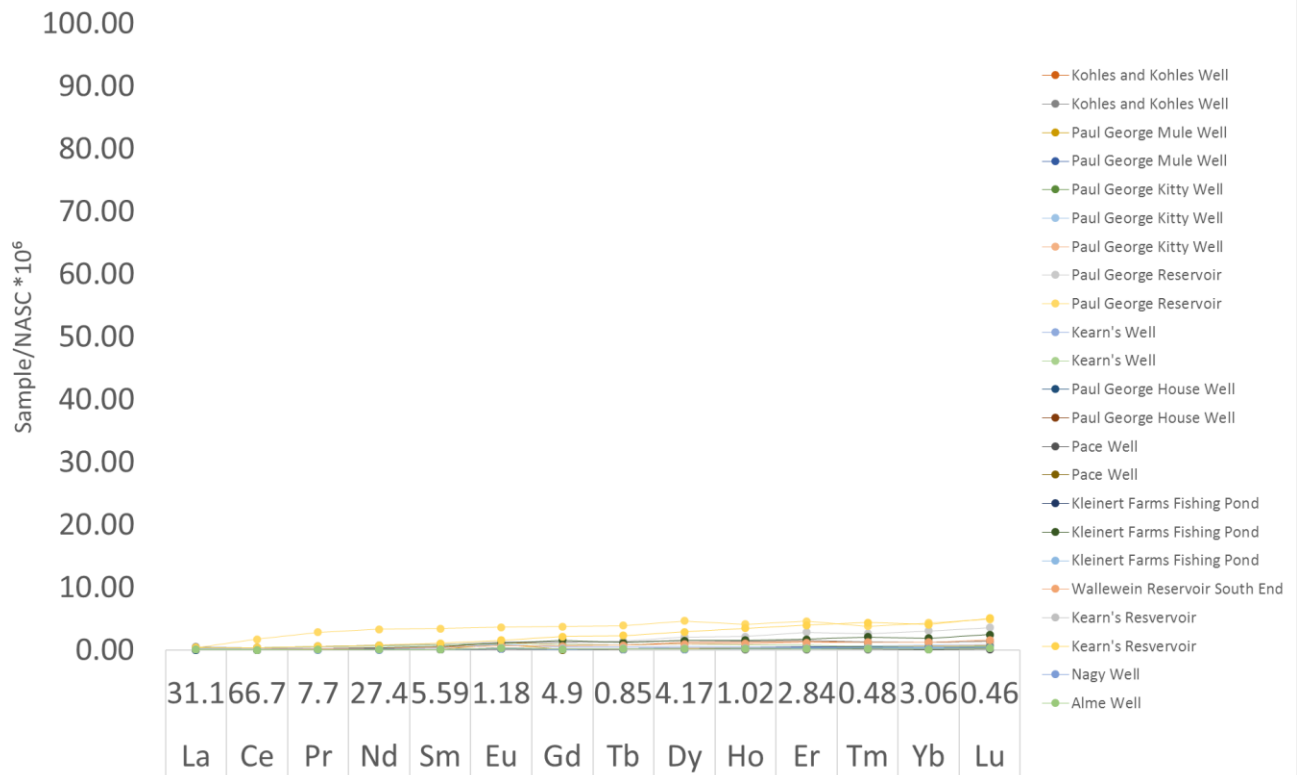
NR=Not Reported

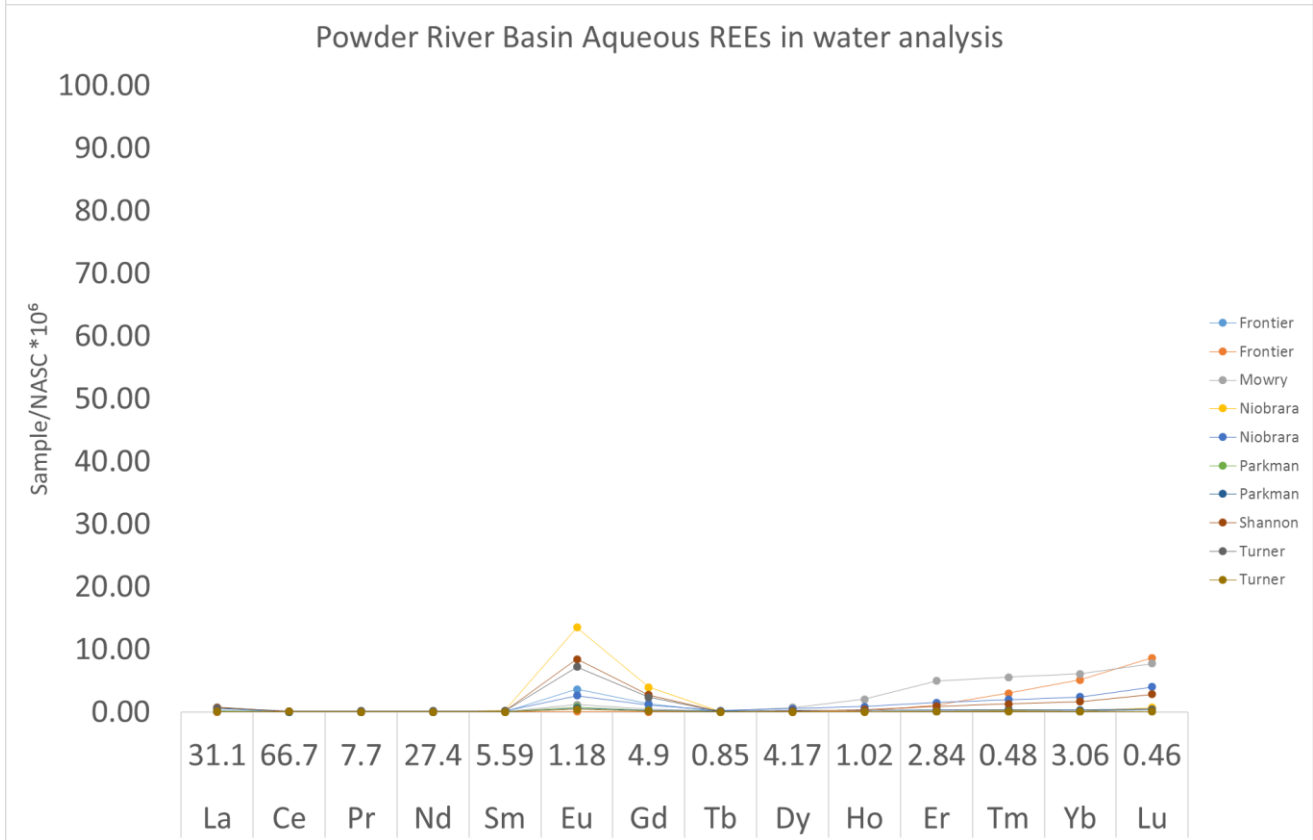
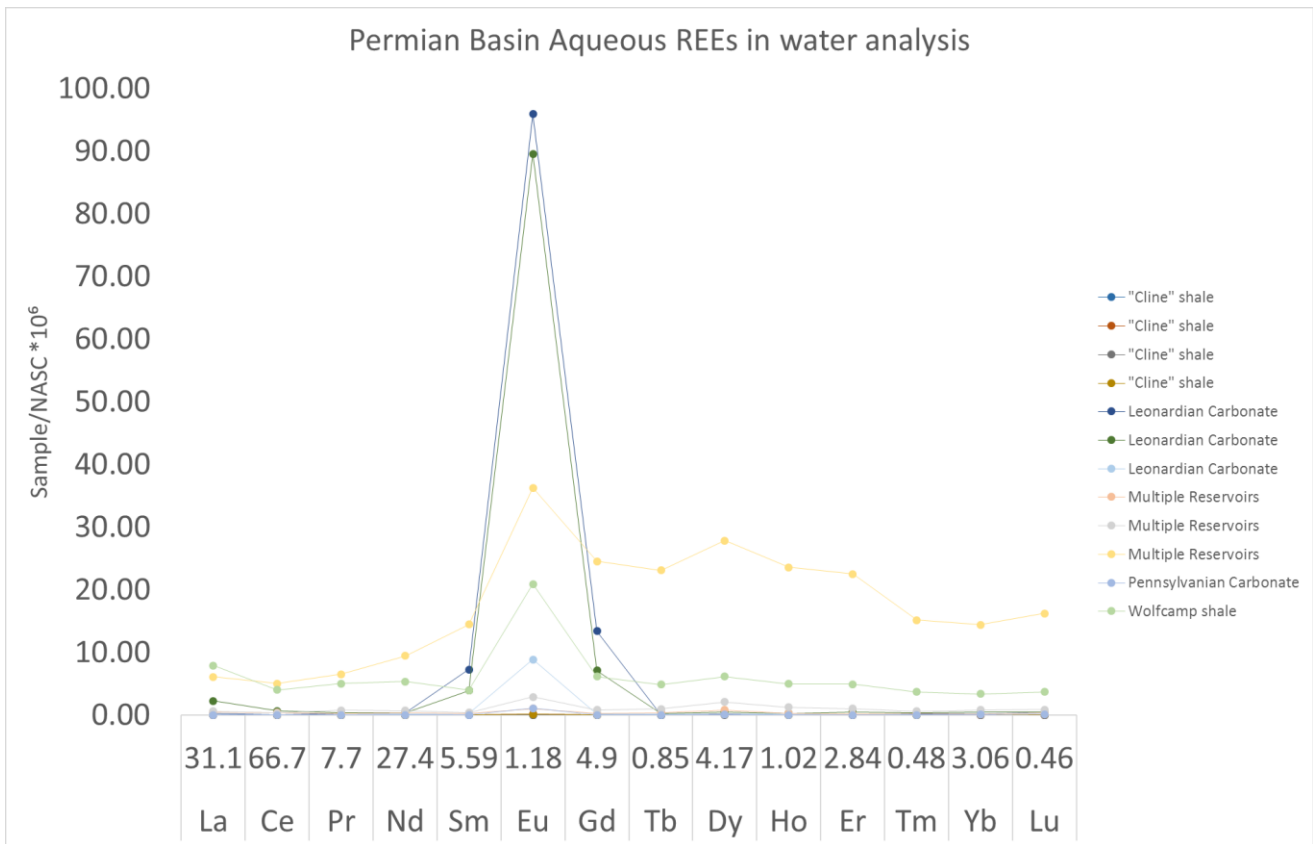


Green River Basin Aqueous REEs in water analysis

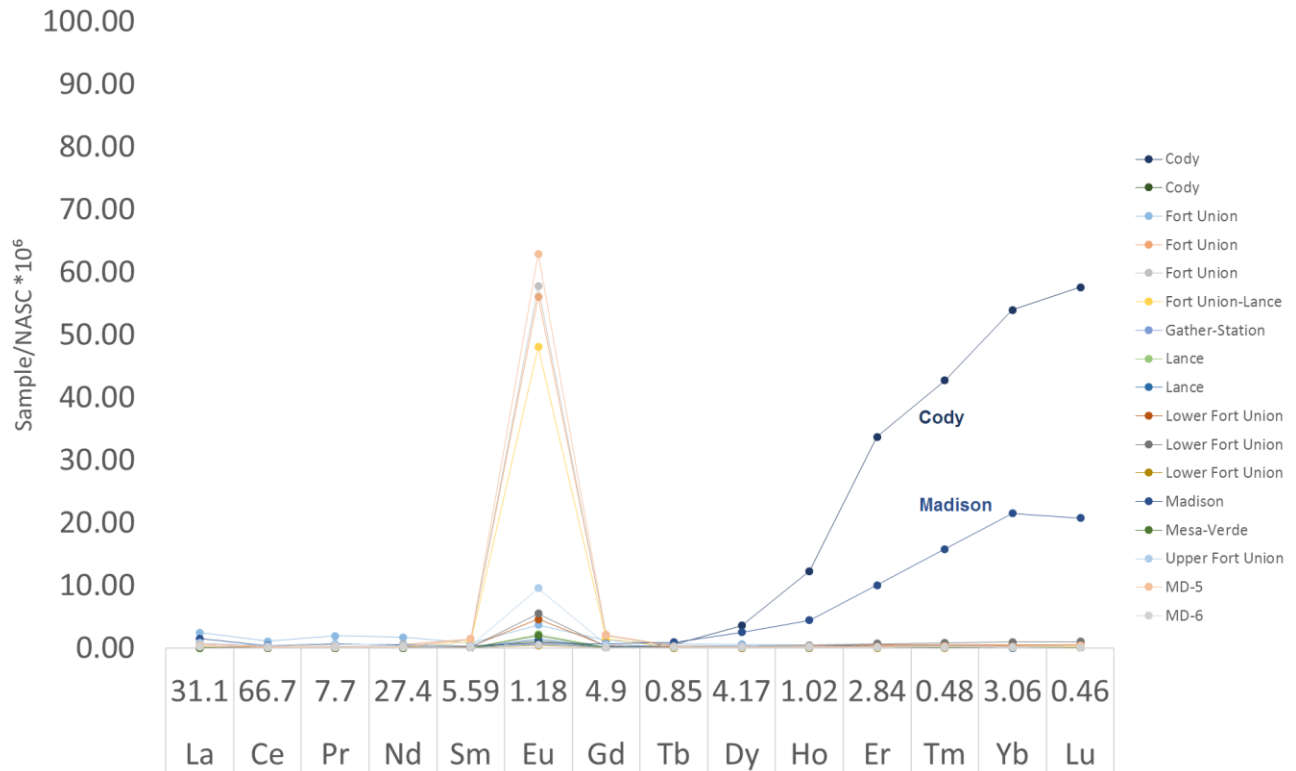


Kevin Dome Aqueous REEs in water analysis





Wind River Basin Aqueous REEs in water analysis



Industrial Power Stations Aqueous REEs in water analysis

